mαcrϕ@ufmg

Universidade Federal de Minas Gerais
Programa de Pós-Graduação em Engenharia Elétrica
Research group MACRO - Mechatronics, Control and Robotics

ROBUST CONTROL FRAMEWORK IN THE WEIGHTED SOBOLEV SPACE

PH.D. THESIS

Daniel Neri Cardoso

Belo Horizonte, Brazil
2021

Daniel Neri Cardoso

ROBUST CONTROL FRAMEWORK IN THE WEIGHTED SOBOLEV SPACE

Manuscript submitted to the Graduate Program in Electrical Engineering of Escola de Engenharia at the Universidade Federal de Minas Gerais, in partial fulfillment of the requirements for the degree of Doctor in Electrical Engineering.

Advisors: Guilherme Vianna Raffo
Sergio Esteban Roncero

Belo Horizonte, Brazil
2021

Cardoso, Daniel Neri.
C268r Robust control framework in the weighted Sobolev space [recurso eletrônico] / Daniel Neri Cardoso. - 2021.
1 recurso online (201 f. : il., color.) : pdf.

Orientador: Guilherme Vianna Raffo.
Coorientador: Sergio Esteban Roncero.

Tese (doutorado) - Universidade Federal de Minas Gerais, Escola de Engenharia.

Bibliografia: f.171-183.
Exigências do sistema: Adobe Acrobat Reader.

1. Engenharia elétrica - Teses. 2. Controle robusto - Teses. 3. Teoria do controle não-linear - Teses. 4. Veículos Aéreos Não Tripulados - Teses. I. Raffo, Guilherme Vianna. II. Esteban Roncero, Sergio. III. Universidade Federal de Minas Gerais. Escola de Engenharia. IV. Título.

CDU: 621.3(043)

Ficha catalográfica elaborada pela Bibliotecária Roseli Alves de Oliveira - CRB-6/2121
Biblioteca Prof. Mário Werneck - Escola de Engenharia da UFMG

UNIVERSIDADE FEDERAL DE MINAS GERAIS
ESCOLA DE ENGENHARIA
Programa de Pós-Graduação em Engenharia Elétrica

ATA DA 363ª DEFESA DE TESE DE DOUTORADO
DO PROGRAMA DE PÓS-GRADUAÇÃO EM ENGENHARIA ELÉTRICA

ATA DE DEFESA DE TESE DE DOUTORADO do aluno **Daniel Neri Cardoso** - registro de matrícula de número 2016752836. Às 11:00 horas do dia 23 do mês de junho de 2021, reuniu-se na Escola de Engenharia da UFMG a Comissão Examinadora da TESE DE DOUTORADO para julgar, em exame final, o trabalho intitulado **"Robust Control Framework In The Weighted Sobolev Space"** da Área de Concentração em Sinais e Sistemas. O Prof. Guilherme Vianna Raffo, orientador do aluno, abriu a sessão apresentando os membros da Comissão e, dando continuidade aos trabalhos, informou aos presentes que, de acordo com o Regulamento do Programa no seu Art. 8.16, será considerado APROVADO na defesa da Tese de Doutorado o candidato que obtiver a aprovação unânime dos membros da Comissão Examinadora. Em seguida deu início à apresentação do trabalho pelo Candidato. Ao final da apresentação seguiu-se a arguição do candidato pelos examinadores. Logo após o término da arguição a Comissão Examinadora se reuniu, sem a presença do Candidato e do público, e elegeu o Prof. Guilherme Vianna Raffo para presidir a fase de avaliação do trabalho, constituída de deliberação individual de APROVAÇÃO ou de REPROVAÇÃO e expedição do resultado final. As deliberações individuais de cada membro da Comissão Examinadora foram as seguintes:

Membro da Comissão Examinadora	Instituição de Origem	Deliberação	Assinatura
Prof. Dr. Guilherme Vianna Raffo - Orientador	DELT (UFMG)	APROVADO	
Prof. Dr. Sergio Esteban Roncero - Co-Orientador	DIAMF (Universidad de Sevilla)	APROVADO	
Prof. Dr. Leonardo Antônio Borges Tôrres	DELT (UFMG)	APROVADO	
Prof. Dr. Víctor Costa da Silva Campos	(UFMG)	APROVADO	
Prof. Dr. Ricardo Hiroshi Caldeira Takahashi	DMAT (UFMG)	APROVADO	
Prof. Dr. Adriano Almeida Gonçalves Siqueira	DEM (USP-SC)	APROVADO	
Prof. Dr. Manuel Gil Ortega Linares	DISA (Universidad de Sevilla)	APROVADO	

Tendo como base as deliberações dos membros da Comissão Examinadora a Tese de Doutorado foi APROVADA. O resultado final de APROVAÇÃO foi comunicado publicamente ao Candidato pelo Presidente da Comissão, ressaltando que a obtenção do Grau de Doutor em ENGENHARIA ELÉTRICA fica condicionada à entrega do TEXTO FINAL da Tese de Doutorado. O Candidato terá um prazo máximo de 30 (trinta) dias, a partir desta data, para fazer as CORREÇÕES DE FORMA e entregar o texto final da Tese de Doutorado na secretaria do PPGEE/UFMG. As correções de forma exigidas pelos membros da Comissão Examinadora deverão ser registradas em um exemplar do texto da Tese de Doutorado, cuja verificação ficará sob a responsabilidade do Presidente da Banca Examinadora. Nada mais havendo a tratar o Presidente encerrou a reunião e lavrou a presente ATA, que será assinada pelo Presidente da Comissão Examinadora. Belo Horizonte, 23 de junho de 2021.

ASSINATURA DO PRESIDENTE DA COMISSÃO EXAMINADORA

Acknowledgements

First of all, I would like to thank God for providing health and intelligence to the accomplishment of this work.

To my parents, Adalcio Cardoso Santos and Maria Wilma Rodrigues Neri, who have supported me in this journey. I have a great pride and admiration for them.

Also to my girlfriend, Ivone Lima Ferreira, who understood my faults, being patient during these times.

Special thanks to Prof. Guilherme Vianna Raffo and Prof. Sergio Esteban who guided me to carry out this work.

To my friends Brenner and Petrus, who cheered me up when things went wrong.

To my colleagues from the laboratories LCR and MACSIN and also from the group MACRO.

Resumo

Esta tese de doutorado propõe novas formulações dos controladores $\mathcal{H}_2$ e $\mathcal{H}_\infty$ nos espaços ponderado de Sobolev. As novas abordagens, aqui chamadas de $\mathcal{W}_2$ e $\mathcal{W}_\infty$, são desenvolvidas levando em consideração a norma ponderada de Sobolev da variável de custo com o objetivo de alcançar uma rápida atenuação de perturbação com um desempenho transiente aprimorado.

Inicialmente, os controladores $\mathcal{W}_2$ e $\mathcal{W}_\infty$ não lineares são formulados para sistemas autônomos em malha fechada, e os problemas de controle são desenvolvidos por meio de programação dinâmica, resultando em equações de Hamilton-Jacobi (HJ) complexas a serem resolvidas. Devido à dificuldade de resolver analiticamente essas equações, o algoritmo de aproximação sucessiva de Galerkin é estendido aos controladores $\mathcal{W}_2$ e $\mathcal{W}_\infty$, e usados para aproximar soluções das equações de HJ. Experimentos numéricos são realizados com um veículo autobalanceado de duas rodas, e uma análise comparativa com o controlador $\mathcal{H}_\infty$ clássico é apresentada. Os resultados demonstram que os controladores resultantes das abordagens no espaço ponderado de Sobolev alcançam um melhor desempenho transiente com uma atenuação mais rápida de perturbação.

Esta tese também propõe novas formulações das abordagens de controle ótimo não linear $\mathcal{H}_2$ e $\mathcal{H}_\infty$ no espaço ponderado de Sobolev para lidar com duas classes de sistemas mecânicos subatuados: a classe de sistemas mecânicos subatuados reduzidos, com o objetivo de obter rastreamento de trajetória de um número reduzido de graus de liberdade, denominado graus de liberdade controlados; e a classe de sistemas mecânicos subatuados com acoplamento de entradas, com o objetivo de conduzir os graus de liberdade controlados ao longo da trajetória desejada enquanto estabiliza os restantes. Para esses sistemas, os problemas de controle ótimo são novamente formulados via programação dinâmica, e soluções particulares são apresentadas para as equações de HJ resultantes com a análise de estabilidade correspondente. Além disso, os conceitos de ganho $\mathcal{W}_{m,p,\boldsymbol{\sigma}}$ e estabilidade $\mathcal{W}_{m,p,\boldsymbol{\sigma}}$ são estabelecidos e aplicados para o caso particular de estudo. Adicionalmente, é mostrado que para a classe particular de sistemas mecânicos subatuados, cujas entradas de controle e o vetor de perturbação abrangem o mesmo espaço vetorial no vetor de forcas generalizadas, os controladores $\mathcal{W}_2$ e $\mathcal{W}_\infty$ tornam-se equivalentes. Resultados numéricos são obtidos com um manipulador totalmente atuado, um veículo autobalanceado de duas

rodas e um veículo aéreo não tribulado (VANT) do tipo *quadrotor*, para demonstrar a eficiência dos controladores propostos. Eles mostram que os controladores $\mathcal{W}_2$ e $\mathcal{W}_\infty$ proporcionam uma melhor resposta transiente com uma rápida atenuação de perturbações externas em comparação com o controlador $\mathcal{H}_\infty$ clássico não linear, além de serem de fácil implementação.

Esta tese de doutorado também formula o controlador $\mathcal{W}_\infty$ linear no espaço ponderado de Sobolev para sistemas lineares invariantes no tempo. São abordados os projetos de controladores lineares baseado em realimentação de estados e de saída, e é apresentado uma nova abordagem em que o comportamento dinâmico das perturbações é levado em consideração na fase de projeto de controle por meio de um modelo de perturbação. Restrições de posicionamento de pólos também são desenvolvidas, permitindo a síntese de controladores $\mathcal{W}_\infty$ com os pólos de malha fechada alocados em uma região prédefinida do plano complexo. Experimentos numéricos são realizados com um sistema linear simples, um veículo autobalanceado de duas rodas e um VANT *quadrotor*, eles mostram que as abordagems de controle linear $\mathcal{W}_\infty$ obtem um melhor desempenho quando comparado com um controlador $\mathcal{H}_\infty$ clássico linear.

Por fim, o controlador $\mathcal{W}_\infty$ é empregado no estudo de caso dos VANTs conversíveis do tipo *Tilt-rotor*. Uma modelagem detalhada da dinâmica não linear multicorpo do VANT *Tilt-rotor* é conduzida usando o formalismo de Euler-Lagrange, e as forças e torques não conservativos gerados pelas hélices, servomotores, fuselagem, asas, superfícies da cauda e interferência aerodinâmica são calculados e mapeados para o vetor de forças generalizadas. Controladores $\mathcal{W}_\infty$ lineares baseado em realimentação de estado e de saída são sintetizados para resolver o problema de rastreamento de trajetória no modo de voo de helicóptero, sendo o modelo de turbulência de Von kármán usado para emular o vento do ambiente e considerado como modelo de perturbação para projeto dos controladores. Além disso, um controlador $\mathcal{W}_\infty$ não linear é projetado para resolver o problema de rastreamento da trajetória ao longo do envelope de vôo completo. Para projetar esse controlador não linear, a abordagem proposta para sistemas mecânicos subactuados com acoplamento de entrada, mencionado anteriormente, é estendida, o sistema mecânico é particionado em relação aos graus de liberadade estabilizados, regulados e controlados, com o objetivo de alcançar o rastreamento da trajetória dos graus de liberdade controlados, e definir referências para os graus de liberdade regulados, enquanto os graus de liberdade restantes são estabilizados. O controlador não linear é implementado levando em consideração um esquema de alocação de controle, que é proposto para lidar com o *rank* variável no tempo da matriz de acoplamento de entrada do VANT conversível *Tilt-rotor*, levando em consideração a magnitude e a orientação da velocidade do vento relativo para mapear adequadamente as entradas generalizadas para os sinais de controle. Experimentos numéricos são conduzidos em um simulador de alta fidelidade, eles demonstram que os controladores $\mathcal{W}_\infty$ propostos alcançam rastreamento de trajetória no modo de voo de helicóptero, utilizando

os controladores $\mathcal{W}_\infty$ lineares, e rastreamento de trajetória ao longo de todo o envelope de vôo, utilizando o controlador $\mathcal{W}_\infty$ não linear, além de atenuar adequadamente efeitos de distúrbios externos e rajadas de vento.

Abstract

This Ph.D. thesis proposes new formulations of the $\mathcal{H}_2$ and $\mathcal{H}_\infty$ controllers in the weighted Sobolev spaces. The novel approaches, here called $\mathcal{W}_2$ and $\mathcal{W}_\infty$, are developed taking into account the weighted Sobolev norm of the cost variable, aiming to achieve an improved transient performance with a faster disturbance attenuation.

Initially, the nonlinear $\mathcal{W}_2$ and $\mathcal{W}_\infty$ control problems are formulated for closed-loop autonomous nonlinear systems, and the control problems are developed via dynamic-programming, resulting in complex Hamilton-Jacobi (HJ) equations to be solved. Due to the difficulty of solving analytically these HJ equations, the Successive Galerkin Approximation Algorithm is extended to the $\mathcal{W}_2$ and $\mathcal{W}_\infty$ controllers, and used to approximate solutions. Numerical experiments are performed with a Two-wheeled Self-balanced vehicle, and a comparative analysis with the classic $\mathcal{H}_\infty$ controller is presented. The results demonstrate that the controllers resulting from the weighted Sobolev approach achieve a better transient performance with a faster disturbance attenuation.

This doctoral thesis also proposes new formulations of the nonlinear $\mathcal{H}_2$ and $\mathcal{H}_\infty$ optimal control approaches in the weighted Sobolev spaces, in order to handle two classes of underactuated mechanical systems: the class of reduced underactuated mechanical systems, with the objective of achieving trajectory tracking for a reduced number of Degrees Of Freedom (DOF), called controlled DOF; and the class of underactuated mechanical systems with input coupling, with the objective of driving the controlled DOF along a desired trajectory while stabilizing the remaining ones. For these systems, the optimal nonlinear $\mathcal{W}_2$ and $\mathcal{W}_\infty$ control problems are formulated via dynamic-programming, and particular solutions are presented for the resulting HJ equations with the corresponding stability analysis. In addition, the concepts of $\mathcal{W}_{m,p,\boldsymbol{\sigma}}$-gain and $\mathcal{W}_{m,p,\boldsymbol{\sigma}}$-stability are established and applied to the particular case studies. It is shown that, for the particular class of underactuated mechanical systems, whose control inputs and disturbances vector span the same space in the vector space of generalized forces, the $\mathcal{W}_2$ and $\mathcal{W}_\infty$ controllers become equivalent. The efficacy of the proposed $\mathcal{W}_2$ and $\mathcal{W}_\infty$ control strategies for mechanical systems are demonstrated via numerical experiments conducted with a fully actuated manipulator, a Two-wheeled Self-balanced vehicle, and a Quadrotor unmanned aerial vehicle (UAV). It is verified that these controllers provide a better transient perfor-

mance with a faster response against external disturbances, in comparison with a more traditional nonlinear $\mathcal{H}_\infty$ controller, in addition to be of simpler design.

This thesis also formulates the linear $\mathcal{W}_\infty$ controller in the weighted Sobolev space for linear time-invariant systems. The design of state and output feedback controllers is addressed, and a new approach in which the dynamic behavior of the disturbances is taken into consideration in the control design stage by means of a disturbance model is introduced. Pole placement constraints are also developed, allowing the synthesis of linear $\mathcal{W}_\infty$ controllers with the closed-loop poles allocated in a predefined region of the complex plane. Numerical experiments are performed with a simple linear system, a Two-wheeled Self-balanced vehicle, and a Quadrotor UAV, which demonstrate that the state and output feedback linear $\mathcal{W}_\infty$ controllers achieve a better transient performance with a faster disturbance attenuation in comparison with a linear $\mathcal{H}_\infty$ controller.

Lastly, the $\mathcal{W}_\infty$ controller is employed in the case study of convertible Tilt-rotor UAVs. A detailed modeling of the nonlinear multi-body dynamics of the Tilt-rotor UAV is conducted using the Euler-Lagrange formalism, and the nonconservative forces and torques generated by the propellers, servomotors, fuselage, wings, tail surfaces, and aerodynamic interference are computed and mapped to the vector of generalized forces. State and output feedback linear $\mathcal{W}_\infty$ controllers are synthesized to solve the trajectory tracking problem of the convertible Tilt-rotor UAV in the helicopter flight mode, being the Von Kármán wind turbulence model used to emulate the environment wind and considered as disturbance model in the linear control design. Besides, a nonlinear $\mathcal{W}_\infty$ controller is designed to solve the full flight envelope trajectory tracking problem of the convertible Tilt-rotor UAV. To design the nonlinear controller, the approach proposed for underactuated mechanical systems with input coupling, previously mentioned, is extended, the mechanical system is partitioned with respect to stabilized, regulated, and controlled DOF, aiming to achieve trajectory tracking of the controller DOF, and set references to the regulated DOF, while stabilizing the remaining DOF. The nonlinear controller is implemented taking into account a control allocation scheme, which is proposed to handle the time-varying rank of the convertible Tilt-rotor UAV input coupling matrix, taking into account the magnitude and orientation of the relative wind-speed to properly map the generalized inputs to the control signals. Numerical experiments are conducted in a high fidelity simulator, they demonstrate that the proposed $\mathcal{W}_\infty$ controllers achieve trajectory tracking in the helicopter flight mode, regarding the linear $\mathcal{W}_\infty$ controllers, and trajectory tracking throughout the full flight envelope, regarding the nonlinear $\mathcal{W}_\infty$ controller, while attenuating effects of external disturbances and wind gusts.

List of Figures

List of Tables

Notation

a	italic lower case letters denote scalars
$\boldsymbol{a}$	boldface italic lowercase letters denote vectors
$\boldsymbol{A}$	boldface italic uppercase letters denote matrices
$\mathbb{N}$	the set of natural numbers, $\mathbb{N} \triangleq \{1, 2, 3...\}$
$\mathbb{C}$	the set of complex numbers
$\mathbb{Z}$	the set of integers, $\mathbb{Z} \triangleq \{..., -3, -2, -1, 0, 1, 2, 3, ...\}$
$\mathbb{R}$	the set of real numbers, $\mathbb{R} \triangleq (-\infty, \ \infty)$
$\mathbb{R}_{>0}$	the set of positive real numbers, $\mathbb{R}_{>0} \triangleq (0, \ \infty)$
$\mathbb{R}_{\geq 0}$	the set of positive real numbers including zero, $\mathbb{R}_{\geq 0} \triangleq [0, \ \infty)$
$\mathbb{R}^n$	the set of real vectors with dimension n, $\mathbb{R}^n \triangleq \{\boldsymbol{r} = [r_1 \ ... \ r_n]' : r_i \in \mathbb{R}, i \in \{1, ..., n\}\}$
$\mathbb{R}^{n \times m}$	the set of real matrices with dimension $n \times m$, $\mathbb{R}^{n \times m} \triangleq \{\boldsymbol{R} = [\boldsymbol{r}_1 \ ... \ \boldsymbol{r}_m] : \boldsymbol{r}_i \in \mathbb{R}^n, i \in \{1, ..., m\}\}$
$a \in \Omega$	a is an element of the set Ω
$\Omega_1 \times \Omega_2$	denotes the Cartesian product between the sets Ω_1 and Ω_2
$(.)'$	denotes the transpose of (.)
$(.)^{-1}$	denotes the inverse of the square matrix (.)
$(.)^{\dagger}$	denotes the pseudo-inverse of matrix (.)
trace$\{\boldsymbol{A}\}$	Trace of A
diag()	Diagonal matrix whose diagonal elements are given in the parentheses

blkdiag(.)	represents a block diagonal matrix whose diagonal elements are the matrices or vectors given in the parentheses, and all off-diagonal blocks are zero matrices.
$\mathbf{0}$	zeros matrix with appropriate dimension
$\boldsymbol{I}$	identity matrix with appropriate dimension
$\mathbf{1}$	ones matrix with appropriate dimension
$\boldsymbol{z}(\cdot) : \Omega \to \Gamma$	a function that maps the domain space Ω to the image space Γ
$\mathcal{U} : \Omega \to \Gamma$	the set of functions that maps the space Ω to Γ
$\dot{\boldsymbol{z}}(t)$	the time-derivative of the function $\boldsymbol{z}(t) : \mathbb{R}_{\geq 0} \to \mathbb{R}^{n_z}$, in which $t \in \mathbb{R}_{\geq 0}$ is the time variable
$\|\|\boldsymbol{z}(t)\|\|_{\mathcal{L}_p}$	the Lebesgue $\mathcal{L}_p$ – norm of $\boldsymbol{z}(t)$
$\|\|\boldsymbol{z}(t)\|\|_{\mathcal{W}_{m,p}}$	the Sobolev $\mathcal{W}_{m,p}$ – norm of $\boldsymbol{z}(t)$
$\|\|\boldsymbol{z}(t)\|\|_{\mathcal{W}_{m,p,\boldsymbol{\sigma}}}$	the weighted Sobolev $\mathcal{W}_{m,p,\boldsymbol{\sigma}}$ – norm of $\boldsymbol{z}(t)$
$\boldsymbol{z}(t) \in \mathcal{L}_p[0, \infty)$	the function $\boldsymbol{z}(t)$ belongs to the $\mathcal{L}_p$-space, i.e. $\|\|\boldsymbol{z}(t)\|\|_{\mathcal{L}_p} < \infty$
$\boldsymbol{z}(t) \in \mathcal{W}_{m,p}[0, \infty)$	the function $\boldsymbol{z}(t)$ belongs to the Sobolev $\mathcal{W}_{m,p}$-space, i.e. $\|\|\boldsymbol{z}(t)\|\|_{\mathcal{W}_{m,p}} < \infty$
$\boldsymbol{z}(t) \in \mathcal{W}_{m,p,\boldsymbol{\sigma}}[0, \infty)$	the function $\boldsymbol{z}(t)$ belongs to the weighted Sobolev $\mathcal{W}_{m,p,\boldsymbol{\sigma}}$-space, i.e. $\|\|\boldsymbol{z}(t)\|\|_{\mathcal{W}_{m,p,\boldsymbol{\sigma}}} < \infty$
$\inf S$	infimum of set S, i.e. $s \in S$, $s \leq s_0$, $\forall s_0 \in S$.

Acronyms

UAV	Unmanned Aerial Vehicle
VANT	Veículo Aéreo Não Tripulado
VTOL	Vertical Take-off and Landing
MPC	Model Predictive Control
LMPC	Linear Model Predictive Control
NN	Neural Network
LPV	Linear Parameter Varying
PSO	Particle Swarm Optimization
LMI	Linear Matrix Inequality
LQR	Linear Quadratic Regulator
DLQR	Discrete time Linear Quadratic Regulator
ISE	Integral of the Square Error
IADU	Integral of the Absolute Derivative of the control signal
PDE	Partial Differential Equation
HJ	Hamilton-Jacobi
HJB	Hamilton-Jacobi-Bellman
HJBI	Hamilton-Jacobi-Bellman-Isacs
SISO	Single-Input Single-Output
MIMO	Multiple-Input Multiple-Output
PID	Proportional Integral Derivative

PI	Proportional Integral Derivative
DOF	Degrees of Freedom
SGAA	Successive Galerkin Approximation Algorithm
SCAA	Successive Collocation Approximation Algorithm

Contents

1 Introduction

1.1 Motivation

The design of controllers aiming to attenuate disturbances is one of the main challenges in the control area due to an inevitable need to deal with the presence of uncertainties. In general, the control design is conducted based on mathematical models; however, it is a complex, if not impossible, task to obtain a mathematical model that describes with perfection a real-life phenomenon. Mathematical models usually are approximations of the system, presenting unmodeled dynamics and parameter uncertainties. Besides, physical systems are often subject to external disturbances and noise added to the measurement reported by sensors, which make the control design even more complex. Robust control strategies emerges due to the inevitable need to deal with uncertainties when it is required to achieve acceptable performance.

Two usual approaches to deal with disturbances and imperfections on the mathematical model in the control design stage are the well known $\mathcal{H}_2$ (Johansson, 1990) and $\mathcal{H}_\infty$ (Van Der Schaft, 1992) control strategies. They have been originally formulated in the frequency domain to cope with single-input-single-output systems represented by transfer functions (Doyle et al., 2013). The $\mathcal{H}_2$ controller designed on the frequency domain seeks to minimize the energy of the disturbance impulse response (Geromel et al., 1999), while the $\mathcal{H}_\infty$ controller minimizes the maximum gain given by the closed-loop system to a disturbance signal (Francis and Doyle, 1987). Due to the need to deal with multiple-input-multiple-output systems, efforts were made to extend these control strategies to

systems represented in state-space, which were firstly introduced in (Doyle et al., 1989) and received considerable attention in the past decades as the initial point to the development of $\mathcal{H}_2$ and $\mathcal{H}_\infty$ controllers based on linear matrix inequalities (Gahinet and Apkarian, 1994). For nonlinear systems, the $\mathcal{H}_\infty$ control strategy was first introduced in Van der Schaft (1991), where the problem is formulated in the $\mathcal{L}_2$ space using the theory of dissipative systems.

Although the $\mathcal{H}_2$ and $\mathcal{H}_\infty$ control strategies have been applied successfully and their effectiveness verified experimentally (Van der Linden and Lambrechts, 1993; Nichols et al., 1993; Sedhom et al., 2020), these methods may present drawbacks. As stated in Chilali and Gahinet (1996), the $\mathcal{H}_2$ and $\mathcal{H}_\infty$ control strategies deal mostly with the aspects of stabilization and disturbance attenuation and provide little control over the transient behavior. On one hand, pole placement constraints can be imposed into the control design stage of linear systems (Chilali and Gahinet, 1996) to achieve a satisfactory transient behavior. On the other hand, just a few works deal with the transient behavior in the control design for nonlinear systems. An alternative approach to overcome this issue is the formulation of both $\mathcal{H}_2$ and $\mathcal{H}_\infty$ controllers in the Sobolev spaces $\mathcal{W}_{m,p}$, which are the spaces of functions in the $\mathcal{L}_p$ space whose generalized derivatives up to order m are also in the $\mathcal{L}_p$ space (Treves, 2016). In the control area, the properties of the Sobolev spaces have been successfully employed, for example, to design state observers (Alessandri and Sanguineti, 2007; Zemouche and Boutayeb, 2008). Furthermore, in Bourles and Colledani (1995), a new input-output stability definition is presented based on the Sobolev spaces, as a local version of the small gain theorem, besides the relationship between $\mathcal{W}$-stability and asymptotic stability. He and Wang (2004) extended the $\mathcal{W}$-stability criterion for the class of nonlinear systems with bounded delay. The idea behind these works relies on the fact that in this kind of space all properties of $\mathcal{L}_p$ space are satisfied.

For control design, Aliyu and Boukas (2011a) proposed the reformulation of the $\mathcal{H}_2$ and $\mathcal{H}_\infty$ control approaches in a Sobolev space to achieve improved transient performance. In their formulation, instead of the $\mathcal{L}_2$-norm, the $\mathcal{W}_{1,2}$-norm of the cost variable is considered.[1] The control problems are developed via dynamic programming, from which the related Hamilton-Jacobi (HJ) equations must be solved to obtain the resulting controllers. Nevertheless, these HJ equations are hard to solve analytically. In particular, Aliyu and Boukas (2011a) consider the HJ equation resulting from the $\mathcal{H}_\infty$ control formulation in the Sobolev space to be intractable and propose an alternative approach through the backstepping technique to simplify the problem. However, the latter approach is quite similar to the classic nonlinear $\mathcal{H}_\infty$ one, differing by an integrator added to the cost variable. Thus, as the rate of change of the cost variable is not considered in the cost functional,

[1] The Sobolev $\mathcal{W}_{m,p}-$norm of a function $\boldsymbol{z}(t) : \mathbb{R}_{\geq 0} \to \mathbb{R}$, for $m \in \mathbb{N}$ and $p \in \mathbb{N} \cup \{\infty\}$, is defined as $||\boldsymbol{z}(t)||_{\mathcal{W}_{m,p}} = \left(\sum_{\alpha=0}^{m} ||\frac{d^\alpha \boldsymbol{z}(t)}{dt^\alpha}||_{\mathcal{L}_p}^p\right)^{1/p}$, where $||\cdot||_{\mathcal{L}_p}$ stands for the $\mathcal{L}_p-$norm, $\mathbb{N} = \{1, 2, 3...\}$.

the improvements on the transient behavior are not achieved. In addition, the approaches presented in Aliyu and Boukas (2011a) lack in the capacity of distinguishing the influences of the cost variable and its time derivatives in the control objectives.

In this context, this doctoral thesis designs the classic $\mathcal{H}_2$ and $\mathcal{H}_\infty$ control approaches in the weighted Sobolev spaces $\mathcal{W}_{m,p,\boldsymbol{\sigma}}$ (Kufner, 1985), aiming to improve the transient performance and allow tuning component-wise the influences of the cost variable and its time derivatives in the cost functional. The $\mathcal{W}_2$ and $\mathcal{W}_\infty$ control problems[2] are developed via dynamic-programming resulting in complex HJ equations to be solved. HJ Partial Differential Equations (PDEs) are hard to solve analytically for the general class of systems. Therefore, to simplify the process of achieving the controller, it is usual to compute either a solution using numerical algorithms or to particularize the control problem to a special class of systems. This work explores both possibilities, initially, the nonlinear $\mathcal{W}_2$ and $\mathcal{W}_\infty$ control problems are formulated for nonlinear systems, and the Successive Galerkin Approximation Algorithm (SGAA) (Beard and McLain, 1998) is extended to solve the HJ equations. In addition, the $\mathcal{W}_2$ and $\mathcal{W}_\infty$ control problems are particularized for mechanical systems represented by the Euler-Lagrange equation, and particular solutions are proposed to the resulting HJ equations for the classes of fully actuated, reduced underactuated, and underactuated mechanical systems with input coupling.

It is worth highlighting that, as stated in Chen et al. (1994), the standard formulation of the nonlinear $\mathcal{H}_\infty$ control and, consequently, of the nonlinear $\mathcal{H}_2$ control for Euler-Lagrange mechanical systems presents a limitation in the way to weight the cost variable. For its appropriate formulation, the weighting matrices must be considered positive real scalars multiplied by the identity matrix, limiting the adjustment of the control law for systems with multiple DOF with similar dynamics. To overcome this shortcoming, in Raffo et al. (2011a) an approach based on diagonalization of the inertia matrix is proposed in order to provide some flexibility to tune the nonlinear $\mathcal{H}_\infty$ controller. That issue does not arise in the proposed $\mathcal{W}_2$ and $\mathcal{W}_\infty$ controllers for mechanical systems and, besides, they are of simpler design.

This doctoral thesis also formulates the linear $\mathcal{W}_\infty$ controller in the weighted Sobolev space for linear time-invariant systems via semidefinite programming written as Linear Matrix Inequalities (LMI) constraints, for which a series of numerical methods can be used to achieve a solution. It is addressed the design of state and output feedback linear controllers, and is introduced a new approach in which the dynamic behavior of the disturbances is taken into consideration in the control design stage by means of a disturbance model. Pole placement constraints are also developed to allow the synthesis of $\mathcal{W}_\infty$ controllers with the closed-loop poles allocated in a predefined region of the complex plane.

[2] In this work, the $\mathcal{H}_2$ and $\mathcal{H}_\infty$ controllers formulated in the weighted Sobolev space are called $\mathcal{W}_2$ and $\mathcal{W}_\infty$ controllers, respectively.

This doctoral thesis also designs a nonlinear $\mathcal{W}_\infty$ controller to solve the full flight envelope trajectory tracking problem of a convertible Tilt-rotor UAV. The Tilt-rotor UAV is a kind of convertible UAV, which can perform hovering and Vertical Take-off and Landing (VTOL) as helicopters and, by tilting the rotors to the horizontal position, improved cruise flight as a fixed-wing aircraft (Maisel et al., 2000; Liu et al., 2017). The relative wind generated by the motion substantially changes the dynamic behaviour of this aircraft between hovering and cruise flight modes. In helicopter-flight mode (VTOL and hovering), the deflections of the aerodynamic control surfaces (aileron, rudder, and elevator) do not produce significant forces and torques, whereas in cruise-flight mode, small deflections produce significant aerodynamic forces that can be used to generate both the necessary forces to sustain forward flight, and the moments that allow control and guidance. These facts pose some challenges for the control design of convertible Tilt-rotor UAVs, which cannot usually be solved using classical linear controllers when it is required to achieve good performance throughout the full flight envelope trajectory tracking. Furthermore, control techniques designed for mechanical systems, such as Johansson (1990); Raffo et al. (2011a), cannot be directly applied to solve this problem since they were developed for systems whose input coupling matrix rank does not vary with time. In addition, convertible plane Tilt-rotor UAVs are usually subjected to uncertainties from many sources as wind gusts, unmodeled dynamics, and parametric uncertainties, which make the design of controllers for these systems even less trivial when it is required to achieve good performance. To the best of the author's knowledge and as commented in Morin (2015), the design of a controller for convertible Tilt-rotor UAVs to accomplish transition between hover and cruise flight modes fully exploiting the aircraft nonlinear dynamics is an open problem. To solve this problem, this doctoral thesis designs a nonlinear $\mathcal{W}_\infty$ controller that is implemented taking into account a control allocation scheme. The control allocation scheme is proposed to handle the time-varying rank of the convertible Tilt-rotor UAV input coupling matrix, taking into account the magnitude and orientation of the relative wind-speed to properly map the generalized inputs to the control signals.

1.2 Justification

In view of the drawbacks of the $\mathcal{H}_2$ and $\mathcal{H}_\infty$ control strategies, this doctoral thesis introduces the $\mathcal{W}_2$ and $\mathcal{W}_\infty$ controllers. These novel controllers are formulated taking into account the weighted Sobolev norm of the cost variable to allow tuning component-wise the influences of the cost variable and its time derivatives in the cost functional. They aggregate an improved transient performance to the $\mathcal{H}_2$ and $\mathcal{H}_\infty$ controllers, providing a faster disturbance attenuation to the closed-loop system. The control problems are developed via dynamic-programming resulting in HJ equations to be solved, for which particular solutions are presented for special classes of mechanical systems and numerical

algorithms are proposed to attain solutions. The state and output feedback linear $\mathcal{W}_\infty$ control problems are also formulated for linear time-invariant systems via semidefinite programming written as LMI constraints, for which several numerical methods can be used to achieve a solution. It is proposed a robust control framework in the weighted Sobolev space that allows handling a wide variety of systems.

1.3 Objectives

The main objective of this thesis is to formulate the classic $\mathcal{H}_2$ and $\mathcal{H}_\infty$ controllers in the weighted Sobolev space, for both linear and nonlinear systems, aiming to achieve faster disturbance attenuation with improved transient performance.

1.3.1 Specific Objectives

Specifically, it is intended to:

1. Formulate the $\mathcal{H}_2$ and $\mathcal{H}_\infty$ control problems in the weighted Sobolev spaces;
2. Develop the $\mathcal{W}_2$ and $\mathcal{W}_\infty$ optimal control problems via dynamic-programming, and propose numerical algorithms to attain solutions of the resulting HJ equations;
3. Formulate the nonlinear $\mathcal{W}_2$ and $\mathcal{W}_\infty$ controllers for mechanical systems represented by the Euler-Lagrange equations, develop the optimal control problems via dynamic-programming, and propose particular solutions to the resulting HJ equations;
4. Formulate the state and output feedback linear $\mathcal{W}_\infty$ controllers in the weighted Sobolev spaces via semidefinite programming written as LMI, and develop pole placement constraints that allow synthesizing these linear controllers with the closed-loop poles allocated in a predefined region $\mathcal{D}$ of the complex plane;
5. Demonstrate the effectiveness of the $\mathcal{W}_2$ and $\mathcal{W}_\infty$ control strategies via numerical experiments and perform comparison analysis with the classic $\mathcal{H}_\infty$ controller.
6. Design $\mathcal{W}_\infty$ controllers for a convertible Tilt-rotor UAV, in order to solve the full flight envelope trajectory tracking problem.

1.4 List of publications

During this Ph.D. research the following scientific works have been elaborated.

Journal papers:

1. (Cardoso et al., 2021c) D. N. Cardoso, S. Esteban and G. V. Raffo. A new robust adaptive mixing control for trajectory tracking with improved forward flight of a Tilt-rotor UAV. Journal ISA transactions.

2. (Cardoso et al., 2021a) D. N. Cardoso, S. Esteban and G. V. Raffo. A robust optimal control approach in the weighted Sobolev space for underactuated mechanical systems. Automatica.

3. (Cardoso et al., 2021b) D. N. Cardoso, S. Esteban and G. V. Raffo. A linear robust control framework in the weighted Sobolev space via LMIs. (in the process of submission).

4. (Cardoso et al., 2021d) D. N. Cardoso, S. Esteban and G. V. Raffo. A Robust Nonlinear Controller in the Weighted Sobolev Space for Trajectory Tracking Throughout the Full Flight Envelope of a Tilt-rotor UAV. (in the process of submission).

5. (Aquino et al., 2021b) J. E. M. Aquino, D. N. Cardoso and G. V. Raffo. Robust nonlinear control of aerial manipulators. (Submitted to Journal of Control, Automation and Electrical Systems JCAE).

Conference papers:

1. (Santos et al., 2017) M. A. Santos, D. N. Cardoso, and B. S. Rego, and G. V. Raffo and S. Esteban. A discrete robust adaptive control of a Tilt-rotor UAV for an enlarged flight envelope. In Proc. of IEEE 56th Annual Conference on Decision and Control (CDC2017).

2. (Cardoso and Raffo, 2018) D. N. Cardoso and G. V. Raffo. Approximated solutions to the nonlinear $\mathcal{H}_2$ and $\mathcal{H}_\infty$ control approaches formulated in the Sobolev space. In Proc. of European Control Conference - 2018 (ECC2018).

3. (Cardoso et al., 2018a) D. N. Cardoso, S. Esteban and G. V. Raffo. Nonlinear $\mathcal{H}_2$ and $\mathcal{H}_\infty$ control formulated in the Sobolev space for mechanical systems. In Proc. of 9th Symposium on Robust Control Design (ROCOND2018)

4. (Cardoso et al., 2018b) D. N. Cardoso, S. Esteban and G. V. Raffo. Nonlinear $\mathcal{H}_2$ and $\mathcal{H}_\infty$ control formulated in the weighted Sobolev space for underactuated mechanical systems with input coupling. In Proc. of 57th IEEE Conference on Decision and Control (CDC2018)

5. (Cardoso et al., 2018c) D. N. Cardoso, S. Esteban and G. V. Raffo. Nonlinear $\mathcal{H}_\infty$ and $\mathcal{W}_\infty$ control approaches - A comparison analysis. In Proc. of XXII Congresso Brasileiro de Automática (CBA2018)

6. (Cardoso, Esteban and Raffo, 2019) D. N. Cardoso, S. Esteban and G. V. Raffo. A Nonlinear $\mathcal{W}_\infty$ Controller of a Tilt-rotor UAV for trajectory tracking. In Proc. of European Control Conference - 2019 (ECC2019)

7. (Cardoso, Campos, Esteban, Normey-rico and Raffo, 2019) D. N. Cardoso, J. Campos, S. Esteban, J.E. Normey-rico and G. V. Raffo. Modelagem e simulação de um VANT convertível Tilt-rotor - In Proc. of 2º Congresso Aeroespacial Brasileiro - 2019 (CAB2019)

8. (Aquino et al., 2020) J. E. M. Aquino, D. N. Cardoso and G. V. Raffo. Robust optimal nonlinear control strategies for an aerial manipulator - In Proc. of XXIII Congresso Brasileiro de Automática - 2020 (CBA2020)

9. (Campos et al., 2021) J. Campos, D. N. Cardoso, and G. V. Raffo. Modeling and Robust Control for Full-Flight Envelope Trajectory Tracking of a QuadCP-VTOL Unmanned Aerial Vehicle. In Proc of The Vertical Flight Society's 77th Annual Forum & Technology Display (VFS2021).

10. (Aquino et al., 2021a) J. E. M. Aquino, D. N. Cardoso and G. V. Raffo. Modeling and Control of an Aerial Manipulator from the Perspective of its End-effector. In Proc. of Simpósio Brasileiro de Automação Inteligente - 2021 (SBAI2021)

1.5 Content of this manuscript

The following chapters are structured as:

- **Chapter** 2 concerns the literature review on the $\mathcal{H}_2$ and $\mathcal{H}_\infty$ control frameworks, Sobolev spaces and its application in the control theory, and approximate solutions to the HJ equation.

- **Chapter** 3 presents some preliminary concepts necessary to better comprehend this manuscript, which include the Lebesgue and the Sobolev spaces, interesting features of the $\mathcal{W}_2$ and $\mathcal{W}_\infty$ control formulations in the weighted Sobolev spaces, the Hamilton-Jacobi-Bellman equation, the method of Galerkin, and the Euler-Lagrange formulation of mechanical systems.

- **Chapter** 4 formulates the nonlinear $\mathcal{H}_2$ and $\mathcal{H}_\infty$ control approaches in the weighted Sobolev space, namely $\mathcal{W}_2$ and $\mathcal{W}_\infty$ controllers, for continuous autonomous nonlinear systems that are affine in the control inputs and disturbances. The control problems are developed via dynamic-programming resulting in complex HJ equations to be solved. Numerical algorithms are proposed to attain solutions of the HJ partial

differential equations (PDE). The efficiency of the proposed controllers and algorithms are demonstrated via numerical experiments conducted with a two-wheeled self-balanced vehicle.

- **Chapter** 5 particularizes the $\mathcal{W}_2$ and $\mathcal{W}_\infty$ control approaches for mechanical systems represented by the Euler-Lagrange equations. The control problems are again formulated via dynamic-programming, and particular solutions are proposed to the classes of fully actuated mechanical systems, reduced underactuated mechanical systems, and underactuated mechanical systems with input coupling. The controllers are synthesized for a fully-actuated manipulator, a two-wheeled self-balanced vehicle, and a quadrotor UAV. The results of numerical experiments are presented to corroborate the efficiency of the controllers.

- **Chapter** 6 formulates the linear $\mathcal{W}_\infty$ control approach in the weighted Sobolev space via semidefinite programming written as LMI constraints. It addresses the design of state and output feedback controllers, and introduces a new approach in which the disturbance behavior is taken into consideration in the control design stage by means of a disturbance model. In addition, pole placement constraints are formulated to allow the synthesis of $\mathcal{W}_\infty$ controllers with the closed-loop poles allocated in a predefined region of the complex plane. The effectiveness of the control strategies are corroborated with numerical experiments conducted with a simple linear system, a two-wheeled self-balanced vehicle and a quadrotor UAV.

- **Chapter** 7 employs the $\mathcal{W}_\infty$ control framework into the case study of convertible Tilt-rotor UAVs. A detailed modeling of the nonlinear multi-body dynamics of a convertible Tilt-rotor UAV is conducted using the Euler-Lagrange formalism, and the nonconservative forces and torques generated by the propellers, servomotors, fuselage, wings, tail surfaces, and aerodynamic interference are computed and mapped to the vector of generalized forces. The state and output feedback linear $\mathcal{W}_\infty$ controllers introduced in Chapter 6 are synthesized to solve the trajectory tracking problem of the convertible Tilt-rotor UAV operating in the helicopter flight mode. The Von Kármán wind turbulence model used to emulate the environment wind and considered as disturbance model in the linear control design. In addition, a nonlinear $\mathcal{W}_\infty$ controller is designed to solve the full flight envelope trajectory tracking problem of the convertible Tilt-rotor UAV. Numerical experiments are conducted in a high fidelity simulator to corroborate the controllers' efficiency.

- **Chapter** 8 concludes the work and presents the final considerations.

2

Literature Review

This chapter presents a literature review on the main topics of interest of this doctoral thesis. It is concerned with the following topics: (i) the $\mathcal{H}_2$ and $\mathcal{H}_\infty$ control frameworks; (ii) Sobolev spaces and their applications in control theory; and (iii) approximate solutions to the HJ equation.

2.1 The $\mathcal{H}_2$ and $\mathcal{H}_\infty$ control frameworks

As commented previously, the classic $\mathcal{H}_2$ and $\mathcal{H}_\infty$ (Van Der Schaft, 1992) control strategies intrinsically provide disturbance attenuation to the closed-loop system. These control strategies were originally formulated based on the frequency domain to cope with single-input-single-output (SISO) systems represented by transfer functions (Doyle et al., 2013). In this domain, the $\mathcal{H}_2$ controller seeks to minimize the energy of the disturbance impulse response (Geromel et al., 1999), while the $\mathcal{H}_\infty$ controller minimizes the maximum gain given by the closed-loop system to a disturbance signal (Francis and Doyle, 1987).

The necessity of dealing with multiple-input-multiple-output (MIMO) systems required the extension of the $\mathcal{H}_2$ and $\mathcal{H}_\infty$ control strategies to systems represented in the state-space, which were first introduced in Doyle et al. (1989). These strategies received considerable attention in the past decades as the initial point to the development of $\mathcal{H}_\infty$ controllers based on a convex optimization problem with Linear Matrix Inequalities (LMIs) constraints (Gahinet and Apkarian, 1994; Hu et al., 2003). Still regarding systems represented in the state-space, the multi-objective linear mixed $\mathcal{H}_2/\mathcal{H}_\infty$ controller

(Khargonekar and Rotea, 1991) was formulated to aggregate an $\mathcal{H}_2$ performance to the $\mathcal{H}_\infty$ control strategy.

Concerning the nonlinear $\mathcal{H}_\infty$ control, it was first introduced in Van der Schaft (1991). In this case, the control problem is formulated based on the $\mathcal{L}_2$-space using the theory of dissipative systems (Willems, 2007). For the $\mathcal{H}_2$ control, Dullerud and Paganini (2013) (p. 191) demonstrated that building the optimizing index based on the $\mathcal{H}_2$-norm of the output variable gives us a direct measure of the energy of the system's outputs. Therefore, one that selects the disturbances equal to a impulse signal, and considers the initial conditions equal to zero, will conclude that the nonlinear $\mathcal{H}_2$ control is a generalization of the Linear Quadratic Regulator (LQR) controller.

In the literature, the optimization problems resulting from the formulation of the nonlinear $\mathcal{H}_2$ and $\mathcal{H}_\infty$ controllers are commonly developed via dynamic-programming resulting in a Hamilton-Jacobi (HJ) equation to be solved. HJ Partial Differential Equations (PDEs) are hard to solve analytically for the general class of systems. Therefore, to simplify the process of achieving the controller, it is usual to compute either a solution using numerical algorithms or to particularize the control problem to a special class of systems. Concerning the former, in Section 2.3 a literature review about approximate solutions to the HJ equation is presented. Regarding the latter, this work is interested in the particular class of mechanical systems represented by the Euler-Lagrange equations.

When dealing with the nonlinear $\mathcal{H}_2$ and $\mathcal{H}_\infty$ control design for mechanical systems, a pioneering work is Johansson (1990). In that work, the nonlinear $\mathcal{H}_2$ control strategy is designed for the special class of fully-actuated mechanical systems represented by Euler-Lagrange equations, with a particular solution being proposed to the HJ PDE related to the problem. Based on this solution and using the same tracking error model, Chen et al. (1994) formulate the nonlinear $\mathcal{H}_\infty$ control strategy for the same class of systems. In the same year, Feng and Postlethwaite (1993) propose a similar approach for robotic systems, where the cost variable considers the coupling between the controlled variables and the control inputs, giving more degrees of freedom to the control design.

From these initial approaches for mechanical systems, several works have been proposed. Chen et al. (1996) present a procedure to develop an $\mathcal{H}_\infty$ controller aiming to achieve robust tracking of perturbed nonholonomic mechanical systems. Aguilar et al. (2003) extend the $\mathcal{H}_\infty$ approach for nonsmooth time-varying mechanical systems with friction. Ortega et al. (2005) enhance the nonlinear $\mathcal{H}_\infty$ control strategy with an integral action on the error vector and establish conditions to formulate the controller in the form of a nonlinear PID. A survey about robust control of robot manipulators, with a brief overview of nonlinear $\mathcal{H}_\infty$ control, is presented in Sage et al. (1999).

Concerning underactuated mechanical systems, the design of nonlinear $\mathcal{H}_2$ and $\mathcal{H}_\infty$ controllers often explore the characteristic of mechanical systems. In Siqueira and Terra (2004) and Siqueira et al. (2006), for example, the nonlinear $\mathcal{H}_\infty$ controller is developed

considering underactuated manipulators. These works explore the passive-active properties of mechanical systems. The active degrees of freedom are defined as the ones that are actuated directly by the control inputs, while the passive ones are unactuated. The control design is conducted considering the dynamic coupling between the passive and active degrees of freedom and it is assumed that the passive joints are equipped with brakes. The strategy consists in controlling all the passive joints in order to reach their desired position by applying torques in the active ones, and then turn the brakes on. After that, all the active joints are controlled as if the manipulator was fully actuated. Also, in Raffo et al. (2011b) the passive-active property of mechanical systems is again explored aiming to design a cascade controller for a quadrotor UAV. In that work, a nonlinear $\mathcal{H}_\infty$ controller is designed to control the active degrees of freedom, while a model predictive controller (MPC) is used to generate references for the active degrees of freedom to guide the passive ones throughout the desired trajectory.

Moreover, in Raffo et al. (2011a), a nonlinear $\mathcal{H}_\infty$ control strategy is proposed to deal with the class of underactuated mechanical systems with input coupling (Olfati-Saber, 2001). In that work, the dynamics of the system are partitioned in controlled and stabilized degrees of freedom, from which the controller is designed to perform trajectory tracking of the controlled degrees of freedom, while the remaining ones are stabilized. The efficiency of the control strategy is corroborated by numerical experiments conducted with a quadrotor UAV. In order to provide input coupling to the dynamics of the system, the authors propose a modification on the mechanical structure of the quadrotor UAV by tilting the thrusters with a small inclination angle towards the geometric center of the aircraft. This small inclination guarantees full controllability to the quadrotor UAV. In Raffo et al. (2015), a similar approach is employed to design a nonlinear $\mathcal{H}_\infty$ controller for a two-wheeled self-balanced vehicle. The objective is to ensure the inclination angle of the pendulum (controlled degrees of freedom) is led to the upper vertical position, while the angular velocity of the wheels (time derivative of the remaining degrees of freedom) is set in a desired reference value.

The nonlinear $\mathcal{H}_2$ and $\mathcal{H}_\infty$ control strategies have been applied successfully to mechanical systems in several experiments. Nevertheless, these methods may present significant drawbacks. As stated in Chen et al. (1994); Raffo et al. (2011a), the standard formulation of the nonlinear $\mathcal{H}_\infty$ control and, consequently, of the nonlinear $\mathcal{H}_2$ control for Euler-Lagrange mechanical systems presents a limitation in the way to weight the cost variable. For its appropriate formulation, the weighting matrices must be considered like positive real scalars multiplied by the identity matrix, limiting the adjustment of the control law for systems with multiple degrees of freedom with different dynamics, such as the tilt-rotor UAV. Secondly, as stated in Chilali and Gahinet (1996), the $\mathcal{H}_\infty$ control strategy deals mostly with the aspect of the highest gain of the disturbances, and provides little control over the transient behavior of the system. Regarding the first drawback, in Raffo

(2011) an approach based on diagonalization of the inertia matrix is proposed in order to give flexibility to tune the nonlinear $\mathcal{H}_\infty$ controller. On the other hand, few works deal with the second drawback for control designing of nonlinear systems.

A singular paper that proposes the reformulation of the nonlinear $\mathcal{H}_2$ and $\mathcal{H}_\infty$ control approaches by making use of signals in the Sobolev space to improve the transient performance of the nonlinear $\mathcal{H}_2$ and $\mathcal{H}_\infty$ controllers is Aliyu and Boukas (2011a). A literature review about the Sobolev space and its application in control theory is presented in the next section.

2.2 Sobolev spaces and applications in control theory

The Sobolev spaces $\mathcal{W}_{m,p}$ and the weighted Sobolev spaces $\mathcal{W}_{m,p,\sigma}$ are normed vector spaces. They are composed of functions in $\mathcal{L}_p$ whose generalized derivatives up to order m are also in $\mathcal{L}_p$ (Adams and Fournier, 2003; Dlotko, 2014; Maz'ya, 2013; Treves, 2016; Kufner, 1985; Goldshtein and Ukhlov, 2009). These spaces have been widely used in the field of partial differential equations. For example, Pavel (2013) considers the global classical solvability of a mixed initial-boundary value problem for semilinear hyperbolic systems with nonlinear reaction coupling of Lotka-Volterra type. He develops mathematical results in Sobolev spaces that can be used as the basis for developing further boundary control results for this type of system. González De Paz (2009) presents a variational principle for several free boundary value problems using a relaxation approach. The equivalence of the solution of the relaxed problem with the solution of several free boundary value problem is proved. Some inequality properties of the weighted Sobolev spaces are discussed in Kilpeläinen (1994).

In the control area, properties of Sobolev spaces have been employed in the design of state observers. In Alessandri and Sanguineti (2007), the optimal estimation problems for nonlinear systems are considered, in which the Luenberger observer is used as case of study. The optimality criterion is taken as the norm of the estimation error in a function space and is dependent on a chosen innovation function. In particular, $\mathcal{L}_p$ and Sobolev optimality criteria are adopted. Relationships between internal (asymptotic and exponential) stability and input-output stability are studied, and upper bounds on the estimation error are given. Zemouche and Boutayeb (2008) deal with an unknown input observer design method for nonlinear systems. The proposed method takes into account the presence of disturbances in both equations of states and output. The main result lies in the use of Sobolev norms to define a new criterion of robustness, called the modified $\mathcal{H}_\infty$ criterion. Contrarily to the standard $\mathcal{H}_\infty$ filtering method (Simon, 2006), the modified $\mathcal{H}_\infty$ criterion offers the possibility to solve the unknown input observer synthesis problem in a noisy context. Aliyu and Boukas (2011b) propose the $\mathcal{W}_{1,2}$ and $\mathcal{W}_{1,\infty}$ estimation problems as an extension of the $\mathcal{H}_2$ and $\mathcal{H}_\infty$ optimization problems. Proportional, proportional-derivative,

and proportional-integral (PI) filters are presented for each problem, and sufficient conditions for the existence of optimal filter gains in terms of new HJB and HJBI equations are provided.

Also, in Bourles and Colledani (1995), a new type of input-output stability is defined based on the use of Sobolev space $\mathcal{W}_{m,p}$, with a local version of the small gain theorem being established in this framework and the relationship between $\mathcal{W}$-stability and asymptotic stability being presented. In He and Wang (2004), the $\mathcal{W}$-stability criterion is extended for a class of nonlinear systems with nonlinear finite time-delay. The idea behind these works relies on the fact that in this kind of space all properties of $\mathcal{L}_2$ space are satisfied. Additionally, Guillard and Bourlès (2000) propose a robust feedback linearization that transform the original nonlinear system into its linear approximation around a given operation point. In this work, the idea of $\mathcal{W}$-stability is employed to prove the improvements of the robust feedback linearization.

Furthermore, seeking to overcome the drawbacks of the nonlinear $\mathcal{H}_2$ and $\mathcal{H}_\infty$ control approaches mentioned in Section 2.1, Aliyu and Boukas (2011a) redesign these control strategies in the Sobolev space. In their work, instead of the $\mathcal{L}_2$-norm, the $\mathcal{W}_{1,2}$-norm of the cost variable is considered. The control problems are developed via dynamic-programming from which the HJ PDE might be solved. In particular, Aliyu and Boukas (2011a) consider the HJ PDE resulting from the redesign of the nonlinear $\mathcal{H}_\infty$ control approach in the Sobolev space to be "horrendous and impossible to compute the solution", proposing an alternative approach using the backstepping technique to simplify the problem. However, since the rate of change of the cost variable is not considered in the cost functional, the improvements on the transient performance are not achieved. Additionally, the approaches addressed in Aliyu and Boukas (2011a) lack in the sense of distinguishing the influences of the cost variable and its time derivatives in the control objectives.

To overcome the drawbacks of the approaches proposed by Aliyu and Boukas (2011a), this thesis formulates the nonlinear $\mathcal{H}_2$ and $\mathcal{H}_\infty$ control approaches in the weighted Sobolev space, which allows tuning component-wise the influences of the cost variable and its time derivative in the cost functional. The control problems are developed via dynamic-programming and numerical algorithms are proposed to attain solutions of the resulting HJ PDEs. In addition, the $\mathcal{W}_2$ and $\mathcal{W}_\infty$ control problems are particularized to the class of mechanical systems represented by the Euler-Lagrange equations, and particular solutions are proposed to the resulting HJ PDEs. The linear version of the $\mathcal{W}_\infty$ controller is also formulated via semidefinite programming written as LMI constraints, for which a series of numerical algorithms can be used to achieve a solution.

2.3 Approximate solutions to the HJ equation

Since HJ PDEs are difficult to solve analytically, several methods have been proposed to approximate solutions. The Taylor series expansion was the first one used with this purpose (Lukes, 1969), which was also used by Van Der Schaft (1992) to achieve approximate solutions to the HJ PDE resulting from the nonlinear $\mathcal{H}_\infty$ control approach. Based on this approach, optimal controllers have been designed for several systems, as for instance: fixed-wing aircrafts (Kang et al., 1992), robot manipulators (Yazdanpanah et al., 1998), jet engine compressors (Hardt et al., 2000), magnetic levitator (Sinha and Pechev, 2004), among others. A systematic procedure to obtain an approximate solution of the HJ PDE via Taylor series expansion is presented in Huang and Lin (1995). Although the approach via Taylor series expansion is attractive from the computational effort point of view, the solution is usually obtained considering a finite number of terms, not ensuring stability to nonlinear systems. Besides, the difficulty to attain a solution increases with respect to the degree of the considered term. In this context, Yazdanpanah et al. (1999) present studies to determine the stability region of the solution obtained via Taylor series expansion truncated in low order terms.

Other usual approaches to solve the HJ PDEs are the method of characteristics (Wise and Sedwick, 1996), finite differences (Fleming and Soner, 2006; Wise and Sedwick, 1994), and finite elements (Xiao and Basar, 1997). The first one tries to find an open-loop solution by integrating the problem forward considering a given initial condition, while the latter consist in obtaining viscosity solutions to the problem. Additionally, Lu and Doyle (1995) and Patpong et al. (1996) characterize the nonlinear $\mathcal{H}_\infty$ control problem as a convex optimization problem and present solutions in terms of nonlinear matrix inequalities. In these methods, the computational effort and memory used to achieve the solution increase exponentially with respect to the states of the system. Approaches based on neural networks have recently received great attention due to the computational efficiency (Vamvoudakis and Lewis, 2010; Zhu and Zhao, 2018; Walters et al., 2018; Xiao et al., 2018).

According to Beard and McLain (1998), the main features to be considered in order to select the numerical procedure are: i) guaranteed stability for finite truncations of the approximation; ii) a simple closed-loop control to be implemented; iii) to guarantee the approximation error goes to zero as the order of the approximation increases; iv) a well-defined region of the state-space where the approximation is guaranteed to work; v) low run-time computation and memory requirements; vi) to effectively deal with the curse of dimensionality. Regarding these features, the Successive Galerkin Approximation Algorithm (SGAA) is among the most interesting numerical procedures, mainly due to the guarantee of stability, which is crucial from the control point of view (Beard, 1995; Beard et al., 1996, 1997; Beard and McLain, 1998; Beard et al., 1998).

SGAA was first introduced in Beard (1995), with the purpose of solving the HJB equation resulting from the development of the nonlinear $\mathcal{H}_2$ control approach via dynamic-programming. Thereafter, in Beard and McLain (1998), it was extended to solve the HJBI equation that arises from the formulation of the nonlinear $\mathcal{H}_\infty$ controller via game theory. SGAA is applicable to a general class of autonomous systems and consists to performing Sucessive Galerkin approximations in order to approximate the solution of the HJ PDE, but with the shortcomings of depending on a chosen initial stabilizing control law. Besides, it requires the calculation of $\mathcal{L}_2$ inner products, which can be significantly time-intensive for higher dimensional systems.

Regarding the Galerkin method, the literature also presents a few works that employ it to solve HJ equations. In Curtis and Beard (2001), for example, a successive collocation approximation algorithm (SCAA) is proposed to solve the HJ equation. Instead of seeking for an approximation to the HJ PDE in a domain, like SGAA, a local approximation is obtained via Galerkin method by solving the HJ equation at a local point of the state space. This approximation does not require the use of inner product, which reduce considerably the computational effort to attain the solution. Also, Wernrud and Rantzer (2005) replace the HJ equation by two inequalities, with the optimal problem replaced by a suboptimal problem in order to simplify computations. In Cheng and Wang (2014) and Cheng and Shu (2007), the Galerkin method is employed to solve the HJ PDE considering one-dimensional and two-dimensional problems.

To the best of the author's knowledge, there are no works in the literature that propose numerical methods to achieve the solution to the HJ PDEs resulting from the formulation of the nonlinear $\mathcal{H}_2$ and $\mathcal{H}_\infty$ controllers in weighted Sobolev spaces. Therefore, this work extends the SGAA to achieve such solutions for the corresponding HJ PDEs.

2.4 Final Remarks

This chapter presented a literature review on the main topics of interest in this doctoral thesis.

Section 2.1 concerned with the state of the art of the $\mathcal{H}_2$ and $\mathcal{H}_\infty$ controllers, and addressed some relevant works that were taken as theoretical basis to the development of this doctoral thesis. It exposed the disadvantage of $\mathcal{H}_2$ and $\mathcal{H}_\infty$ controllers in providing little control over the transient behavior of the system, which motivated the development of the $\mathcal{W}_2$ and $\mathcal{W}_\infty$ control frameworks in weighted Sobolev spaces.

Section 2.2 addressed some relevant works related to Sobolev spaces and their applications in control theory, including the work by Aliyu and Boukas (2011a), which introduced the redesign of the $\mathcal{H}_2$ and $\mathcal{H}_\infty$ controllers in a Sobolev space. It was commented that the approaches introduced in Aliyu and Boukas (2011a) lacked in the sense of distinguishing the influences of the cost variable and its time derivatives in the control objective, and

resulted in HJ PDEs that were hard to solve algebraically.

Finally, Section 2.3 addressed a brief review of the literature on the most popular techniques used to obtain numerical solutions for HJ equations, including the Successive Galerkin Approximation Algorithm, which is extended in this doctoral thesis to achieve solutions of the $\mathcal{W}_2$ and $\mathcal{W}_\infty$ control problems.

The next chapter presents some basic concepts and definitions used in this doctoral thesis.

3

Mathematical background

This chapter presents some preliminary concepts and definitions necessary to the development of this doctoral thesis. The following topics are introduced: (i) the Lebesgue and Sobolev spaces; (ii) interesting features of the $\mathcal{W}_2$ and $\mathcal{W}_\infty$ control formulations in the weighted Sobolev space; (iii) the Hamilton-Jacobi-Bellman equation; (iv) the method of Galerkin; and (v) the Euler-Lagrange formulation.

3.1 The Lebesgue and Sobolev spaces

This section is concerned with the definitions of the Lebesgue, Sobolev, and weighted Sobolev spaces. The latter is used to formulate the nonlinear $\mathcal{W}_2$ and $\mathcal{W}_\infty$ control strategies proposed in this work. For further details, we refer the readers to Adams and Fournier (2003); Dlotko (2014); Maz'ya (2013); Treves (2016); Kufner (1985); Goldshtein and Ukhlov (2009).

As commented, the nonlinear $\mathcal{H}_2$ and $\mathcal{H}_\infty$ control strategies can be formulated in the Lebesgue space making use of the $\mathcal{L}_p-$norm. The $\mathcal{L}_p-$norm of a function $\boldsymbol{z}(t) : \mathbb{R}_{\geq 0} \to \mathbb{R}^{n_z}$, in which $t \in \mathbb{R}_{\geq 0}$ is the time variable, is computed by

$$||\boldsymbol{z}(t)||_{\mathcal{L}_p} \triangleq \left(\int_0^\infty \sum_{j=1}^{n_z} |\boldsymbol{z}_j(t)|^p dt \right)^{\frac{1}{p}}, \tag{3.1}$$

for $p \in \mathbb{N} \cup \{\infty\}$, where $\boldsymbol{z}_j(t)$ stands for the j-th element of the vector $\boldsymbol{z}(t)$.

Remark 1. *Regarding (3.1), one can show that* $||\boldsymbol{z}(t)||_{\mathcal{L}_2}^2 = \int_0^\infty \boldsymbol{z}'(t)\boldsymbol{z}(t)dt$ *and* $||\boldsymbol{z}(t)||_{\mathcal{L}_\infty} = \inf\{a \geq 0 : |\boldsymbol{z}_j(t)| \leq a, \forall t \in \mathbb{R}_{\geq 0}, j \in \{1, ..., n_z\}\}$.

The $\mathcal{L}_p$ space is composed of functions whose $\mathcal{L}_p$ – norm is bounded and is defined as follows.

Definition 1. *(Adapted from van der Schaft (2000)) A function* $\boldsymbol{z}(t) : \mathbb{R}_{\geq 0} \to \mathbb{R}^{n_z}$, *for some* $n_z \in \mathbb{N}$, *belongs to the* $\mathcal{L}_p$ *space (i.e.* $\boldsymbol{z}(t) \in \mathcal{L}_p[0, \infty)$*) if and only if* $||\boldsymbol{z}(t)||_{\mathcal{L}_p} < \infty$.

The weighted $\mathcal{L}_{p,\boldsymbol{\varphi}}$-norm of the function $\boldsymbol{z}(t)$ is computed as (Nielsen, 2012)

$$||\boldsymbol{z}(t)||_{\mathcal{L}_{p,\boldsymbol{\varphi}}} \triangleq \left(\int_0^\infty ||\boldsymbol{\varphi}^{1/p}\boldsymbol{z}(t)||_p^p \, dt \right)^{1/p}, \tag{3.2}$$

for $p \in \mathbb{N} \cup \{\infty\}$, where $\boldsymbol{\varphi}$ is a symmetric matrix with appropriate dimension, in which $|\boldsymbol{\varphi}_{ij}| < \infty$, $\forall i, j \in \{1, ..., n_z\}$, and $||\boldsymbol{\varphi}^{1/p}\boldsymbol{z}(t)||_p \triangleq (\sum_{i=1}^{n_z} |\left(\boldsymbol{\varphi}^{1/p}\boldsymbol{z}(t)\right)_i|^p)^{1/p}$, in which $\left(\boldsymbol{\varphi}^{1/p}\boldsymbol{z}(t)\right)_i$ stands for the i-th element of the vector resulting from the product $\boldsymbol{\varphi}^{1/p}\boldsymbol{z}(t)$. Accordingly, the $\mathcal{L}_p$ space is a subspace of the weighted $\mathcal{L}_p$ space, which is defined as follows.

Definition 2. *A function* $\boldsymbol{z}(t) : \mathbb{R}_{\geq 0} \to \mathbb{R}^{n_z}$, *for some* $n_z \in \mathbb{N}$, *belongs to the weighted* $\mathcal{L}_{p,\boldsymbol{\varphi}}$ *space (i.e.* $\boldsymbol{z}(t) \in \mathcal{L}_{p,\boldsymbol{\varphi}}[0, \infty)$*) if and only if* $||\boldsymbol{z}(t)||_{\mathcal{L}_{p,\boldsymbol{\varphi}}} < \infty$.

The formulation of the $\mathcal{H}_2$ and $\mathcal{H}_\infty$ control approaches in the time-domain into the Sobolev space is based on the Sobolev $\mathcal{W}_{m,p}-$norm of functions. The Sobolev $\mathcal{W}_{m,p}-$norm of a function $\boldsymbol{z}(t)$ is computed as

$$||\boldsymbol{z}(t)||_{\mathcal{W}_{m,p}} \triangleq \left(\sum_{\alpha=0}^{m} \left|\left| \frac{d^\alpha \boldsymbol{z}(t)}{dt^\alpha} \right|\right|_{\mathcal{L}_p}^p \right)^{\frac{1}{p}}, \tag{3.3}$$

where $p \in \mathbb{N} \cup \{\infty\}$ and $m \in \mathbb{N}$.

It is worth highlighting that (3.3) takes into account the $\mathcal{L}_p-$norm of the function $\boldsymbol{z}(t)$ and of its time derivatives. Consequently, the $\mathcal{W}_{m,p}$ space is a subspace of the $\mathcal{L}_p$ space that is composed of functions whose generalized derivatives up to degree m are also in the $\mathcal{L}_p$ space. The $\mathcal{W}_{m,p}$ space is defined as follows:

Definition 3. *A generic function* $\boldsymbol{z}(t) : \mathbb{R}_{\geq 0} \to \mathbb{R}^{n_z}$, *for some* $n_z \in \mathbb{N}$, *belongs to the* $\mathcal{W}_{m,p}$ *space (i.e.* $\boldsymbol{z}(t) \in \mathcal{W}_{m,p}[0, \infty)$*) if and only if* $||\boldsymbol{z}(t)||_{\mathcal{W}_{m,p}} < \infty$.

The $\mathcal{W}_2$ and $\mathcal{W}_\infty$ controllers proposed in this doctoral thesis are formulated on the weighted Sobolev space, they require the satisfaction of the weighted Sobolev $\mathcal{W}_{m,p,\boldsymbol{\sigma}}-$norm of the function $\boldsymbol{z}(t)$, that is given by

$$||\boldsymbol{z}(t)||_{\mathcal{W}_{m,p,\boldsymbol{\sigma}}} = \left(\sum_{\alpha=0}^{m} \left|\left| \frac{d^\alpha \boldsymbol{z}(t)}{dt^\alpha} \right|\right|_{\mathcal{L}_{p,\boldsymbol{\sigma}\alpha}}^p \right)^{\frac{1}{p}}, \tag{3.4}$$

where $\boldsymbol{\sigma} = (\boldsymbol{\sigma}_0, ..., \boldsymbol{\sigma}_m)$ is a set of positive definite matrices with appropriate dimension and $||(\cdot)||_{\mathcal{L}_{p,\boldsymbol{\sigma}_\alpha}}$ stands for the $\mathcal{L}_p$ – norm of function $(\cdot)$ weighted by the matrix $\boldsymbol{\sigma}_\alpha$, for $\alpha \in \{0, 1, ..., m\}$.

Remark 2. *Regarding (3.4), it is of special interest of this work the case* $||\boldsymbol{z}(t)||^2_{\mathcal{W}_{m,2,\boldsymbol{\sigma}}} = ||\boldsymbol{z}(t)||_{\mathcal{L}_{2,\boldsymbol{\sigma}_0}} + \cdots + \left|\left|\frac{d^m \boldsymbol{z}(t)}{dt^m}\right|\right|_{\mathcal{L}_{2,\boldsymbol{\sigma}_m}} = \int_0^\infty \boldsymbol{z}'(t)\boldsymbol{\sigma}_0\boldsymbol{z}(t)dt + \cdots + \int_0^\infty \left(\frac{d^m \boldsymbol{z}(t)}{dt^m}\right)' \boldsymbol{\sigma}_m \frac{d^m \boldsymbol{z}(t)}{dt^m} dt$, *which is used to formulate the proposed* $\mathcal{W}_2$ *and* $\mathcal{W}_\infty$ *controllers in the next chapters.*

Then, the $\mathcal{W}_{m,p,\boldsymbol{\sigma}}$ space is defined as follows:

Definition 4. *A generic function* $\boldsymbol{z}(t) : \mathbb{R}_{\geq 0} \to \mathbb{R}^{n_z}$, *for some* $n_z \in \mathbb{N}$, *belongs to the* $\mathcal{W}_{m,p,\boldsymbol{\sigma}}$ *space (i.e.* $\boldsymbol{z}(t) \in \mathcal{W}_{m,p,\boldsymbol{\sigma}}[0, \infty)$*) if and only if* $||\boldsymbol{z}(t)||_{\mathcal{W}_{m,p,\boldsymbol{\sigma}}} < \infty$.

Since it is a weighted space, one can show that any function that belongs to this space also belongs to the Sobolev space. Besides, the $\mathcal{W}_{m,p}$-norm is a particular case of the $\mathcal{W}_{m,p,\boldsymbol{\sigma}}$-norm, in which $\boldsymbol{\sigma}_\alpha = \boldsymbol{I}$, for $\alpha \in \{0, 1, ..., m\}$.

3.2 Interesting features of the $\mathcal{W}_2$ and $\mathcal{W}_\infty$ control formulations in weighted Sobolev spaces

This section highlights some interesting features of $\mathcal{W}_2$ and $\mathcal{W}_\infty$ control formulation in weighted Sobolev space.

Consider the following linear system represented in state-space

$$\mathcal{P} : \begin{cases} \dot{\boldsymbol{x}}(t) = \boldsymbol{A}\boldsymbol{x}(t) + \boldsymbol{B}_\tau \boldsymbol{\tau}(t) + \boldsymbol{B}_w \boldsymbol{w}(t), \\ \boldsymbol{h}(t) = \boldsymbol{Q}\boldsymbol{x}(t) + \boldsymbol{R}\boldsymbol{\tau}(t), \end{cases} \tag{3.5}$$

where $\boldsymbol{x}(t) : \mathbb{R}_{\geq 0} \to \mathbb{R}^{n_x}$ is the state vector, $\boldsymbol{\tau}(t) : \mathbb{R}_{\geq 0} \to \mathbb{R}^{n_\tau}$ is the input vector, $\boldsymbol{w}(t) : \mathbb{R}_{\geq 0} \to \mathbb{R}^{n_w}$ is the disturbance vector, $\boldsymbol{h}(t) : \mathbb{R}_{\geq 0} \to \mathbb{R}^{n_x}$ is the output vector, $\boldsymbol{A} \in \mathbb{R}^{n_x \times n_x}$, $\boldsymbol{B}_\tau \in \mathbb{R}^{n_x \times n_\tau}$, and $\boldsymbol{B}_w \in \mathbb{R}^{n_x \times n_w}$ are matrices with appropriate dimensions that give the dynamics of the linear system, and $\boldsymbol{Q} > 0$ and $\boldsymbol{R} > 0$ are weighting matrices.

Regarding (3.5), the classic $\mathcal{H}_2$ control strategy is formulated in the frequency domain in order to find a control law that minimizes the energy of the output vector $\boldsymbol{h}(t)$ when the system is subjected to an impulsive disturbance $\boldsymbol{w}(t)$. In this domain, the $\mathcal{H}_2$ control problem can be stated as the following optimization problem (Dullerud and Paganini, 2013):

$$\min_{\tau \in \mathbb{C}} \frac{1}{2\pi} \int_{-\infty}^{\infty} \text{trace}\left[\boldsymbol{H}^*(j\omega)\boldsymbol{H}(j\omega)\right] d\omega, \tag{3.6}$$

where $\boldsymbol{H}(j\omega)$ is the transfer function of $\mathcal{P}$ from $\boldsymbol{w}(t)$ to $\boldsymbol{h}(t)$.

This work is interested in the formulation of the $\mathcal{H}_2$ controller in the time-domain. Therefore, making use of Parseval's Theorem, and assuming $\boldsymbol{w}(t) \in \mathcal{L}_2[0,\infty)$, the optimization problem (3.6) can be written as (Trofino et al., 2003)

$$\begin{aligned} &\min_{\boldsymbol{\tau}\in\mathcal{L}_2} \int_0^\infty \operatorname{trace}\left[\boldsymbol{h}'(t)\boldsymbol{h}(t)\right] dt, \\ &s.t. \quad \mathcal{P}. \end{aligned} \tag{3.7}$$

In addition, Khalaf et al. (2006) have demonstrated that if we let $\boldsymbol{x}(0) = \boldsymbol{0}$, $\boldsymbol{h}(t) = \bar{\boldsymbol{W}}\begin{bmatrix}\boldsymbol{x}(t)\\ \boldsymbol{\tau}(t)\end{bmatrix}$, with $\bar{\boldsymbol{W}} \triangleq \begin{bmatrix}\boldsymbol{Q} & 0\\ 0 & \boldsymbol{R}\end{bmatrix}$, and $\boldsymbol{w}(t) = \boldsymbol{\delta}(t)$, in which $\boldsymbol{\delta}(t)$ is a vector with appropriate dimension composed of delta Dirac functions, the classic $\mathcal{H}_2$ control problem can be equivalently posed for $\mathcal{P}$ as

$$\begin{aligned} &\min_{\tau(t)\in\mathcal{L}_2} \frac{1}{2}||\boldsymbol{h}(t)||^2_{\mathcal{L}_2}, \\ &s.t. \quad \mathcal{P}, \end{aligned} \tag{3.8}$$

which is the so-called formulation of the $\mathcal{H}_2$ controller in the Lebesgue space.

Remark 3. *In $\mathcal{H}_2$ control problem (3.8) the output vector is required to belong to the $\mathcal{L}_2$ space, i.e. $\boldsymbol{h}(t) \in \mathcal{L}_2[0,\infty)$, but there are no requirements for its rate of change. The rate of change is tuned indirectly by weighting the energy of the states and control action in the cost functional.*

Note that, the control problem (3.8) can be employed, for example, to synthesize a $\mathcal{H}_2$ controller for the nonlinear system

$$\mathcal{Y}: \begin{cases} \dot{\boldsymbol{x}}(t) = \boldsymbol{f}(\boldsymbol{x}(t),t) + \boldsymbol{g}(\boldsymbol{x}(t),t)\boldsymbol{\tau}(t) + \boldsymbol{k}(\boldsymbol{x}(t),t)\boldsymbol{w}(t), \\ \boldsymbol{h}(t) = \bar{\boldsymbol{W}}\begin{bmatrix}\boldsymbol{x}(t)\\ \boldsymbol{\tau}(t)\end{bmatrix}, \end{cases} \tag{3.9}$$

where $\boldsymbol{x}(t)$, $\boldsymbol{\tau}(t)$, $\boldsymbol{w}(t)$, and $\boldsymbol{h}(t)$ are defined as in (3.5), and $\boldsymbol{f}(\boldsymbol{x}(t),t)$, $\boldsymbol{g}(\boldsymbol{x}(t),t)$, and $\boldsymbol{k}(\boldsymbol{x}(t),t)$, with $\boldsymbol{f}(0,t) = 0$, are matrices with appropriate dimension that represent the dynamics of the nonlinear system.

This doctoral thesis extends the $\mathcal{H}_2$ control problem (3.8) to the weighted Sobolev space $\mathcal{W}_{1,2,\boldsymbol{\sigma}}$. In this space, the control problem is posed as

$$\begin{aligned} &\min_{\tau(t)\in\mathbb{U}} \frac{1}{2}||\boldsymbol{z}(t)||^2_{\mathcal{W}_{1,2,\boldsymbol{\sigma}}}, \\ &s.t. \quad \mathcal{Y}, \end{aligned} \tag{3.10}$$

where $\mathbb{U}: \mathbb{R}_{\geq 0} \to \mathbb{R}^{n_\tau}$, with the output variable given by $\boldsymbol{z}(t) = \boldsymbol{x}(t)$, and $\boldsymbol{\sigma} = (\boldsymbol{\sigma}_0, \boldsymbol{\sigma}_1)$, in which $\boldsymbol{\sigma}_0, \boldsymbol{\sigma}_1$ are weighting matrices.

Remark 4. *The $\mathcal{H}_2$ control approach in the Sobolev space proposed by Aliyu and Boukas (2011a) is a particular case of (3.10), in which the control problem is posed regarding the Sobolev norm $\mathcal{W}_{1,2}$ of the output variable.*

Remark 5. *The optimal control problem (3.10) weights component-wise the output vector and its rate of change in the optimizing index. Therefore, the resulting controller tends to generate less oscillating behavior, in addition to provide a faster response to disturbances, in comparison to the classic $\mathcal{H}_2$ controller.*

Note that, in the $\mathcal{H}_2$ control problem (3.8) the cost functional can be expanded as

$$\begin{aligned}\mathcal{J}_{\mathcal{L}} &= \frac{1}{2}||\boldsymbol{h}(t)||^2_{\mathcal{L}_2},\\ &= \frac{1}{2}\int_0^\infty \boldsymbol{h}'(t)\boldsymbol{h}(t)dt,\\ &= \begin{bmatrix}\boldsymbol{x}'(t) & \boldsymbol{u}'(t)\end{bmatrix}\bar{\boldsymbol{W}}'\bar{\boldsymbol{W}}\begin{bmatrix}\boldsymbol{x}(t)\\ \boldsymbol{u}(t)\end{bmatrix},\end{aligned} \tag{3.11}$$

while in the $\mathcal{W}_2$ control problem (3.10) one has that

$$\begin{aligned}\mathcal{J}_{\mathcal{W}} &= \frac{1}{2}||\boldsymbol{z}(t)||^2_{\mathcal{W}_{1,2}},\\ &= \frac{1}{2}||\boldsymbol{z}(t)||^2_{\mathcal{L}_{2,\boldsymbol{\sigma}_0}} + \frac{1}{2}||\dot{\boldsymbol{z}}(t)||^2_{\mathcal{L}_{2,\boldsymbol{\sigma}_1}},\\ &= \begin{bmatrix}\boldsymbol{x}'(t) & \dot{\boldsymbol{x}}'(t)\end{bmatrix}\begin{bmatrix}\boldsymbol{\sigma}_0 & \boldsymbol{0}\\ \boldsymbol{0} & \boldsymbol{\sigma}_1\end{bmatrix}\begin{bmatrix}\boldsymbol{x}(t)\\ \dot{\boldsymbol{x}}(t)\end{bmatrix}.\end{aligned} \tag{3.12}$$

From (3.11) and (3.12), one can see that the $\mathcal{H}_2$ approach requires that $\boldsymbol{x}(t), \boldsymbol{u}(t) \in \mathcal{L}_2[0,\infty)$, while the $\mathcal{W}_2$ approach requires that $\boldsymbol{x}(t), \dot{\boldsymbol{x}}(t) \in \mathcal{L}_2[0,\infty)$. This is an interesting feature of the latter approach, which relaxes the necessity of $\boldsymbol{u}(t) \in \mathcal{L}_2[0,\infty)$ and, consequently, $\lim_{t\to\infty}\boldsymbol{u}(t) = 0$. For example, notice that

$$\begin{aligned}||\dot{\boldsymbol{x}}(t)||_{\mathcal{L}_2} &= ||\boldsymbol{f}(\boldsymbol{x}(t),t) + \boldsymbol{g}(\boldsymbol{x}(t),t)\boldsymbol{\tau}(t) + \boldsymbol{k}(\boldsymbol{x}(t),t)\boldsymbol{w}(t)||_{\mathcal{L}_2},\\ &\neq ||\boldsymbol{f}(\boldsymbol{x}(t),t)||_{\mathcal{L}_2} + ||\boldsymbol{g}(\boldsymbol{x}(t),t)\boldsymbol{\tau}(t)||_{\mathcal{L}_2} + ||\boldsymbol{k}(\boldsymbol{x}(t),t)\boldsymbol{w}(t)||_{\mathcal{L}_2}.\end{aligned} \tag{3.13}$$

This feature allows the design of the $\mathcal{W}_2$ controller for system (3.9) when $\boldsymbol{f}(0,t) \neq 0$, since to keep such system at the origin of the state space the controller must inject energy indefinitely, even when in the steady state, requiring a control signal that is not in $\mathcal{L}_2$ space in order to achieve asymptotic stability.

Remark 6. *The case in which $\boldsymbol{f}(0,t) \neq 0$ in (3.9) is quite common in nonlinear systems, especially for mechanical systems as highlighted in Chapter 5.*

Remark 7. *Regarding the case in which $\boldsymbol{f}(0,t) \neq 0$ in system (3.9), in order to design an $\mathcal{H}_2$ controller it is usual to split $\boldsymbol{f}(x(t),t) = \bar{\boldsymbol{f}}(x(t),t) + \hat{\boldsymbol{f}}(x(t),t)$, with $\bar{\boldsymbol{f}}(0,t) = 0$ and*

$\hat{\boldsymbol{f}}(0,t) \neq 0$, then perform the following change of variables in the control input vector: $\boldsymbol{u}(t) = \hat{\boldsymbol{f}}(x(t),t) + \boldsymbol{v}(t)$. The controller is designed considering the new input vector $\boldsymbol{v}(t)$.

Similarly to the $\mathcal{H}_2$ controller, the classic $\mathcal{H}_\infty$ controller is originally formulated in the frequency domain in order to find a control law that minimizes the maximum ratio between the norm of the performance output signal and the norm of the disturbance signal. Regarding the LTI system (3.5), this control problem can be shown to be equivalent to

$$\min_{\tau \in \mathbb{C}} E\{\boldsymbol{H}(j\omega)\}, \tag{3.14}$$

where $E\{\boldsymbol{H}(j\omega)\}$ denotes the maximum singular value of $\boldsymbol{H}(j\omega)$, in which $\boldsymbol{H}(j\omega)$ is the transfer function of $\mathcal{P}$ from $\boldsymbol{w}(t)$ to $\boldsymbol{h}(t)$.

Alternatively, from the Parseval's theorem we have that

$$||\boldsymbol{z}(t)||^2_{\mathcal{L}_2} = \frac{1}{2\pi}\int_{-\infty}^{\infty} \boldsymbol{Z}'(j\omega)\boldsymbol{Z}(j\omega)d\omega, \tag{3.15}$$

and

$$||\boldsymbol{w}(t)||^2_{\mathcal{L}_2} = \frac{1}{2\pi}\int_{-\infty}^{\infty} \boldsymbol{W}'(j\omega)\boldsymbol{W}(j\omega)d\omega. \tag{3.16}$$

where $\boldsymbol{Z}(j\omega)$ and $\boldsymbol{W}(j\omega)$ are, respectively, the signals $\boldsymbol{z}(t)$ and $\boldsymbol{w}(t)$ represented in the frequency domain. Thereby,

$$\begin{aligned} ||\boldsymbol{z}(t)||^2_{\mathcal{L}_2} &= \frac{1}{2\pi}\int_{-\infty}^{\infty} \boldsymbol{W}'(j\omega)\boldsymbol{H}'(j\omega)\boldsymbol{H}(j\omega)\boldsymbol{W}(j\omega)d\omega, \\ &\leq \sup_{\omega} E\{\boldsymbol{H}(j\omega)\}^2 \frac{1}{2\pi}\int_{-\infty}^{\infty} \boldsymbol{W}'(j\omega)\boldsymbol{W}(j\omega)d\omega, \\ &\leq \sup_{\omega} E\{\boldsymbol{H}(j\omega)\}^2 ||\boldsymbol{w}(t)||^2_{\mathcal{L}_2}, \\ &\leq \gamma^2 ||\boldsymbol{w}(t)||^2_{\mathcal{L}_2}, \end{aligned} \tag{3.17}$$

in which $\gamma = \sup_\omega E\{\boldsymbol{H}(j\omega)\}$ is the $\mathcal{H}_\infty$ attenuation level.

Remark 8. *In (3.17), the $\mathcal{H}_\infty$ attenuation level γ can be seen as the maximum gain in terms of the ratio between performance output and input signal energies that system (3.5) gives to a disturbance signal.*

Accordingly, the $\mathcal{H}_\infty$ controller can be formulated in the time-domain as

$$\begin{aligned} &\min_{\tau \in \mathcal{L}_2} \gamma, \\ &s.t. \quad ||\boldsymbol{h}(t)||^2_{\mathcal{L}_2} - \gamma^2 ||\boldsymbol{w}(t)||^2_{\mathcal{L}_2} \leq 0. \end{aligned} \tag{3.18}$$

The control problem (3.18) is the so-called $\mathcal{H}_\infty$ control formulation in the Lebesgue space. This problem can be employed, for example, to synthesize $\mathcal{H}_\infty$ controllers for nonlinear

systems (3.9).

Remark 9. *In the $\mathcal{H}_\infty$ control problem (3.18), the effects of the disturbances in the transient behavior of the closed-loop system are taken into account indirectly through the energy of the output vector $\boldsymbol{h}(t)$.*

This doctoral thesis extends the $\mathcal{H}_\infty$ control problem (3.18) to the weighted Sobolev space. In this space, the control problem is posed as

$$\begin{aligned} &\min_{\tau(t)\in\mathbb{U}} \gamma, \\ &s.t. \quad \frac{1}{2}||\boldsymbol{z}(t)||^2_{\mathcal{W}_{1,2,\boldsymbol{\sigma}}} - \gamma^2||\boldsymbol{w}(t)||^2_{\mathcal{L}_2} \leq 0, \end{aligned} \tag{3.19}$$

for all $\boldsymbol{w}(t) \in \mathcal{L}_2[0,\infty)$, where γ is the $\mathcal{W}_\infty$ attenuation level. Besides, $\mathbb{U} : \mathbb{R}_{\geq 0} \to \mathbb{R}^{n_\tau}$, $\boldsymbol{z}(t) = \boldsymbol{x}(t)$, and $\boldsymbol{\sigma} = (\boldsymbol{\sigma}_0, \boldsymbol{\sigma}_1)$, in which $\boldsymbol{\sigma}_0, \boldsymbol{\sigma}_1$ are weighting matrices.

Remark 10. *The $\mathcal{H}_\infty$ control approach in the Sobolev space proposed by Aliyu and Boukas (2011a) is a particular case of (3.19), in which the control problem is posed regarding the Sobolev norm $\mathcal{W}_{1,2}$ of the output variable.*

Remark 11. *Remarks 5 also applies to the $\mathcal{W}_\infty$ control problem (3.19).*

Remark 12. *In the control problem (3.19), the $\mathcal{W}_\infty$ attenuation level γ can be seen as the maximum gain in terms of energy that a disturbance signal induces on the output variable and its time derivative.*

Note that, the control problem (3.19) takes into account the cost variables and its time derivative, therefore, the minimization of γ results in controllers that provide faster disturbances attenuation. This is the main feature of the $\mathcal{W}_\infty$ control formulation in the weighted Sobolev space.

In this doctoral thesis, the optimal control problems are developed via dynamic-programming resulting in Hamilton-Jacobi partial differential equations to be solved. The next section presents the mathematical background for such development.

3.3 The Hamilton-Jacobi-Bellman equation

The content of this section was adapted from Kirk (2004).

Consider a nonlinear system

$$\mathcal{P} : \Big\{ \dot{\boldsymbol{x}}(t) = \boldsymbol{a}(\boldsymbol{x}, \boldsymbol{u}, t), \tag{3.20}$$

for which it is desired to design a control law $\boldsymbol{u}(\boldsymbol{x}, t)$ that minimizes the cost functional

$$\mathcal{J} = h(\boldsymbol{x}(t_f), t_f) + \int_{t_0}^{t_f} g(\boldsymbol{x}(\tau), \boldsymbol{u}(\tau), \tau) d\tau \tag{3.21}$$

where $t \in [t_0, t_f]$ is the time variable, $\boldsymbol{x}(t) : \mathbb{R}_{\geq 0} \to \mathbb{R}^{n_x}$ is the state vector, $\boldsymbol{u}(t) : \mathbb{R}_{\geq 0} \to \mathbb{R}^{u}$ is the input vector, and $\boldsymbol{a}(\boldsymbol{x}, \boldsymbol{u}, t) : \mathbb{R}^{n_x} \times \mathbb{R}^{n_u} \times \mathbb{R}_{\geq 0} \to \mathbb{R}^{n_x}$, $g(\boldsymbol{x}, \boldsymbol{u}, t) : \mathbb{R}^{n_x} \times \mathbb{R}^{n_u} \times \mathbb{R}_{\geq 0} \to \mathbb{R}_{\geq 0}$ and $h(\boldsymbol{x}(t_f), t_f) : \mathbb{R}^{n_x} \times \mathbb{R}_{\geq 0} \to \mathbb{R}_{\geq 0}$ are specified functions. This control problem can be stated as

$$\begin{aligned} \mathcal{J}^*(\boldsymbol{x}(t_0), t_0) = \min_{\boldsymbol{u}(t) \in \mathcal{U}} & \left[h(\boldsymbol{x}(t_f), t_f) + \int_{t_0}^{t_f} g(\boldsymbol{x}(\tau), \boldsymbol{u}(\tau), \tau) d\tau \right], \\ & s.t. \quad \mathcal{P}, \end{aligned} \tag{3.22}$$

where $\mathcal{U}$ is a space where the control input signal belongs to.

The fundamentals of dynamic programming relies on Bellman's Principle of Optimality, which can be summarized as follows (Raffo, 2011):

"Given an optimal trajectory between the initial time, t_0, and an intermediate time, t, the optimal trajectory between t_0 and a terminal time $t_f > t$ can be found concatenating the initial optimal trajectory to the computed one between t and t_f for the system starting at $\boldsymbol{x}(t)$ with $\boldsymbol{u}(t)$ at time t, which are the terminal states and control signals of the previous computed trajectory between t_0 and t."

Thus, by applying the Bellman principle of optimality to (3.22), yields

$$\begin{aligned} \mathcal{J}^*(\boldsymbol{x}(t_0), t_0) &= \min_{\boldsymbol{u}(t) \in \mathcal{U}} \left[h(\boldsymbol{x}(t_f), t_f) + \int_{t_0}^{t_0 + \Delta t} g(\boldsymbol{x}(\tau), \boldsymbol{u}(\tau), \tau) d\tau + \int_{t_0 + \Delta t}^{t_f} g(\boldsymbol{x}(\tau), \boldsymbol{u}(\tau), \tau) d\tau \right], \\ &= \min_{\boldsymbol{u}(t) \in \mathcal{U}} \left[\int_{t_0}^{t_0 + \Delta t} g(\boldsymbol{x}(\tau), \boldsymbol{u}(\tau), \tau) d\tau + \mathcal{J}^*(\boldsymbol{x}(t_0 + \Delta t), t_0 + \Delta t) \right], \end{aligned} \tag{3.23}$$

where $\mathcal{J}^*(\boldsymbol{x}(t_0 + \Delta t), t_0 + \Delta t)$ is the minimum cost of the process in the time interval $[t_0 + \Delta t,\ t_f]$, when starting from the initial state $\boldsymbol{x}(t_0 + \Delta t)$.

By assuming that the second partial derivatives of $\mathcal{J}^*(\boldsymbol{x}(t), t)$ exist and are bounded for $t \in [t_0,\ t_f]$, the term $\mathcal{J}^*(\boldsymbol{x}(t_0 + \Delta t), t_0 + \Delta t)$ in (3.23) can be expanded using the Taylor series at a generic point ($\boldsymbol{x}(t)$,t), yielding

$$\begin{aligned} \mathcal{J}^*(\boldsymbol{x}(t), t) = \min_{\boldsymbol{u}(t) \in \mathcal{U}} \Bigg[& \int_{t_0}^{t_0 + \Delta t} g(\boldsymbol{x}(\tau), \boldsymbol{u}(\tau), \tau) d\tau + \mathcal{J}^*(\boldsymbol{x}(t), t) + \frac{\partial \mathcal{J}^*(\boldsymbol{x}(t), t)}{\partial t} \Delta t \\ & + \left(\frac{\partial \mathcal{J}^*(\boldsymbol{x}(t), t)}{\partial \boldsymbol{x}} \right)' (\boldsymbol{x}(t + \Delta t) - \boldsymbol{x}(t)) + \mathcal{O}(\boldsymbol{x}(t), t) \Bigg], \end{aligned} \tag{3.24}$$

where $\mathcal{O}(\boldsymbol{x}(t), t)$ is composed by terms of higher order of the Taylor series expansion. Accordingly, for a small Δt, it is possible to approximate (3.24) by

$$\begin{aligned} \mathcal{J}^*(\boldsymbol{x}(t), t) = \min_{\boldsymbol{u}(t) \in \mathcal{U}} \Bigg[& g(\boldsymbol{x}(t), \boldsymbol{u}(t), t) \Delta t + \mathcal{J}^*(\boldsymbol{x}(t), t) + \frac{\partial \mathcal{J}^*(\boldsymbol{x}(t), t)}{\partial t} \Delta t + \\ & \left(\frac{\partial \mathcal{J}^*(\boldsymbol{x}(t), t)}{\partial \boldsymbol{x}} \right)' \boldsymbol{a}(\boldsymbol{x}, \boldsymbol{u}, t) \Delta t + \mathcal{O}(\boldsymbol{x}, \boldsymbol{u}, t) \Bigg]. \end{aligned} \tag{3.25}$$

In addition, since the terms $\mathcal{J}^*(\boldsymbol{x}(t),t)$ and $\dfrac{\partial \mathcal{J}^*(\boldsymbol{x}(t),t)}{\partial t}\Delta t$ are not influenced directly by the control inputs, they can be removed from the minimization, resulting in

$$\frac{\partial \mathcal{J}^*(\boldsymbol{x}(t),t)}{\partial t}\Delta t + \min_{\boldsymbol{u}(t)\in\mathcal{U}}\left[g(\boldsymbol{x}(t),\boldsymbol{u}(t),t)\Delta t + \left(\frac{\partial \mathcal{J}^*(\boldsymbol{x}(t),t)}{\partial \boldsymbol{x}}\right)' \boldsymbol{a}(\boldsymbol{x},\boldsymbol{u},t)\Delta t + \mathcal{O}(\boldsymbol{x},\boldsymbol{u},t)\right] = 0, \tag{3.26}$$

Then, dividing (3.26) by Δt and taking the limit of the resulting equation as $\Delta t \to 0$, leads to

$$\frac{\partial \mathcal{J}^*(\boldsymbol{x}(t),t)}{\partial t} + \min_{\boldsymbol{u}(t)\in\mathcal{U}}\left[g(\boldsymbol{x}(t),\boldsymbol{u}(t),t) + \left(\frac{\partial \mathcal{J}^*(\boldsymbol{x}(t),t)}{\partial \boldsymbol{x}}\right)' \boldsymbol{a}(\boldsymbol{x},\boldsymbol{u},t)\right] = 0, \tag{3.27}$$

which is the so-called Hamilton-Jacobi-Bellman equation, with the boundary value $\mathcal{J}^*(\boldsymbol{x}(t_f),t_f) = h(\boldsymbol{x}(t_f),t_f)$.

Therefore, by defining the Hamiltonian as follows

$$\mathbb{H}(\boldsymbol{x},\boldsymbol{u},\mathcal{J}^*,t) \triangleq g(\boldsymbol{x}(t),\boldsymbol{u}(t),t) + \left(\frac{\partial \mathcal{J}^*(\boldsymbol{x}(t),t)}{\partial \boldsymbol{x}}\right)' \boldsymbol{a}(\boldsymbol{x},\boldsymbol{u},t), \tag{3.28}$$

and the optimized Hamiltonian as

$$\mathbb{H}(\boldsymbol{x},\boldsymbol{u}^*,\mathcal{J}^*,t) \triangleq \min_{\boldsymbol{u}\in\mathcal{U}}\left(\mathbb{H}(\boldsymbol{x},\boldsymbol{u}^*,\mathcal{J}^*,t)\right), \tag{3.29}$$

where $\boldsymbol{u}^*(\boldsymbol{x},t) : \mathbb{R}^{n_x}\times\mathbb{R}_{\geq 0} \to \mathbb{R}^{n_u}$ is the optimal control law, the Hamilton-Jacobi equation is given by

$$\frac{\partial \mathcal{J}^*(\boldsymbol{x}(t),t)}{\partial t} + \mathbb{H}(\boldsymbol{x},\boldsymbol{u}^*,\mathcal{J}^*,t) = 0. \tag{3.30}$$

Therefore, by using dynamic-programming one can represent the optimal control problem (3.22) by the partial differential equation (3.30), whose solution is a function $\mathcal{J}^*(\boldsymbol{x}(t),t)$ that satisfies the boundary condition $\mathcal{J}^*(\boldsymbol{x}(t_f),t_f) = h(\boldsymbol{x}(t_f),t_f)$.

3.4 The method of Galerkin

The Galerkin's method is commonly used to approximate the solution of Partial Differential Equations (PDE) (Mikhlin and Smolitskiy, 1967). In this work, it is applied to achieve solutions of the HJB and HJBI equations associated to the nonlinear $\mathcal{W}_2$ and $\mathcal{W}_\infty$ control problems, respectively.

Therefore, consider a generic PDE in the compact form

$$\mathcal{A}(V(\boldsymbol{x})) = 0, \tag{3.31}$$

with the boundary condition $V(\boldsymbol{x}_0) = a$, for some $\boldsymbol{x}_0 \in \mathbb{R}^{n_x}$ and $a \in \mathbb{R}$, where the function $V(\boldsymbol{x}) : \mathbb{R}^{n_x} \to \mathbb{R}$ is an unknown solution of this PDE. The first step in applying the method of Galerkin is to constrain the domain of (3.31) to a compact subset, $\Omega \subset \mathbb{R}^{n_x}$, thus $V(\boldsymbol{x}) : \Omega \to \mathbb{R}$. In this context, if one select a complete vector of basis functions $\Phi(\boldsymbol{x}) = \left[\phi_1(\boldsymbol{x})\ \phi_2(\boldsymbol{x})\ ...\ \phi_{n_\phi}(\boldsymbol{x})\right], n_\phi \in \mathbb{N}$, and consider $V_N(\boldsymbol{x}) = \sum_{j=1}^{n_\phi} c_j \phi_j(\boldsymbol{x}) = \boldsymbol{c}'\Phi(\boldsymbol{x})$, with $V_N(\boldsymbol{x}_0) = a$, then there exist coefficients $c_j \in \mathbb{R}$, such that

$$\int_\Omega (V(\boldsymbol{x}) - V_N(\boldsymbol{x}))\, d\Omega = 0, \tag{3.32}$$

where $\int_\Omega (\cdot) d\Omega$ stands for the integral over the domain of the problem. Nevertheless, in practice the vector of basis functions is not usually a complete basis in the domain of interest Thus, the following approximation error is obtained for any selection of the coefficients c_j,

$$\mathcal{A}(V_N(\boldsymbol{x})) = \text{Error}(\boldsymbol{x}). \tag{3.33}$$

In the Galerkin's method the vector of coefficients $\boldsymbol{c}$ is determined by setting the projection of the error on the finite basis $\Phi(\boldsymbol{x})$ to zero, $\forall \boldsymbol{x} \in \Omega$, as follows

$$< \mathcal{A}(V_N(\boldsymbol{x})), \boldsymbol{\phi}_j(\boldsymbol{x}) > \triangleq \int_\Omega \mathcal{A}(V_N(\boldsymbol{x}))\boldsymbol{\phi}_j(\boldsymbol{x}) d\boldsymbol{\Omega} = 0, \quad j = 1,\ 2,\ ...\ n_\phi. \tag{3.34}$$

The method of Galerkin is employed in this doctoral thesis to approximate the solution of the HJB and HJBI equations that arise from the formulation of the $\mathcal{W}_2$ and $\mathcal{W}_\infty$ control strategies via dynamic-programming.

3.5 The Euler-Lagrange formulation

This section concerns some mathematical aspects of the Euler-Lagrange formulation of mechanical systems. For further details about the Euler-Lagrange approach, the readers may refer to Spong et al. (2006).

Mechanical systems can be described by the Lagrangian function

$$\mathcal{L}(\boldsymbol{q}, \dot{\boldsymbol{q}}) = \mathcal{K}(\boldsymbol{q}, \dot{\boldsymbol{q}}) - \mathcal{P}(\boldsymbol{q}, \dot{\boldsymbol{q}}), \tag{3.35}$$

where $\mathcal{K}(\boldsymbol{q}, \dot{\boldsymbol{q}}) : (\mathbb{R}^{n_q} \times \mathbb{R}^{n_q}) \to \mathbb{R}$ is the kinetic energy, $\mathcal{P}(\boldsymbol{q}, \dot{\boldsymbol{q}}) : (\mathbb{R}^{n_q} \times \mathbb{R}^{n_q}) \to \mathbb{R}$ is the potential energy, $\boldsymbol{q}(t) : \mathbb{R}_{\geq 0} \to \mathbb{R}^{n_q}$ is the vector of generalized coordinates that describes the position and orientation of rigid bodies composing a mechanical system with respect to the inertial reference frame $\mathcal{I}$, and $\dot{\boldsymbol{q}}(t) : \mathbb{R}_{\geq 0} \to \mathbb{R}^{n_q}$ is the vector of generalized velocities, in which n_q is the number of degrees of freedom of the mechanical system.

Regarding (3.35) and through the D'Alembert's principle, the Euler-Lagrange equa-

tions that describe the mechanical system are given by

$$\frac{d}{dt}\left(\frac{\partial \mathcal{L}(\boldsymbol{q},\dot{\boldsymbol{q}})}{\partial \dot{\boldsymbol{q}}(t)}\right) - \frac{\partial \mathcal{L}(\boldsymbol{q},\dot{\boldsymbol{q}})}{\partial \boldsymbol{q}(t)} = \boldsymbol{\vartheta}(t), \tag{3.36}$$

where $\boldsymbol{\vartheta}(t) : \mathbb{R}_{\geq 0} \to \mathbb{R}^{n_q}$ is the vector of generalized forces, which is composed by nonconservative forces and torques that actuate on the system.

For the special class of mechanical systems whose kinetic energy can be written as a quadratic function of the generalized velocities and the potential energy is independent of them, the Lagrangian function (3.35) can be written as

$$\mathcal{L}(\boldsymbol{q},\dot{\boldsymbol{q}}) = \frac{1}{2}\dot{\boldsymbol{q}}'(t)\boldsymbol{M}(\boldsymbol{q})\dot{\boldsymbol{q}}(t) - \mathcal{P}(\boldsymbol{q}), \tag{3.37}$$

where $\boldsymbol{M}(\boldsymbol{q}) : \mathbb{R}^{n_q} \to \mathbb{R}^{n_q \times n_q}$ is the inertia matrix, which possess the following properties (Spong et al., 2006):

Property 1. *The inertia matrix in (3.37) is positive definite, i.e.* $\boldsymbol{M}(\boldsymbol{q}) > 0$.

Property 2. *The inertia matrix in (3.37) is symmetric, i.e.* $\boldsymbol{M}'(\boldsymbol{q}) = \boldsymbol{M}(\boldsymbol{q})$.

Consequently, by replacing equation (3.37) in (3.36), yields

$$\begin{aligned}
&\frac{d}{dt}\left(\frac{\partial}{\partial \dot{\boldsymbol{q}}(t)}\left(\frac{1}{2}\dot{\boldsymbol{q}}'(t)\boldsymbol{M}(\boldsymbol{q})\dot{\boldsymbol{q}}(t)\right)\right) - \left(\frac{\partial}{\partial \boldsymbol{q}(t)}\left(\frac{1}{2}\dot{\boldsymbol{q}}'(t)\boldsymbol{M}(\boldsymbol{q})\dot{\boldsymbol{q}}(t)\right)\right) + \frac{\partial \mathcal{P}(\boldsymbol{q})}{\partial \boldsymbol{q}(t)} = \boldsymbol{\vartheta}(t), \\
&\boldsymbol{M}(\boldsymbol{q})\ddot{\boldsymbol{q}}(t) + \underbrace{\frac{\partial \boldsymbol{M}(\boldsymbol{q})\dot{\boldsymbol{q}}(t)}{\partial t} - \frac{\partial}{\partial \boldsymbol{q}(t)}\left(\frac{1}{2}\dot{\boldsymbol{q}}'(t)\boldsymbol{M}(\boldsymbol{q})\dot{\boldsymbol{q}}(t)\right)}_{\boldsymbol{C}(\boldsymbol{q},\dot{\boldsymbol{q}})\dot{\boldsymbol{q}}} + \underbrace{\frac{\partial \mathcal{P}}{\partial \boldsymbol{q}(t)}}_{\boldsymbol{g}(\boldsymbol{q})} = \boldsymbol{\vartheta}(t),
\end{aligned} \tag{3.38}$$

which, when considering input affine mechanical systems, can also be written in the canonical form of the Euler-Lagrange equations as

$$\boldsymbol{M}(\boldsymbol{q})\ddot{\boldsymbol{q}}(t) + \boldsymbol{C}(\boldsymbol{q}.\dot{\boldsymbol{q}})\dot{\boldsymbol{q}}(t) + \boldsymbol{g}(\boldsymbol{q}) = \boldsymbol{B}(\boldsymbol{q},\dot{\boldsymbol{q}})\boldsymbol{\tau}(t) + \boldsymbol{w}(t), \tag{3.39}$$

where $\boldsymbol{C}(\boldsymbol{q},\dot{\boldsymbol{q}}) : (\mathbb{R}^{n_q} \times \mathbb{R}^{n_q}) \to \mathbb{R}^{n_q \times n_q}$ is the Coriolis and centripetal forces matrix, $\boldsymbol{g}(\boldsymbol{q}) : \mathbb{R}^{n_q} \to \mathbb{R}^{n_q}$ is related to the gravitational forces, and $\boldsymbol{\vartheta}(t) = \boldsymbol{B}(\boldsymbol{q},\dot{\boldsymbol{q}})\boldsymbol{\tau}(t) + \boldsymbol{w}(t)$, in which $\boldsymbol{\tau}(t) : \mathbb{R}_{\geq 0} \to \mathbb{R}^{n_\tau}$ is the vector of control inputs, $\boldsymbol{B}(\boldsymbol{q},\dot{\boldsymbol{q}}) : (\mathbb{R}^{n_q} \times \mathbb{R}^{n_q}) \to \mathbb{R}^{n_q \times n_\tau}$ is the input coupling matrix, and $\boldsymbol{w}(t) : \mathbb{R}_{\geq 0} \to \mathbb{R}^{n_q}$ is the disturbances vector, that represents the total effects of unmodeled dynamics, parametric uncertainties and external disturbances actuating on the mechanical system.

The Coriolis and centrifugal forces matrix $\boldsymbol{C}(\boldsymbol{q}.\dot{\boldsymbol{q}})$ is not unique. Thus, for the sake of convenience, in this manuscript this matrix is computed through the Christoffel symbols of first kind, which is defined as

$$\boldsymbol{C}_{k,j}(\boldsymbol{q},\dot{\boldsymbol{q}}) = \sum_{l=1}^{n_q} \frac{1}{2}\left[\frac{\partial \boldsymbol{M}_{k,j}(\boldsymbol{q})}{\partial \boldsymbol{q}_l(t)} + \frac{\partial \boldsymbol{M}_{k,l}(\boldsymbol{q})}{\partial \boldsymbol{q}_j(t)} - \frac{\partial \boldsymbol{M}_{l,j}(\boldsymbol{q})}{\partial \boldsymbol{q}_k(t)}\right]\dot{\boldsymbol{q}}_l(t), \tag{3.40}$$

where $\boldsymbol{C}_{k,j}(\boldsymbol{q},\dot{\boldsymbol{q}})$, $\boldsymbol{M}_{k,j}(\boldsymbol{q})$, and $\boldsymbol{q}_k(t)$ are elements of the Coriolis and centripetal forces matrix, the inertia matrix, and the vector of generalized coordinates, respectively, corresponding to the k-th row and j-th column. By computing the Coriolis and centripetal forces matrix through the Christoffel symbols of first kind (3.40), it ensures that the following property holds for the mechanical system (3.39),

Property 3. *(Adapted from Spong et al. (2006)) If the Coriolis and centripetal forces matrix $\boldsymbol{C}(\boldsymbol{q},\dot{\boldsymbol{q}})$ in (3.39) is computed through the Christoffel symbols (3.40), then the expression $\dot{\boldsymbol{M}}(\boldsymbol{q}) - 2\boldsymbol{C}(\boldsymbol{q},\dot{\boldsymbol{q}})$ is a skew-symmetric matrix.*

In order to compute the generalized forces, consider an external force actuating at the point $\mathcal{P}$ belonging to a rigid body $\mathcal{D}$ of the mechanical system. This force can be mapped as follows (Kane and Levinson, 1985, pag. 106)

$$\boldsymbol{\vartheta}(t) = (\boldsymbol{J}_{\mathcal{P}}(\boldsymbol{q}))'\boldsymbol{f}^{\mathcal{I}}(t), \tag{3.41}$$

where $\boldsymbol{f}^{\mathcal{I}}(t) : \mathbb{R}_{\geq 0} \to \mathbb{R}^{n_{\mathcal{P}}}$ is the applied external force expressed in the inertial reference frame $\mathcal{I}$, $\boldsymbol{J}_{\mathcal{P}}(\boldsymbol{q}) : \mathbb{R}^{n_q} \to \mathbb{R}^{n_{\mathcal{P}} \times n_q}$ is the linear velocity Jacobian of $\mathcal{P}$ in $\mathcal{I}$, given by

$$\boldsymbol{J}_{\mathcal{P}}(\boldsymbol{q}) \triangleq \frac{\partial \boldsymbol{v}^{\mathcal{I}}_{\mathcal{I},\mathcal{P}}(\boldsymbol{q},\dot{\boldsymbol{q}})}{\partial \dot{\boldsymbol{q}}(t)} = \frac{\partial \boldsymbol{p}^{\mathcal{I}}_{\mathcal{I},\mathcal{P}}(\boldsymbol{q})}{\partial \boldsymbol{q}(t)}, \tag{3.42}$$

with $\boldsymbol{v}^{\mathcal{I}}_{\mathcal{I},\mathcal{P}}(\boldsymbol{q},\dot{\boldsymbol{q}}) = \dot{\boldsymbol{p}}^{\mathcal{I}}_{\mathcal{I},\mathcal{P}}(\boldsymbol{q},\dot{\boldsymbol{q}}) : (\mathbb{R}^{n_q} \times \mathbb{R}^{n_q}) \to \mathbb{R}^{n_{\mathcal{P}}}$, being the vector of linear velocity of $\mathcal{P}$ with respect to $\mathcal{I}$ expressed in $\mathcal{I}$, and $\boldsymbol{p}^{\mathcal{I}}_{\mathcal{I},\mathcal{P}}(t) : \mathbb{R}_{\geq 0} \to \mathbb{R}^{n_{\mathcal{P}}}$ the position vector of $\mathcal{P}$ with respect to $\mathcal{I}$ expressed in $\mathcal{I}$.

Similarly, the external torque actuating on a rigid body $\mathcal{D}$ of the mechanical system can be mapped to the generalized forces through (Kane and Levinson, 1985, pag. 106)

$$\boldsymbol{\vartheta}(t) = (\boldsymbol{W}_{\mathcal{D}}(\boldsymbol{q}))'\boldsymbol{\tau}^{\mathcal{I}}(t), \tag{3.43}$$

where $\boldsymbol{\tau}^{\mathcal{I}}(t) : \mathbb{R}_{\geq 0} \to \mathbb{R}^{n_{\mathcal{D}}}$ is the applied torque expressed in the inertial reference frame $\mathcal{I}$,

$$\boldsymbol{W}_{\mathcal{D}} \triangleq \frac{\partial \boldsymbol{w}^{\mathcal{I}}_{\mathcal{I},\mathcal{D}}(\boldsymbol{q},\dot{\boldsymbol{q}})}{\partial \dot{\boldsymbol{q}}}, \tag{3.44}$$

is the angular velocity Jacobian, and $\boldsymbol{w}^{\mathcal{I}}_{\mathcal{I},\mathcal{D}}(\boldsymbol{q},\dot{\boldsymbol{q}}) : \mathbb{R}^{n_q} \times \mathbb{R}^{n_q} \to \mathbb{R}^{n_{\mathcal{D}}}$ is the angular velocity of $\mathcal{D}$ with respect to $\mathcal{I}$ expressed in $\mathcal{I}$, this angular velocity can be obtained doing $\dot{\boldsymbol{R}}^{\mathcal{I}}_{\mathcal{D}}(\boldsymbol{R}^{\mathcal{I}}_{\mathcal{D}})' = \boldsymbol{S}(\boldsymbol{w}^{\mathcal{I}}_{\mathcal{I},\mathcal{D}})$, where $\boldsymbol{S}(\cdot) : \mathbb{R}^3 \to \mathbb{R}^{3\times 3}$ denotes a skew-symmetric matrix (Spong et al., 2006) and $\boldsymbol{R}^{\mathcal{I}}_{\mathcal{D}}$ the rotation matrix that gives the orientation of $\mathcal{D}$ with respect to $\mathcal{I}$.

The mechanical system (3.39) can be classified according to its degree of actuation.

Definition 5. *The mechanical system (3.39) is fully actuated in the domain $\Omega \subseteq (\mathbb{R}^{n_q} \times \mathbb{R}^{n_q})$ if $\boldsymbol{q}(t) : \mathbb{R}_{\geq 0} \to \mathbb{R}^{n_q}$ and $rank(\boldsymbol{B}(\boldsymbol{q},\dot{\boldsymbol{q}})) = n_q$, $\forall (\boldsymbol{q},\dot{\boldsymbol{q}}) \in \Omega$, where $n_q \in \mathbb{N}$ is the number of DOF of the system.*

Definition 6. *The mechanical system* (3.39) *is underactuated in the domain* $\Omega \subseteq (\mathbb{R}^{n_q} \times \mathbb{R}^{n_q})$ *if* $\boldsymbol{q}(t) : \mathbb{R}_{\geq 0} \to \mathbb{R}^{n_q}$ *and* $rank(\boldsymbol{B}(\boldsymbol{q}, \dot{\boldsymbol{q}})) < n_q$, $\forall (\boldsymbol{q}, \dot{\boldsymbol{q}}) \in \Omega$, *where* $n_q \in \mathbb{N}$ *is the number of DOF of the system.*

Remark 13. *The degree of actuation of a mechanical system in the domain* Ω *is given by* $\inf\{rank(\boldsymbol{B}(\boldsymbol{q}, \dot{\boldsymbol{q}}))\}$, $\forall (\boldsymbol{q}, \dot{\boldsymbol{q}}) \in \Omega$, *in which the rank of a input coupling matrix is the dimension of the image space spawned by its columns.*

Remark 14. *According to definitions 5 and 6, overactuated mechanical systems are a particular case of fully actuated mechanical systems, that possess* $\boldsymbol{q}(t) : \mathbb{R}_{\geq 0} \to \mathbb{R}^{n_q}$, $\boldsymbol{\tau}(t) : \mathbb{R}_{\geq 0} \to \mathbb{R}^{n_\tau}$, $rank(\boldsymbol{B}(\boldsymbol{q}, \dot{\boldsymbol{q}})) = n_q$, *with* $n_\tau, n_q \in \mathbb{N}$, *and* $n_\tau > n_q$. *In addition, a mechanical system that possess* $\boldsymbol{q}(t) : \mathbb{R}_{\geq 0} \to \mathbb{R}^{n_q}$, $\boldsymbol{\tau}(t) : \mathbb{R}_{\geq 0} \to \mathbb{R}^{n_\tau}$, $rank(\boldsymbol{B}(\boldsymbol{q}, \dot{\boldsymbol{q}})) < n_q$, *with* $n_\tau, n_q \in \mathbb{N}$, *and* $n_\tau > n_q$ *is also underactuated.*

3.6 Final Remarks

This chapter introduced most of the required concepts, notations, and definitions used in this doctoral thesis. The following topics were addressed: (i) the Lebesgue and Sobolev spaces; (ii) interesting features of the $\mathcal{W}_2$ and $\mathcal{W}_\infty$ control formulations in the weighted Sobolev space; (iii) the Hamilton-Jacobi-Bellman equation; (iv) the method of Galerkin; and (v) the Euler-Lagrange formulation.

The next chapter develops the nonlinear $\mathcal{W}_2$ and $\mathcal{W}_\infty$ controllers in the weighted Sobolev space via dynamic-programming, and proposes numerical algorithms to achieve solutions of the resulting Hamilton-Jacobi equations. In addition to present results of numerical experiments with a Two-wheeled Self-balanced vehicle, and perform comparative analysis with the classic $\mathcal{H}_\infty$ controller.

4

$\mathcal{W}_2$ and $\mathcal{W}_\infty$ controllers formulated in the weighted Sobolev space and approximate solutions

This chapter presents novel formulations of the nonlinear $\mathcal{H}_2$ and $\mathcal{H}_\infty$ control in the weighted Sobolev space for nonlinear systems, here called $\mathcal{W}_2$ and $\mathcal{W}_\infty$ control problems. These formulations allow to weight component-wise the influences of the cost variable and its time derivatives in the cost function. The $\mathcal{W}_2$ and $\mathcal{W}_\infty$ control problems are developed using dynamic-programming, and the Successive Galerkin Approximation Algorithm is extended to achieve solutions of the resulting HJ equations. Numerical results with a Two-wheeled Self-balanced vehicle are presented, and comparison analysis are performed with a nonlinear $\mathcal{H}_\infty$ controller. The content presented in this chapter was published in Cardoso and Raffo (2018) and Cardoso et al. (2018c).

4.1 The nonlinear $\mathcal{W}_2$ control problem

In this section, the nonlinear $\mathcal{W}_2$ control approach is formulated in the weighted Sobolev space for nonlinear systems represented in the form

$$\mathcal{P}_1 : \begin{cases} \dot{\boldsymbol{x}}(t) = \boldsymbol{f}(\boldsymbol{x}) + \boldsymbol{g}(\boldsymbol{x})\boldsymbol{u}(t), \quad \boldsymbol{x}(0) = \boldsymbol{x}_0, \\ \boldsymbol{z}(t) = \boldsymbol{h}(\boldsymbol{x}), \end{cases} \tag{4.1}$$

where $t \in \mathbb{R}_{\geq 0}$ is the time variable, $\boldsymbol{x}(t) : \mathbb{R}_{\geq 0} \to \mathbb{R}^{n_x}$ is the state vector, $\boldsymbol{u}(t) : \mathbb{R}_{\geq 0} \to \mathbb{R}^{n_u}$ is the input vector, and $\boldsymbol{z}(t) : \mathbb{R}_{\geq 0} \to \mathbb{R}^{n_z}$ is the cost variable. It is assumed that,

Assumption 1. *System $\mathcal{P}_1$ is controllable (See Definition 13),*

Assumption 2. *The state vector $\boldsymbol{x}$ is available,*

Assumption 3. *The origin of the state-space is an equilibrium point, i.e. $f(\mathbf{0}) = \mathbf{0}$, with $h(\mathbf{0}) = \mathbf{0}$.*

Assumption 4. *The matrices $\dfrac{\partial \boldsymbol{h}(x)}{\partial \boldsymbol{x}}$ and $\boldsymbol{g}(x)$ have full column rank.*

Remark 15. *Assumption 4 ensures that all states are observable from the cost variable $\boldsymbol{z}(t)$, and also that the column vectors in $\boldsymbol{g}(x)$ are linearly independent.*

The nonlinear $\mathcal{H}_2$ controller formulated in the weighted Sobolev space is designed in order to obtain a state feedback control law that minimizes the following cost functional:

$$\begin{aligned} \mathcal{J}_2 &= \frac{1}{2}||\boldsymbol{z}(t)||^2_{\mathcal{W}_{1,2,\boldsymbol{\sigma}}}, \\ &= \frac{1}{2}||\boldsymbol{z}(t)||^2_{\boldsymbol{\sigma}_0} + \frac{1}{2}||\dot{\boldsymbol{z}}(t)||^2_{\boldsymbol{\sigma}_1}, \end{aligned} \tag{4.2}$$

where $\boldsymbol{\sigma} = (\boldsymbol{\sigma}_0, \boldsymbol{\sigma}_1)$, in which $\boldsymbol{\sigma}_0, \boldsymbol{\sigma}_1 \in \mathbb{R}^{n_z \times n_z}$ are symmetric and positive definite weighting matrices.

Remark 16. *In the nonlinear $\mathcal{W}_2$ and $\mathcal{W}_\infty$ control approaches presented here, the control inputs are not weighted directly in the optimizing index. The transient and steady-state performance are reached by tuning component-wise the influence of the cost variable and its time derivative in the cost functional.*

In this context, the control problem is stated as

$$\begin{aligned} V_2 &= \min_{u \in \mathcal{U}} \mathcal{J}_2, \\ &= \min_{u \in \mathcal{U}} \frac{1}{2} \int_0^\infty \left(||\boldsymbol{z}(t)||^2_{\boldsymbol{\sigma}_0} + ||\dot{\boldsymbol{z}}(t)||^2_{\boldsymbol{\sigma}_1} \right) dt, \\ &\text{s.t.} \quad \mathcal{P}_1, \end{aligned} \tag{4.3}$$

in which $\mathcal{U} : \mathbb{R}^{n_x} \to \mathbb{R}^{n_u}$.

In order to solve this problem, in this doctoral thesis, the $\mathcal{W}_2$ optimal control problem is formulated via dynamic-programming (Kirk, 2004), from which the associated Hamiltonian is given by

$$\mathbb{H}_2\left(V_2, \boldsymbol{x}, \boldsymbol{u}\right) = \left(\frac{\partial V_2(\boldsymbol{x})}{\partial \boldsymbol{x}} \right)' \left[f(\boldsymbol{x}) + g(\boldsymbol{x})\boldsymbol{u} \right] + \frac{1}{2} \left(||\boldsymbol{z}(t)||^2_{\boldsymbol{\sigma}_0} + ||\dot{\boldsymbol{z}}(t)||^2_{\boldsymbol{\sigma}_1} \right), \tag{4.4}$$

with the boundary condition $V_2(\mathbf{0}) = 0$. Equation (4.4) in the expanded form yields[1]

$$\begin{aligned}\mathbb{H}_2\left(V_2, \boldsymbol{x}, \boldsymbol{u}\right) &= \left(\frac{\partial V_2}{\partial \boldsymbol{x}}\right)' [\boldsymbol{f} + \boldsymbol{g}\boldsymbol{u}] + \frac{1}{2}\boldsymbol{h}'\boldsymbol{\sigma}_0\boldsymbol{h} + \frac{1}{2}\dot{\boldsymbol{x}}'\nabla\boldsymbol{h}'\boldsymbol{\sigma}_1\nabla\boldsymbol{h}\dot{\boldsymbol{x}} \\ &= \left(\frac{\partial V_2}{\partial \boldsymbol{x}}\right)' [\boldsymbol{f} + \boldsymbol{g}\boldsymbol{u}] + \frac{1}{2}\boldsymbol{h}'\boldsymbol{\sigma}_0\boldsymbol{h} + \frac{1}{2}\boldsymbol{f}'\nabla\boldsymbol{h}'\boldsymbol{\sigma}_1\nabla\boldsymbol{h}\boldsymbol{f} + \boldsymbol{u}'\boldsymbol{g}'\nabla\boldsymbol{h}'\boldsymbol{\sigma}_1\nabla\boldsymbol{h}\boldsymbol{f} \\ &+ \frac{1}{2}\boldsymbol{u}'\boldsymbol{g}'\nabla\boldsymbol{h}'\boldsymbol{\sigma}_1\nabla\boldsymbol{h}\boldsymbol{g}\boldsymbol{u}, \end{aligned} \tag{4.5}$$

where $\nabla\boldsymbol{h} \triangleq \dfrac{\partial \boldsymbol{h}(x)}{\partial \boldsymbol{x}}$.

The Hamilton-Jacobi-Bellman equation is obtained from (4.3) using the Hamiltonian (4.5), which in a compact form is given by

$$\frac{\partial V_2(\boldsymbol{x}, t)}{\partial t} + \min_{\boldsymbol{u}\in\mathcal{U}} \left\{\mathbb{H}_2\left(V_2, \boldsymbol{x}, \boldsymbol{u}\right)\right\} = 0. \tag{4.6}$$

Consequently, the optimal control law $\boldsymbol{u}^*$ can be obtained by minimizing the Hamiltonian (4.5) with respect to the control inputs as follows

$$\frac{\partial \mathbb{H}_2}{\partial \boldsymbol{u}} = \boldsymbol{g}'\frac{\partial V_2}{\partial \boldsymbol{x}} + \boldsymbol{g}'\nabla\boldsymbol{h}'\boldsymbol{\sigma}_1\nabla\boldsymbol{h}\boldsymbol{f} + \boldsymbol{g}(\boldsymbol{x})'\nabla\boldsymbol{h}'\boldsymbol{\sigma}_1\nabla\boldsymbol{h}\boldsymbol{g}\boldsymbol{u}^* = 0, \tag{4.7}$$

which leads to

$$\boldsymbol{u}^* = -\boldsymbol{R}^{-1}\boldsymbol{g}'\left(\frac{\partial V_2}{\partial \boldsymbol{x}} + \boldsymbol{B}\boldsymbol{f}\right), \tag{4.8}$$

where $\boldsymbol{R} \triangleq \boldsymbol{g}'\boldsymbol{B}\boldsymbol{g}$, with $\boldsymbol{B} \triangleq \nabla\boldsymbol{h}'\boldsymbol{\sigma}_1\nabla\boldsymbol{h} > 0$. The invertibility of $\boldsymbol{R}$ is ensured by Assumption 4.

The HJ equation associated with this optimal control problem is obtained by replacing the optimal control law (4.8) in the HJB equation (4.6), and assuming the now autonomous system (4.1), which is written in the compact form

$$\frac{\partial V_2(\boldsymbol{x}, t)}{\partial t} + \mathbb{H}_2(V_2, \boldsymbol{x}, \boldsymbol{u}^*) = 0. \tag{4.9}$$

Consequently, the control problem (4.3) results in finding a function $V_2(\boldsymbol{x}, t)$ that satisfies (4.9).

4.2 The nonlinear $\mathcal{W}_\infty$ control problem

In this section, the nonlinear $\mathcal{W}_\infty$ control approach is formulated in the weighted Sobolev space for autonomous nonlinear systems. Now, the control law is designed considering perturbed systems represented by the following standard form of input-affine

[1]For the sake of simplicity, throughout the manuscript, some functional dependencies are omitted.

systems:

$$\mathcal{P}_2 : \begin{cases} \dot{\boldsymbol{x}}(t) = \boldsymbol{f}(\boldsymbol{x}) + \boldsymbol{g}(\boldsymbol{x})\boldsymbol{u}(t) + \boldsymbol{k}(\boldsymbol{x})\boldsymbol{w}(t), \quad \boldsymbol{x}(0) = \boldsymbol{x}_0, \\ \boldsymbol{z}(t) = \boldsymbol{h}(\boldsymbol{x}), \end{cases} \tag{4.10}$$

where $\boldsymbol{x}(t)$, $\boldsymbol{u}(t)$, $\boldsymbol{z}(t)$ are defined as in (4.1), and $\boldsymbol{w}(t) : \mathbb{R}_{\geq 0} \to \mathbb{R}^{n_w}$ is the disturbance vector. In addition, Assumptions 1-4 hold for $\mathcal{P}_2$.

The nonlinear $\mathcal{H}_\infty$ control problem in the weighted Sobolev space is posed as finding an optimal control law that ensures the following inequality

$$||\boldsymbol{z}(t)||^2_{W_{1,2,\boldsymbol{\sigma}}} \leq \gamma^2 ||\boldsymbol{w}(t)||^2_{\mathcal{L}_2}, \tag{4.11}$$

where $\gamma \in \mathbb{R}_{\geq 0}$ is a given sufficiently large $\mathcal{W}_\infty$ attenuation level.

Accordingly, the controller is designed based on the following cost functional:

$$\mathcal{J}_\infty = \frac{1}{2}||\boldsymbol{z}(t)||^2_{W_{1,2,\boldsymbol{\Sigma}}} - \frac{1}{2}\gamma^2 ||\boldsymbol{w}(t)||^2_{\mathcal{L}_2}. \tag{4.12}$$

Therefore, the optimal control problem is stated as

$$V_\infty = \min_{\boldsymbol{u}\in\mathcal{U}} \max_{\boldsymbol{w}\in\mathcal{W}} \int_0^\infty \frac{1}{2}\left(||\boldsymbol{z}(t)||^2_{\boldsymbol{\sigma}_0} + ||\dot{\boldsymbol{z}}(t)||^2_{\boldsymbol{\sigma}_1} - \gamma^2 ||\boldsymbol{w}(t)||^2\right) dt, \tag{4.13}$$

in which $\mathcal{U} : \mathbb{R}^{n_x} \to \mathbb{R}^{n_u}$ and $\mathcal{W} = \mathcal{L}_2[0, \infty)$.

The control design is derived by solving a Min-Max optimization problem, which can be formulated via differential game theory. The associated Hamiltonian is given by

$$\mathbb{H}_\infty = \left(\frac{\partial V_\infty(\boldsymbol{x})}{\partial \boldsymbol{x}}\right)' [\boldsymbol{f}(\boldsymbol{x}) + \boldsymbol{g}(\boldsymbol{x})\boldsymbol{u}(t) + \boldsymbol{k}(\boldsymbol{x})\boldsymbol{w}(t)] + \frac{1}{2}(||\boldsymbol{z}(t)||^2_{\boldsymbol{\sigma}_0} + ||\dot{\boldsymbol{z}}(t)||^2_{\boldsymbol{\sigma}_1} - \gamma^2 ||\boldsymbol{w}(t)||^2), \tag{4.14}$$

which in its expanded form yields

$$\begin{aligned} \mathbb{H}_\infty = &\left(\frac{\partial V_\infty}{\partial \boldsymbol{x}}\right)' [\boldsymbol{f} + \boldsymbol{g}\boldsymbol{u} + \boldsymbol{k}\boldsymbol{w}] + \frac{1}{2}\boldsymbol{h}'\boldsymbol{\sigma}_0\boldsymbol{h} + \frac{1}{2}\boldsymbol{f}'\nabla\boldsymbol{h}'\boldsymbol{\sigma}_1\nabla\boldsymbol{h}\boldsymbol{f} - \gamma^2\boldsymbol{w}'\boldsymbol{w} + \frac{1}{2}\boldsymbol{f}'\nabla\boldsymbol{h}'\boldsymbol{\sigma}_1\nabla\boldsymbol{h}\boldsymbol{g}\boldsymbol{u} \\ &+ \frac{1}{2}\boldsymbol{f}'\nabla\boldsymbol{h}'\boldsymbol{\sigma}_1\nabla\boldsymbol{h}\boldsymbol{k}\boldsymbol{w} + \frac{1}{2}\boldsymbol{u}'\boldsymbol{g}'\nabla\boldsymbol{h}'\boldsymbol{\sigma}_1\nabla\boldsymbol{h}\boldsymbol{g}\boldsymbol{u} + +\boldsymbol{u}'\boldsymbol{g}'\nabla\boldsymbol{h}'\boldsymbol{\sigma}_1\nabla\boldsymbol{h}\boldsymbol{k}\boldsymbol{w} + \frac{1}{2}\boldsymbol{w}'\boldsymbol{k}'\nabla\boldsymbol{h}'\boldsymbol{\sigma}_1\nabla\boldsymbol{h}\boldsymbol{f} \\ &+ \frac{1}{2}\boldsymbol{w}'\boldsymbol{k}'\nabla\boldsymbol{h}'\boldsymbol{\sigma}_1\nabla\boldsymbol{h}\boldsymbol{g}\boldsymbol{u} + \frac{1}{2}\boldsymbol{w}'\boldsymbol{k}'\nabla\boldsymbol{h}'\boldsymbol{\sigma}_1\nabla\boldsymbol{h}\boldsymbol{k}\boldsymbol{w}. \end{aligned} \tag{4.15}$$

The Hamilton-Jacobi-Bellman-Isaacs equation is obtained from (4.13) using the Hamiltonian (4.15), which in a compact form is given by

$$\frac{\partial V_\infty(\boldsymbol{x}, t)}{\partial t} + \min_{u\in\mathcal{U}} \max_{\boldsymbol{w}\in\mathcal{W}} \{\mathbb{H}_\infty (V_\infty, \boldsymbol{x}, \boldsymbol{u}, \boldsymbol{w})\} = 0. \tag{4.16}$$

The worst case of the disturbance, $\boldsymbol{w}^*$, and the optimal control law, $\boldsymbol{u}^*$, are obtained by computing the partial derivatives of (4.15) with respect to these variables as follows

$$\frac{\partial \mathbb{H}_\infty}{\partial \boldsymbol{u}} = \boldsymbol{g}' \frac{\partial V_\infty}{\partial \boldsymbol{x}} + \boldsymbol{g}' \nabla \boldsymbol{h}' \boldsymbol{\sigma}_1 \nabla \boldsymbol{h} \boldsymbol{f} + \boldsymbol{g}' \nabla \boldsymbol{h}' \boldsymbol{\sigma}_1 \nabla \boldsymbol{h} \boldsymbol{g} \boldsymbol{u}^* + \boldsymbol{g}' \nabla \boldsymbol{h}' \boldsymbol{\sigma}_1 \nabla \boldsymbol{h} \boldsymbol{k} \boldsymbol{w}^* = 0 \tag{4.17}$$

$$\frac{\partial \mathbb{H}_\infty}{\partial \boldsymbol{w}} = \boldsymbol{k}' \frac{\partial V_\infty}{\partial \boldsymbol{x}} + \boldsymbol{k}' \nabla \boldsymbol{h}' \boldsymbol{\sigma}_1 \nabla \boldsymbol{h} \boldsymbol{f} + \boldsymbol{k}' \nabla \boldsymbol{h}' \boldsymbol{\sigma}_1 \nabla \boldsymbol{h} \boldsymbol{g} \boldsymbol{u}^* + \boldsymbol{k}' \nabla \boldsymbol{h}' \boldsymbol{\sigma}_1 \nabla \boldsymbol{h} \boldsymbol{k} \boldsymbol{w}^* - \gamma^2 \boldsymbol{w}^* = 0. \tag{4.18}$$

Thereby, by manipulating algebraically (4.17) and (4.18), yields

$$\boldsymbol{w}^* = \left(\gamma^2 \boldsymbol{I} - \boldsymbol{k}' \boldsymbol{B} \boldsymbol{k} + \boldsymbol{k}' \boldsymbol{B} \boldsymbol{g} \boldsymbol{R}^{-1} \boldsymbol{g}' \boldsymbol{B} \boldsymbol{k}\right)^{-1} \boldsymbol{k}' \left[\frac{\partial V_\infty}{\partial \boldsymbol{x}} + \boldsymbol{B} \boldsymbol{f} - \boldsymbol{B} \boldsymbol{g} \boldsymbol{R}^{-1} \left(\boldsymbol{g}' \frac{\partial V_\infty}{\partial \boldsymbol{x}} + \boldsymbol{g}' \boldsymbol{B} \boldsymbol{f}\right)\right], \tag{4.19}$$

$$\boldsymbol{u}^* = -\boldsymbol{R}^{-1} \boldsymbol{g}' \left(\frac{\partial V_\infty}{\partial \boldsymbol{x}} + \boldsymbol{B} \boldsymbol{f} + \boldsymbol{B} \boldsymbol{k} \boldsymbol{w}^*\right), \tag{4.20}$$

in which $(\boldsymbol{u}^*, \boldsymbol{w}^*)$ is the saddle-point solution to the problem (4.16). This can be verified by computing the second order partial derivative of (4.17) and (4.18), which results in

$$\frac{\partial^2 \mathbb{H}_\infty}{\partial \boldsymbol{u}^2} = \boldsymbol{g}' \nabla \boldsymbol{h}' \nabla \boldsymbol{h} \boldsymbol{g} > 0, \tag{4.21}$$

$$\frac{\partial^2 \mathbb{H}_\infty}{\partial \boldsymbol{w}^2} = \boldsymbol{k}' \nabla \boldsymbol{h}' \nabla \boldsymbol{h} \boldsymbol{k} - \gamma^2 \boldsymbol{I} < 0. \tag{4.22}$$

Remark 17. *The $\mathcal{W}_\infty$ attenuation level must be selected appropriately such that the inequality (4.22) holds, ensuring feasibility to the optimization problem.*

In order to obtain the HJ equation associated with the problem, it is necessary to replace (4.19) and (4.20) in (4.16) and, assuming now the autonomous system (4.10), it yields to the partial differential equation

$$\frac{\partial V_\infty(\boldsymbol{x}, t)}{\partial t} + \mathbb{H}_\infty \left(V_\infty, \boldsymbol{x}, \boldsymbol{u}^*, \boldsymbol{w}^*\right) = 0, \tag{4.23}$$

which is hard to solve analytically for the general case.

In Aliyu and Boukas (2011a), a similar HJ equation is presented, which results from the original formulation of $\mathcal{W}_\infty$ control problem in the Sobolev space. The authors assume it to be analytically intractable and propose an alternative approach to simplify the problem, which makes use of the backstepping technique. From the best knowledge of the author, there are no works in the literature proposing analytical solutions for this HJ equation. Therefore, in the next section a numerical algorithm is proposed to approximate solutions to the HJB and HJBI PDEs resulting from the $\mathcal{W}_2$ and $\mathcal{W}_\infty$ control approaches in the weighted Sobolev space for input-affine autonomous nonlinear systems.

4.3 Successive Galerkin Approximation Algorithm

The HJ equations resulting from the formulation of the nonlinear $\mathcal{W}_2$ and $\mathcal{W}_\infty$ control problems in the weighted Sobolev space are represented in a quadratic form, which is not suitable to apply directly the Galerkin's method, since it leads to multiple solutions in which one generates an optimal control law. In order to ensure that the obtained solution corresponds to a stabilizing control law, the Sucessive Galerkin Approximation Algorithm is applied. This algorithm decreases the complexity of the problem to a non-quadratic form, leading to a single solution.

In this doctoral thesis, we present two SGAAs which are based on the algorithms proposed in Beard and McLain (1998). On one hand, Algorithm 4.1 is developed to find a solution of the HJ equation derived from the nonlinear $\mathcal{W}_2$ control approach. On the other hand, for the nonlinear $\mathcal{W}_\infty$ control problem, the proposed SGAA is described in Algorithm 4.2. The convergence proofs of the presented SGAAs follow the same procedure as in Beard and McLain (1998).

Remark 18. *In Algorithms 4.1 and 4.2, although the number of iterations goes from* 1 *to* ∞*, the stopping criterion* $V^{(i)} = V^{(i+1)}$ *can be used when seeking for the approximate solution of the HJ equations.*

Remark 19. *In particular,* $\boldsymbol{u}^{(i)}$ *will ensure stability of the system* (4.1) *in the same region of the state space as* $\boldsymbol{u}^{(0)}$ *does, even though in the experiments the final optimal control law have presented an enlarged domain of attraction. In addition, as stated in Beard et al. (1998), it is not possible to find an admissible control that can stabilize an initial condition that is unstable.*

Remark 20. *Algorithm 4.2 does not converge if Remark 17 is not satisfied.*

Algorithm 4.1 SGAA to the nonlinear $\mathcal{W}_2$ control problem.

1: Let $\boldsymbol{u}^{(0)}$ be any initial stabilizing control law for system (4.1) with stability region Ω.
2: **for** $i = 0$ to ∞ **do**
3: Solve for $V_2^{(i)}$ from:

$$\left(\frac{\partial V_2^{(i)}}{\partial \boldsymbol{x}}\right)' \left[\boldsymbol{f}(\boldsymbol{x}) + \boldsymbol{g}(\boldsymbol{x})\boldsymbol{u}^{(i)}\right] + \frac{1}{2}\left(||\boldsymbol{z}||^2_{\boldsymbol{\sigma}_0} + ||\dot{\boldsymbol{z}}(\boldsymbol{u}^{(i)})||^2_{\boldsymbol{\sigma}_1}\right) = 0$$

4: Update the Control:

$$\boldsymbol{u}^{(i+1)} = -\boldsymbol{R}^{-1}\boldsymbol{g}'(\boldsymbol{x})\left(\frac{\partial V_2^{(i)}}{\partial \boldsymbol{x}} + \boldsymbol{B}\boldsymbol{f}(\boldsymbol{x})\right)$$

5: **end for**

In order to use the proposed algorithms and approximate the solutions of the HJ equations (4.9) and (4.23), the Galerkin's method is applied to solve numerically the

Algorithm 4.2 SGAA to nonlinear $\mathcal{W}_\infty$ control problem.

1: Let $\boldsymbol{u}^{(0)}$ be any initial stabilizing control law for the system (4.1) with $\boldsymbol{w} = \boldsymbol{0}$ and stability region Ω.
2: Set $\boldsymbol{w}^{(0,0)} = \boldsymbol{0}$
3: **for** $i = 0$ to ∞ **do**
4: **for** $j = 0$ to ∞ **do**
5: Solve for $V_\infty^{(i,j)}$ from:

$$\left(\frac{\partial V_\infty^{(i,j)}}{\partial \boldsymbol{x}}\right)' [\boldsymbol{f}(\boldsymbol{x}) + \boldsymbol{g}(\boldsymbol{x})\boldsymbol{u}^{(i)} + \boldsymbol{k}(\boldsymbol{x})\boldsymbol{w}^{(i,j)}] + \frac{1}{2}(||\boldsymbol{z}||^2_{\boldsymbol{\sigma}_0} + ||\dot{\boldsymbol{z}}(u^{(i)}, \boldsymbol{w}^{(i,j)})||^2_{\boldsymbol{\sigma}_1} - \gamma^2 ||\boldsymbol{w}^{(i,j)}||^2) = 0$$

6: Update the Disturbance:

$$\boldsymbol{w}^{(i,j+1)} = (\gamma^2 \boldsymbol{I} - \boldsymbol{k}'\boldsymbol{B}\boldsymbol{k} + \boldsymbol{k}'\boldsymbol{B}\boldsymbol{g}\boldsymbol{R}^{-1}\boldsymbol{g}'\boldsymbol{B}\boldsymbol{k})^{-1} \left[\boldsymbol{k}'\frac{\partial V_\infty^{(i,j)}}{\partial \boldsymbol{x}} + \boldsymbol{k}'\boldsymbol{B}\boldsymbol{f} - \boldsymbol{k}'\boldsymbol{B}\boldsymbol{g}\boldsymbol{R}^{-1}\left(\boldsymbol{g}'\frac{\partial V_\infty^{(i,j)}}{\partial \boldsymbol{x}} + \boldsymbol{g}'\boldsymbol{B}\boldsymbol{f}\right)\right]$$

7: **end for**
8: Update the Control:

$$\boldsymbol{u}^{(i+1)} = -\boldsymbol{R}^{-1}\left(\boldsymbol{g}'\frac{\partial V_\infty^{(i,\infty)}}{\partial \boldsymbol{x}} + \boldsymbol{g}'(\boldsymbol{x})\boldsymbol{B}\boldsymbol{f}(\boldsymbol{x}) + \boldsymbol{g}'(\boldsymbol{x})\boldsymbol{B}\boldsymbol{k}(\boldsymbol{x})\boldsymbol{w}^{(i,\infty)}\right)$$

9: **end for**

respective PDEs. The general formulation of the Galerkin's method is briefly presented in Chapter 3, Section 3.4, taking into account this formulation and Algorithm 4.1, which is proposed to solve the nonlinear $\mathcal{W}_2$ control problem and the HJB equation (4.9), the procedure to achieve an approximate solution $V_2(\boldsymbol{x})$, $\forall \boldsymbol{x} \in \Omega$, is performed as follows. First, we require that the residual resulting from the use of the approximate solution in the HJ equation (4.9) will be orthogonal to the vector of basis function in the domain Ω, as

$$\int_\Omega \left[\left(\frac{\partial \boldsymbol{\Phi}'\boldsymbol{c}}{\partial \boldsymbol{x}}\right)' [\boldsymbol{f}(\boldsymbol{x}) + \boldsymbol{g}(\boldsymbol{x})\boldsymbol{u}] + \frac{1}{2}\left(||\boldsymbol{z}||^2_{\boldsymbol{\sigma}_0} + ||\dot{\boldsymbol{z}}||^2_{\boldsymbol{\sigma}_1}\right)\right] \boldsymbol{\Phi}' d\Omega = 0, \tag{4.24}$$

which, after some manipulation, can be rewritten as

$$\boldsymbol{c}' \int_\Omega \nabla \boldsymbol{\Phi}' [\boldsymbol{f}(\boldsymbol{x}) + \boldsymbol{g}(\boldsymbol{x})\boldsymbol{u}] \boldsymbol{\Phi}' d\Omega = -\frac{1}{2}\int_\Omega (||\boldsymbol{z}||^2_{\boldsymbol{\sigma}_0} + ||\dot{\boldsymbol{z}}||^2_{\boldsymbol{\sigma}_1}) \boldsymbol{\Phi}' d\Omega. \tag{4.25}$$

Hence, the vector of coefficients $\boldsymbol{c}$ is obtained by

$$\boldsymbol{c}' = \left(-\frac{1}{2}\int_\Omega (||\boldsymbol{z}||^2_{\boldsymbol{\sigma}_0} + ||\dot{\boldsymbol{z}}||^2_{\boldsymbol{\sigma}_1}) \boldsymbol{\Phi}' d\Omega\right)\left(\int_\Omega \nabla \boldsymbol{\Phi}' \left[\boldsymbol{f}(\boldsymbol{x}) + \boldsymbol{g}(\boldsymbol{x})\boldsymbol{u}\right] \boldsymbol{\Phi}' d\Omega\right)^{-1}. \tag{4.26}$$

Similarly, for Algorithm 4.2 and considering the HJ equation (4.23), the procedure to obtain an approximated solution of $V_\infty(\boldsymbol{x})$, $\forall \boldsymbol{x} \in \Omega$, is conducted as follows. Initially, we

have that

$$\int_{\Omega}\Big[\Big(\frac{\partial \boldsymbol{\Phi}'\boldsymbol{c}}{\partial \boldsymbol{x}}\Big)'\big[\boldsymbol{f}(\boldsymbol{x})+\boldsymbol{g}(\boldsymbol{x})\boldsymbol{u}+\boldsymbol{k}(\boldsymbol{x})\boldsymbol{w}\big]+\frac{1}{2}(||\boldsymbol{z}||^2_{\boldsymbol{\sigma}_0}+||\dot{\boldsymbol{z}}||^2_{\boldsymbol{\sigma}_1}-\gamma^2||\boldsymbol{w}||^2)\Big]\boldsymbol{\Phi}'d\Omega=0, \tag{4.27}$$

leading to

$$\boldsymbol{c}'\int_{\Omega}\nabla\boldsymbol{\Phi}'\big[\boldsymbol{f}(\boldsymbol{x})+\boldsymbol{g}(\boldsymbol{x})\boldsymbol{u}+\boldsymbol{k}(\boldsymbol{x})\boldsymbol{w}\big]\boldsymbol{\Phi}'d\Omega=-\frac{1}{2}\int_{\Omega}(||\boldsymbol{z}||^2_{\boldsymbol{\sigma}_0}+||\dot{\boldsymbol{z}}||^2_{\boldsymbol{\sigma}_1}-\gamma^2||\boldsymbol{w}||^2)\boldsymbol{\Phi}'d\Omega. \tag{4.28}$$

Consequently, in this case the vector of coefficients $\boldsymbol{c}$ is obtained as

$$\boldsymbol{c}'=\Big(-\frac{1}{2}\int_{\Omega}(||\boldsymbol{z}||^2_{\boldsymbol{\sigma}_0}+||\dot{\boldsymbol{z}}||^2_{\boldsymbol{\sigma}_1}-\gamma^2||\boldsymbol{w}||^2)\boldsymbol{\Phi}'d\Omega\Big)\Big(\int_{\Omega}\nabla\boldsymbol{\Phi}'\big[\boldsymbol{f}(\boldsymbol{x})+\boldsymbol{g}(\boldsymbol{x})\boldsymbol{u}+\boldsymbol{k}(\boldsymbol{x})\boldsymbol{w}\big]\boldsymbol{\Phi}'d\Omega\Big)^{-1}. \tag{4.29}$$

Remark 21. *The finite set of basis functions must be selected to provide small approximation error in the domain of interest, ensuring convergence of the algorithms.*

In the a following section, equations (4.26) and (4.29) are computed with Algorithms 4.1 and 4.2 in order to design the nonlinear $\mathcal{W}_2$ and $\mathcal{W}_\infty$ controllers for a Two-wheeled Self-balanced vehicle.

4.4 Numerical examples

This section corroborates the efficacy of the nonlinear $\mathcal{W}_2$ and $\mathcal{W}_\infty$ controllers, by using Algorithms 4.1 and 4.2, via numerical experiments with a Two-wheeled Self-balanced vehicle. The objective is to keep the Two-wheeled Self-balanced vehicle standing in the upper vertical position, while it is subject to external disturbances.

The equations of motion of the Two-wheeled Self-balanced vehicle (see Figure 4.1) were obtained from (Madero et al., 2010; Raffo et al., 2015) and are given by the Euler-Lagrange equations

$$\boldsymbol{M}(\boldsymbol{q})\ddot{\boldsymbol{q}}+\boldsymbol{C}(\boldsymbol{q},\dot{\boldsymbol{q}})\dot{\boldsymbol{q}}+\boldsymbol{K}(\dot{\boldsymbol{q}})+\boldsymbol{G}(\boldsymbol{q})=\boldsymbol{F}(\boldsymbol{q})u+\boldsymbol{w}, \tag{4.30}$$

with

$$\boldsymbol{M}(\boldsymbol{q})=\begin{bmatrix}(M+m)r^2+I_r & mlr\cos(\theta)\\ mlr\cos(\theta) & ml^2+I_p\end{bmatrix},\quad \boldsymbol{q}=\begin{bmatrix}\phi\\ \theta\end{bmatrix},$$
$$\boldsymbol{C}(\boldsymbol{q},\dot{\boldsymbol{q}})=\begin{bmatrix}0 & -mlr\sin(\theta)\dot{\theta}\\ 0 & 0\end{bmatrix},\qquad \boldsymbol{K}(\dot{\boldsymbol{q}})=\begin{bmatrix}k\dot{\phi}\\ -k\dot{\phi}\end{bmatrix},$$
$$\boldsymbol{G}(\boldsymbol{q})=\begin{bmatrix}0\\ -mgl\sin(\theta)\end{bmatrix},\ \boldsymbol{F}(\boldsymbol{q})=\begin{bmatrix}1\\ -1\end{bmatrix},\ \boldsymbol{w}=\begin{bmatrix}w_\phi\\ w_\theta\end{bmatrix},$$

where $u\in\mathbb{R}$ is the torque applied on vehicles' wheels, $w_1, w_2\in\mathbb{R}$ are disturbances applied

to the system, m is the mass of the pendulum, M is the mass of the wheels, l is the distance from the axle to the pendulum center of mass, r is the wheel's radius, I_p is the pendulum moment of inertia, I_r is the inertia of the wheel, k is the static friction of the motor, and g is the gravity acceleration. The physical parameters used in the numerical simulations are presented in Table 4.1.

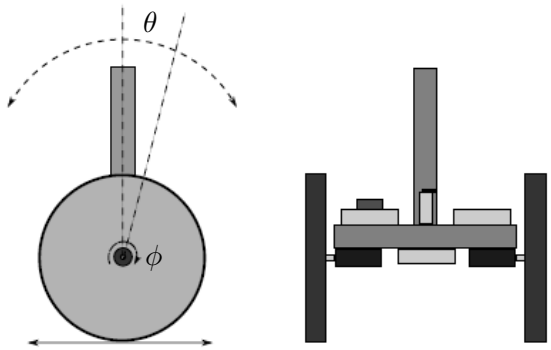

Figure 4.1: The Two-wheeled Self-balanced vehicle.

Table 4.1: Vehicle parameters.

Parameter	Value	Unit of Measure
I_r	0.0421	kg· m²
Ip	0.201	kg· m²
k	0.00215	N· m · s/rad
m	2.75	kg
M	3.75	kg
l	0.1435	m
r	0.25	m
g	9.8	m/s²

In order to design the nonlinear $\mathcal{W}_2$ and $\mathcal{W}_\infty$ controllers, initially, the Two-wheeled Self-balanced vehicle equations of motion (4.30) are represented in the state-space standard form (4.10), yielding

$$\boldsymbol{f}(\boldsymbol{x}) = \begin{bmatrix} \dot{\theta} \\ -\boldsymbol{M}^{-1}(\boldsymbol{q})\left[\boldsymbol{C}(\boldsymbol{q},\dot{\boldsymbol{q}})\dot{\boldsymbol{q}} + \boldsymbol{K}(\dot{\boldsymbol{q}}) + \boldsymbol{G}(\boldsymbol{q})\right] \end{bmatrix}, \boldsymbol{g}(\boldsymbol{x}) = \begin{bmatrix} 0 \\ \boldsymbol{M}^{-1}(\boldsymbol{q})\boldsymbol{F}(\boldsymbol{q}) \end{bmatrix}, \boldsymbol{k}(\boldsymbol{x}) = \begin{bmatrix} 0 & 0 \\ \boldsymbol{M}^{-1}(\boldsymbol{q}) \end{bmatrix},$$

with $\boldsymbol{x} = \begin{bmatrix} \theta & \dot{\phi} & \dot{\theta} \end{bmatrix}'$.

The controllers are designed by iterating Algorithms 4.1 and 4.2 and considering the Galerkin's approximations (4.26) and (4.29). A complete polynomial basis with degree four is used as basis functions, which is given by

$$\Phi(\boldsymbol{x}) = \begin{bmatrix} \theta & \dot{\phi} & \dot{\theta} & \dot{\phi}\theta & \theta\dot{\theta} & \dot{\phi}\dot{\theta} & \dot{\phi}^2 & \theta^2 & \dot{\theta}^2 & \cdots & \theta^4 & \dot{\phi}^4 & \dot{\theta}^4 \end{bmatrix}. \tag{4.31}$$

In order to decrease the computational time taken to obtain the solution, it is used the stopping criteria $||\boldsymbol{c}^{i-1} - \boldsymbol{c}^{i}||_2 < 0.1$.

The set Ω is the domain in which the approximation is valid, and it must be selected as the region of the state-space in which the system evolves with time. In this experiment, it is chosen as $\Omega = \theta_\Omega \times \dot{\phi}_\Omega \times \dot{\theta}_\Omega = [-\frac{\pi}{4}, \frac{\pi}{4}] \times [-3, 3] \times [-1.2, 1.2]$.

The integrals of domain, presented in (4.26) and (4.29), were computed using rectangular integration using the midpoint rule, which is illustrated in Figure 4.2, and computed as

$$\int_a^b \psi(\xi) d\xi = (b-a)\psi\left(\frac{b+a}{2}\right). \tag{4.32}$$

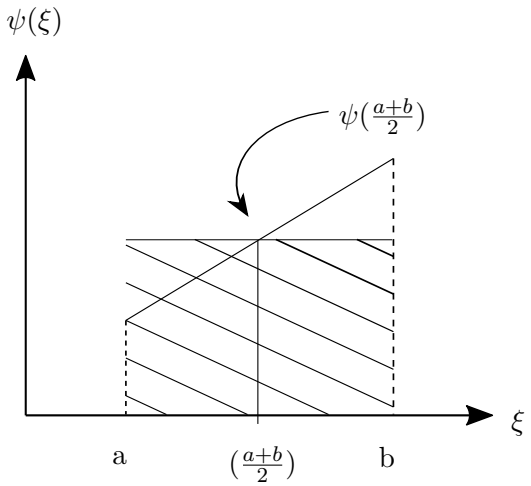

Figure 4.2: Gaussian Quadrature with one point.

In order to apply the Gaussian quadrature, the domain Ω is split in several squares with width $\Delta = 0.1$. The function is approximated as uncoupled, such that the following holds:

$$\int_a^b \int_c^d \int_e^f \psi(\theta, \dot{\phi}, \dot{\theta}) d\theta \; d\dot{\phi} \; d\dot{\theta} = \int_a^b \psi(\theta) d\theta \int_c^d \psi(\dot{\phi}) d\dot{\phi} \int_e^f \psi(\dot{\theta}) d\dot{\theta}. \tag{4.33}$$

During the iterations of Algorithms 4.1 and 4.2, the coefficients $\boldsymbol{c}$ of the Galerkin's method converge asymptotically to the solution (Beard and McLain, 1998).

In addition, a linear state feedback LQR controller was designed as the initial stabilizing control law for both controllers, which resulted in

$$u^{(0)} = \begin{bmatrix} 11.3132 & 1.0022 & 3.2589 \end{bmatrix} \boldsymbol{x}. \tag{4.34}$$

For comparison purposes, an $\mathcal{H}_\infty$ controller is designed through the SGAA presented in Beard and McLain (1998). The $\mathcal{W}_\infty$ and $\mathcal{H}_\infty$ attenuation levels were set as $\gamma = 5$. Besides, the controllers were tuned to provide almost the same settling time, using the criteria of 5%, as shown in Figure 4.3. This choice resulted in the following adjustments

$\boldsymbol{\sigma}_0 = \boldsymbol{I}$ and $\boldsymbol{\sigma}_1 = \text{diag}([0.64 \;\; 0.1 \;\; 0.1])$.

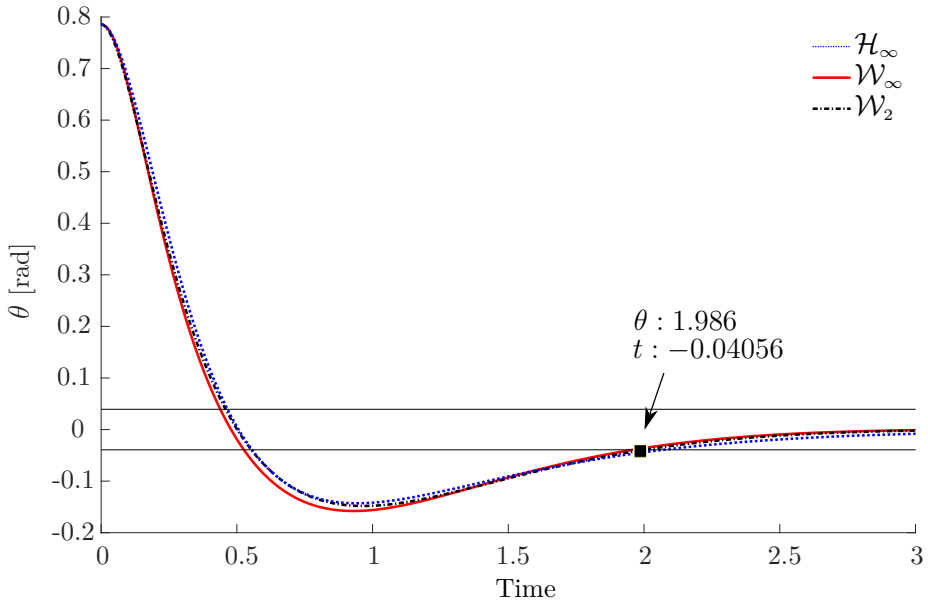

Figure 4.3: Settling time of the Two-wheeled Self-balanced vehicle, resulting from the application of the $\mathcal{H}_\infty$, $\mathcal{W}_\infty$ and $\mathcal{W}_2$ controllers.

The system was simulated starting from the initial condition $\boldsymbol{x}(0) = [\frac{\pi}{4} \;\; 0 \;\; 0]'$. The results are presented in Figure 4.4.

At the beginning, the pendulum starts displaced from the desired upper vertical position and asymptotically converges to it, remaining in this position until external disturbances $\boldsymbol{w}_\phi(t) = 1$ N·m, for $t \in [7, 14]$, and $\boldsymbol{w}_\theta(t) = 1$ N·m, for $t \in [22, 32]$, are applied to the wheels and to the pendulum, respectively. Due to the coupled dynamics of the system, the effects of external disturbances affect all states. Moreover, since the nonlinear $\mathcal{W}_2$ and $\mathcal{W}_\infty$ controllers considers the time derivative of the cost variable in the cost functional, they react faster to external disturbances than the $\mathcal{H}_\infty$ controller, presenting smaller overshoots with faster transients, as can be seen in Figures 4.4 and 4.5.

The control effort and the system error were evaluated by means of the Integral of the Absolute Derivative of the control signal (IADU) and the Integral of the Square Error (ISE) performance indexes, which are shown in Table 4.2. Note that, although the results do not present significant differences on states $\theta(t)$ and $\dot{\theta}(t)$, the $\mathcal{W}_\infty$ controller achieved considerable improvement on the angular velocity of the wheels with less control effort.

4.5 Final remarks

In this chapter, the nonlinear $\mathcal{W}_2$ and $\mathcal{W}_\infty$ control strategies were formulated in the weighted Sobolev space for autonomous nonlinear systems, and numerical algorithms were proposed to solve the resulting HJB and HJBI equations. The efficiency of these

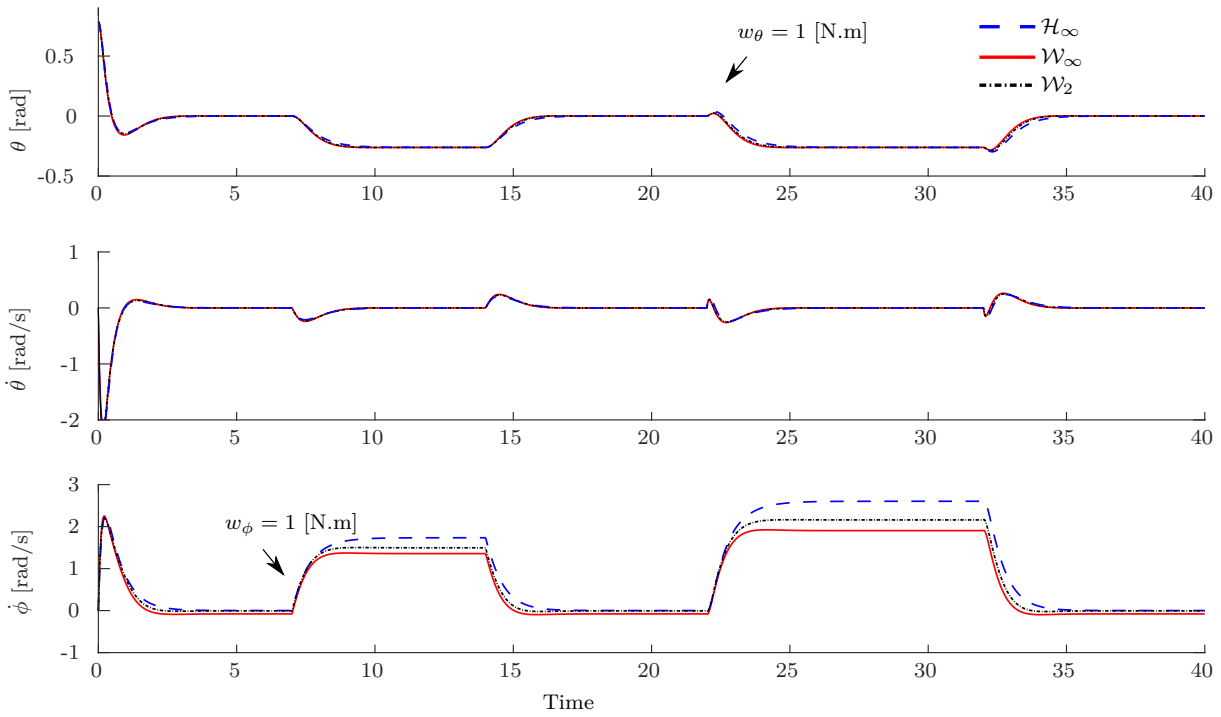

Figure 4.4: Time evolution of the states of the Two-wheeled Self-balanced vehicle, resulting from the application of the $\mathcal{H}_\infty$, $\mathcal{W}_\infty$ and $\mathcal{W}_2$ controllers.

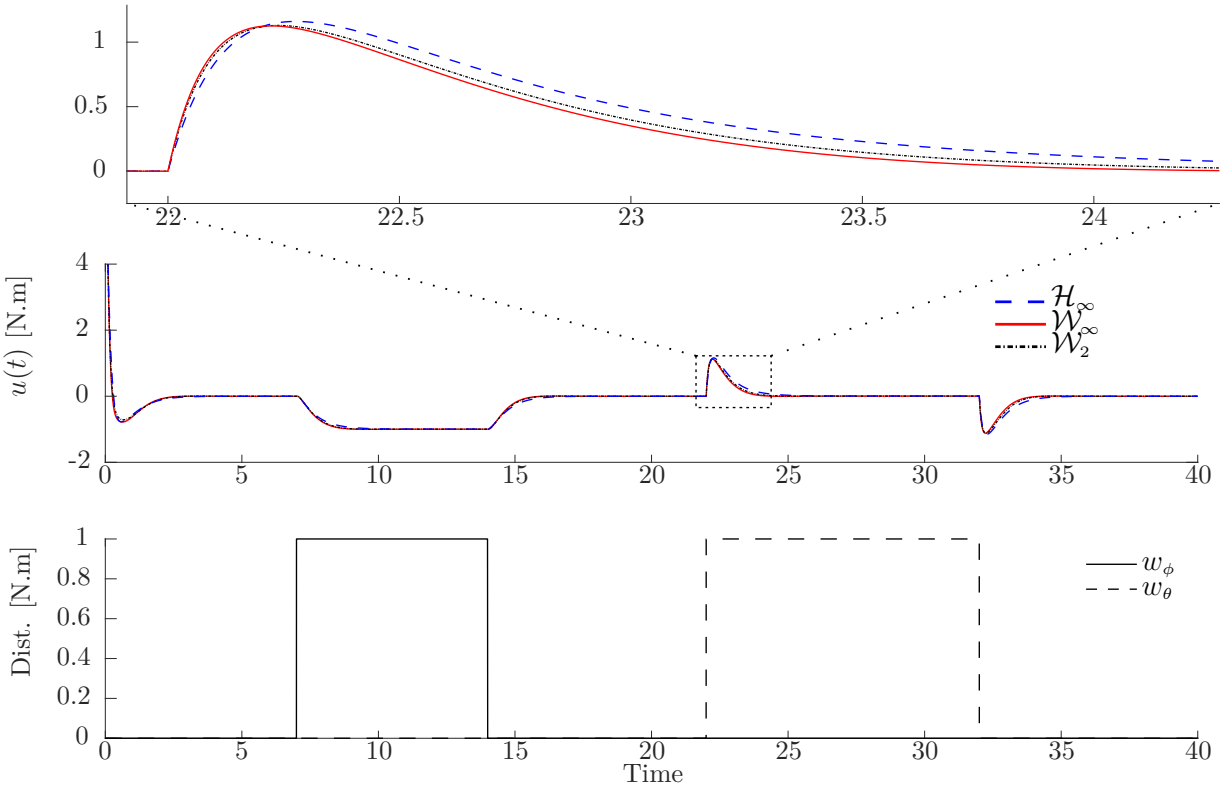

Figure 4.5: Control inputs, resulting from the application of the $\mathcal{H}_\infty$, $\mathcal{W}_\infty$, and $\mathcal{W}_2$ controllers to the Two-wheeled Self-balanced vehicle, and the disturbance signals.

controllers and numerical algorithms were demonstrated via numerical experiments conducted with a Two-wheeled Self-balanced vehicle, and comparison analysis were performed

Table 4.2: Table of performance indexes computed from the results of the $\mathcal{H}_\infty$, $\mathcal{W}_\infty$ and $\mathcal{W}_2$ controllers applied to the Two-wheeled Self-balanced vehicle.

P. Index	Computed by	$\mathcal{H}_\infty$	$\mathcal{W}_\infty$	$\mathcal{W}_2$
IADU	$\int_0^{t_f} \left\lvert \frac{du(t)}{dt} \right\rvert dt$	16.809 (100%)	**16.117** (95%)	18.1953 (108%)
ISE	$\int_0^{t_f} \theta^2(t)dt$	**1.199** (100%)	1.217 (101%)	1.2125 (101%)
	$\int_0^{t_f} \dot{\phi}^2(t)dt$	85.254 (100%)	**49.682** (58.2%)	61.8686 (72%)
	$\int_0^{t_f} \dot{\theta}^2(t)dt$	**1.604** (100%)	1.736 (108%)	1.6393 (102%)

with a nonlinear $\mathcal{H}_\infty$ controller. It was demonstrated that the $\mathcal{W}_2$ and $\mathcal{W}_\infty$ controllers provided better transient responses with smaller overshot, besides a faster reaction to external disturbances.

Unfortunately, the algorithms presented in this chapter depend on a feasible initial solution to be iterated, are limited to an admissible domain of the state-space, and suffer from the curse of dimensionality. Therefore, aiming to propose analytical solutions to the resulting HJ equations, in the next chapter the $\mathcal{W}_2$ and $\mathcal{W}_\infty$ control strategies are particularized for the class of mechanical systems described by the Euler-Lagrange equations.

5

Nonlinear $\mathcal{W}_2$ and $\mathcal{W}_\infty$ control of mechanical systems

This chapter proposes new formulations of the nonlinear $\mathcal{H}_2$ and $\mathcal{H}_\infty$ optimal control approaches in weighted Sobolev spaces in order to handle two classes of underactuated mechanical systems: the reduced ones, aiming achieve trajectory tracking of a reduced number of DOF; and the underactuated mechanical systems with input coupling, in order to drive the controlled DOF along a desired trajectory while stabilizing the remaining ones. Additionally, to improve the closed-loop performance with robustness against parametric uncertainties and constant disturbances, an integral action is considered in the problem formulation. The optimal control problems are formulated via dynamic-programming and particular solutions are presented for the resulting Hamilton-Jacobi equations with the corresponding stability analysis. Also, the concepts of $\mathcal{W}_{m,p,\boldsymbol{\sigma}}$-stability and $\mathcal{W}_{m,p,\boldsymbol{\sigma}}$-gain for a general class of systems are established, with the demonstration for the particular case studies. The novel $\mathcal{W}_2$ and $\mathcal{W}_\infty$ controllers are synthesized for a fully actuated manipulator, a Two-wheeled Self-balanced vehicle, and a Quadrotor UAV. The results demonstrate that these controllers provide better transient performance with faster response against external disturbances in comparison with a classic nonlinear $\mathcal{H}_\infty$ controller, in addition to have a simple design. The content presented in this chapter was published in Cardoso et al. (2021a).

5.1 Control of fully actuated and reduced underactuated mechanical systems

The development in this Chapter is conducted by considering mechanical systems represented by the Euler-Lagrange equations in the canonical form (Spong et al., 2006)

$$\boldsymbol{M}(\boldsymbol{q})\ddot{\boldsymbol{q}}(t) + \boldsymbol{C}(\boldsymbol{q},\dot{\boldsymbol{q}})\dot{\boldsymbol{q}}(t) + \boldsymbol{g}(\boldsymbol{q}) = \boldsymbol{B}(\boldsymbol{q},\dot{\boldsymbol{q}})\boldsymbol{\tau}(t) + \boldsymbol{w}(t), \tag{5.1}$$

where $\boldsymbol{q}(t) : \mathbb{R}_{\geq 0} \to \mathbb{R}^{n_q}$ is the vector of generalized coordinates, $\boldsymbol{M}(\boldsymbol{q}) : \mathbb{R}^{n_q} \to \mathbb{R}^{n_q \times n_q}$ is the inertia matrix, $\boldsymbol{C}(\boldsymbol{q},\dot{\boldsymbol{q}}) : (\mathbb{R}^{n_q} \times \mathbb{R}^{n_q}) \to \mathbb{R}^{n_q \times n_q}$ is the Coriolis and centripetal forces matrix, $\boldsymbol{g}(\boldsymbol{q}) : \mathbb{R}^{n_q} \to \mathbb{R}^{n_q}$ is the gravitational force vector, $\boldsymbol{B}(\boldsymbol{q},\dot{\boldsymbol{q}}) : (\mathbb{R}^{n_q} \times \mathbb{R}^{n_q}) \to \mathbb{R}^{n_q \times n_\tau}$ is the input coupling matrix, $\boldsymbol{\tau}(t) : \mathbb{R}_{\geq 0} \to \mathbb{R}^{n_\tau}$ is the control input vector, and $\boldsymbol{w}(t) : \mathbb{R}_{\geq 0} \to \mathbb{R}^{n_q}$ is the vector of generalized disturbances.

In the case of underactuated mechanical systems (See Definition 6 in Section 3.5), it is well known that no more than n_τ DOF can be controlled (i.e. to be regulated at a desired position or to track a reference trajectory) simultaneously through the control inputs, since the system has fewer manipulated variables than DOF. Due to the inability of performing simultaneous tracking of all DOF, for control design purposes, in this section we partition the system (5.1) in controlled and uncontrolled DOF as follows (Raffo, 2011),

$$\underbrace{\begin{bmatrix} \boldsymbol{M}_{uu}(\boldsymbol{q}) & \boldsymbol{M}_{uc}(\boldsymbol{q}) \\ \boldsymbol{M}_{cu}(\boldsymbol{q}) & \boldsymbol{M}_{cc}(\boldsymbol{q}) \end{bmatrix}}_{\boldsymbol{M}(\boldsymbol{q})} \underbrace{\begin{bmatrix} \ddot{\boldsymbol{q}}_u \\ \ddot{\boldsymbol{q}}_c \end{bmatrix}}_{\ddot{\boldsymbol{q}}(t)} + \underbrace{\begin{bmatrix} \boldsymbol{C}_{uu}(\boldsymbol{q},\dot{\boldsymbol{q}}) & \boldsymbol{C}_{uc}(\boldsymbol{q},\dot{\boldsymbol{q}}) \\ \boldsymbol{C}_{cu}(\boldsymbol{q},\dot{\boldsymbol{q}}) & \boldsymbol{C}_{cc}(\boldsymbol{q},\dot{\boldsymbol{q}}) \end{bmatrix}}_{\boldsymbol{C}(\boldsymbol{q},\dot{\boldsymbol{q}})} \underbrace{\begin{bmatrix} \dot{\boldsymbol{q}}_u \\ \dot{\boldsymbol{q}}_c \end{bmatrix}}_{\dot{\boldsymbol{q}}(t)} + \underbrace{\begin{bmatrix} \boldsymbol{g}_u(\boldsymbol{q}) \\ \boldsymbol{g}_c(\boldsymbol{q}) \end{bmatrix}}_{\boldsymbol{g}(\boldsymbol{q})} = \underbrace{\begin{bmatrix} \boldsymbol{B}_u(\boldsymbol{q},\dot{\boldsymbol{q}}) \\ \boldsymbol{B}_c(\boldsymbol{q},\dot{\boldsymbol{q}}) \end{bmatrix}}_{\boldsymbol{B}(\boldsymbol{q},\dot{\boldsymbol{q}})} \boldsymbol{\tau} + \underbrace{\begin{bmatrix} \boldsymbol{w}_u \\ \boldsymbol{w}_c \end{bmatrix}}_{\boldsymbol{w}(t)}, \tag{5.2}$$

in which $\boldsymbol{q}(t) = [\boldsymbol{q}_u'(t) \;\; \boldsymbol{q}_c'(t)]'$, where $\boldsymbol{q}_u(t) : \mathbb{R}_{\geq 0} \to (\mathbb{R}^{n_q - n_\tau} = \mathbb{R}^{n_u})$ corresponds to the uncontrolled DOF and $\boldsymbol{q}_c(t) : \mathbb{R}_{\geq 0} \to \mathbb{R}^{n_\tau}$ corresponds to the controlled ones.

Considering this partition, it is possible to deal only with the controlled DOF. Therefore, from the first row of (5.2), we have

$$\ddot{\boldsymbol{q}}_u = -\boldsymbol{M}_{uu}^{-1}\boldsymbol{M}_{uc}\ddot{\boldsymbol{q}}_c - \boldsymbol{M}_{uu}^{-1}\boldsymbol{C}_{uu}\ddot{\boldsymbol{q}}_u - \boldsymbol{M}_{uu}^{-1}\boldsymbol{C}_{uc}\dot{\boldsymbol{q}}_c - \boldsymbol{M}_{uu}^{-1}\boldsymbol{G}_u + \boldsymbol{M}_{uu}^{-1}\boldsymbol{B}_u\boldsymbol{\tau} + \boldsymbol{M}_{uu}^{-1}\boldsymbol{w}_u. \tag{5.3}$$

By replacing $\ddot{\boldsymbol{q}}_u$ in the second row of (5.2), yields to

$$\begin{aligned} \boldsymbol{M}_{cu}(-\boldsymbol{M}_{uu}^{-1}\boldsymbol{M}_{uc}\ddot{\boldsymbol{q}}_c - \boldsymbol{M}_{uu}^{-1}\boldsymbol{C}_{uu}\dot{\boldsymbol{q}}_u - \boldsymbol{M}_{uu}^{-1}\boldsymbol{C}_{uc}\dot{\boldsymbol{q}}_c - \boldsymbol{M}_{uu}^{-1}\boldsymbol{g}_u + \boldsymbol{M}_{uu}^{-1}\boldsymbol{B}_u\boldsymbol{\tau} + \boldsymbol{M}_{uu}^{-1}\boldsymbol{w}_u) \\ + \boldsymbol{M}_{cc}\ddot{\boldsymbol{q}}_c + \boldsymbol{C}_{cu}\dot{\boldsymbol{q}}_u + \boldsymbol{C}_{cc}\dot{\boldsymbol{q}}_c + \boldsymbol{g}_c = \boldsymbol{B}_c\boldsymbol{\tau} + \boldsymbol{w}_c. \end{aligned} \tag{5.4}$$

Then, the equations of motion that describe the dynamics of the controlled DOF, here

called the reduced underactuated mechanical system, are written as

$$\bar{\boldsymbol{M}}(\boldsymbol{q})\ddot{\boldsymbol{q}}_c(t) + \bar{\boldsymbol{C}}(\boldsymbol{q},\dot{\boldsymbol{q}})\dot{\boldsymbol{q}}_c(t) + \bar{\boldsymbol{e}}(\boldsymbol{q},\dot{\boldsymbol{q}}) = \bar{\boldsymbol{B}}(\boldsymbol{q},\dot{\boldsymbol{q}})\boldsymbol{\tau}(t) + \bar{\boldsymbol{\delta}}(t), \tag{5.5}$$

where $\bar{\boldsymbol{M}}(\boldsymbol{q}) \triangleq \boldsymbol{M}_{cc} - \boldsymbol{M}_{cu}\boldsymbol{M}_{uu}^{-1}\boldsymbol{M}_{uc}$, $\bar{\boldsymbol{C}}(\boldsymbol{q},\dot{\boldsymbol{q}}) \triangleq \boldsymbol{C}_{cc} - \boldsymbol{M}_{cu}\boldsymbol{M}_{uu}^{-1}\boldsymbol{C}_{uc}$, $\bar{\boldsymbol{e}}(\boldsymbol{q},\dot{\boldsymbol{q}}) \triangleq \boldsymbol{g}_c - \boldsymbol{M}_{cu}\boldsymbol{M}_{uu}^{-1}\boldsymbol{g}_u + (\boldsymbol{C}_{cu} - \boldsymbol{M}_{cu}\boldsymbol{M}_{uu}^{-1}\boldsymbol{C}_{uu})\dot{\boldsymbol{q}}_u$, $\bar{\boldsymbol{B}}(\boldsymbol{q},\dot{\boldsymbol{q}}) = \boldsymbol{B}_c - \boldsymbol{M}_{cu}\boldsymbol{M}_{uu}^{-1}\boldsymbol{B}_u$, and $\bar{\boldsymbol{\delta}}(t) \triangleq \boldsymbol{w}_c + \boldsymbol{M}_{cu}\boldsymbol{M}_{uu}^{-1}\boldsymbol{w}_u$.

Accordingly, the system (5.2) must be partitioned such that the following assumption holds for the reduced underactuated mechanical system (5.5).

Assumption 5. *The matrix $\bar{\boldsymbol{B}}(\boldsymbol{q},\dot{\boldsymbol{q}})$ is invertible, i.e. $rank(\bar{\boldsymbol{B}}(\boldsymbol{q},\dot{\boldsymbol{q}})) = n_\tau$, $\forall(\boldsymbol{q},\dot{\boldsymbol{q}}) \in \Omega \subseteq (\mathbb{R}^{n_q} \times \mathbb{R}^{n_q})$.*

Remark 22. *The control approaches presented in this section are developed for reduced underactuated mechanical systems described by (5.8). It is assumed the remaining uncontrolled DOF have stable dynamics or are input to state stable with respect to $\boldsymbol{q}_c$; hence, they can be stabilized through an additional control strategy imposed on the time evolution of $\boldsymbol{q}_c(t)$.*

Remark 23. *Regarding a fully-actuated mechanical system (See Definition 5), the controlled DOF are given by $\boldsymbol{q}_c = \boldsymbol{q}$, yielding $\bar{\boldsymbol{M}}(\boldsymbol{q}) = \boldsymbol{M}(\boldsymbol{q})$, $\bar{\boldsymbol{C}}(\boldsymbol{q},\dot{\boldsymbol{q}}) = \boldsymbol{C}(\boldsymbol{q},\dot{\boldsymbol{q}})$, $\bar{\boldsymbol{e}}(\boldsymbol{q},\dot{\boldsymbol{q}}) = \boldsymbol{g}(\boldsymbol{q})$, $\bar{\boldsymbol{B}}(\boldsymbol{q},\dot{\boldsymbol{q}}) = \boldsymbol{B}(\boldsymbol{q},\dot{\boldsymbol{q}})$, and $\bar{\boldsymbol{\delta}}(t) = \boldsymbol{w}(t)$. Consequently, (5.5) becomes equal to (5.1). Then, the approaches presented in this section are also valid for fully-actuated mechanical systems.*

Additionally, aiming to perform trajectory tracking, the error dynamics can be written as

$$\begin{aligned}\bar{\boldsymbol{M}}(\tilde{\boldsymbol{q}}_c + \boldsymbol{q}_{cr}, \boldsymbol{q}_u)(\ddot{\tilde{\boldsymbol{q}}}_c + \ddot{\boldsymbol{q}}_{cr}) + \bar{\boldsymbol{C}}(\tilde{\boldsymbol{q}}_c + \boldsymbol{q}_{cr}, \dot{\tilde{\boldsymbol{q}}}_c + \dot{\boldsymbol{q}}_{cr}, \boldsymbol{q}_u, \dot{\boldsymbol{q}}_u)(\dot{\tilde{\boldsymbol{q}}}_c + \dot{\boldsymbol{q}}_{cr}) \\ + \bar{\boldsymbol{e}}(\tilde{\boldsymbol{q}}_c + \boldsymbol{q}_{cr}, \dot{\tilde{\boldsymbol{q}}}_c + \dot{\boldsymbol{q}}_{cr}, \boldsymbol{q}_u, \dot{\boldsymbol{q}}_u) = \bar{\boldsymbol{B}}(\tilde{\boldsymbol{q}}_c + \boldsymbol{q}_{cr}, \dot{\tilde{\boldsymbol{q}}}_c + \dot{\boldsymbol{q}}_{cr}, \boldsymbol{q}_u, \dot{\boldsymbol{q}}_u)\boldsymbol{\tau} + \bar{\boldsymbol{\delta}}(t),\end{aligned} \tag{5.6}$$

with $\tilde{\boldsymbol{q}}_c(t) \triangleq \boldsymbol{q}_c(t) - \boldsymbol{q}_{cr}(t)$, and $\boldsymbol{q}_{cr}(t)$, $\dot{\boldsymbol{q}}_{cr}(t)$ and $\ddot{\boldsymbol{q}}_{cr}(t)$ being the desired values of the controlled DOF and their time derivatives, in which $\boldsymbol{q}_{cr}(t) \in \mathcal{C}^2$.

Besides, given the state vector $\boldsymbol{x}(t) : \mathbb{R}_{\geq 0} \to \mathbb{R}^{n_x}$, with

$$\boldsymbol{x}(t) \triangleq [\dot{\tilde{\boldsymbol{q}}}_c'(t)\ \tilde{\boldsymbol{q}}_c'(t)\ \int_0^t \tilde{\boldsymbol{q}}_c'(\tau)d\tau]', \tag{5.7}$$

in which an integral action is considered over the error of the controlled DOF to provide parametric uncertainty and constant disturbance rejection capability for the closed-loop system, equation (5.6) can be represented in the state-space form as

$$\dot{\boldsymbol{x}}(t) = \underbrace{\begin{bmatrix} -\bar{\boldsymbol{M}}^{-1}\bar{\boldsymbol{C}} & \boldsymbol{0} & \boldsymbol{0} \\ \boldsymbol{I} & \boldsymbol{0} & \boldsymbol{0} \\ \boldsymbol{0} & \boldsymbol{I} & \boldsymbol{0} \end{bmatrix}}_{\boldsymbol{f}(\boldsymbol{x},\boldsymbol{q}_u,\dot{\boldsymbol{q}}_u)} \boldsymbol{x}(t) + \underbrace{\begin{bmatrix} -\bar{\boldsymbol{M}}^{-1}\bar{\boldsymbol{d}} \\ \boldsymbol{0} \\ \boldsymbol{0} \end{bmatrix}}_{\bar{\boldsymbol{f}}(\boldsymbol{x},\boldsymbol{q}_u,\dot{\boldsymbol{q}}_u,t)} + \underbrace{\begin{bmatrix} \bar{\boldsymbol{M}}^{-1}\bar{\boldsymbol{B}} \\ \boldsymbol{0} \\ \boldsymbol{0} \end{bmatrix}}_{\boldsymbol{g}(\boldsymbol{x},\boldsymbol{q}_u,\dot{\boldsymbol{q}}_u)} \boldsymbol{\tau}(t) + \underbrace{\begin{bmatrix} \bar{\boldsymbol{M}}^{-1} \\ \boldsymbol{0} \\ \boldsymbol{0} \end{bmatrix}}_{\boldsymbol{k}(\boldsymbol{x},\boldsymbol{q}_u,\dot{\boldsymbol{q}}_u)} \bar{\boldsymbol{\delta}}(t), \tag{5.8}$$

where $\bar{\boldsymbol{d}} \triangleq \bar{\boldsymbol{M}}(\tilde{\boldsymbol{q}}_c + \boldsymbol{q}_{cr}, \boldsymbol{q}_u)\ddot{\boldsymbol{q}}_{cr}(t) + \bar{\boldsymbol{C}}(\tilde{\boldsymbol{q}}_c + \boldsymbol{q}_{cr}, \dot{\tilde{\boldsymbol{q}}}_c + \dot{\boldsymbol{q}}_{cr}, \boldsymbol{q}_u, \dot{\boldsymbol{q}}_u)\dot{\boldsymbol{q}}_{cr}(t) + \bar{\boldsymbol{e}}(\tilde{\boldsymbol{q}}_c + \boldsymbol{q}_{cr}, \dot{\tilde{\boldsymbol{q}}}_c + \dot{\boldsymbol{q}}_{cr}, \boldsymbol{q}_u, \dot{\boldsymbol{q}}_u)$, and $\boldsymbol{I}$ and $\boldsymbol{0}$ are the identity and zeros matrices, respectively, with appropriate dimensions.

5.1.1 Nonlinear $\mathcal{W}_2$ control approach

In order to derive the nonlinear $\mathcal{W}_2$ optimal control law, the following standard form is obtained from (5.8), considering no disturbances affecting the system ($\bar{\boldsymbol{\delta}}(t) = \boldsymbol{0}$),

$$\mathcal{P}_3 : \begin{cases} \dot{\boldsymbol{x}}(t) = \boldsymbol{f}(\boldsymbol{x}, \boldsymbol{q}_u, \dot{\boldsymbol{q}}_u) + \bar{\boldsymbol{f}}(\boldsymbol{x}, \boldsymbol{q}_u, \dot{\boldsymbol{q}}_u, t) + \boldsymbol{g}(\boldsymbol{x}, \boldsymbol{q}_u, \dot{\boldsymbol{q}}_u)\boldsymbol{\tau}(t), \\ \boldsymbol{z}(t) = \int_0^t \tilde{\boldsymbol{q}}_c(\tau)d\tau, \end{cases} \tag{5.9}$$

in which $\boldsymbol{z}(t)$ is the cost variable, chosen in order to ensure that all states and the system dynamics are included in the cost functional.

The nonlinear $\mathcal{W}_2$ controller is designed in order to obtain a control law $\boldsymbol{\tau}(\boldsymbol{x}, \boldsymbol{q}_u, \dot{\boldsymbol{q}}_u, t)$ that minimizes the cost functional

$$\begin{aligned} J_2 &= \frac{1}{2}||\boldsymbol{z}(t)||^2_{\mathcal{W}_{3,2,\boldsymbol{\mathcal{Y}}}}, \\ &= \frac{1}{2}\int_0^\infty \left(||\boldsymbol{z}(t)||^2_{\boldsymbol{\mathcal{Y}}_0} + ||\dot{\boldsymbol{z}}(t)||^2_{\boldsymbol{\mathcal{Y}}_1} + ||\ddot{\boldsymbol{z}}(t)||^2_{\boldsymbol{\mathcal{Y}}_2} + ||\dddot{\boldsymbol{z}}(t)||^2_{\boldsymbol{\mathcal{Y}}_3}\right) dt, \end{aligned} \tag{5.10}$$

where $||(\cdot)||^2_{\boldsymbol{\mathcal{Y}}_i} \triangleq (\cdot)'\boldsymbol{\mathcal{Y}}_i(\cdot)$, with $\boldsymbol{\mathcal{Y}}_i$, for $i \in \{0,\ 1,\ 2,\ 3\}$, being a symmetric positive definite tuning matrix, that weights the influence of the states in the control objective.

Remark 24. *In (5.10), the weighted Sobolev norm takes into account tree time-derivatives of the cost variable $\boldsymbol{z}(t)$. The objective is to include the dynamics of the system, i.e. $\dddot{\tilde{\boldsymbol{q}}}_c$, in the cost functional.*

Hence, the optimal control problem is stated as finding $\boldsymbol{\tau}^*(\boldsymbol{x}, \boldsymbol{q}_u, \dot{\boldsymbol{q}}_u, t)$ that leads to

$$\begin{aligned} \boldsymbol{V}_2 = &\min_{\boldsymbol{\tau}\in\mathcal{U}} \frac{1}{2}||\boldsymbol{z}(t)||^2_{\mathcal{W}_{3,2,\boldsymbol{\mathcal{Y}}}}\ , \\ &\text{s.t.}\ \ \mathcal{P}_3, \end{aligned} \tag{5.11}$$

with $\mathcal{U} : (\mathbb{R}^{n_x} \times \mathbb{R}^{n_u} \times \mathbb{R}^{n_u} \times \mathbb{R}_{\geq 0}) \to \mathbb{R}^{n_\tau}$. The goal is to provide a smooth decay of the error between the generalized coordinates (as well as their time derivatives) and their references over time.

Remark 25. *The presence of the time derivatives of the cost variable into the cost functional (5.10) provides improved transient performance for the closed-loop system.*

Remark 26. *In contrast to the nonlinear $\mathcal{H}_2$ and $\mathcal{H}_\infty$ control approaches for mechanical systems (Johansson, 1990; Chen et al., 1994; Feng and Postlethwaite, 1993; Raffo et al., 2011a), the proposed $\mathcal{W}_2$ and $\mathcal{W}_\infty$ controllers do not include the control inputs directly in the cost functional, which relaxes the requirement that $\tau(t) \in \mathcal{L}_2[0, \infty)$. In addition, this*

relaxation allows formulating the control problem without any prior compensation of the gravity vector and the terms related to the desired trajectory.

Remark 27. *In the nonlinear $\mathcal{W}_2$ and $\mathcal{W}_\infty$ control approaches the control inputs are not weighted directly in the optimizing index. The transient and steady-state performance are reached by tuning component-wise the influence of the cost variable and its time derivatives into the cost functional.*

Therefore, aiming to solve (5.11), it is formulated via dynamic-programming (Kirk, 2004), the associated Hamiltonian is given by

$$\mathbb{H}_2 = \frac{\partial' \boldsymbol{V}_2}{\partial \boldsymbol{x}} \dot{\boldsymbol{x}} + \frac{1}{2} \boldsymbol{z}' \boldsymbol{\mathcal{Y}}_0 \boldsymbol{z} + \frac{1}{2} \dot{\boldsymbol{z}}' \boldsymbol{\mathcal{Y}}_1 \dot{\boldsymbol{z}} + \frac{1}{2} \ddot{\boldsymbol{z}}' \boldsymbol{\mathcal{Y}}_2 \ddot{\boldsymbol{z}} + \frac{1}{2} \dddot{\boldsymbol{z}}' \boldsymbol{\mathcal{Y}}_3 \dddot{\boldsymbol{z}}, \tag{5.12}$$

with the boundary condition $\boldsymbol{V}_2(\boldsymbol{0}, t) = 0$. Expanding (5.12) with (5.9) yields

$$\begin{aligned} \mathbb{H}_2 = \frac{\partial' \boldsymbol{V}_2}{\partial \boldsymbol{x}} \Big(\boldsymbol{f}(\boldsymbol{x}, \boldsymbol{q}_u, \dot{\boldsymbol{q}}_u, t) + \bar{\boldsymbol{f}}(\boldsymbol{x}, \boldsymbol{q}_u, \dot{\boldsymbol{q}}_u, t) + \boldsymbol{g}(\boldsymbol{x}, \boldsymbol{q}_u, t) \boldsymbol{\tau} \Big) + \frac{1}{2} \boldsymbol{x}' \begin{bmatrix} \boldsymbol{\mathcal{Y}}_2 & \boldsymbol{0} & \boldsymbol{0} \\ \boldsymbol{0} & \boldsymbol{\mathcal{Y}}_1 & \boldsymbol{0} \\ \boldsymbol{0} & \boldsymbol{0} & \boldsymbol{\mathcal{Y}}_0 \end{bmatrix} \boldsymbol{x} \\ + \frac{1}{2} \Big[\dot{\tilde{\boldsymbol{q}}}_c' \bar{\boldsymbol{C}}' \Pi \bar{\boldsymbol{C}} \dot{\tilde{\boldsymbol{q}}}_c + 2 \dot{\tilde{\boldsymbol{q}}}_c' \bar{\boldsymbol{C}}' \Pi \bar{\boldsymbol{d}} - 2 \boldsymbol{\tau}' \bar{\boldsymbol{B}}' \Pi \bar{\boldsymbol{C}} \dot{\tilde{\boldsymbol{q}}}_c - 2 \boldsymbol{\tau}' \bar{\boldsymbol{B}}' \Pi \bar{\boldsymbol{d}} + \boldsymbol{\tau}' \bar{\boldsymbol{B}}' \Pi \bar{\boldsymbol{B}} \boldsymbol{\tau} + \bar{\boldsymbol{d}}' \Pi \bar{\boldsymbol{d}} \Big], \end{aligned} \tag{5.13}$$

where $\Pi \triangleq \bar{\boldsymbol{M}}^{-1} \boldsymbol{\mathcal{Y}}_3 \bar{\boldsymbol{M}}^{-1}$. The HJB equation is obtained from (5.11) using the Hamiltonian (5.13), which in a compact form is given by

$$\frac{\partial \boldsymbol{V}_2(\boldsymbol{x}, t)}{\partial t} + \min_{\boldsymbol{\tau} \in \mathcal{U}} \{ \mathbb{H}_2(\boldsymbol{V}_2, \boldsymbol{x}, \boldsymbol{q}_u, \dot{\boldsymbol{q}}_u, \boldsymbol{\tau}, t) \} = 0. \tag{5.14}$$

The optimal control law $\boldsymbol{\tau}^*(\boldsymbol{x}, \boldsymbol{q}_u, \dot{\boldsymbol{q}}_u, t)$ can be obtained by minimizing the Hamiltonian (5.13) with respect to $\boldsymbol{\tau}$ as follows

$$\frac{\partial \mathbb{H}_2}{\partial \boldsymbol{\tau}} = \boldsymbol{g}' \frac{\partial \boldsymbol{V}_2}{\partial \boldsymbol{x}} - \bar{\boldsymbol{B}}' \Pi \bar{\boldsymbol{C}} \dot{\tilde{q}}_c - \bar{\boldsymbol{B}}' \Pi \bar{\boldsymbol{d}} + \bar{\boldsymbol{B}}' \Pi \bar{\boldsymbol{B}} \boldsymbol{\tau}^* = 0, \tag{5.15}$$

leading to

$$\boldsymbol{\tau}^* = \bar{\boldsymbol{B}}^{-1} \bar{\boldsymbol{M}} \Big(\begin{bmatrix} -\boldsymbol{\mathcal{Y}}_3^{-1} & \boldsymbol{0} & \boldsymbol{0} \end{bmatrix} \frac{\partial \boldsymbol{V}_2}{\partial \boldsymbol{x}} + \bar{\boldsymbol{M}}^{-1} \bar{\boldsymbol{C}} \dot{\tilde{\boldsymbol{q}}}_c + \bar{\boldsymbol{M}}^{-1} \bar{\boldsymbol{d}} \Big). \tag{5.16}$$

This is indeed a minimum value of the optimization problem, since $\dfrac{\partial^2 \mathbb{H}_\infty}{\partial \boldsymbol{\tau}^2} = \bar{\boldsymbol{B}}' \Pi \bar{\boldsymbol{B}} > 0$.

The HJ equation associated with the problem is obtained by replacing the optimal control law (5.16) in (5.13), and considering the time-varying nonlinear system (5.9),

$$\frac{\partial \boldsymbol{V}_2(\boldsymbol{x}, t)}{\partial t} + \mathbb{H}_2(\boldsymbol{V}_2, \boldsymbol{x}, \boldsymbol{q}_u, \dot{\boldsymbol{q}}_u, \boldsymbol{\tau}^*, t) = 0. \tag{5.17}$$

A particular solution $\boldsymbol{V}_2(\boldsymbol{x}, t)$ of the HJ equation (5.17) is proposed in the following theorem.

Theorem 1. *Let $\boldsymbol{V}_2$ be the parameterized scalar function*

$$\boldsymbol{V}_2(\boldsymbol{x}) = \frac{1}{2}\boldsymbol{x}' \begin{bmatrix} \boldsymbol{Q} & \boldsymbol{K} & \boldsymbol{T} \\ \boldsymbol{K} & \boldsymbol{R} & \boldsymbol{S} \\ \boldsymbol{T} & \boldsymbol{S} & \boldsymbol{P} \end{bmatrix} \boldsymbol{x} > 0, \tag{5.18}$$

such that the matrices $\boldsymbol{Q}$, $\boldsymbol{K}$, $\boldsymbol{T}$, $\boldsymbol{R}$, $\boldsymbol{S}$, and $\boldsymbol{P}$ are positive definite and verify $\boldsymbol{Q}-\boldsymbol{K}\boldsymbol{R}^{-1}\boldsymbol{K} > 0$ and $\begin{bmatrix} \boldsymbol{Q} & \boldsymbol{K} \\ \boldsymbol{K} & \boldsymbol{R} \end{bmatrix} - \begin{bmatrix} \boldsymbol{T} \\ \boldsymbol{S} \end{bmatrix} \boldsymbol{P}^{-1} \begin{bmatrix} \boldsymbol{T} & \boldsymbol{S} \end{bmatrix} > 0$, with $\boldsymbol{T}$, $\boldsymbol{Q}$, and $\boldsymbol{K}$ obtained by solving the following Riccati equations

$$-\boldsymbol{T}\boldsymbol{\mathcal{Y}}_3^{-1}\boldsymbol{T} + \boldsymbol{\mathcal{Y}}_0 = \boldsymbol{0}, \tag{5.19}$$

$$-\boldsymbol{Q}\boldsymbol{\mathcal{Y}}_3^{-1}\boldsymbol{Q}+2\boldsymbol{K}+\boldsymbol{\mathcal{Y}}_2 = \boldsymbol{0}, \tag{5.20}$$

$$-\boldsymbol{K}\boldsymbol{\mathcal{Y}}_3^{-1}\boldsymbol{K}+2\boldsymbol{Q}\boldsymbol{\mathcal{Y}}_3^{-1}\boldsymbol{T} + \boldsymbol{\mathcal{Y}}_1 = \boldsymbol{0}, \tag{5.21}$$

and $\boldsymbol{R}$, $\boldsymbol{S}$, and $\boldsymbol{P}$, are given by

$$\boldsymbol{R} = \boldsymbol{Q}\boldsymbol{\mathcal{Y}}_3^{-1}\boldsymbol{K} - \boldsymbol{T}, \tag{5.22}$$

$$\boldsymbol{S} = \boldsymbol{Q}\boldsymbol{\mathcal{Y}}_3^{-1}\boldsymbol{T}, \tag{5.23}$$

$$\boldsymbol{P} = \boldsymbol{K}\boldsymbol{\mathcal{Y}}_3^{-1}\boldsymbol{T}. \tag{5.24}$$

Then, function $\boldsymbol{V}_2(\boldsymbol{x})$ is a solution of the HJ equation (5.17).

Proof. The proof is conducted by replacing (5.18) in (5.17) and using the properties of the inertia matrix. In the following the computation is performed by parts. Consider the HJ equation (5.17). Since (5.18) is a time-invariant function, we have that $\dfrac{\partial \boldsymbol{V}_2}{\partial t} = 0$, and (5.17) results in

$$\frac{\partial' \boldsymbol{V}_2}{\partial \boldsymbol{x}}\dot{\boldsymbol{x}} + \frac{1}{2}\boldsymbol{x}' \begin{bmatrix} \boldsymbol{\mathcal{Y}}_2 & \boldsymbol{0} & \boldsymbol{0} \\ \boldsymbol{0} & \boldsymbol{\mathcal{Y}}_1 & \boldsymbol{0} \\ \boldsymbol{0} & \boldsymbol{0} & \boldsymbol{\mathcal{Y}}_0 \end{bmatrix} \boldsymbol{x} + \frac{1}{2}\ddot{\tilde{\boldsymbol{q}}}_c' \boldsymbol{\mathcal{Y}}_3 \ddot{\tilde{\boldsymbol{q}}}_c = 0. \tag{5.25}$$

In addition, considering the candidate solution (5.18), the optimal control law (5.16) is given by

$$\boldsymbol{\tau}^* = \bar{\boldsymbol{B}}^{-1}\Big(\begin{bmatrix} -\bar{\boldsymbol{M}}\boldsymbol{\mathcal{Y}}_3^{-1}\boldsymbol{Q} & -\bar{\boldsymbol{M}}\boldsymbol{\mathcal{Y}}_3^{-1}\boldsymbol{K} & -\bar{\boldsymbol{M}}\boldsymbol{\mathcal{Y}}_3^{-1}\boldsymbol{T} \end{bmatrix} \boldsymbol{x} + \bar{\boldsymbol{C}}\dot{\tilde{\boldsymbol{q}}}_c + \bar{\boldsymbol{d}} \Big), \tag{5.26}$$

which leads to the following acceleration error dynamics

$$\begin{aligned} \ddot{\tilde{\boldsymbol{q}}}_c &= -\bar{\boldsymbol{M}}^{-1}\bar{\boldsymbol{C}}\dot{\tilde{\boldsymbol{q}}}_c - \bar{\boldsymbol{M}}^{-1}\bar{\boldsymbol{d}} + \bar{\boldsymbol{M}}^{-1}\bar{\boldsymbol{B}}\boldsymbol{\tau}^*, \\ &= \begin{bmatrix} -\boldsymbol{\mathcal{Y}}_3^{-1}\boldsymbol{Q} & -\boldsymbol{\mathcal{Y}}_3^{-1}\boldsymbol{K} & -\boldsymbol{\mathcal{Y}}_3^{-1}\boldsymbol{T} \end{bmatrix} \boldsymbol{x}. \end{aligned}$$

Accordingly, the closed-loop dynamics are given by

$$\dot{\boldsymbol{x}} = \begin{bmatrix} -\boldsymbol{\mathcal{Y}}_3^{-1}\boldsymbol{Q} & -\boldsymbol{\mathcal{Y}}_3^{-1}\boldsymbol{K} & -\boldsymbol{\mathcal{Y}}_3^{-1}\boldsymbol{T} \\ \boldsymbol{I} & \boldsymbol{0} & \boldsymbol{0} \\ \boldsymbol{0} & \boldsymbol{I} & \boldsymbol{0} \end{bmatrix} \boldsymbol{x}, \tag{5.27}$$

which is a closed-loop time-invariant system. Then, by replacing (5.27) in the first term of (5.25) yields

$$\frac{\partial' \boldsymbol{V}_2}{\partial \boldsymbol{x}} \dot{\boldsymbol{x}} = \boldsymbol{x}' \begin{bmatrix} -\boldsymbol{Q}\boldsymbol{\mathcal{Y}}_3^{-1}\boldsymbol{Q} + \boldsymbol{K} & -\boldsymbol{Q}\boldsymbol{\mathcal{Y}}_3^{-1}\boldsymbol{K} + \boldsymbol{T} & -\boldsymbol{Q}\boldsymbol{\mathcal{Y}}_3^{-1}\boldsymbol{T} \\ -\boldsymbol{K}\boldsymbol{\mathcal{Y}}_3^{-1}\boldsymbol{Q} + \boldsymbol{R} & -\boldsymbol{K}\boldsymbol{\mathcal{Y}}_3^{-1}\boldsymbol{K} + \boldsymbol{S} & -\boldsymbol{K}\boldsymbol{\mathcal{Y}}_3^{-1}\boldsymbol{T} \\ -\boldsymbol{T}\boldsymbol{\mathcal{Y}}_3^{-1}\boldsymbol{Q} + \boldsymbol{S} & -\boldsymbol{T}\boldsymbol{\mathcal{Y}}_3^{-1}\boldsymbol{K} + \boldsymbol{P} & -\boldsymbol{T}\boldsymbol{\mathcal{Y}}_3^{-1}\boldsymbol{T} \end{bmatrix} \boldsymbol{x}. \tag{5.28}$$

Moreover, the last term of (5.25) is computed as

$$\frac{1}{2}\ddot{\tilde{\boldsymbol{q}}}' \boldsymbol{Y}_3 \ddot{\tilde{\boldsymbol{q}}} = \frac{1}{2}\boldsymbol{x}' \begin{bmatrix} \boldsymbol{Q}\boldsymbol{\mathcal{Y}}_3^{-1}\boldsymbol{Q} & \boldsymbol{Q}\boldsymbol{\mathcal{Y}}_3^{-1}\boldsymbol{K} & \boldsymbol{Q}\boldsymbol{\mathcal{Y}}_3^{-1}\boldsymbol{T} \\ \boldsymbol{K}\boldsymbol{\mathcal{Y}}_3^{-1}\boldsymbol{Q} & \boldsymbol{K}\boldsymbol{\mathcal{Y}}_3^{-1}\boldsymbol{K} & \boldsymbol{K}\boldsymbol{\mathcal{Y}}_3^{-1}\boldsymbol{T} \\ \boldsymbol{T}\boldsymbol{\mathcal{Y}}_3^{-1}\boldsymbol{Q} & \boldsymbol{T}\boldsymbol{\mathcal{Y}}_3^{-1}\boldsymbol{K} & \boldsymbol{T}\boldsymbol{\mathcal{Y}}_3^{-1}\boldsymbol{T} \end{bmatrix} \boldsymbol{x}. \tag{5.29}$$

Thus, considering (5.28) and (5.29), the HJ equation (5.25) results in

$$\boldsymbol{x}'\boldsymbol{N}\boldsymbol{x} = \boldsymbol{x}' \begin{bmatrix} \boldsymbol{N}_{11} & \boldsymbol{N}_{12} & \boldsymbol{N}_{13} \\ \boldsymbol{N}_{21} & \boldsymbol{N}_{22} & \boldsymbol{N}_{23} \\ \boldsymbol{N}_{31} & \boldsymbol{N}_{32} & \boldsymbol{N}_{33} \end{bmatrix} \boldsymbol{x} = 0, \tag{5.30}$$

with $\boldsymbol{N}_{11} \triangleq -\frac{1}{2}\boldsymbol{Q}\boldsymbol{\mathcal{Y}}_3^{-1}\boldsymbol{Q} + \boldsymbol{K} + \frac{1}{2}\boldsymbol{\mathcal{Y}}_2$, $\boldsymbol{N}_{12} \triangleq -\frac{1}{2}\boldsymbol{Q}\boldsymbol{\mathcal{Y}}_3^{-1}\boldsymbol{K} + \boldsymbol{T}$, $\boldsymbol{N}_{13} \triangleq -\frac{1}{2}\boldsymbol{Q}\boldsymbol{\mathcal{Y}}_3^{-1}\boldsymbol{T}$, $\boldsymbol{N}_{21} \triangleq -\frac{1}{2}\boldsymbol{K}\boldsymbol{\mathcal{Y}}_3^{-1}\boldsymbol{Q} + \boldsymbol{R}$, $\boldsymbol{N}_{22} \triangleq -\frac{1}{2}\boldsymbol{K}\boldsymbol{\mathcal{Y}}_3^{-1}\boldsymbol{K} + \boldsymbol{S} + \frac{1}{2}\boldsymbol{\mathcal{Y}}_1$, $\boldsymbol{N}_{23} \triangleq -\frac{1}{2}\boldsymbol{K}\boldsymbol{\mathcal{Y}}_3^{-1}\boldsymbol{T}$, $\boldsymbol{N}_{31} \triangleq -\frac{1}{2}\boldsymbol{T}\boldsymbol{\mathcal{Y}}_3^{-1}\boldsymbol{Q} + \boldsymbol{S}$, $\boldsymbol{N}_{32} \triangleq -\frac{1}{2}\boldsymbol{T}\boldsymbol{\mathcal{Y}}_3^{-1}\boldsymbol{K} + \boldsymbol{P}$, $\boldsymbol{N}_{33} \triangleq -\frac{1}{2}\boldsymbol{T}\boldsymbol{\mathcal{Y}}_3^{-1}\boldsymbol{T} + \frac{1}{2}\boldsymbol{\mathcal{Y}}_0$.

The matrix $\boldsymbol{N}$ is decomposed by its symmetric and skew-symmetric components, resulting in

$$\frac{1}{2}\boldsymbol{x}'(\boldsymbol{N} + \boldsymbol{N}')\boldsymbol{x} = \boldsymbol{x}' \begin{bmatrix} \boldsymbol{A}_{11} & \boldsymbol{A}_{12} & \boldsymbol{A}_{13} \\ * & \boldsymbol{A}_{22} & \boldsymbol{A}_{23} \\ * & * & \boldsymbol{A}_{33} \end{bmatrix} \boldsymbol{x} = 0, \tag{5.31}$$

where the * terms indicate the corresponding symmetric block matrix component. One way to satisfy (5.31) is by solving the following set of algebraic Riccati equations

$$\boldsymbol{A}_{11} = -\boldsymbol{Q}\boldsymbol{\mathcal{Y}}_3^{-1}\boldsymbol{Q} + 2\boldsymbol{K} + \boldsymbol{\mathcal{Y}}_2 = \boldsymbol{0}, \tag{5.32}$$

$$\boldsymbol{A}_{12} = -\boldsymbol{Q}\boldsymbol{\mathcal{Y}}_3^{-1}\boldsymbol{K} + \boldsymbol{T} + \boldsymbol{R} = \boldsymbol{0}, \tag{5.33}$$

$$\boldsymbol{A}_{13} = -\boldsymbol{Q}\boldsymbol{\mathcal{Y}}_3^{-1}\boldsymbol{T} + \boldsymbol{S} = \boldsymbol{0}, \tag{5.34}$$

$$\boldsymbol{A}_{22} = -\boldsymbol{K}\boldsymbol{\mathcal{Y}}_3^{-1}\boldsymbol{K}+2\boldsymbol{S}+\boldsymbol{\mathcal{Y}}_1 = \boldsymbol{0}, \tag{5.35}$$

$$\boldsymbol{A}_{23} = -\boldsymbol{K}\boldsymbol{\mathcal{Y}}_3^{-1}\boldsymbol{T}+\boldsymbol{P} = \boldsymbol{0}, \tag{5.36}$$

$$\boldsymbol{A}_{33} = -\boldsymbol{T}\boldsymbol{\mathcal{Y}}_3^{-1}\boldsymbol{T}+\boldsymbol{\mathcal{Y}}_0 = \boldsymbol{0}. \tag{5.37}$$

Firstly, $\boldsymbol{T}$ is computed by solving (5.37). Afterwards, equations (5.22), (5.23) and (5.24) are obtained through (5.33), (5.34), and (5.36), respectively. Finally, $\boldsymbol{Q}$ and $\boldsymbol{K}$ are computed through (5.32) and (5.35) by solving the following pair of cross-coupled Riccati equations

$$-\boldsymbol{Q}\boldsymbol{\mathcal{Y}}_3^{-1}\boldsymbol{Q}+2\boldsymbol{K}+\boldsymbol{\mathcal{Y}}_2 = \boldsymbol{0}, \tag{5.38}$$

$$-\boldsymbol{K}\boldsymbol{\mathcal{Y}}_3^{-1}\boldsymbol{K}+2\boldsymbol{Q}\boldsymbol{\mathcal{Y}}_3^{-1}\boldsymbol{T}+\boldsymbol{\mathcal{Y}}_1 = \boldsymbol{0}. \tag{5.39}$$

Thus, with the solutions of (5.32)-(5.37), we conclude the proof. □

Furthermore, the stability of the closed-loop system (5.27) is verified by the following Theorem.

Theorem 2. *Let $\boldsymbol{V}_2(\boldsymbol{x}) > 0$ be a solution of (5.17) given by the parameterized scalar function (5.18). Therefore, the closed-loop system, formed by the control law (5.16) and system (5.9), is asymptotically stable within the domain Ω.*

Proof. From (5.17) and (5.18) we have that

$$\frac{d\boldsymbol{V}_2}{dt} = -\frac{1}{2}\boldsymbol{z}'\boldsymbol{\mathcal{Y}}_0\boldsymbol{z} - \frac{1}{2}\dot{\boldsymbol{z}}'\boldsymbol{\mathcal{Y}}_1\dot{\boldsymbol{z}} - \frac{1}{2}\ddot{\boldsymbol{z}}'\boldsymbol{\mathcal{Y}}_2\ddot{\boldsymbol{z}} - \frac{1}{2}\dddot{\boldsymbol{z}}'\boldsymbol{\mathcal{Y}}_3\dddot{\boldsymbol{z}}, \tag{5.40}$$

$$= -\frac{1}{2}\boldsymbol{x}'\begin{bmatrix} \boldsymbol{Q}\boldsymbol{\mathcal{Y}}_3^{-1}\boldsymbol{Q}+\boldsymbol{\mathcal{Y}}_2 & \boldsymbol{Q}\boldsymbol{\mathcal{Y}}_3^{-1}\boldsymbol{K} & \boldsymbol{Q}\boldsymbol{\mathcal{Y}}_3^{-1}\boldsymbol{T} \\ \boldsymbol{K}\boldsymbol{\mathcal{Y}}_3^{-1}\boldsymbol{Q} & \boldsymbol{K}\boldsymbol{\mathcal{Y}}_3^{-1}\boldsymbol{K}+\boldsymbol{\mathcal{Y}}_1 & \boldsymbol{K}\boldsymbol{\mathcal{Y}}_3^{-1}\boldsymbol{T} \\ \boldsymbol{T}\boldsymbol{\mathcal{Y}}_3^{-1}\boldsymbol{Q} & \boldsymbol{T}\boldsymbol{\mathcal{Y}}_3^{-1}\boldsymbol{K} & \boldsymbol{T}\boldsymbol{\mathcal{Y}}_3^{-1}\boldsymbol{T}+\boldsymbol{\mathcal{Y}}_0 \end{bmatrix}\boldsymbol{x}, \tag{5.41}$$

$$= -\frac{1}{2}\boldsymbol{x}'\boldsymbol{G}\boldsymbol{x}, \tag{5.42}$$

where

$$\boldsymbol{G} = \boldsymbol{\Lambda}_1\begin{bmatrix} \boldsymbol{\mathcal{Y}}_3^{-1} & \boldsymbol{\mathcal{Y}}_3^{-1} & \boldsymbol{\mathcal{Y}}_3^{-1} \\ \boldsymbol{\mathcal{Y}}_3^{-1} & \boldsymbol{\mathcal{Y}}_3^{-1} & \boldsymbol{\mathcal{Y}}_3^{-1} \\ \boldsymbol{\mathcal{Y}}_3^{-1} & \boldsymbol{\mathcal{Y}}_3^{-1} & \boldsymbol{\mathcal{Y}}_3^{-1} \end{bmatrix}\boldsymbol{\Lambda}_1 + \begin{bmatrix} \boldsymbol{\mathcal{Y}}_2 & \boldsymbol{0} & \boldsymbol{0} \\ \boldsymbol{0} & \boldsymbol{\mathcal{Y}}_1 & \boldsymbol{0} \\ \boldsymbol{0} & \boldsymbol{0} & \boldsymbol{\mathcal{Y}}_0 \end{bmatrix}, \tag{5.43}$$

with $\boldsymbol{\Lambda}_1 \triangleq \text{blkdiag}(\boldsymbol{Q}, \boldsymbol{K}, \boldsymbol{T})$, and blkdiag$(\cdot)$ represents a block diagonal matrix whose diagonal elements are square matrices given in parentheses, and all off-diagonal blocks are zero matrices. Matrix (5.43) is composed of two terms, where the first is positive semi-definite and the second is positive definite, yielding $\boldsymbol{G} > 0$. Then, $\dot{\boldsymbol{V}}_2(\boldsymbol{x}) < 0$, which ensures asymptotic stability for the closed-loop system in the Lyapunov sense. Accordingly, from

(5.42) we have that

$$\begin{aligned}\int_0^\infty \frac{d\boldsymbol{V}_2(\boldsymbol{x})}{dt}dt &= \lim_{t\to\infty}\boldsymbol{V}_2(\boldsymbol{x}(t)) - \boldsymbol{V}_2(\boldsymbol{x}(0)),\\ &= -\int_0^\infty \frac{1}{2}\boldsymbol{x}'(t)\boldsymbol{G}\boldsymbol{x}(t)\mathrm{dt}\\ &= -\frac{1}{2}||\boldsymbol{z}(t)||^2_{\mathcal{W}_{3,2,\boldsymbol{\mathcal{Y}}}} = -c_1,\end{aligned} \tag{5.44}$$

where $\boldsymbol{x}(0)$ is the value of the states $\boldsymbol{x}$ at the time instant $t = 0$, and $c_1 \in \mathbb{R}_{\geq 0}$. Then, the $\mathcal{W}_{3,2,\boldsymbol{\mathcal{Y}}}$ weighted Sobolev norm of the cost variable exists and is finite, consequently $\lim_{t\to\infty}\boldsymbol{x}(t) = \boldsymbol{0}$. □

5.1.2 Nonlinear $\mathcal{W}_\infty$ control approach

Consider again system (5.8), from which the following compact standard form is obtained

$$\mathcal{P}_4\!:\!\begin{cases}\dot{\boldsymbol{x}}(t) = \boldsymbol{f}(\boldsymbol{x},\boldsymbol{q}_u,\dot{\boldsymbol{q}}_u)+\bar{\boldsymbol{f}}(\boldsymbol{x},\boldsymbol{q}_u,\dot{\boldsymbol{q}}_u,t) + \boldsymbol{g}(\boldsymbol{x},\boldsymbol{q}_u,\dot{\boldsymbol{q}}_u)\boldsymbol{\tau}(t)+\boldsymbol{k}(\boldsymbol{x},\boldsymbol{q}_u)\bar{\boldsymbol{\delta}}(t),\\ \boldsymbol{z}(t) = \int_0^t \tilde{\boldsymbol{q}}_c(\tau)d\tau,\end{cases} \tag{5.45}$$

with $\boldsymbol{z}(t)$ being the cost variable. The nonlinear $\mathcal{W}_\infty$ control in the weighted Sobolev space is posed in order to achieve the control law $\boldsymbol{\tau}(\boldsymbol{x},\boldsymbol{q}_u,\dot{\boldsymbol{q}}_u,t)$ that minimizes the following cost functional

$$\mathcal{J}_\infty = \frac{1}{2}||\boldsymbol{z}(t)||^2_{\mathcal{W}_{3,2,\boldsymbol{\mathcal{Y}}}} - \frac{1}{2}\gamma^2||\bar{\boldsymbol{\delta}}(t)||^2_{\mathcal{L}_2}, \tag{5.46}$$

for the worst case of the disturbances $\bar{\boldsymbol{\delta}}(t) \in \mathcal{L}_2[0,\infty)$, considering a given sufficiently large $\mathcal{W}_\infty$-index $\gamma \in \mathbb{R}_{\geq 0}$, where $||\bar{\boldsymbol{\delta}}(t)||^2_{\mathcal{L}_2} = \int_0^\infty \bar{\boldsymbol{\delta}}'(t)\bar{\boldsymbol{\delta}}(t)\ dt$.

Remark 28. *It is assumed that the time derivatives of the disturbance vector are unknown, and because of that, only the $\mathcal{L}_2$-norm of the disturbance vector is considered into the cost functional* (5.46).

Therefore, the optimization problem is posed as

$$\begin{aligned}\boldsymbol{V}_\infty = &\min_{\boldsymbol{\tau}\in\mathcal{U}}\max_{\bar{\boldsymbol{\delta}}\in\mathcal{D}}\left\{\frac{1}{2}||\boldsymbol{z}(t)||^2_{\mathcal{W}_{3,2,\boldsymbol{\mathcal{Y}}}} - \frac{1}{2}\gamma^2||\bar{\boldsymbol{\delta}}(t)||^2_{\mathcal{L}_2}\right\},\\ &\text{s.t.}\quad \mathcal{P}_4,\end{aligned} \tag{5.47}$$

with $\mathcal{U} : (\mathbb{R}^{n_x}\times\mathbb{R}^{n_u}\times\mathbb{R}^{n_u}\times\mathbb{R}_{\geq 0}) \to \mathbb{R}^{n_\tau}$ and $\mathcal{D} = \mathcal{L}_2[0,\infty)$. The goal is to provide trajectory tracking for the controlled DOF while being robust against external disturbances, unmodeled dynamics, and parametric uncertainties.

The control law is obtained by solving a Min-Max optimization problem, which can be formulated via dynamic programming, using differential game theory. The HJBI

(Hamilton-Jacobi-Bellman-Isaacs) equation associated to this problem is

$$\frac{\partial \boldsymbol{V}_\infty}{\partial t} + \min_{\boldsymbol{\tau}\in\mathcal{U}} \max_{\bar{\boldsymbol{\delta}}\in\mathcal{D}} \{\mathbb{H}_\infty(\boldsymbol{V}_\infty, \boldsymbol{q}_u, \dot{\boldsymbol{q}}_u, \boldsymbol{x}, \boldsymbol{\tau}, \bar{\boldsymbol{\delta}}, t)\} = 0, \tag{5.48}$$

with the Hamiltonian

$$\mathbb{H}_\infty \triangleq \frac{\partial' \boldsymbol{V}_\infty}{\partial \boldsymbol{x}} \dot{\boldsymbol{x}} + \frac{1}{2}\left(\boldsymbol{z}'\boldsymbol{\mathcal{Y}}_0\boldsymbol{z} + \dot{\boldsymbol{z}}'\boldsymbol{\mathcal{Y}}_1\dot{\boldsymbol{z}} + \ddot{\boldsymbol{z}}'\boldsymbol{\mathcal{Y}}_2\ddot{\boldsymbol{z}} + \dddot{\boldsymbol{z}}'\boldsymbol{\mathcal{Y}}_3\dddot{\boldsymbol{z}} - \gamma^2\bar{\boldsymbol{\delta}}'\bar{\boldsymbol{\delta}}\right), \tag{5.49}$$

and boundary condition $\boldsymbol{V}_\infty(\boldsymbol{0}, t) = 0$. The equation (5.49), in its expanded form, is written as

$$\begin{aligned}\mathbb{H}_\infty = {} & \frac{\partial' \boldsymbol{V}_\infty}{\partial \boldsymbol{x}}\left(\boldsymbol{f}(\boldsymbol{x}, \boldsymbol{q}_u, \dot{\boldsymbol{q}}_u, t) + \bar{\boldsymbol{f}}(\boldsymbol{x}, \boldsymbol{q}_u, \dot{\boldsymbol{q}}_u, t) + \boldsymbol{g}(\boldsymbol{x}, \boldsymbol{q}_u, t)\boldsymbol{\tau}\right) + \frac{1}{2}\boldsymbol{x}'\begin{bmatrix}\boldsymbol{\mathcal{Y}}_2 & \boldsymbol{0} & \boldsymbol{0}\\ \boldsymbol{0} & \boldsymbol{\mathcal{Y}}_1 & \boldsymbol{0}\\ \boldsymbol{0} & \boldsymbol{0} & \boldsymbol{\mathcal{Y}}_0\end{bmatrix}\boldsymbol{x} - \frac{1}{2}\gamma^2\bar{\boldsymbol{\delta}}'\bar{\boldsymbol{\delta}} \\ & + \frac{1}{2}\Big[\dot{\bar{\boldsymbol{q}}}_c'\bar{\boldsymbol{C}}'\Pi\bar{\boldsymbol{C}}\dot{\bar{\boldsymbol{q}}}_c + 2\dot{\bar{\boldsymbol{q}}}_c'\bar{\boldsymbol{C}}'\Pi\bar{\boldsymbol{d}} - 2\boldsymbol{\tau}'\bar{\boldsymbol{B}}'\Pi\bar{\boldsymbol{C}}\dot{\bar{\boldsymbol{q}}}_c - 2\boldsymbol{\tau}'\bar{\boldsymbol{B}}'\Pi\bar{\boldsymbol{d}} \\ & + \boldsymbol{\tau}'\bar{\boldsymbol{B}}'\Pi\bar{\boldsymbol{B}}\boldsymbol{\tau} + \bar{\boldsymbol{d}}'\Pi\bar{\boldsymbol{d}} - 2\dot{\bar{\boldsymbol{q}}}_c'\bar{\boldsymbol{C}}'\Pi\bar{\boldsymbol{\delta}} - 2\bar{\boldsymbol{d}}'\Pi\bar{\boldsymbol{\delta}} + 2\boldsymbol{\tau}'\bar{\boldsymbol{B}}'\Pi\bar{\boldsymbol{\delta}} + \bar{\boldsymbol{\delta}}'\Pi\bar{\boldsymbol{\delta}}\Big].\end{aligned} \tag{5.50}$$

The optimal control law, $\boldsymbol{\tau}^*$, and the worst case of the disturbances, $\bar{\boldsymbol{\delta}}^*$, are obtained by computing the partial derivatives of (5.50) with respect to these variables and equaling them to zero as follows

$$\frac{\partial \mathbb{H}_\infty}{\partial \boldsymbol{\tau}} = \boldsymbol{g}'\frac{\partial \boldsymbol{V}_\infty}{\partial \boldsymbol{x}} - \bar{\boldsymbol{B}}'\Pi\bar{\boldsymbol{C}}\dot{\bar{\boldsymbol{q}}} - \bar{\boldsymbol{B}}'\Pi\bar{\boldsymbol{d}} + \bar{\boldsymbol{B}}'\Pi\bar{\boldsymbol{\delta}}^* + \bar{\boldsymbol{B}}'\Pi\bar{\boldsymbol{B}}\boldsymbol{\tau}^* = 0, \tag{5.51}$$

$$\frac{\partial \mathbb{H}_\infty}{\partial \bar{\boldsymbol{\delta}}} = \boldsymbol{k}'\frac{\partial \boldsymbol{V}_\infty}{\partial \boldsymbol{x}} - \Pi\bar{\boldsymbol{C}}\dot{\bar{\boldsymbol{q}}} - \Pi\bar{\boldsymbol{d}} + \Pi\bar{\boldsymbol{B}}\boldsymbol{\tau}^* + \Pi\bar{\boldsymbol{\delta}}^* - \gamma^2\bar{\boldsymbol{\delta}}^* = 0. \tag{5.52}$$

Thus, considering (5.51), the optimal control law is given by

$$\boldsymbol{\tau}^* = -(\bar{\boldsymbol{B}}'\Pi\bar{\boldsymbol{B}})^{-1}\boldsymbol{g}'\frac{\partial \boldsymbol{V}_\infty}{\partial \boldsymbol{x}} + \bar{\boldsymbol{B}}\bar{\boldsymbol{C}}\dot{\bar{\boldsymbol{q}}} + \bar{\boldsymbol{B}}\bar{\boldsymbol{d}} - \bar{\boldsymbol{B}}\bar{\boldsymbol{\delta}}^*. \tag{5.53}$$

In addition, the worst case of the disturbances can be computed by premultiplying both sides of (5.52) by $\bar{\boldsymbol{B}}'(\boldsymbol{q}, \dot{\boldsymbol{q}})$, and using (5.53), which yields

$$\bar{\boldsymbol{\delta}}^* = \frac{(\bar{\boldsymbol{B}}')^{-1}}{\gamma^2}(\boldsymbol{k}\bar{\boldsymbol{B}} - \boldsymbol{g})'\frac{\partial \boldsymbol{V}_\infty}{\partial \boldsymbol{x}}. \tag{5.54}$$

Furthermore, through the second order partial derivatives of (5.50), which are given by

$$\frac{\partial^2 \mathbb{H}_\infty}{\partial \boldsymbol{\tau}^2} = \bar{\boldsymbol{B}}'\Pi\bar{\boldsymbol{B}} > 0, \tag{5.55}$$

$$\frac{\partial^2 \mathbb{H}_\infty}{\partial \bar{\boldsymbol{\delta}}^2} = \Pi - \gamma^2\boldsymbol{I} < 0, \tag{5.56}$$

it can be verified that (5.53) and (5.54) are a Min-Max extremum of the optimization

problem for a sufficiently large γ.

Remark 29. *The $\mathcal{W}_\infty$-index γ must be selected appropriately such that the inequality (5.56) holds, ensuring feasibility to the optimization problem.*

The HJ PDE associated to this problem is obtained by replacing the optimal control law (5.53) and the worst case of the disturbances (5.54) in (5.48), yielding

$$\frac{\partial \boldsymbol{V}_\infty(\boldsymbol{x},t)}{\partial t} + \mathbb{H}_\infty(\boldsymbol{V}_\infty, \boldsymbol{x}, \boldsymbol{\tau}^*, \bar{\boldsymbol{\delta}}^*, t) = 0. \tag{5.57}$$

Therefore, the optimal control problem (5.47) results in finding a function $\boldsymbol{V}_\infty(\boldsymbol{x},t)$ that solves (5.57).

Remark 30. *For the particular case of interest (see (5.8)) $\boldsymbol{k}\bar{\boldsymbol{B}} = \boldsymbol{g}$ in (5.54), which leads the $\mathcal{W}_2$ and $\mathcal{W}_\infty$ controllers being equivalent. Therefore, the particular solution proposed in Theorem 1 is also a solution to (5.57).*

The stability of the closed-loop system is stated in the following Theorem.

Theorem 3. *Let $\boldsymbol{V}_\infty(\boldsymbol{x}) > 0$ be a solution of (5.57) given by the parameterized scalar function (5.18). Therefore, the closed-loop system, with the control law (5.53) and system (5.45), is asymptotically stable.*

Proof. From (5.57) and (5.18) we have that

$$\begin{aligned}\frac{d\boldsymbol{V}_\infty(\boldsymbol{x})}{dt} &= -\frac{1}{2}\boldsymbol{z}'\boldsymbol{\mathcal{Y}}_0\boldsymbol{z} - \frac{1}{2}\dot{\boldsymbol{z}}'\boldsymbol{\mathcal{Y}}_1\dot{\boldsymbol{z}} - \frac{1}{2}\ddot{\boldsymbol{z}}'\boldsymbol{\mathcal{Y}}_2\ddot{\boldsymbol{z}} - \frac{1}{2}\dddot{\boldsymbol{z}}'\boldsymbol{\mathcal{Y}}_3\dddot{\boldsymbol{z}} + \frac{1}{2}\gamma^2\bar{\boldsymbol{\delta}}^{*\prime}\bar{\boldsymbol{\delta}}^*, \\ &= -\frac{1}{2}\boldsymbol{x}'\boldsymbol{G}\boldsymbol{x} + \frac{1}{2}\gamma^2\bar{\boldsymbol{\delta}}^{*\prime}\bar{\boldsymbol{\delta}}^*,\end{aligned} \tag{5.58}$$

where $\boldsymbol{G} > 0$ is given by (5.43). In addition, from (5.8) in which $\boldsymbol{k}\bar{\boldsymbol{B}} = \boldsymbol{g}$, the worst case of the disturbances is $\bar{\boldsymbol{\delta}}^*(t) = \boldsymbol{0}$ (see (5.54)). This implies that $\dot{\boldsymbol{V}}_\infty(\boldsymbol{x}) < 0$, ensuring asymptotic stability for the closed-loop system in the Lyapunov sense. Consequently, similarly to (5.44), the $\mathcal{W}_{3,2,\boldsymbol{\mathcal{Y}}}$ weighted Sobolev norm of the cost variable exists and is finite, which implies that $\lim_{t\to\infty}\boldsymbol{x}(t) = \boldsymbol{0}$. □

In the following we extend the definitions of $\mathcal{L}_q$-stability and $\mathcal{L}_q$-gain (van der Schaft, 2000) and also of $\mathcal{W}$-stability and $\mathcal{W}$-gain (Bourles and Colledani, 1995), considering the weighted Sobolev norm.

Definition 7. *Suppose $\bar{\boldsymbol{\delta}}(t) : \mathbb{R}_{\geq 0} \to \mathbb{R}^{n_q}$, $\boldsymbol{z}(t) : \mathbb{R}_{\geq 0} \to \mathbb{R}^{n_\tau}$, for some $n_q, n_\tau \in \mathbb{N}$, and $\boldsymbol{z}(t) = \boldsymbol{\Psi}(\bar{\boldsymbol{\delta}}(t))$, such that $\boldsymbol{\Psi} : \mathbb{R}^{n_q} \to \mathbb{R}^{n_\tau}$. The map $\boldsymbol{\Psi}$ is said to be $\mathcal{W}_{m,p,\boldsymbol{\sigma}}$-stable if there exist finite constants $\gamma, v \in \mathbb{R}_{\geq 0}$ such that the inequality*

$$||\boldsymbol{z}(t)||^2_{\mathcal{W}_{m,p,\boldsymbol{\sigma}}} \leq \gamma^2 ||\bar{\boldsymbol{\delta}}(t)||^2_{\mathcal{L}_p} + v \tag{5.59}$$

holds for any $\bar{\boldsymbol{\delta}}(t) \in \mathcal{L}_p[0,\infty)$. *Moreover, if* $\gamma = \inf S$ *in which* $S = \{\bar{\gamma} \in \mathbb{R}_{\geq 0} : ||\boldsymbol{z}(t)||^2_{\mathcal{W}_{m,p,\boldsymbol{\sigma}}} \leq \bar{\gamma}^2 ||\bar{\boldsymbol{\delta}}(t)||^2_{\mathcal{L}_p} + v,\ \forall \bar{\boldsymbol{\delta}}(t) \in \mathcal{L}_p[0,\infty),\ v \in \mathbb{R}_{\geq 0}\}$, *then* γ *is said to be the* $\mathcal{W}_{m,p,\boldsymbol{\sigma}}$*-gain of the system.*

Note that, $\bar{\boldsymbol{\delta}}^*$ is the worst case of the disturbances, thus it maximizes the Hamiltonian. Consequently, from (5.58), for a generic $\bar{\boldsymbol{\delta}}(t) \in \mathcal{L}_2[0,\infty)$, we have that

$$\begin{aligned} &\frac{d\boldsymbol{V}_\infty(\boldsymbol{x})}{dt} + \frac{1}{2}\boldsymbol{x}'\boldsymbol{G}\boldsymbol{x} - \frac{1}{2}\gamma^2 \bar{\boldsymbol{\delta}}'\bar{\boldsymbol{\delta}} \leq 0, \\ &\frac{d\boldsymbol{V}_\infty(\boldsymbol{x})}{dt} \leq -\frac{1}{2}\boldsymbol{x}'\boldsymbol{G}\boldsymbol{x} + \frac{1}{2}\gamma^2 \bar{\boldsymbol{\delta}}'\bar{\boldsymbol{\delta}}. \end{aligned} \tag{5.60}$$

Thus, by integrating both sides of (5.60) in time, we have that

$$\begin{aligned} \int_0^\infty \frac{d\boldsymbol{V}_\infty(\boldsymbol{x})}{dt} dt &\leq \int_0^\infty \left(-\frac{1}{2}\boldsymbol{x}'\boldsymbol{G}\boldsymbol{x} + \frac{1}{2}\gamma^2 \bar{\boldsymbol{\delta}}'\bar{\boldsymbol{\delta}}\right) \mathrm{dt}, \\ \lim_{t\to\infty} \boldsymbol{V}_\infty(\boldsymbol{x}(t)) - \boldsymbol{V}_\infty(\boldsymbol{x}(0)) &\leq -\frac{1}{2}||\boldsymbol{z}(t)||^2_{\mathcal{W}_{3,2,\boldsymbol{\mathcal{Y}}}} + \frac{1}{2}\gamma^2 ||\bar{\boldsymbol{\delta}}(t)||^2_{\mathcal{L}_2}, \end{aligned} \tag{5.61}$$

which implies $||\boldsymbol{z}(t)||^2_{\mathcal{W}_{3,2,\boldsymbol{\mathcal{Y}}}} \leq \gamma^2 ||\bar{\boldsymbol{\delta}}(t)||^2_{\mathcal{L}_2} + 2\boldsymbol{V}_\infty(\boldsymbol{x}(0))$. Then, from (5.59) and assuming a finite initial condition, the closed-loop system is $\mathcal{W}_{3,2,\boldsymbol{\mathcal{Y}}}$-stable. The related $\mathcal{W}_{3,2,\boldsymbol{\mathcal{Y}}}$-gain, i.e. the smallest $\gamma \in \mathbb{R}_{\geq 0}$, can be obtained from inequality (5.56).

5.2 Control of underactuated mechanical systems with input coupling

Another class of special interest in this work is the underactuated mechanical system with input coupling. Examples of mechanical systems with input coupling include the Quadrotor UAV with tilted rotors (Raffo et al., 2011a), two-wheeled self-balanced pendulum (Raffo et al., 2015), autonomous helicopter (Olfati-Saber, 2001), VTOL aircraft (Olfati-Saber, 2001; Cardoso, Esteban and Raffo, 2019), among others. This class comprehends underactuated mechanical systems whose all DOF of the system are directly affected by the control inputs due to the input coupling matrix.

As commented previously, when dealing with underactuated mechanical systems, no more than n_τ degrees of freedom can track a desired reference simultaneously. However, for systems with input coupling one can select n_τ DOF to track a desired trajectory while the remaining ones are stabilized at an equilibrium point.

Therefore, by assuming the mechanical system (5.1) with input coupling, for control design purposes, it can be partitioned in controlled and stabilized DOF as (Raffo et al.,

2011a)

$$\underbrace{\begin{bmatrix} \boldsymbol{M}_{ss}(\boldsymbol{q}) & \boldsymbol{M}_{sc}(\boldsymbol{q}) \\ \boldsymbol{M}_{cs}(\boldsymbol{q}) & \boldsymbol{M}_{cc}(\boldsymbol{q}) \end{bmatrix}}_{\boldsymbol{M}(\boldsymbol{q})} \underbrace{\begin{bmatrix} \ddot{\boldsymbol{q}}_s \\ \ddot{\boldsymbol{q}}_c \end{bmatrix}}_{\ddot{\boldsymbol{q}}(t)} + \underbrace{\begin{bmatrix} \boldsymbol{C}_{ss}(\boldsymbol{q},\dot{\boldsymbol{q}}) & \boldsymbol{C}_{sc}(\boldsymbol{q},\dot{\boldsymbol{q}}) \\ \boldsymbol{C}_{cs}(\boldsymbol{q},\dot{\boldsymbol{q}}) & \boldsymbol{C}_{cc}(\boldsymbol{q},\dot{\boldsymbol{q}}) \end{bmatrix}}_{\boldsymbol{C}(\boldsymbol{q},\dot{\boldsymbol{q}})} \underbrace{\begin{bmatrix} \dot{\boldsymbol{q}}_s \\ \dot{\boldsymbol{q}}_c \end{bmatrix}}_{\dot{\boldsymbol{q}}(t)} + \underbrace{\begin{bmatrix} \boldsymbol{g}_s(\boldsymbol{q}) \\ \boldsymbol{g}_c(\boldsymbol{q}) \end{bmatrix}}_{\boldsymbol{g}(\boldsymbol{q})} = \underbrace{\begin{bmatrix} \boldsymbol{B}_s(\boldsymbol{q},\dot{\boldsymbol{q}}) \\ \boldsymbol{B}_c(\boldsymbol{q},\dot{\boldsymbol{q}}) \end{bmatrix}}_{\boldsymbol{B}(\boldsymbol{q},\dot{\boldsymbol{q}})} \boldsymbol{\tau}(t) + \boldsymbol{w}(t), \tag{5.62}$$

in which $\boldsymbol{q}(t) = [\boldsymbol{q}_s'(t)\ \boldsymbol{q}_c'(t)]'$, with $\boldsymbol{q}_s(t) : \mathbb{R}_{\geq 0} \to (\mathbb{R}^{n_q - n_\tau} = \mathbb{R}^{n_s})$ corresponding to the stabilized DOF and $\boldsymbol{q}_c(t) : \mathbb{R}_{\geq 0} \to \mathbb{R}^{n_\tau}$ to the controlled ones. The controlled DOF must be selected so that the following assumptions hold.

Assumption 6. *The matrix $\boldsymbol{B}_c(\boldsymbol{q},\dot{\boldsymbol{q}})$ is invertible within the domain $\Omega \subseteq (\mathbb{R}^{n_q} \times \mathbb{R}^{n_q})$, i.e. $rank(\boldsymbol{B}_c(\boldsymbol{q},\dot{\boldsymbol{q}})) = n_\tau$, $\forall (\boldsymbol{q},\dot{\boldsymbol{q}}) \in \Omega$.*

Assumption 7. *The rows of $\boldsymbol{B}_s(\boldsymbol{q},\dot{\boldsymbol{q}})$ are linearly independent within the domain $\Omega \subseteq (\mathbb{R}^{n_q} \times \mathbb{R}^{n_q})$, i.e. $rank(\boldsymbol{B}_s(\boldsymbol{q},\dot{\boldsymbol{q}})) = n_s$, $\forall (\boldsymbol{q},\dot{\boldsymbol{q}}) \in \Omega$.*

Remark 31. *Assumption 6 ensures that matrix $\boldsymbol{B}_c(\boldsymbol{q},\dot{\boldsymbol{q}})$ is square and span a image space with dimension n_τ, the same as $\boldsymbol{q}_c$, that allows to perform tracking of the controlled DOF. In addition, Assumption 7 ensures the image space generated by the matrix $\boldsymbol{B}_s(\boldsymbol{q},\dot{\boldsymbol{q}})$ is not null, which provides actuation on the stabilized DOF by the control inputs. Physically, these assumptions ensure the system has input coupling, so the control inputs directly influence all system DOF.*

Aiming trajectory tracking, the error dynamics are written considering the entire system dynamics

$$\begin{aligned} \boldsymbol{M}(\boldsymbol{q}_s, \tilde{\boldsymbol{q}}_c{+}\boldsymbol{q}_{c_r}) \begin{bmatrix} \ddot{\boldsymbol{q}}_s \\ \ddot{\tilde{\boldsymbol{q}}}_c{+}\ddot{\boldsymbol{q}}_{c_r} \end{bmatrix} + \boldsymbol{C}(\boldsymbol{q}_s, \tilde{\boldsymbol{q}}_c{+}\boldsymbol{q}_{c_r}, \dot{\boldsymbol{q}}_s, \dot{\tilde{\boldsymbol{q}}}_c{+}\dot{\boldsymbol{q}}_{c_r}) \begin{bmatrix} \dot{\boldsymbol{q}}_s \\ \dot{\tilde{\boldsymbol{q}}}_c{+}\dot{\boldsymbol{q}}_{c_r} \end{bmatrix} \\ + \boldsymbol{g}(\boldsymbol{q}_s, \tilde{\boldsymbol{q}}_c{+}\boldsymbol{q}_{c_r}) = \boldsymbol{B}(\boldsymbol{q}_s, \tilde{\boldsymbol{q}}_c{+}\boldsymbol{q}_{c_r}, \dot{\boldsymbol{q}}_s, \dot{\tilde{\boldsymbol{q}}}_c{+}\dot{\boldsymbol{q}}_{c_r})\boldsymbol{\tau} + \boldsymbol{w}, \end{aligned} \tag{5.63}$$

with $\tilde{\boldsymbol{q}}_c(t) \triangleq \boldsymbol{q}_c(t) - \boldsymbol{q}_{cr}(t)$, where $\boldsymbol{q}_{cr}(t)$, $\dot{\boldsymbol{q}}_{cr}(t)$ and $\ddot{\boldsymbol{q}}_{cr}(t)$ are the desired values of the controlled DOF and their time derivatives, in which $\boldsymbol{q}_{cr}(t) \in \mathcal{C}^2$.

Hence, by defining the state vector

$$\boldsymbol{x}(t) \triangleq [\dot{\boldsymbol{q}}_s'(t)\ \dot{\tilde{\boldsymbol{q}}}_c'(t)\ \tilde{\boldsymbol{q}}_c'(t)\ \int_0^t \tilde{\boldsymbol{q}}_c'(\tau)d\tau]', \tag{5.64}$$

equation (7.64) is represented in the state-space form as

$$\dot{\boldsymbol{x}}(t) = \underbrace{\begin{bmatrix} -\boldsymbol{M}^{-1}\boldsymbol{C} & \boldsymbol{0} & \boldsymbol{0} \\ [\boldsymbol{0}\ \ \boldsymbol{I}] & \boldsymbol{0} & \boldsymbol{0} \\ \boldsymbol{0} & \boldsymbol{I} & \boldsymbol{0} \end{bmatrix}}_{\boldsymbol{f}(\boldsymbol{x},\boldsymbol{q}_s)} \boldsymbol{x}(t) + \underbrace{\begin{bmatrix} -\boldsymbol{M}^{-1}\boldsymbol{d} \\ \boldsymbol{0} \\ \boldsymbol{0} \end{bmatrix}}_{\bar{\boldsymbol{f}}(\boldsymbol{x},\boldsymbol{q}_s,t)} + \underbrace{\begin{bmatrix} \boldsymbol{M}^{-1} \\ \boldsymbol{0} \\ \boldsymbol{0} \end{bmatrix}}_{\boldsymbol{g}(\boldsymbol{x},\boldsymbol{q}_s)} \boldsymbol{u}(t) + \underbrace{\begin{bmatrix} \boldsymbol{M}^{-1} \\ \boldsymbol{0} \\ \boldsymbol{0} \end{bmatrix}}_{\boldsymbol{k}(\boldsymbol{x},\boldsymbol{q}_s)} \boldsymbol{w}(t), \tag{5.65}$$

where $\boldsymbol{d} \triangleq \boldsymbol{g}(\boldsymbol{q}_s, \tilde{\boldsymbol{q}}_c + \boldsymbol{q}_{c_r}) + \boldsymbol{M}(\boldsymbol{q}_s, \tilde{\boldsymbol{q}}_c + \boldsymbol{q}_{c_r}) \begin{bmatrix} \boldsymbol{0} \\ \ddot{\boldsymbol{q}}_{c_r} \end{bmatrix} + \boldsymbol{C}(\boldsymbol{q}_s, \tilde{\boldsymbol{q}}_c + \boldsymbol{q}_{c_r}, \dot{\boldsymbol{q}}_s, \dot{\tilde{\boldsymbol{q}}}_c + \dot{\boldsymbol{q}}_{c_r}) \begin{bmatrix} \boldsymbol{0} \\ \dot{\boldsymbol{q}}_{c_r} \end{bmatrix}$, and $\boldsymbol{u} = \boldsymbol{B}(\boldsymbol{x}, \boldsymbol{q}_s)\boldsymbol{\tau}$ is the generalized input vector.

In order to design the $\mathcal{W}_2$ and $\mathcal{W}_\infty$ controllers for underactuated mechanical systems with input coupling, we also assume that the desired trajectory is feasible and the forces and torques induced on the system by gravity and external disturbances can be handled using the control inputs. Accordingly, the following assumption is posed.

Assumption 8. *There exists $\boldsymbol{q}_s$ such that $\boldsymbol{B}^\perp(\boldsymbol{x}, \boldsymbol{q}_s)(\boldsymbol{w} - \boldsymbol{d}) = \boldsymbol{0}$, where $\boldsymbol{B}^\perp(\boldsymbol{x}, \boldsymbol{q}_s)$ is a full rank left annihilator of $\boldsymbol{B}(\boldsymbol{x}, \boldsymbol{q}_s)$ (i.e $\boldsymbol{B}^\perp\boldsymbol{B} = \boldsymbol{0}$).*

Remark 32. *The vector $\boldsymbol{d}$ comprehends three terms, the first is related to the generalized forces induced on the mechanical system by gravity, the others are the generalized forces required to perform the desired trajectory.*

Remark 33. *Assumption 8 ensures that there exists the image space (or exact map using pseudo-inverse (Ortega et al., 2002)) of vectors $\boldsymbol{d}$ and $\boldsymbol{w}$ from the generalized inputs $\boldsymbol{u}$ to the control inputs $\boldsymbol{\tau}$, for some configuration of the stabilized DOF.*

5.2.1 Nonlinear $\mathcal{W}_2$ control approach

In order to derive the nonlinear $\mathcal{W}_2$ optimal control law, system (5.65) is written in the following compact form

$$\mathcal{P}_5 : \begin{cases} \dot{\boldsymbol{x}}(t) & = \boldsymbol{f}(\boldsymbol{x}, \boldsymbol{q}_s) + \bar{\boldsymbol{f}}(\boldsymbol{x}, \boldsymbol{q}_s, t) + \boldsymbol{g}(\boldsymbol{x}, \boldsymbol{q}_s)\boldsymbol{u}(t), \\ \boldsymbol{z}_c(t) & = \int_0^t \tilde{\boldsymbol{q}}_c(\tau)d\tau, \\ \boldsymbol{z}_s(t) & = \dot{\boldsymbol{q}}_s(t), \end{cases} \tag{5.66}$$

where $\boldsymbol{z}_c(t)$ and $\boldsymbol{z}_s(t)$ are the cost variables related to the controlled and stabilized DOF, respectively. They allow the appearance of the states and both, stabilizable and controllable, dynamics in the cost functional. Besides, it is assumed no disturbances affecting the system ($\boldsymbol{w}(t) = \boldsymbol{0}$).

The nonlinear $\mathcal{W}_2$ controller is designed in order to obtain the control law $\boldsymbol{u}(\boldsymbol{x}, \boldsymbol{q}_s) \in \mathcal{U}$ that minimizes the cost functional

$$\mathcal{J}_2 = \frac{1}{2}||\boldsymbol{z}_c(t)||^2_{\mathcal{W}_{3,2,\boldsymbol{\Gamma}}} + \frac{1}{2}||\boldsymbol{z}_s(t)||^2_{\mathcal{W}_{1,2,\boldsymbol{\Upsilon}}}, \tag{5.67}$$

with $\mathcal{U} : (\mathbb{R}^{n_x} \times \mathbb{R}^{n_s}) \to \mathbb{R}^{n_q}$.

Therefore, the optimal control problem is posed as finding the optimal control law $\boldsymbol{u}^*$ that leads to

$$\boldsymbol{V}_2 = \min_{\boldsymbol{u} \in \mathcal{U}} \left\{ \frac{1}{2}||\boldsymbol{z}_c(t)||^2_{\mathcal{W}_{3,2,\boldsymbol{\Gamma}}} + \frac{1}{2}||\boldsymbol{z}_s(t)||^2_{\mathcal{W}_{1,2,\boldsymbol{\Upsilon}}} \right\}, \tag{5.68}$$

$$\text{s.t.} \quad \mathcal{P}_5,$$

in which $\boldsymbol{\Gamma} = \{\boldsymbol{\Gamma}_0, ..., \boldsymbol{\Gamma}_3\}$ and $\boldsymbol{\Upsilon} = \{\boldsymbol{\Upsilon}_0, \boldsymbol{\Upsilon}_1\}$, where $\boldsymbol{\Gamma}_i$ and $\boldsymbol{\Upsilon}_j$, for $i \in \{0,\ 1,\ 2,\ 3\}$ and $j \in \{0,\ 1\}$, are symmetric, positive definite tuning matrices, that weight the influence of the states in the control objective.

Remark 34. *In the optimal control problem (5.68), the time derivatives of the stabilized DOF are required to converge to zero, but there are no references for the stabilized DOF. This allows the controller to manipulate $\boldsymbol{q}_s(t)$ in order to achieve $\boldsymbol{B}^{\perp}(\boldsymbol{x}, \boldsymbol{q}_s)\,(\boldsymbol{w} - \boldsymbol{d}) = \boldsymbol{0}$.*

Aiming to solve this problem, it can be formulated via dynamic programming, from which the HJB PDE is obtained

$$\frac{\partial \boldsymbol{V}_2(\boldsymbol{x}, t)}{\partial t} + \min_{\boldsymbol{u} \in \boldsymbol{\mathcal{U}}} \{\mathbb{H}_2(\boldsymbol{V}_2(\boldsymbol{x}, t), \boldsymbol{x}, \boldsymbol{q}_s, \boldsymbol{u}, t)\} = 0, \tag{5.69}$$

where the associated Hamiltonian is given by

$$\begin{aligned}\mathbb{H}_2 \triangleq & \frac{\partial' \boldsymbol{V}_2}{\partial \boldsymbol{x}}\dot{\boldsymbol{x}} + \frac{1}{2}\boldsymbol{z}_c'\boldsymbol{\Gamma}_0\boldsymbol{z}_c + \frac{1}{2}\dot{\boldsymbol{z}}_c'\boldsymbol{\Gamma}_1\dot{\boldsymbol{z}}_c + \frac{1}{2}\ddot{\boldsymbol{z}}_c'\boldsymbol{\Gamma}_2\ddot{\boldsymbol{z}}_c + \frac{1}{2}\dddot{\boldsymbol{z}}_c'\boldsymbol{\Gamma}_3\dddot{\boldsymbol{z}}_c + \frac{1}{2}\boldsymbol{z}_s'\boldsymbol{\Upsilon}_0\boldsymbol{z}_s + \frac{1}{2}\dot{\boldsymbol{z}}_s'\boldsymbol{\Upsilon}_1\dot{\boldsymbol{z}}_s, \\ = & \frac{\partial' \boldsymbol{V}_2}{\partial \boldsymbol{x}}\Big(\boldsymbol{f} + \bar{\boldsymbol{f}} + \boldsymbol{g}\boldsymbol{u}\Big) + \frac{1}{2}\boldsymbol{x}'\boldsymbol{D}\boldsymbol{x} + \frac{1}{2}\ddot{\tilde{\boldsymbol{q}}}'\boldsymbol{E}\ddot{\tilde{\boldsymbol{q}}},\end{aligned} \tag{5.70}$$

with $\boldsymbol{D} \triangleq \text{blkdiag}(\boldsymbol{\Upsilon}_0, \boldsymbol{\Gamma}_2, \boldsymbol{\Gamma}_1, \boldsymbol{\Gamma}_0)$, $\boldsymbol{E} \triangleq \text{blkdiag}(\boldsymbol{\Upsilon}_1, \boldsymbol{\Gamma}_3)$, and the boundary condition $\boldsymbol{V}_2(\boldsymbol{0}, t) = 0$.

By expanding (5.70), yields

$$\begin{aligned}\mathbb{H}_2 = & \frac{\partial' \boldsymbol{V}_2}{\partial \boldsymbol{x}}\dot{\boldsymbol{x}} + \frac{1}{2}\boldsymbol{x}' \underbrace{\begin{bmatrix} \boldsymbol{\Upsilon}_0 & \boldsymbol{0} & \boldsymbol{0} & \boldsymbol{0} \\ \boldsymbol{0} & \boldsymbol{\Gamma}_2 & \boldsymbol{0} & \boldsymbol{0} \\ \boldsymbol{0} & \boldsymbol{0} & \boldsymbol{\Gamma}_1 & \boldsymbol{0} \\ \boldsymbol{0} & \boldsymbol{0} & \boldsymbol{0} & \boldsymbol{\Gamma}_0 \end{bmatrix}}_{\boldsymbol{D}} \boldsymbol{x} + \frac{1}{2}\ddot{\tilde{\boldsymbol{q}}}' \underbrace{\begin{bmatrix} \boldsymbol{\Upsilon}_1 & \boldsymbol{0} \\ \boldsymbol{0} & \boldsymbol{\Gamma}_3 \end{bmatrix}}_{\boldsymbol{E}} \ddot{\tilde{\boldsymbol{q}}}, \\ = & \frac{\partial' \boldsymbol{V}_2}{\partial \boldsymbol{x}}\Big(\boldsymbol{f} + \bar{\boldsymbol{f}} + \boldsymbol{g}\boldsymbol{u}\Big) + \frac{1}{2}\boldsymbol{x}'\boldsymbol{D}\boldsymbol{x} + \frac{1}{2}\ddot{\tilde{\boldsymbol{q}}}'\boldsymbol{E}\ddot{\tilde{\boldsymbol{q}}}, \\ = & \frac{\partial' \boldsymbol{V}_2}{\partial \boldsymbol{x}}\Big(\boldsymbol{f} + \bar{\boldsymbol{f}} + \boldsymbol{g}\boldsymbol{u}\Big) + \frac{1}{2}\boldsymbol{x}'\boldsymbol{D}\boldsymbol{x} \\ & + \frac{1}{2}\Big[\dot{\tilde{\boldsymbol{q}}}'\boldsymbol{C}'\Pi\boldsymbol{C}\dot{\tilde{\boldsymbol{q}}} + 2\dot{\tilde{\boldsymbol{q}}}'\boldsymbol{C}'\Pi\boldsymbol{d} - 2\boldsymbol{u}'\Pi\boldsymbol{C}\dot{\tilde{\boldsymbol{q}}} - 2\boldsymbol{u}'\Pi\boldsymbol{d} + \boldsymbol{u}'\Pi\boldsymbol{u} + \boldsymbol{d}'\Pi\boldsymbol{d}\Big],\end{aligned} \tag{5.71}$$

in which $\dot{\tilde{\boldsymbol{q}}} = \begin{bmatrix} \dot{\boldsymbol{q}}_s' & \dot{\tilde{\boldsymbol{q}}}_c' \end{bmatrix}'$ and $\boldsymbol{\Pi} \triangleq \boldsymbol{M}^{-1}\boldsymbol{E}\boldsymbol{M}^{-1}$.

Then, the optimal control law, $\boldsymbol{u}^*$, is obtained by minimizing (5.70) with respect to $\boldsymbol{u}$, as follows

$$\frac{\partial \mathbb{H}_2}{\partial \boldsymbol{u}} = \boldsymbol{g}'\frac{\partial \boldsymbol{V}_2}{\partial \boldsymbol{x}} - \boldsymbol{\Pi}\boldsymbol{d} - \boldsymbol{\Pi}\boldsymbol{C}\dot{\tilde{\boldsymbol{q}}} + \boldsymbol{\Pi}\boldsymbol{u}^* = 0, \tag{5.72}$$

yielding

$$\begin{aligned}\boldsymbol{u}^* &= -\boldsymbol{\Pi}^{-1}\Big(\boldsymbol{g}'\frac{\partial \boldsymbol{V}_2}{\partial \boldsymbol{x}} - \boldsymbol{\Pi}\boldsymbol{C}\dot{\boldsymbol{q}} - \boldsymbol{\Pi}\boldsymbol{d}\Big),\\ &= -\boldsymbol{\Pi}^{-1}\boldsymbol{g}'\frac{\partial \boldsymbol{V}_2}{\partial \boldsymbol{x}} + \boldsymbol{C}\dot{\boldsymbol{q}} + \boldsymbol{d},\end{aligned} \tag{5.73}$$

which is a minimum value of the optimization problem, since $\dfrac{\partial^2 \mathbb{H}_2}{\partial \boldsymbol{u}^2} = \boldsymbol{\Pi} > 0$. The HJ equation associated to the problem, obtained by replacing the optimal control law (5.73) in (5.70), is written as

$$\frac{\partial \boldsymbol{V}_2(\boldsymbol{x},t)}{\partial t} + \mathbb{H}_2(\boldsymbol{V}_2, \boldsymbol{x}, \boldsymbol{q}_s, \boldsymbol{u}^*, t) = 0. \tag{5.74}$$

Therefore, the optimal control problem (5.68) results in solving the PDE (5.74) to obtain the solution $\boldsymbol{V}_2(\boldsymbol{x},t)$. Then, similar to Theorem 1, a particular solution to (5.74) is proposed in the following theorem.

Theorem 4. *Let $\boldsymbol{V}_2$ be the parametrized scalar function*

$$\boldsymbol{V}_2(\boldsymbol{x}) = \frac{1}{2}\boldsymbol{x}'\begin{bmatrix}\boldsymbol{U} & \boldsymbol{0} & \boldsymbol{0} & \boldsymbol{0}\\ \boldsymbol{0} & \boldsymbol{Q} & \boldsymbol{K} & \boldsymbol{T}\\ \boldsymbol{0} & \boldsymbol{K} & \boldsymbol{R} & \boldsymbol{S}\\ \boldsymbol{0} & \boldsymbol{T} & \boldsymbol{S} & \boldsymbol{P}\end{bmatrix}\boldsymbol{x} > 0, \tag{5.75}$$

such that $\boldsymbol{U}$, $\boldsymbol{Q}$, $\boldsymbol{K}$, $\boldsymbol{T}$, $\boldsymbol{R}$, $\boldsymbol{S}$, and $\boldsymbol{P}$ are positive definite matrices and verify $\boldsymbol{Q}-\boldsymbol{K}\boldsymbol{R}^{-1}\boldsymbol{K} > 0$ and $\begin{bmatrix}\boldsymbol{Q} & \boldsymbol{K}\\ \boldsymbol{K} & \boldsymbol{R}\end{bmatrix} - \begin{bmatrix}\boldsymbol{T}\\ \boldsymbol{S}\end{bmatrix}\boldsymbol{P}^{-1}\begin{bmatrix}\boldsymbol{T} & \boldsymbol{S}\end{bmatrix} > 0$, with $\boldsymbol{U}$, $\boldsymbol{Q}$, $\boldsymbol{K}$, and $\boldsymbol{T}$ obtained from the following Riccati equations

$$-\boldsymbol{U}\boldsymbol{\Upsilon}_1^{-1}\boldsymbol{U} + \boldsymbol{\Upsilon}_0 = \boldsymbol{0}, \tag{5.76}$$

$$-\boldsymbol{T}\boldsymbol{\Gamma}_3^{-1}\boldsymbol{T} + \boldsymbol{\Gamma}_0 = \boldsymbol{0}, \tag{5.77}$$

$$-\boldsymbol{Q}\boldsymbol{\Gamma}_3^{-1}\boldsymbol{Q} + 2\boldsymbol{K} + \boldsymbol{\Gamma}_2 = \boldsymbol{0}, \tag{5.78}$$

$$-\boldsymbol{K}\boldsymbol{\Gamma}_3^{-1}\boldsymbol{K} + 2\boldsymbol{S} + \boldsymbol{\Gamma}_1 = \boldsymbol{0}, \tag{5.79}$$

and $\boldsymbol{R}$, $\boldsymbol{S}$, and $\boldsymbol{P}$ are given by

$$\boldsymbol{R} = \boldsymbol{Q}\boldsymbol{\Gamma}_3^{-1}\boldsymbol{K} - \boldsymbol{T}, \tag{5.80}$$

$$\boldsymbol{S} = \boldsymbol{Q}\boldsymbol{\Gamma}_3^{-1}\boldsymbol{T}, \tag{5.81}$$

$$\boldsymbol{P} = \boldsymbol{K}\boldsymbol{\Gamma}_3^{-1}\boldsymbol{T}. \tag{5.82}$$

Then, function $\boldsymbol{V}_2(\boldsymbol{x})$ is a solution to the HJ equation (5.74).

Proof. The proof is conducted similarly to the proof of Theorem 1, by replacing (5.75)

in (5.74) and using the properties of inertia matrix. In the following, it is computed by parts.

Consider the HJ equation (5.74), since (5.75) is a time-invariant function, $\frac{\partial \boldsymbol{V}_2}{\partial t} = 0$, it leads to

$$\begin{aligned} \mathbb{H}_2(\boldsymbol{V}_2, \boldsymbol{x}, \boldsymbol{u}^*, t) = 0, \\ \frac{\partial' \boldsymbol{V}_2}{\partial \boldsymbol{x}} \dot{\boldsymbol{x}} + \frac{1}{2} \boldsymbol{x}' \boldsymbol{D} \boldsymbol{x} + \frac{1}{2} \ddot{\tilde{\boldsymbol{q}}}' \boldsymbol{E} \ddot{\tilde{\boldsymbol{q}}}, = 0. \end{aligned} \tag{5.83}$$

In addition, considering the candidate solution (5.75), the optimal control law (5.73) yields

$$\boldsymbol{u}^* = \boldsymbol{C} \dot{\tilde{q}} + \boldsymbol{d} - \boldsymbol{M} \begin{bmatrix} \boldsymbol{\Upsilon}_1^{-1} \boldsymbol{U} & \boldsymbol{0} & \boldsymbol{0} & \boldsymbol{0} \\ \boldsymbol{0} & \boldsymbol{\Gamma}_3^{-1} \boldsymbol{Q} & \boldsymbol{\Gamma}_3^{-1} \boldsymbol{K} & \boldsymbol{\Gamma}_3^{-1} \boldsymbol{T} \end{bmatrix} \boldsymbol{x}. \tag{5.84}$$

Accordingly, the acceleration dynamics are given by

$$\begin{aligned} \ddot{\tilde{\boldsymbol{q}}} &= -\boldsymbol{M}^{-1} \boldsymbol{C} \dot{\tilde{\boldsymbol{q}}} - \boldsymbol{M}^{-1} \boldsymbol{d} + \boldsymbol{M}^{-1} \boldsymbol{u}^*, \\ &= \begin{bmatrix} -\boldsymbol{\Upsilon}_1^{-1} \boldsymbol{U} & \boldsymbol{0} & \boldsymbol{0} & \boldsymbol{0} \\ \boldsymbol{0} & -\boldsymbol{\Gamma}_3^{-1} \boldsymbol{Q} & -\boldsymbol{\Gamma}_3^{-1} \boldsymbol{K} & -\boldsymbol{\Gamma}_3^{-1} \boldsymbol{T} \end{bmatrix} \boldsymbol{x}, \end{aligned} \tag{5.85}$$

leading to the following closed-loop dynamics

$$\dot{\boldsymbol{x}} = \begin{bmatrix} -\boldsymbol{\Upsilon}_1^{-1} \boldsymbol{U} & \boldsymbol{0} & \boldsymbol{0} & \boldsymbol{0} \\ \boldsymbol{0} & -\boldsymbol{\Gamma}_3^{-1} \boldsymbol{Q} & -\boldsymbol{\Gamma}_3^{-1} \boldsymbol{K} & -\boldsymbol{\Gamma}_3^{-1} \boldsymbol{T} \\ \boldsymbol{0} & \boldsymbol{I} & \boldsymbol{0} & \boldsymbol{0} \\ \boldsymbol{0} & \boldsymbol{0} & \boldsymbol{I} & \boldsymbol{0} \end{bmatrix} \boldsymbol{x}, \tag{5.86}$$

which is a time-invariant system. Then, by replacing (5.86) in the first term of (5.83), results in

$$\frac{\partial' \boldsymbol{V}_2}{\partial \boldsymbol{x}} \dot{\boldsymbol{x}} = \boldsymbol{x}' \begin{bmatrix} -\boldsymbol{U} \boldsymbol{\Upsilon}_1^{-1} \boldsymbol{U} & \boldsymbol{0} & \boldsymbol{0} & \boldsymbol{0} \\ \boldsymbol{0} & -\boldsymbol{Q} \boldsymbol{\Gamma}_3^{-1} \boldsymbol{Q} + \boldsymbol{K} & -\boldsymbol{Q} \boldsymbol{\Gamma}_3^{-1} \boldsymbol{K} + \boldsymbol{T} & -\boldsymbol{Q} \boldsymbol{\Gamma}^{-1} \boldsymbol{T} \\ \boldsymbol{0} & -\boldsymbol{K} \boldsymbol{\Gamma}_3^{-1} \boldsymbol{Q} + \boldsymbol{R} & -\boldsymbol{K} \boldsymbol{\Gamma}_3^{-1} \boldsymbol{K} + \boldsymbol{S} & -\boldsymbol{K} \boldsymbol{\Gamma}^{-1} \boldsymbol{T} \\ \boldsymbol{0} & -\boldsymbol{T} \boldsymbol{\Gamma}_3^{-1} \boldsymbol{Q} + \boldsymbol{S} & -\boldsymbol{T} \boldsymbol{\Gamma}_3^{-1} \boldsymbol{K} + \boldsymbol{P} & -\boldsymbol{T} \boldsymbol{\Gamma}^{-1} \boldsymbol{T} \end{bmatrix} \boldsymbol{x}. \tag{5.87}$$

Moreover, by replacing (5.85) in the last term of (5.83) yields

$$\frac{1}{2} \ddot{\tilde{\boldsymbol{q}}}' \boldsymbol{E} \ddot{\tilde{\boldsymbol{q}}} = \frac{1}{2} \boldsymbol{x}' \begin{bmatrix} \boldsymbol{U} \boldsymbol{\Upsilon}_1^{-1} \boldsymbol{U} & \boldsymbol{0} & \boldsymbol{0} & \boldsymbol{0} \\ \boldsymbol{0} & \boldsymbol{Q} \boldsymbol{\Gamma}_3^{-1} \boldsymbol{Q} & \boldsymbol{Q} \boldsymbol{\Gamma}_3^{-1} \boldsymbol{K} & \boldsymbol{Q} \boldsymbol{\Gamma}_3^{-1} \boldsymbol{T} \\ \boldsymbol{0} & \boldsymbol{K} \boldsymbol{\Gamma}_3^{-1} \boldsymbol{Q} & \boldsymbol{K} \boldsymbol{\Gamma}_3^{-1} \boldsymbol{K} & \boldsymbol{K} \boldsymbol{\Gamma}_3^{-1} \boldsymbol{T} \\ \boldsymbol{0} & \boldsymbol{T} \boldsymbol{\Gamma}_3^{-1} \boldsymbol{Q} & \boldsymbol{T} \boldsymbol{\Gamma}_3^{-1} \boldsymbol{K} & \boldsymbol{T} \boldsymbol{\Gamma}_3^{-1} \boldsymbol{T} \end{bmatrix} \boldsymbol{x}. \tag{5.88}$$

Therefore, considering (5.87) and (5.88), the equation (5.83) is written in the compact

form

$$\boldsymbol{x}'\boldsymbol{N}\boldsymbol{x} = \boldsymbol{x}' \begin{bmatrix} \boldsymbol{N}_{11} & \boldsymbol{0} & \boldsymbol{0} & \boldsymbol{0} \\ \boldsymbol{0} & \boldsymbol{N}_{22} & \boldsymbol{N}_{23} & \boldsymbol{N}_{24} \\ \boldsymbol{0} & \boldsymbol{N}_{32} & \boldsymbol{N}_{33} & \boldsymbol{N}_{34} \\ \boldsymbol{0} & \boldsymbol{N}_{42} & \boldsymbol{N}_{43} & \boldsymbol{N}_{44} \end{bmatrix} \boldsymbol{x} = 0, \tag{5.89}$$

with

$$\begin{aligned}
\boldsymbol{N}_{11} &\triangleq -\frac{1}{2}\boldsymbol{U}\boldsymbol{\Upsilon}_1^{-1}\boldsymbol{U}+\frac{1}{2}\boldsymbol{\Upsilon}_0, & \boldsymbol{N}_{22} &\triangleq -\frac{1}{2}\boldsymbol{Q}\boldsymbol{\Gamma}_3^{-1}\boldsymbol{Q}+\boldsymbol{K}+\frac{1}{2}\boldsymbol{\Gamma}_2, \\
\boldsymbol{N}_{23} &\triangleq -\frac{1}{2}\boldsymbol{Q}\boldsymbol{\Gamma}_3^{-1}\boldsymbol{K}+\boldsymbol{T}, & \boldsymbol{N}_{24} &\triangleq -\frac{1}{2}\boldsymbol{Q}\boldsymbol{\Gamma}_3^{-1}\boldsymbol{T}, \\
\boldsymbol{N}_{32} &\triangleq -\frac{1}{2}\boldsymbol{K}\boldsymbol{\Gamma}_3^{-1}\boldsymbol{Q}+\boldsymbol{R}, & \boldsymbol{N}_{33} &\triangleq -\frac{1}{2}\boldsymbol{K}\boldsymbol{\Gamma}_3^{-1}\boldsymbol{K}+\boldsymbol{S}+\frac{1}{2}\boldsymbol{\Gamma}_1, \\
\boldsymbol{N}_{34} &\triangleq -\frac{1}{2}\boldsymbol{K}\boldsymbol{\Gamma}_3^{-1}\boldsymbol{T}, & \boldsymbol{N}_{42} &\triangleq -\frac{1}{2}\boldsymbol{T}\boldsymbol{\Gamma}_3^{-1}\boldsymbol{Q}+\boldsymbol{S}, \\
\boldsymbol{N}_{43} &\triangleq -\frac{1}{2}\boldsymbol{T}\boldsymbol{\Gamma}_3^{-1}\boldsymbol{K}+\boldsymbol{P}, & \boldsymbol{N}_{44} &\triangleq -\frac{1}{2}\boldsymbol{T}\boldsymbol{\Gamma}_3^{-1}\boldsymbol{T}+\frac{1}{2}\boldsymbol{\Gamma}_0.
\end{aligned}$$

Thereafter, the matrix $\boldsymbol{N}$ is represented by its symmetric and skew-symmetric parts, yielding

$$\boldsymbol{x}' \begin{bmatrix} \boldsymbol{A}_{11} & \boldsymbol{0} & \boldsymbol{0} & \boldsymbol{0} \\ * & \boldsymbol{A}_{22} & \boldsymbol{A}_{23} & \boldsymbol{A}_{24} \\ * & * & \boldsymbol{A}_{33} & \boldsymbol{A}_{34} \\ * & * & * & \boldsymbol{A}_{44} \end{bmatrix} \boldsymbol{x} = 0, \tag{5.90}$$

where the * terms indicates symmetry.

One way to satisfy the equality (5.90) is by solving the following set of algebraic Riccati equations:

$$\boldsymbol{A}_{11} = -\boldsymbol{U}\boldsymbol{\Upsilon}_1^{-1}\boldsymbol{U} + \boldsymbol{\Upsilon}_0 = \boldsymbol{0}, \tag{5.91}$$

$$\boldsymbol{A}_{22} = -\boldsymbol{Q}\boldsymbol{\Gamma}_3^{-1}\boldsymbol{Q} + 2\boldsymbol{K}+\boldsymbol{\Gamma}_2 = \boldsymbol{0}, \tag{5.92}$$

$$\boldsymbol{A}_{23} = -\boldsymbol{Q}\boldsymbol{\Gamma}_3^{-1}\boldsymbol{K} + \boldsymbol{T} + \boldsymbol{R} = \boldsymbol{0}, \tag{5.93}$$

$$\boldsymbol{A}_{24} = -\boldsymbol{Q}\boldsymbol{\Gamma}_3^{-1}\boldsymbol{T} + \boldsymbol{S} = \boldsymbol{0}, \tag{5.94}$$

$$\boldsymbol{A}_{33} = -\boldsymbol{K}\boldsymbol{\Gamma}_3^{-1}\boldsymbol{K} + 2\boldsymbol{S} + \boldsymbol{\Gamma}_1 = \boldsymbol{0}, \tag{5.95}$$

$$\boldsymbol{A}_{34} = -\boldsymbol{K}\boldsymbol{\Gamma}_3^{-1}\boldsymbol{T} + \boldsymbol{P} = \boldsymbol{0}, \tag{5.96}$$

$$\boldsymbol{A}_{44} = -\boldsymbol{T}\boldsymbol{\Gamma}_3^{-1}\boldsymbol{T} + \boldsymbol{\Gamma}_0 = \boldsymbol{0}. \tag{5.97}$$

First, from (5.93), (5.94), and (5.96), we have $\boldsymbol{R} = \boldsymbol{Q}\boldsymbol{\Gamma}_3^{-1}\boldsymbol{K}-\boldsymbol{T}$, $\boldsymbol{S} = \boldsymbol{Q}\boldsymbol{\Gamma}_3^{-1}\boldsymbol{T}$, and $\boldsymbol{P} = \boldsymbol{K}\boldsymbol{\Gamma}_3^{-1}\boldsymbol{T}$. In addition, $\boldsymbol{U}$ and $\boldsymbol{T}$ are computed from (5.91) and (5.97). Then, $\boldsymbol{K}$ and $\boldsymbol{Q}$ are computed through the pair of cross-coupled Riccati equations (5.92) and (5.95).

Therefore, with the solutions of (5.91)-(5.97), we conclude the proof. □

The stability of the closed-loop system is demonstrated in the following Theorem.

Theorem 5. *Let $\boldsymbol{V}_2(\boldsymbol{x},t) > 0$ be a solution of (5.74) given by the parametrized scalar function (5.75). Therefore, the closed-loop system, with the control law (5.73) and system (5.66), is asymptotically stable.*

Proof. From (5.74) and (5.75), we have that

$$\begin{aligned}\frac{d\boldsymbol{V}_2(\boldsymbol{x},t)}{dt} &= -\frac{1}{2}\boldsymbol{z}_c'\boldsymbol{\Gamma}_0\boldsymbol{z}_c - \frac{1}{2}\dot{\boldsymbol{z}}_c'\boldsymbol{\Gamma}_1\dot{\boldsymbol{z}}_c - \frac{1}{2}\ddot{\boldsymbol{z}}_c'\boldsymbol{\Gamma}_2\ddot{\boldsymbol{z}}_c - \frac{1}{2}\dddot{\boldsymbol{z}}_c'\boldsymbol{\Gamma}_3\dddot{\boldsymbol{z}}_c - \frac{1}{2}\boldsymbol{z}_s'\boldsymbol{\Upsilon}_0\boldsymbol{z}_s - \frac{1}{2}\dot{\boldsymbol{z}}_s'\boldsymbol{\Upsilon}_1\dot{\boldsymbol{z}}_s,\\ &= -\frac{1}{2}\boldsymbol{x}'\boldsymbol{F}\boldsymbol{x},\end{aligned} \tag{5.98}$$

in which

$$\boldsymbol{F} \triangleq \boldsymbol{\Lambda}_2 \begin{bmatrix} \boldsymbol{\Upsilon}_1^{-1} & \boldsymbol{0} & \boldsymbol{0} & \boldsymbol{0} \\ \boldsymbol{0} & \boldsymbol{\Gamma}_3^{-1} & \boldsymbol{\Gamma}_3^{-1} & \boldsymbol{\Gamma}_3^{-1} \\ \boldsymbol{0} & \boldsymbol{\Gamma}_3^{-1} & \boldsymbol{\Gamma}_3^{-1} & \boldsymbol{\Gamma}_3^{-1} \\ \boldsymbol{0} & \boldsymbol{\Gamma}_3^{-1} & \boldsymbol{\Gamma}_3^{-1} & \boldsymbol{\Gamma}_3^{-1} \end{bmatrix} \boldsymbol{\Lambda}_2 + \boldsymbol{D}, \tag{5.99}$$

with $\boldsymbol{\Lambda}_2 \triangleq \text{blkdiag}(\boldsymbol{U},\ \boldsymbol{Q},\ \boldsymbol{K},\ \boldsymbol{T})$. Matrix (5.99) is composed of two terms, where the first is positive semidefinite and the second is positive definite (the matrix $\boldsymbol{D}$ is defined in (5.71)), yielding $\boldsymbol{F} > 0$. Then, $\dot{\boldsymbol{V}}_2(\boldsymbol{x},t) < 0$, which ensures asymptotically stability for the closed-loop system in the Lyapunov sense. Accordingly, the weighted Sobolev norms of the cost variables $\boldsymbol{z}_c(t)$ and $\boldsymbol{z}_s(t)$ exist, such that $\frac{1}{2}||\boldsymbol{z}_c(t)||^2_{\mathcal{W}_{3,2,\boldsymbol{\Gamma}}} + \frac{1}{2}||\boldsymbol{z}_s(t)||^2_{\mathcal{W}_{1,2,\boldsymbol{\Upsilon}}} < \infty$ and, consequently, $\lim\limits_{t\to\infty} \boldsymbol{x}(t) = \boldsymbol{0}$. □

As commented in Remark 34, there are no desired trajectory for the stabilized DOF, they are accommodated by the controller to physically provide disturbance rejection while the controlled DOF track the trajectory. The following proposition analyzes the convergence of the stabilized DOF to a bounded stable condition.

Proposition 1. *Let $\boldsymbol{q}_s(t) : \mathbb{R}_{\geq 0} \to \mathbb{R}^{n_s}$, for some $n_s \in \mathbb{N}$, be differentiable and its time derivative, $\dot{\boldsymbol{q}}_s(t)$, be a uniformly continuous function, and $||\dot{\boldsymbol{q}}_s(t)||^2_{\mathcal{W}_{1,2,\boldsymbol{\Upsilon}}} < \infty$. Suppose $||\boldsymbol{q}_s(0)|| < \infty$, and $\boldsymbol{\Upsilon} = \{\boldsymbol{\Upsilon}_0, \boldsymbol{\Upsilon}_1\}$, such that $||\boldsymbol{\Upsilon}_0|| + ||\boldsymbol{\Upsilon}_1|| < \infty$. Therefore, $\lim_{t\to\infty} \boldsymbol{q}_s(t) = c_s$, for some $c_s \in \mathbb{R}$, requires that $\lim_{t\to\infty} \dot{\boldsymbol{q}}_s(t) = 0$.*

Proof. Suppose $||\boldsymbol{q}_s(0)|| < \infty$, $c_s \in \mathbb{R}$, and let $\dot{\boldsymbol{q}}_s(t)$ be a uniformly continuous function, from Barbalat's lemma (Slotine et al., 1991), $\lim_{t\to\infty} \boldsymbol{q}_s(t) = c_s$ implies $\lim_{t\to\infty} \dot{\boldsymbol{q}}_s(t) = 0$. In addition, from the definition of the $\mathcal{W}_{1,2,\boldsymbol{\Upsilon}}$-norm, $||\dot{\boldsymbol{q}}_s(t)||^2_{\mathcal{W}_{1,2,\boldsymbol{\Upsilon}}} < \infty$ implies $\lim_{t\to\infty} \dot{\boldsymbol{q}}_s(t) = 0$. □

Thus, assuming the system starts from a finite initial condition, $||\boldsymbol{q}_s(0)|| < \infty$, and since the closed-loop system ensures $||\dot{\boldsymbol{q}}_s(t)||^2_{\mathcal{W}_{1,2,\boldsymbol{\Upsilon}}} < \infty$, Lemma 1 applies to the closed-loop system composed of (5.66) with the control law (5.73).

Under Assumptions 6, 7, and 8, the applied control inputs are obtained by mapping the generalized inputs (5.73) provided by $\mathcal{W}_2$ controllers as follows

$$\boldsymbol{\tau} = \boldsymbol{B}^{\dagger}(\boldsymbol{x}, \boldsymbol{q}_s)\boldsymbol{u}^*, \tag{5.100}$$

where $(.)^{\dagger}$ denotes the pseudo-inverse operation.

5.2.2 Nonlinear $\mathcal{W}_\infty$ control approach

Consider again system (5.65) to obtain the plant $\mathcal{P}_6$ as follows

$$\mathcal{P}_6 : \begin{cases} \dot{\boldsymbol{x}}(t) & = \boldsymbol{f}(\boldsymbol{x}, \boldsymbol{q}_s) + \bar{\boldsymbol{f}}(\boldsymbol{x}, \boldsymbol{q}_s, t) + \boldsymbol{g}(\boldsymbol{x}, \boldsymbol{q}_s)\boldsymbol{u}(t) + \boldsymbol{k}(\boldsymbol{x}, \boldsymbol{q}_s)\boldsymbol{w}(t), \\ \boldsymbol{z}_c(t) & = \int_0^t \tilde{\boldsymbol{q}}_c(\tau)d\tau, \\ \boldsymbol{z}_s(t) & = \dot{\boldsymbol{q}}_s(t). \end{cases} \tag{5.101}$$

The nonlinear $\mathcal{W}_\infty$ control of underactuated mechanical systems with input coupling is posed as finding the control law $\boldsymbol{u} \in \mathcal{U}$ that minimizes the cost functional,

$$J_\infty = ||\boldsymbol{z}_c(t)||^2_{\mathcal{W}_{3,2,\boldsymbol{\Gamma}}} + \frac{1}{2}||\boldsymbol{z}_s(t)||^2_{\mathcal{W}_{1,2,\boldsymbol{\Upsilon}}} - \frac{1}{2}\gamma^2||\boldsymbol{w}(t)||^2_{\mathcal{L}_2}, \tag{5.102}$$

for the worst case of the disturbances $\boldsymbol{w}(t) \in \mathcal{L}_2[0, \infty)$, considering a given sufficiently large $\gamma \in \mathbb{R}_{\geq 0}$. Hence, the optimal control problem is given by

$$\begin{aligned} \boldsymbol{V}_\infty = & \min_{\boldsymbol{u}\in\mathcal{U}} \max_{\boldsymbol{w}\in\mathcal{D}} \left\{ \frac{1}{2}||\boldsymbol{z}_c(t)||^2_{\mathcal{W}_{3,2,\boldsymbol{\Gamma}}} + \frac{1}{2}||\boldsymbol{z}_s(t)||^2_{\mathcal{W}_{1,2,\boldsymbol{\Upsilon}}} - \gamma^2||\boldsymbol{w}(t)||^2_{\mathcal{L}_2} \right\}, \\ & \text{s.t.} \quad \mathcal{P}_6. \end{aligned} \tag{5.103}$$

The optimal control law is obtained by solving a Min-Max optimization problem, which is formulated again via dynamic programming using differential game theory. Therefore, the HJBI PDE is given by

$$\frac{\partial \boldsymbol{V}_\infty(\boldsymbol{x}, t)}{\partial t} + \min_{\boldsymbol{u}\in\mathcal{U}} \max_{\boldsymbol{w}\in\mathcal{D}} \left\{ \mathbb{H}_\infty(\boldsymbol{V}_\infty, \boldsymbol{x}, \boldsymbol{q}_s, \boldsymbol{u}, \boldsymbol{w}, t) \right\} = 0, \tag{5.104}$$

where the associated Hamiltonian is defined as

$$\begin{aligned} \mathbb{H}_\infty \triangleq & \frac{\partial \boldsymbol{V}_\infty(\boldsymbol{x}, t)}{\partial \boldsymbol{x}}\dot{\boldsymbol{x}} + \frac{1}{2}\boldsymbol{z}_c'\boldsymbol{\Gamma}_0\boldsymbol{z}_c + \frac{1}{2}\dot{\boldsymbol{z}}_c'\boldsymbol{\Gamma}_1\dot{\boldsymbol{z}}_c + \frac{1}{2}\ddot{\boldsymbol{z}}_c'\boldsymbol{\Gamma}_2\ddot{\boldsymbol{z}}_c + \frac{1}{2}\dddot{\boldsymbol{z}}_c'\boldsymbol{\Gamma}_3\dddot{\boldsymbol{z}}_c \\ & + \frac{1}{2}\boldsymbol{z}_s'\boldsymbol{\Upsilon}_0\boldsymbol{z}_s + \frac{1}{2}\dot{\boldsymbol{z}}_s'\boldsymbol{\Upsilon}_1\dot{\boldsymbol{z}}_s - \frac{1}{2}\gamma^2\boldsymbol{w}'\boldsymbol{w}, \end{aligned}$$

$$= \frac{\partial' \boldsymbol{V}_\infty}{\partial \boldsymbol{x}}\Big(\boldsymbol{f} + \bar{\boldsymbol{f}} + \boldsymbol{g}\boldsymbol{u} + \boldsymbol{k}\boldsymbol{w}\Big) + \frac{1}{2}\boldsymbol{x}'\boldsymbol{D}\boldsymbol{x} + \frac{1}{2}\ddot{\tilde{\boldsymbol{q}}}'\boldsymbol{E}\ddot{\tilde{\boldsymbol{q}}} - \frac{1}{2}\gamma^2\boldsymbol{w}'\boldsymbol{w} \tag{5.105}$$

with the boundary condition $\boldsymbol{V}_\infty(\boldsymbol{0}, t) = 0$.

In order to obtain the worst case of the disturbances, $\boldsymbol{w}^*$, and the optimal control law, $\boldsymbol{u}^*$, the partial derivatives of (5.105) with respect to these variables are computed as follows

$$\frac{\partial \mathbb{H}_\infty}{\partial \boldsymbol{u}} = \boldsymbol{g}'\frac{\partial \boldsymbol{V}_\infty}{\partial \boldsymbol{x}} - \Pi\boldsymbol{C}\dot{\tilde{\boldsymbol{q}}} - \Pi\boldsymbol{d} + \Pi\boldsymbol{w}^* + \Pi\boldsymbol{u}^* = 0, \tag{5.106}$$

$$\frac{\partial \mathbb{H}_\infty}{\partial \boldsymbol{w}} = \boldsymbol{k}'\frac{\partial \boldsymbol{V}_\infty}{\partial \boldsymbol{x}} - \Pi\boldsymbol{C}\dot{\tilde{\boldsymbol{q}}} - \Pi\boldsymbol{d} + \Pi\boldsymbol{u}^* + \Pi\boldsymbol{w}^* - \gamma^2\boldsymbol{w}^* = 0. \tag{5.107}$$

Thus, from (5.106), the optimal control law is given by

$$\boldsymbol{u}^* = -\Pi^{-1}\boldsymbol{g}'\frac{\partial \boldsymbol{V}_\infty}{\partial \boldsymbol{x}} + \boldsymbol{C}\dot{\tilde{\boldsymbol{q}}} + \boldsymbol{d} - \boldsymbol{w}^*. \tag{5.108}$$

In addition, the worst case of disturbance is computed by subtracting (5.107) from (5.106), leading to

$$\boldsymbol{w}^* = \frac{1}{\gamma^2}\Big(\boldsymbol{k}' - \boldsymbol{g}'\Big)\frac{\partial \boldsymbol{V}_\infty}{\partial \boldsymbol{x}}. \tag{5.109}$$

Through the second order partial derivatives of (5.105), it is possible to verify that (5.108) and (5.109) are a Min-Max extremum of the optimization problem,

$$\frac{\partial^2 \mathbb{H}_\infty}{\partial \boldsymbol{u}^2} = \Pi > 0, \tag{5.110}$$

$$\frac{\partial^2 \mathbb{H}_\infty}{\partial \boldsymbol{w}^2} = \Pi - \gamma^2\boldsymbol{I} < 0. \tag{5.111}$$

Remark 35. *Remark 29 holds similarly for* (5.111).

The HJ PDE associated to the problem is obtained by replacing the optimal control law (5.108) and the worst case of disturbance (5.109) in (5.104), which in a compact form is written as

$$\frac{\partial \boldsymbol{V}_\infty(\boldsymbol{x}, t)}{\partial t} + \mathbb{H}_\infty(\boldsymbol{V}_\infty, \boldsymbol{x}, \boldsymbol{q}_s, \boldsymbol{u}^*, \boldsymbol{w}^*, t) = 0. \tag{5.112}$$

The optimal control problem (5.103) results in solving the PDE (5.112) in order to find the solution $\boldsymbol{V}_\infty(\boldsymbol{x}, t)$.

Remark 36. *For the underactuated mechanical system with input coupling* (5.62)*, assuming* $\boldsymbol{u} = \boldsymbol{B}(\boldsymbol{x}, \boldsymbol{q}_s)\boldsymbol{\tau}$*, the error dynamics* (5.65) *possess* $\boldsymbol{k}(\boldsymbol{x}, \boldsymbol{q}_s, t) = \boldsymbol{g}(\boldsymbol{x}, \boldsymbol{q}_s, t)$*. Therefore, from* (5.109) *the* $\mathcal{W}_2$ *and the* $\mathcal{W}_\infty$ *controllers become equivalent and the particular solution* (5.75) *proposed in Theorem 4 is also a solution to* (5.112).

From equation (5.109), one verifies that the worst case of the disturbances $\boldsymbol{w}^*$ is a vector that depends on the difference $\boldsymbol{k}(\boldsymbol{x}) - \boldsymbol{g}(\boldsymbol{x})$. By analyzing this equation, it can bee

seen that two cases can occur: $\boldsymbol{k}(\boldsymbol{x})$ and $\boldsymbol{g}(\boldsymbol{x})$ span the same columns space; and $\boldsymbol{k}(\boldsymbol{x})$ and $\boldsymbol{g}(\boldsymbol{x})$ span different columns spaces.

If $\boldsymbol{k}(\boldsymbol{x})$ and $\boldsymbol{g}(\boldsymbol{x})$ span the same columns space, i.e. $\exists n \in \mathbb{N}$, $rank(\boldsymbol{k}(\boldsymbol{x})) = \text{rank}(\boldsymbol{g}(\boldsymbol{x})) = n$, $\forall \boldsymbol{x} \in \mathbb{R}^x$, there are three possibilities, $\boldsymbol{k}(\boldsymbol{x}) = \boldsymbol{g}(\boldsymbol{x})$, $\boldsymbol{k}(x) = \boldsymbol{g}(\boldsymbol{x})\boldsymbol{a}(\boldsymbol{x})$, or $\boldsymbol{g}(x) = \boldsymbol{k}(\boldsymbol{x})\boldsymbol{a}(\boldsymbol{x})$, in which $\boldsymbol{a}(\boldsymbol{x})$ is a matrix with appropriated dimension and $\text{rank}(\boldsymbol{a}(\boldsymbol{x})) \geq n$. The first possibility leads straightforward to $\boldsymbol{w}^* = 0$. For the second possibility, the state-space system (5.101) is given by

$$\dot{\boldsymbol{x}}(t) = \boldsymbol{f}(\boldsymbol{x}, \boldsymbol{q}_s) + \bar{\boldsymbol{f}}(\boldsymbol{x}, \boldsymbol{q}_s, t) + \boldsymbol{g}(\boldsymbol{x}, \boldsymbol{q}_s)\boldsymbol{u}(t) + \boldsymbol{k}(\boldsymbol{x}, \boldsymbol{q}_s)\boldsymbol{a}(\boldsymbol{x})\boldsymbol{w}(t). \tag{5.113}$$

So, there exists a transformation over the disturbances vector such that the system can be expressed as (We used a similar transformation to derive the $\mathcal{W}_\infty$ controller for reduced underactuated mechanical system, see Subsection 5.1.2)

$$\dot{\boldsymbol{x}}(t) = \boldsymbol{f}(\boldsymbol{x}, \boldsymbol{q}_s) + \bar{\boldsymbol{f}}(\boldsymbol{x}, \boldsymbol{q}_s, t) + \boldsymbol{g}(\boldsymbol{x}, \boldsymbol{q}_s)\boldsymbol{u}(t) + \boldsymbol{k}(\boldsymbol{x}, \boldsymbol{q}_s)\bar{\boldsymbol{w}}(t), \tag{5.114}$$

in which $\bar{\boldsymbol{w}} = \boldsymbol{a}(\boldsymbol{x})\boldsymbol{w}$. Accordingly, one can see that the computation of (5.109) for (5.114) leads to $\boldsymbol{w}^* = 0$. The same idea can be used to show that $\boldsymbol{w}^* = 0$ also holds for the third possibility.

These results mean that any disturbance $\boldsymbol{w} \in \mathcal{L}_2[0, \infty)$ can be handled by an appropriated control input $\boldsymbol{u} \in \mathbb{R}^c$, since both actuate in the same space. This justifies Remark 36, which states, in this case, that the $\mathcal{W}_2$ and $\mathcal{W}_\infty$ controllers become equivalent.

The closed-loop stability is proven in the following Theorem.

Theorem 6. *Let $\boldsymbol{V}_\infty(\boldsymbol{x}, t) > 0$ be a solution of (5.112) given by (5.75). Therefore, the closed-loop system, with the control law (5.108) and system (5.101), is asymptotically stable.*

Proof. The proof of this Theorem is similar to the proof of Theorem 5, since $\boldsymbol{w}^*(t) = \boldsymbol{0}$. □

In addition, for a generic $\boldsymbol{w}(t) \in \mathcal{L}_2[0, \infty)$ and a finite initial condition $\boldsymbol{x}(0)$, considering the control law (5.108) and the function $\boldsymbol{V}_\infty(\boldsymbol{x}, t)$ given by (5.75), from (5.112) one can obtain

$$\int_0^\infty \frac{d\boldsymbol{V}_\infty(\boldsymbol{x}, t)}{dt} dt \leq \int_0^\infty \left(-\frac{1}{2}\boldsymbol{x}'\boldsymbol{F}\boldsymbol{x} + \frac{1}{2}\gamma^2 \boldsymbol{w}'\boldsymbol{w} \right) \text{dt}, \tag{5.115}$$

$$\lim_{t\to\infty} \boldsymbol{V}_\infty(\boldsymbol{x}(t), t) - \boldsymbol{V}_\infty(\boldsymbol{x}(0), 0) \leq -\frac{1}{2}||\boldsymbol{z}_c(t)||^2_{\mathcal{W}_{3,2,\boldsymbol{\Gamma}}} - \frac{1}{2}||\boldsymbol{z}_s(t)||^2_{\mathcal{W}_{1,2,\boldsymbol{\Upsilon}}} + \frac{1}{2}\gamma^2||\boldsymbol{w}(t)||^2_{\mathcal{L}_2},$$

and so $||\boldsymbol{z}_c(t)||^2_{\mathcal{W}_{3,2,\boldsymbol{\Gamma}}} + ||\boldsymbol{z}_s(t)||^2_{\mathcal{W}_{1,2,\boldsymbol{\Upsilon}}} \leq \gamma^2||\boldsymbol{w}(t)||^2_{\mathcal{L}_2} + 2\boldsymbol{V}_\infty(\boldsymbol{x}(0), 0)$. Accordingly, the following inequalities are true

$$||\boldsymbol{z}_c(t)||^2_{\mathcal{W}_{3,2,\boldsymbol{\Gamma}}} \leq \gamma^2||\boldsymbol{w}(t)||^2_{\mathcal{L}_2} + 2\boldsymbol{V}_\infty(\boldsymbol{x}(0), 0) - ||\boldsymbol{z}_s(t)||^2_{\mathcal{W}_{1,2,\boldsymbol{\Upsilon}}}, \tag{5.116}$$

$$||\boldsymbol{z}_s(t)||^2_{\mathcal{W}_{1,2,\boldsymbol{\Upsilon}}} \leq \gamma^2 ||\boldsymbol{w}||^2_{\mathcal{L}_2} + 2\boldsymbol{V}_\infty(\boldsymbol{x}(0), 0) - ||\boldsymbol{z}_c(t)||^2_{\mathcal{W}_{3,2,\boldsymbol{\Gamma}}}. \tag{5.117}$$

Thus, from Theorem 6, we have that $||\boldsymbol{z}_c(t)||^2_{\mathcal{W}_{3,2,\boldsymbol{\Gamma}}} + ||\boldsymbol{z}_s(t)||^2_{\mathcal{W}_{1,2,\boldsymbol{\Upsilon}}} < \infty$, which implies $||\boldsymbol{z}_c(t)||^2_{\mathcal{W}_{3,2,\boldsymbol{\Gamma}}} < \infty$ and $||\boldsymbol{z}_s(t)||^2_{\mathcal{W}_{1,2,\boldsymbol{\Upsilon}}} < \infty$. Thereby, we can verify, from Definition 7 and through inequalities (5.116) and (5.117), that the closed-loop system is $\mathcal{W}_{3,2,\boldsymbol{\Gamma}}$-stable from the disturbance to the output $\boldsymbol{z}_c(t)$, and $\mathcal{W}_{1,2,\boldsymbol{\Upsilon}}$-stable from the disturbance to the output $\boldsymbol{z}_s(t)$. In addition, the $\mathcal{W}_{3,2,\boldsymbol{\Gamma}}/\mathcal{W}_{1,2,\boldsymbol{\Upsilon}}$-gain is the smallest $\gamma \in \mathbb{R}_{\geq 0}$ that satisfies $\dfrac{\partial^2 \mathbb{H}_\infty}{\partial \boldsymbol{w}^2} = \Pi - \gamma^2 \boldsymbol{I} < 0$.

Finally, under Assumptions 6, 7, and 8, the applied control inputs are obtained by mapping the generalized input (5.108) provided by the $\mathcal{W}_\infty$ controller as follows

$$\boldsymbol{\tau} = \boldsymbol{B}^\dagger(\boldsymbol{x}, \boldsymbol{q}_s)\boldsymbol{u}^*. \tag{5.118}$$

5.3 Numerical examples

This section corroborates the efficacy of the nonlinear $\mathcal{W}_2$ and $\mathcal{W}_\infty$ control strategies proposed in this chapter with numerical experiments conducted with a fully actuated manipulator, a Two-wheeld Self-balanced vehicle, and a Quadrotor UAV. In addition it performs a comparative analysis of these controllers with respect to a nonlinear $\mathcal{H}_\infty$ controller.

5.3.1 Fully actuated and reduced underactuated mechanical systems

In this subsection, the approaches addressed in Section 5.1 are employed to synthesize controllers for a fully actuated manipulator and for a Quadrotor UAV in order to achieve trajectory tracking of the attitude (Euler angles) and altitude motion.

Fully actuated manipulator

The fully actuated manipulator equations of motion were obtained from Spong et al. (2006) and are given by the Euler-Lagrange equations

$$\boldsymbol{M}(\boldsymbol{q})\ddot{\boldsymbol{q}}(t) + \boldsymbol{C}(\boldsymbol{q}, \dot{\boldsymbol{q}})\dot{\boldsymbol{q}}(t) + \boldsymbol{g}(\boldsymbol{q}) = \boldsymbol{B}(\boldsymbol{q})\boldsymbol{\tau}(t) + \boldsymbol{w}(t), \tag{5.119}$$

where $\boldsymbol{q}(t) = \begin{bmatrix} q_1(t) & q_2(t) \end{bmatrix}'$, $\boldsymbol{\tau}(t) = \begin{bmatrix} \tau_1(t) & \tau_2(t) \end{bmatrix}'$, $\boldsymbol{w}(t) = \begin{bmatrix} w_1(t) & w_2(t) \end{bmatrix}'$,

$$\boldsymbol{M}(\boldsymbol{q}) = \begin{bmatrix} d_{11} & d_{12} \\ d_{21} & d_{22} \end{bmatrix}, \tag{5.120}$$

$$
\begin{aligned}
d_{11} &\triangleq m_1\left(\frac{l_1}{2}\right)^2 + m_2\left(l_1^2 + \left(\frac{l_2}{2}\right)^2 + 2l_1\left(\frac{l_2}{2}\right)^2 + 2l_1\left(\frac{l_2}{2}\right)\cos(q_2)\right) + I_1 + I_2,\\
d_{12} &\triangleq m_2\left(\left(\frac{l_2}{2}\right)^2 + l_1\left(\frac{l_2}{2}\right)^2\cos(q_2)\right) + I_2,\\
d_{21} &\triangleq d_{12},\\
d_{22} &\triangleq m_2\left(\frac{l_2}{2}\right)^2 + I_2,\\
\boldsymbol{C}(\boldsymbol{q}) &= \begin{bmatrix} h\dot{q}_2 & h\dot{q}_2 + h\dot{q}_1 \\ -h\dot{q}_1 & 0 \end{bmatrix}, \qquad (5.121)\\
h &\triangleq -m_2 l_1\left(\frac{l_2}{2}\right)\sin(q_2),\\
\boldsymbol{g}(\boldsymbol{q}) &= \begin{bmatrix} \left(m_1\left(\frac{l_1}{2}\right) + m_2 l_1\right) g\cos(q_1) + m_2\left(\frac{l_2}{2}\right) g\cos(q_1+q_2) \\ m_2\left(\frac{l_2}{2}\right) g\cos(q_1+q_2) \end{bmatrix}, \qquad (5.122)
\end{aligned}
$$

in which q_i is angular position of joint i, for $i \in \{1,\ 2\}$, τ_i is the torque applied at joint i, w_i is the disturbance applied at joint i, I_i is the moment of inertia of link i, L_i is the length of link i, m_i is the mass of link i, and g is the gravity acceleration. The fully actuated manipulator is illustrated in Figure 5.1 and the parameters used to perform the numerical experiments are presented in Table 5.1.

Figure 5.1: The fully actuated manipulator.

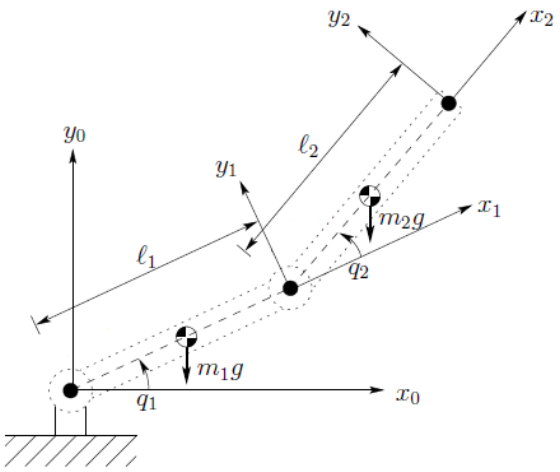

Table 5.1: Fully actuated manipulator physical parameters

Parameter	Value	Unit of measurement
$I_1,\ I_2$	1	$Kg.m^2$
$m_1,\ m_2$	1	Kg
$l_1,\ l_2$	1	m
g	9.8	m/s^2

In order to synthesize the controllers proposed in Section 5.1 for this manipulator, initially, the system (5.119) is partitioned with $\boldsymbol{q}_c(t) = \boldsymbol{q}(t) = \begin{bmatrix} q_1(t) & q_2(t) \end{bmatrix}'$ and no uncontrolled DOF, and rewritten in the form of system (5.8). It is noteworthy that, Remark 23 applies in this case. Thereafter, the optimal control law (5.53) is applied to the system considering the particular solution (5.18) of the HJ PDE proposed in Theorem 5.18. The controller was tuned via trial and error with $\boldsymbol{\mathcal{Y}}_0 = \text{diag}([100 \;\; 200])$, $\boldsymbol{\mathcal{Y}}_1 = \text{diag}([500 \;\; 400])$, $\boldsymbol{\mathcal{Y}}_2 = \text{diag}([40 \;\; 40])$, and $\boldsymbol{\mathcal{Y}}_3 = \text{diag}([0.0720 \;\; 0.0126])$. For this particular case, Remark 30 applies and, consequently, the $\mathcal{W}_2$ and $\mathcal{W}_\infty$ controllers are equivalent, from now on called $\mathcal{W}_{2/\infty}$ controller.

For the sake of comparison analysis, a nonlinear $\mathcal{H}_\infty$ controller was also designed and tuned to achieve almost the same control effort as the $\mathcal{W}_{2/\infty}$ controller, measured by the Absolute Derivative of the control signal (IADU) index. In order to analyze the results, the integral of the square error (ISE) index was evaluated over the controlled DOF. The resulting values are shown in Table 5.3.

The simulation was conducted with the manipulator starting from the initial conditions $\boldsymbol{q}(0) = [\frac{\pi}{4} \;\; 0]'$ and $\dot{\boldsymbol{q}}(0) = \boldsymbol{0}$ and designated to perform trajectory tracking of the desired trajectory described in Table 5.2. In addition, constant and time-varying external disturbances, $w_1(t) = 40$ N·m, for $10 \geq t \geq 20$ s, and $w_2(t) = -40\sin(\frac{2\pi t}{10})$ N·m, for $25 \geq t \geq 35$ s, are applied to the system. The time evolution of the states, external disturbances and control signals are shown in Figure 5.2.

Table 5.2: Desired trajectory for the fully actuated manipulator.

	$q_{1_r}(t)$	$q_{2_r}(t)$
$t \geq 0$	$\frac{\pi}{2}$	$\frac{\pi}{2}\sin(\frac{2\pi}{10}t)$

Table 5.3: Table of performance indexes computed from the results of nonlinear $\mathcal{W}_{2/\infty}$ and $\mathcal{H}_\infty$ controllers applied to the fully actuated manipulator.

P. Index	computed as	$\mathcal{W}_{2/\infty}$	$\mathcal{H}_\infty$
IADU	$\int_0^\tau \sum_{i=1}^2 \lvert\frac{d\tau_i(t)}{dt}\rvert dt$	845.8 (100.3%)	**843.29** (100%)
ISE	$\int_0^\tau (q_1(t) - q_{1_r}(t))^2 dt$	**0.2545** (44%)	0.5686 (100%)
	$\int_0^\tau (q_2(t) - q_{2_r}(t))^2 dt$	**0.1370** (58%)	0.2362 (100%)

As can be observed in Figure 5.2, the $\mathcal{W}_\infty$ controller achieved a faster convergence to the reference and a better disturbances attenuation. It is worth mentioning that although both controllers, $\mathcal{W}_{2,\infty}$ and $\mathcal{H}_\infty$, were tuned to achieve the similar control effort measured

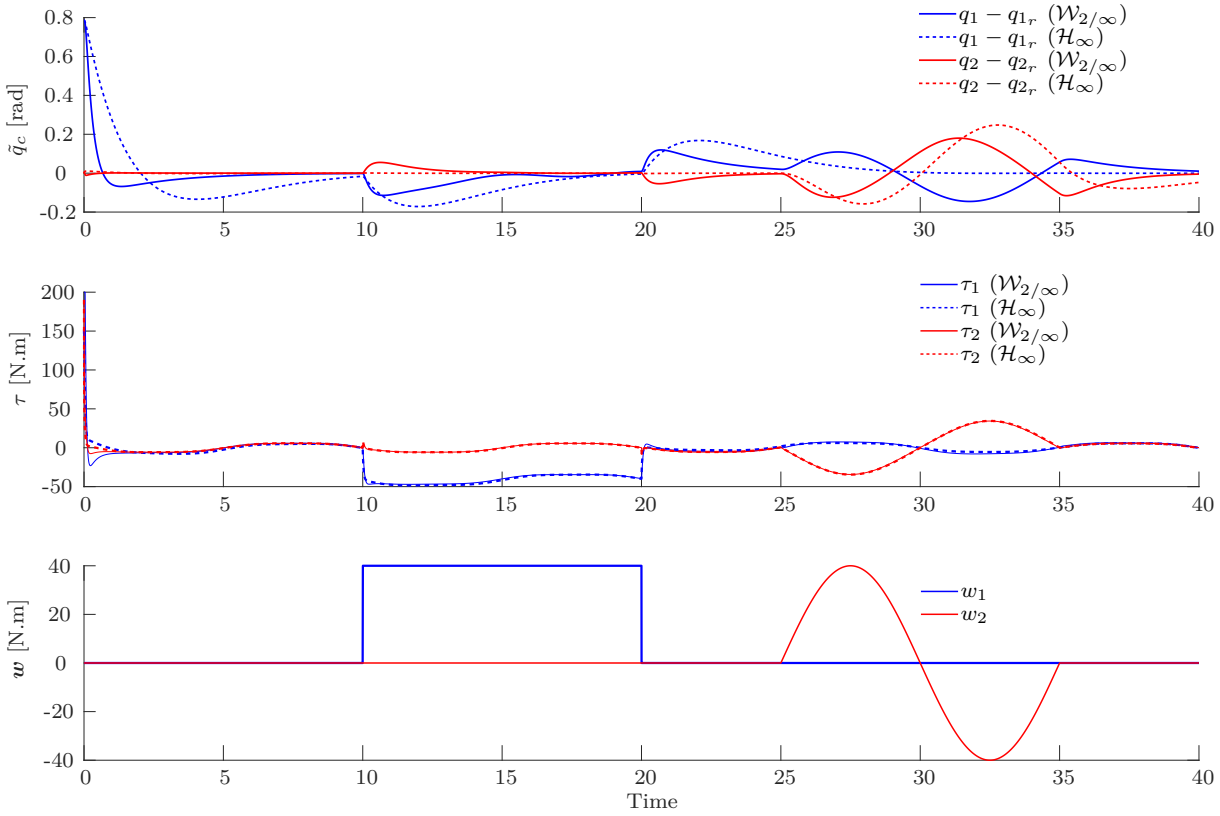

Figure 5.2: Time evolution of the controlled DOF errors, resulting from the application of the nonlinear $\mathcal{W}_{2/\infty}$ and $\mathcal{H}_\infty$ controllers to the fully actuated manipulator, and the disturbance signals.

by the IADU index (See Table 5.3), the $\mathcal{W}_\infty$ controller achieved better results with respect to the ISE index.

Quadrotor UAV

The Quadrotor UAV equations of motion were obtained from Raffo et al. (2011a) and are given by the Euler-Lagrange equations

$$\boldsymbol{M}(\boldsymbol{q})\ddot{\boldsymbol{q}}(t) + \boldsymbol{C}(\boldsymbol{q},\dot{\boldsymbol{q}})\dot{\boldsymbol{q}}(t) + \boldsymbol{g}(\boldsymbol{q}) = \boldsymbol{B}(\boldsymbol{q})\boldsymbol{\tau}(t) + \boldsymbol{w}(t), \tag{5.123}$$

where $\boldsymbol{q}(t) = [\phi(t)\ \theta(t)\ \psi(t)\ x(t)\ y(t)\ z(t)]'$, $\boldsymbol{g}(\boldsymbol{q}) = [\boldsymbol{0}\ \ mg]'$,

$$\boldsymbol{M}(\boldsymbol{q}) = \begin{bmatrix} \boldsymbol{\mathcal{W}}_\eta' \mathbb{I} \boldsymbol{\mathcal{W}}_\eta & \boldsymbol{0} \\ \boldsymbol{0} & m\boldsymbol{I} \end{bmatrix}, \qquad \boldsymbol{\mathcal{W}}_\eta' = \begin{bmatrix} 1 & 0 & -s(\theta) \\ 0 & c(\phi) & s(\phi)c(\theta) \\ 0 & -s(\phi) & c(\phi)c(\theta) \end{bmatrix},$$

$$\boldsymbol{B}(\boldsymbol{q}) = \begin{bmatrix} \boldsymbol{\mathcal{W}}'_{\eta} & \mathbf{0} \\ \mathbf{0} & \boldsymbol{R} \end{bmatrix} \begin{bmatrix} 0 & lbc(\alpha) & 0 & -lbc(\alpha) \\ -lbc(\alpha) & 0 & lbc(\alpha) & 0 \\ dc(\alpha) & -dc(\alpha) & dc(\alpha) & -dc(\alpha) \\ -bs(\alpha) & 0 & bs(\alpha) & 0 \\ 0 & -bs(\alpha) & 0 & bs(\alpha) \\ bc(\alpha) & bc(\alpha) & bc(\alpha) & bc(\alpha) \end{bmatrix},$$

in which $s(\cdot) \triangleq \sin(\cdot)$; $c(\cdot) \triangleq \cos(\cdot)$; $\mathbb{I} = \text{diag}([I_{xx}\ I_{yy}\ I_{zz}])$, with I_{xx}, I_{yy}, I_{zz} the Quadrotor's moments of inertia; $\boldsymbol{R} = \boldsymbol{R}_{z,\psi}\boldsymbol{R}_{y,\theta}\boldsymbol{R}_{x,\phi}$, with $\boldsymbol{R}_{a,\beta}$ the rotation matrix of angle β about the a axis, for $\beta \in \{\psi\ \theta\ \phi\}$ and $a \in \{\vec{z},\ \vec{y},\ \vec{x}\}$; x, y and z are the Quadrotor UAV planar position and altitude, respectively; ϕ, θ and ψ are the Quadrotor UAV orientation described by Euler angles using ZYX convention about the local axes; $\boldsymbol{\tau}$=$[\Omega_1^2 \quad \Omega_2^2 \quad \Omega_3^2 \quad \Omega_4^2]'$ is the vector of control inputs with Ω_i, for $i = \{1,\ 2,\ 3,\ 4\}$, the propellers' angular velocities; $\boldsymbol{w}$=$[\delta_\phi\ \delta_\theta\ \delta_\psi\ \delta_x\ \delta_y\ \delta_z]'$ is the vector of generalized disturbances; m is the Quadrotor mass; g is the gravitational acceleration; α is a small propellers inclination angle, which provides the mentioned input coupling in the control input matrix; l is the displacement between the Quadrotor center of mass and the propellers application point of forces; d and b are the propellers drag and thrust constants.

The Coriolis and centrifugal force matrix $\boldsymbol{C}(\boldsymbol{q}, \dot{\boldsymbol{q}})$, can be obtained from the Christoffel symbols of first kind as

$$\boldsymbol{C}_{k,j} = \sum_{l=1}^{8} \frac{1}{2} \left[\frac{\partial \boldsymbol{M}_{k,j}}{\partial \boldsymbol{q}_l} + \frac{\partial \boldsymbol{M}_{k,l}}{\partial \boldsymbol{q}_j} - \frac{\partial \boldsymbol{M}_{l,j}}{\partial \boldsymbol{q}_k} \right] \dot{\boldsymbol{q}}_l,$$

where $\boldsymbol{C}_{k,j}$ and $\boldsymbol{M}_{k,j}$ are elements of the Coriolis and inertia matrices, respectively, corresponding to the k-th row and j-th column. The quad-rotor UAV parameters are presented in Table 5.4.

Table 5.4: Quadrotor UAV physical parameters

Parameter	Value	Unit of measurement
I_{xx}, I_{yy}, I_{zz}	$\{0.0363, 0.0363, 0.0615\}$	$Kg.m^2$
m	2.2	Kg
α	5	deg
l	0.21	m
g	9.8	m/s^2
b	$2.9 \cdot 10^{-5}$	$N.s^2$
d	$6 \cdot 10^{-6}$	$N.m.s^2$

In order to synthesize the controllers proposed in Section 5.1 for the Quadrotor UAV, initially, the system (5.123) is partitioned with $\boldsymbol{q}_c(t) = [z(t)\ \phi(t)\ \theta(t)\ \psi(t)]'$ and $\boldsymbol{q}_u(t) = [x(t)\ y(t)]'$ and rewritten in the form of system (5.8). Based on this partition, Assumption 5 is ensured with $\phi \neq \frac{\pi}{2} + 2\pi n_\phi$, for any $n_\phi \in \mathbb{Z}$ (the well known Euler angles singularity). Thereafter, the optimal control law (5.53) is applied to the system con-

sidering the particular solution (5.18) of the HJ PDE proposed in Theorem 5.18. The controller was tuned via trial and error with $\boldsymbol{\mathcal{Y}}_0 = \text{diag}([1 \;\; 1 \;\; 1 \;\; 1])$, $\boldsymbol{\mathcal{Y}}_1 = \text{diag}([1 \;\; 1 \;\; 1 \;\; 1])$, , $\boldsymbol{\mathcal{Y}}_2 = \text{diag}([0.61 \;\; 0.6 \;\; 0.6 \;\; 0.6])$, and $\boldsymbol{\mathcal{Y}}_3 = \text{diag}([2{\cdot}10^{-3} \;\; 1{\cdot}10^{-7} \;\; 1{\cdot}10^{-7} \;\; 1{\cdot}10^{-7}])$. For this particular case, Remark 30 applies and, consequently, the $\mathcal{W}_2$ and $\mathcal{W}_\infty$ controllers are also equivalent, from now on called again $\mathcal{W}_{2/\infty}$ controller.

For comparison analysis, the nonlinear $\mathcal{H}_\infty$ controller presented in Raffo et al. (2011b) was used. Both, the $\mathcal{W}_{2/\infty}$ and the $\mathcal{H}_\infty$ controllers, were tuned to achieve the same control effort, which was measured by the Absolute Derivative of the control signal (IADU) index. In order to analyze the results, the integral of the square error (ISE) was evaluated over the controlled DOF. These performance indexes are shown in Table 5.6.

The simulation was conducted with the Quadrotor UAV starting from initial conditions $\boldsymbol{q}_c(0) = [4.5 \;\; \pi/4 \;\; -\pi/4 \;\; \pi/4]'$, $\dot{\boldsymbol{q}}_c(0) = \mathbf{0}$, and $\dot{\boldsymbol{q}}_u(0) = \boldsymbol{q}_u(0) = \mathbf{0}$ and designated to perform trajectory tracking of the desired trajectory described in Table 5.5. In addition, constant and time-varying external disturbances, $\delta_z(t) = -10[N]$, for $10 \geq t \geq 15$, and $\delta_\phi(t) = -3sin(2\pi t)$, for $16 \geq t \geq 20$, are applied to the system. The external disturbances and control signals are shown in Figure 5.3, and the time evolution of the states are showed in Figure 5.4.

Table 5.5: Desired trajectory for the Quadrotor UAV altitude and attitude.

	$z_r(t)$	$\phi_r(t)$	$\theta_r(t)$	$\psi_r(t)$
$t \leq 8$	$5 - \sin\left(\frac{2\pi}{8}t\right)/2$	$\frac{\pi}{4}\sin\left(\frac{2\pi}{5}t\right)$	$\frac{\pi}{4}\sin\left(\frac{2\pi}{5}t\right)$	$\frac{\pi}{4}\sin\left(\frac{2\pi}{5}t\right)$
$8 < t \leq 30$	5	0	$\frac{\pi}{4}\sin\left(\frac{2\pi}{5}t\right)$	$2\pi\sin\left(\frac{2\pi}{40}t\right)$

At the beginning of the simulation, the Quadrotor UAV starts displaced from the desired trajectory and is designated to track a sinusoidal signal on the altitude and attitude dynamics. The purpose is to evaluate the capacity of tracking a time-varying trajectory. Note that, it converges to the reference along with time. After eight seconds of simulation, the altitude and roll dynamics are required to track constant references. The changes from the sinusoidal to the constant stretches are not smooth. Consequently, the Quadrotor UAV is pushed out of the trajectory due to its inertia, converging again to it after some seconds.

Note that, the $\mathcal{W}_{2/\infty}$ controller reacts faster than the $\mathcal{H}_\infty$ controller when the system is affected by external disturbances and provides better disturbance attenuation. Further, when the disturbance δ_z affects the Quadrotor UAV, the $\mathcal{H}_\infty$ controller achieves oscillatory behavior on the altitude motion. This is because the nonlinear $\mathcal{H}_\infty$ control approach weights all the dynamics of the mechanical system equally in the cost functional, while the proposed controllers allow a component wise tuning of the system dynamics, achieving

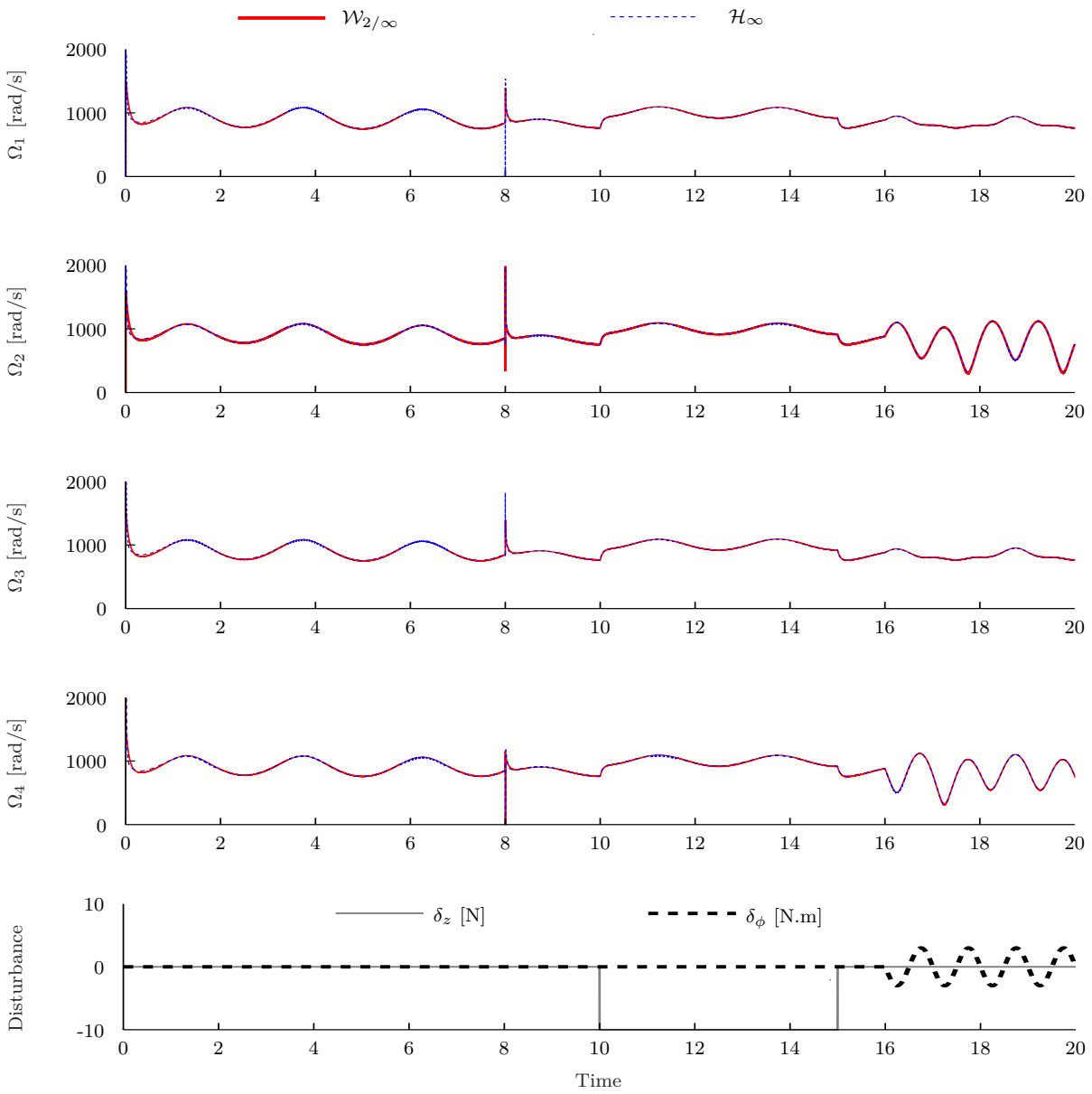

Figure 5.3: Time evolution of the control inputs, resulting from the application of the nonlinear $\mathcal{W}_{2/\infty}$ and $\mathcal{H}_\infty$ controllers to the Quadrotor UAV, and the disturbance signals.

better performance.

Finally, as shown in Table 5.6, even both controllers have been adjusted to obtain the same control effort, the $\mathcal{W}_{2/\infty}$ controller achieved better results with respect to the ISE performance index in comparison with the classic nonlinear $\mathcal{H}_\infty$ controller.

5.3.2 Underactuated mechanical systems with input coupling

In this subsection, the approaches addressed in Section 5.2 are employed to synthesize controllers for a Two-wheeled Self-balanced vehicle in order to keep it standing in the upper vertical position, while subject to external disturbances, and a Quadrotor UAV in order to achieve trajectory tracking of the translational position and yaw angle while the

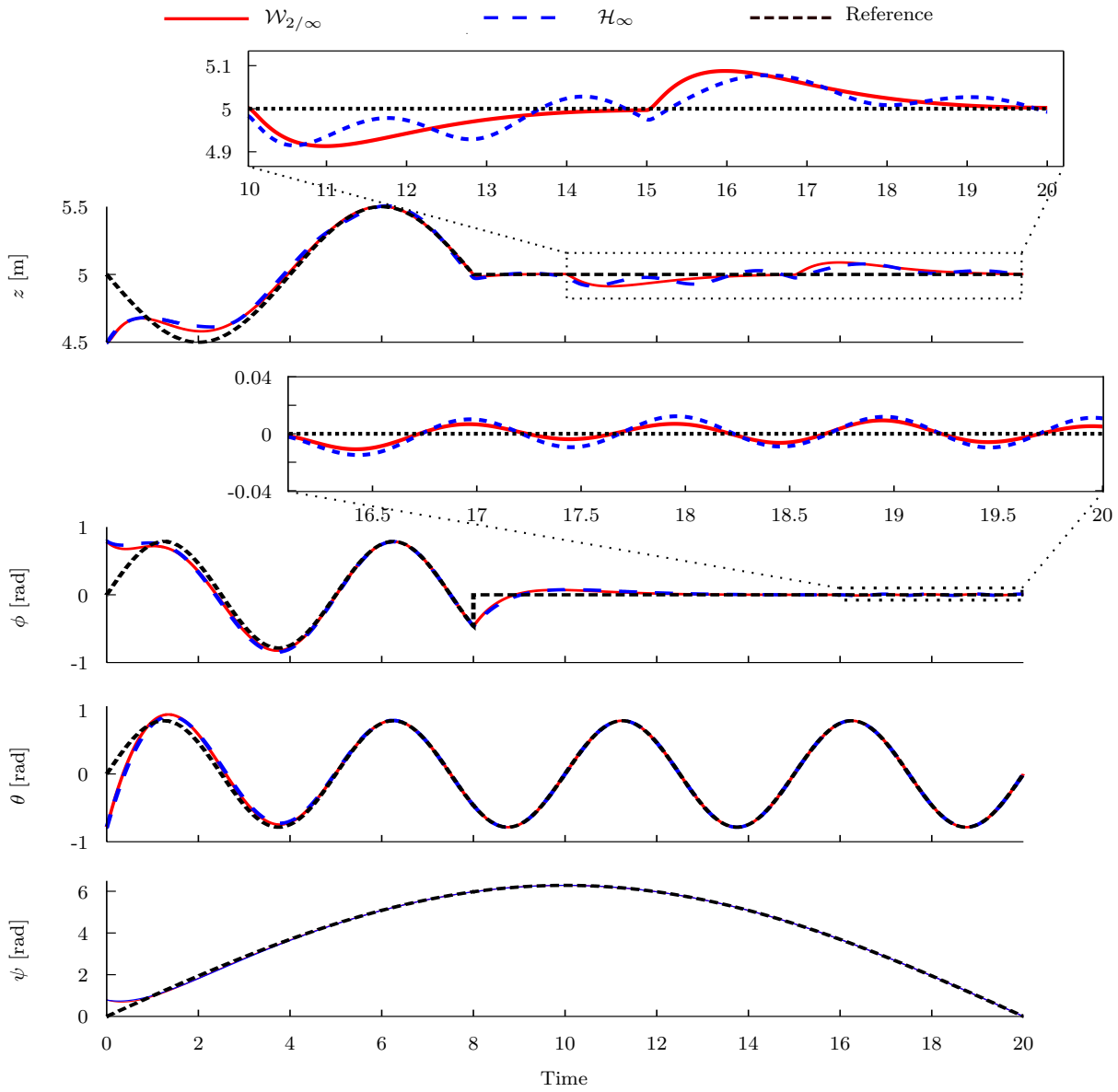

Figure 5.4: Time evolution of the controlled DOF resulting from the application of the nonlinear $\mathcal{W}_{2/\infty}$ and $\mathcal{H}_\infty$ controllers to the Quadrotor UAV.

roll and pitch dynamics are stabilized.

Two-wheeled self-balanced vehicle

The Two-wheeled Self-balanced vehicle equations of motion are presented in Section 4.4. In order to synthesize the controllers proposed in Section 5.2 for this system, initially, the equation (4.30) is partitioned with $\boldsymbol{q}_c(t) = \theta(t)$ and $\boldsymbol{q}_s(t) = \phi(t)$. Thereafter, considering (5.118) and the particular solution of the HJ PDE proposed in Theorem 4, the control law (5.73) is applied to the system. The controller was tuned via trial and error with $\boldsymbol{\Upsilon}_0 = 0.1$, $\boldsymbol{\Upsilon}_1 = 1.1$, $\boldsymbol{\Gamma}_0 = 1000$, $\boldsymbol{\Gamma}_1 = 300$, $\boldsymbol{\Gamma}_2 = 2$, $\boldsymbol{\Gamma}_3 = 0.001$. It is worth mentioning that, Remark 36 applies to this particular case, thus, from now on this controller is also called $\mathcal{W}_{2/\infty}$ controller.

Table 5.6: Table of performance indexes computed from the results of the nonlinear $\mathcal{W}_{2/\infty}$ and $\mathcal{H}_\infty$ controllers applied to the Quadrotor UAV.

P. Index	computed by	$\mathcal{W}_{2/\infty}$	$\mathcal{H}_\infty$
IADU	$\int_0^\tau \sum_{i=1}^4 \lvert\frac{d\Omega_i(t)}{dt}\rvert dt$	**5.4×10^4** (100%)	**5.4×10^4** (100%)
ISE	$\int_0^\tau (z(t) - z_r(t))^2 dt$	**0.093** (95%)	0.097 (100%)
	$\int_0^\tau (\phi(t) - \phi_r(t))^2 dt$	**0.202** (83%)	0.243 (100%)
	$\int_0^\tau (\theta(t) - \theta_r(t))^2 dt$	**0.153** (84%)	0.181 (100%)
	$\int_0^\tau (\psi(t) - \psi_r(t))^2 dt$	**0.151** (84%)	0.178 (100%)

The nonlinear $\mathcal{H}_\infty$ controller presented in Raffo et al. (2015) was also designed for this system. For the sake of comparison analysis, this controller was tuned to achieve similar ISE performance index as the $\mathcal{W}_{2/\infty}$ controller, computed for the variable θ.

The numerical experiment was conducted with the Two-wheeled Self-balanced vehicle starting from $\dot{\boldsymbol{q}}_s(0) = \boldsymbol{q}_s(0) = 0$, $\boldsymbol{q}_c(0) = \frac{\pi}{4}$, $\dot{\boldsymbol{q}}_c(0) = 0$ and designated to stand at the upper vertical position. Along the experiment, time-varying and constant disturbances with magnitudes $w_\phi(t) = 4\sin(\frac{2\pi t}{5})$ N·m, for $7 \leq t \leq 14$ s, and $w_\theta(t) = 4$ N·m, for $22 \leq t \geq 32$ s, are applied to the system. The results are shown in Figure 5.5.

Table 5.7: Table of performance indexes computed from the results of the nonlinear $\mathcal{W}_{2/\infty}$ and $\mathcal{H}_\infty$ controllers applied to the Two-wheeled Self-balanced vehicle.

P. Index	computed by	$\mathcal{W}_{2/\infty}$	$\mathcal{H}_\infty$
IADU	$\int_0^\tau \lvert\frac{du(t)}{dt}\rvert dt$	**79.5** (73%)	108.3 (100%)
ISE	$\int_0^\tau \theta^2(t) dt$	0.047 (100.4%)	**0.0468** (100%)
	$\int_0^\tau \dot{\phi}^2(t) dt$	**$4.975 \cdot 10^4$** (98%)	$5.032 \cdot 10^4$ (100%)

As can be observed from the results of Figure 5.5 and Table 5.7, both controllers attenuated the effects of the external disturbances and achieved a similar performance with respect to the ISE index. However, in this case, the $\mathcal{W}_{2/\infty}$ controller employed a smaller control effort, with respect to the IADU index.

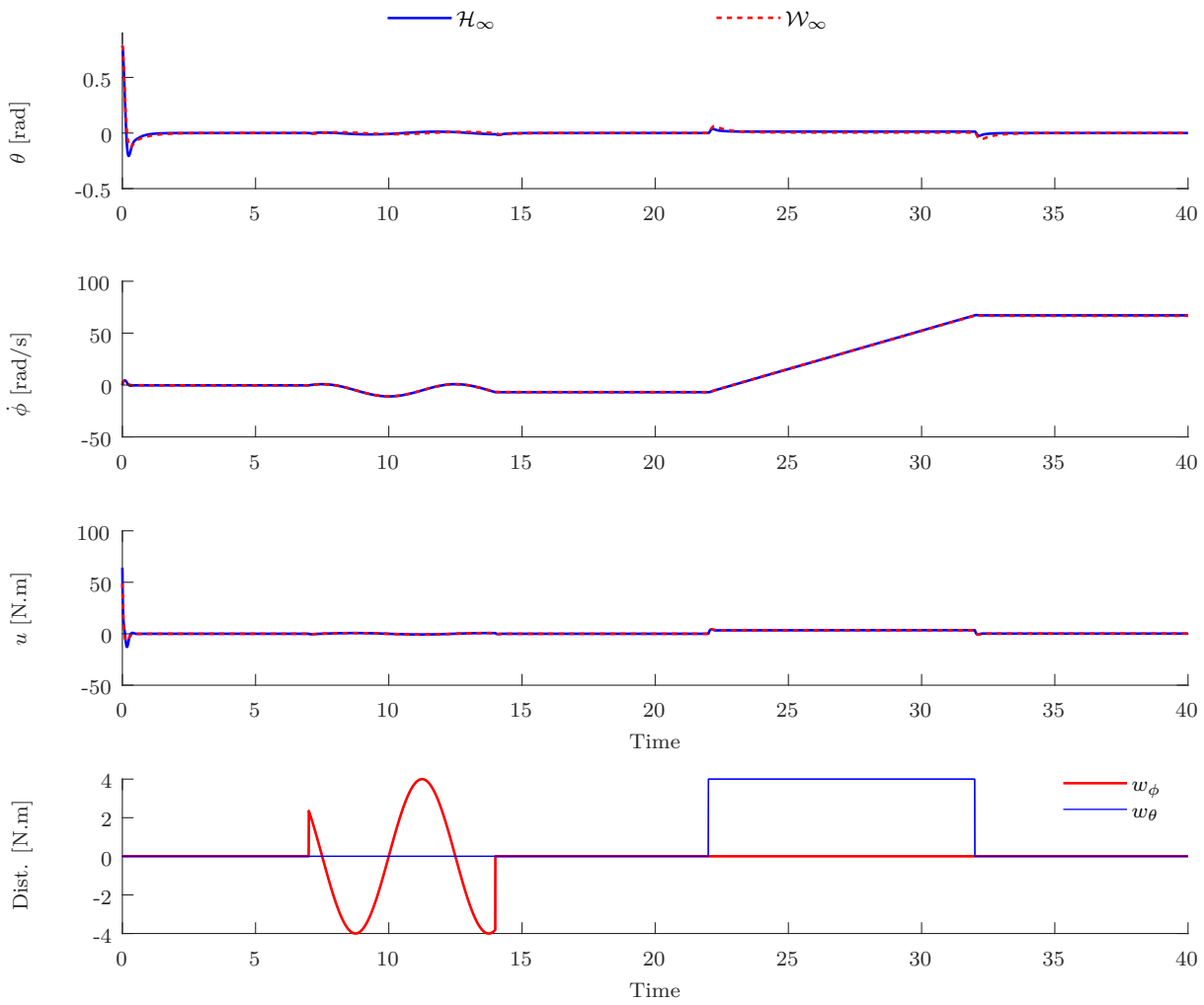

Figure 5.5: Time evolution of the states and control inputs, resulting from the application of the nonlinear $\mathcal{W}_{2/\infty}$ and $\mathcal{H}_\infty$ controllers to the Two-wheeled Self-balanced vehicle, and the disturbance signals.

Quadrotor UAV

The Quadrotor UAV equations of motion are presented in Section (5.3) and are given by (5.123).

In order to synthesize the controllers proposed in Section 5.2 for the Quadrotor UAV, initially, the system (5.123) is partitioned with $\boldsymbol{q}_c(t) = [\psi(t)\ x(t)\ y(t)\ z(t)]'$ and $\boldsymbol{q}_s(t) = [\phi(t)\ \theta(t)]'$. This partition ensures Assumptions 6 and 7 with $\phi \neq \frac{\pi}{2} + 2\pi n_\phi$ for any $n_\phi \in \mathbb{Z}$. Thereafter, considering (5.118) and the particular solution of the HJ PDE proposed in Theorem 4, the control law (5.73) is applied to the system. Note that Remark 36 applies to this particular case, thus, from now on the controller is also called $\mathcal{W}_{2/\infty}$ controller.

The controller was tuned again via trial and error with $\boldsymbol{\Upsilon}_0 = \text{diag}([2\ 2])$, $\boldsymbol{\Upsilon}_1 = \text{diag}([0.01\ 0.01])$, $\boldsymbol{\Gamma}_0 = \text{diag}([10\ 10\ 10\ 10])$, $\boldsymbol{\Gamma}_1 = \text{diag}([12.8\ 18.8\ 18.8\ 12.8])$, $\boldsymbol{\Gamma}_2 = \text{diag}([0.01\ 0.1\ 0.1\ 0.1])$, $\boldsymbol{\Gamma}_3 = \text{diag}([0.00004\ 0.08\ 0.07\ 0.09])$. In addition, to verify the robustness of the controller against parametric uncertainties, the emulated Quadrotor was considered without

tilted rotors, which denies Assumption 7 and cancels the input coupling of the emulated system (see Raffo (2011)). Also, disturbances are applied to the system according to Figure 5.7.

Table 5.8: Desired trajectory for the Quadrotor UAV translational position and yaw angle.

	$x_r(t)$	$y_r(t)$	$z_r(t)$	$\psi_r(t)$
$t \geq 0$	$8\cos\left(\frac{\pi t}{20}\right)$	$8\sin\left(\frac{\pi t}{10}\right)$	$3-\cos\left(\frac{\pi t}{20}t\right)$	0

For comparison analysis, the nonlinear $\mathcal{H}_\infty$ controller presented in Raffo et al. (2011a) was used. The numerical experiment was conducted with the UAV starting from $\dot{\boldsymbol{q}}_s(0) = \boldsymbol{q}_s(0) = \mathbf{0}$, $\boldsymbol{q}_c(0) = [0\ 7\ 0\ 1]'$, $\dot{\boldsymbol{q}}_c(0) = \mathbf{0}$ and designated to track the 8-shape trajectory shown in Figure 5.6 and described in Table 5.8.

From Figures 5.6 and 5.8 it is observed that the Quadrotor UAV starts far from the desired trajectory and converges to it, remaining on the trajectory until the external disturbances are applied to the system. The effects of the constant external disturbances were rejected because both $\mathcal{W}_{2/\infty}$ and $\mathcal{H}_\infty$ controllers consider an integral action on the controlled DOF. In adition, the effects of the time-varying disturbance and parametric uncertainty were attenuated, the latter not being perceptible through the results. For this particular case, although the small tilt angle of the rotors is mathematically necessary to achieve Assumption 7 and provide the image space which allows to actuate on the stabilized DOF, it is not physically necessary to be implemented in the mechanical structure of the Quadrotor UAV.

Again, the $\mathcal{W}_{2/\infty}$ controller achieved less oscillatory behavior with faster disturbance attenuation. In addition, although both $\mathcal{W}_{2/\infty}$ and $\mathcal{H}_\infty$ controllers were tuned to achieve the same control effort, the $\mathcal{W}_{2/\infty}$ controller achieved better results with respect to the ISE performance index of the controlled DOF, as shown in Table 5.9.

Table 5.9: Table of performance indexes computed from the results of the nonlinear $\mathcal{W}_{2/\infty}$ and $\mathcal{H}_\infty$ controllers applied to the Quadrotor UAV.

P. Index	computed by	$\mathcal{W}_{2/\infty}$	$\mathcal{H}_\infty$
IADU	$\int_0^\tau \sum_{i=1}^4 \lvert\frac{d\Omega_i(t)}{dt}\rvert dt$	$\mathbf{2.4 \cdot 10^4}$ (100%)	$\mathbf{2.4 \cdot 10^4}$ (100%)
ISE	$\int_0^\tau (x - x_r)^2 dt$	**0.496** (44%)	1.105 (100%)
	$\int_0^\tau (y - y_r)^2 dt$	**0.030** (29%)	0.102 (100%)
	$\int_0^\tau (z - z_r)^2 dt$	**0.313** (77%)	0.404 (100%)
	$\int_0^\tau (\psi - \psi_r)^2 dt$	$\mathbf{9.5 \cdot 10^{-5}}$ (20%)	$4.6 \cdot 10^{-4}$ (100%)

Figure 5.7 shows the control inputs and external disturbances applied to the system along the simulation. Besides, the time evolution of the norm $||\boldsymbol{B}^\perp(\boldsymbol{w} - \boldsymbol{d})||_2^2$ is presented, which is related to Assumption 8, where $||(\cdot)||_2^2 \triangleq (\cdot)'(\cdot)$. Note that, when the external disturbances affect the system this norm increases, and the controller manipulates the stabilized DOF to achieve $\boldsymbol{B}^\perp(\boldsymbol{x}, \boldsymbol{q}_s)(\boldsymbol{w} - \boldsymbol{d}) = \boldsymbol{0}$, i.e. the exact map that allows handling with the forces and torques induced by gravity and rejecting the disturbances, while tracking the desired trajectory.

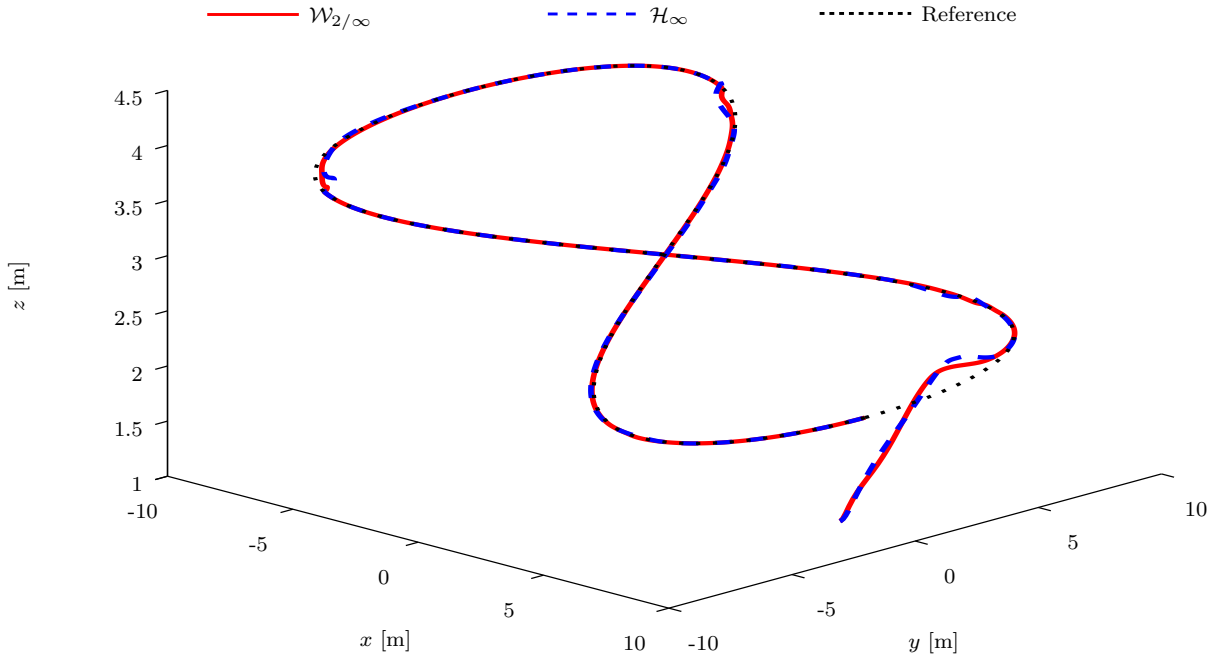

Figure 5.6: Three-dimensional view of the Quadrotor UAV trajectory, resulting from the application of the nonlinear $\mathcal{W}_{2/\infty}$ and $\mathcal{H}_\infty$ controllers.

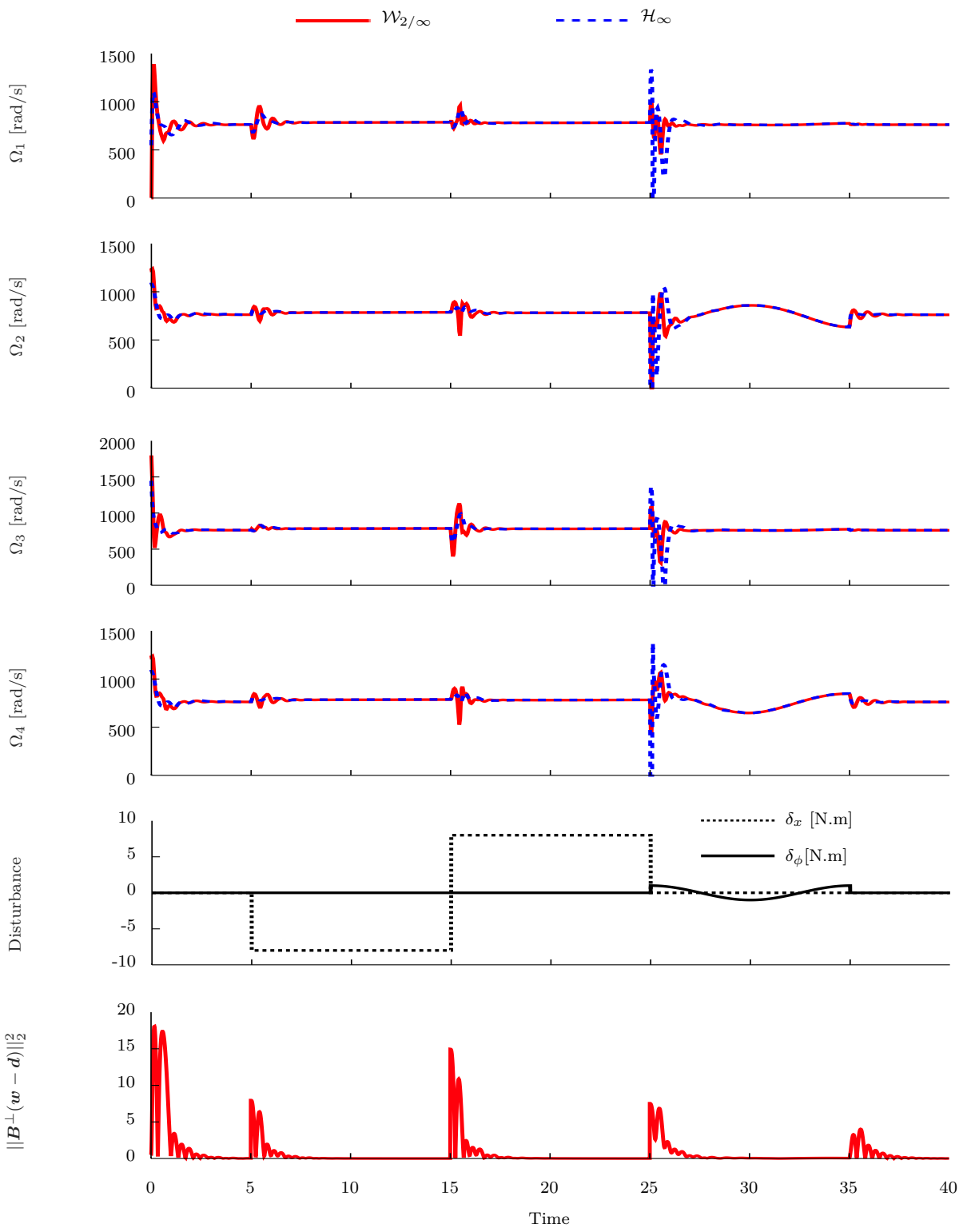

Figure 5.7: Time evolution of the control inputs and the norm of the projection of the vectors $\boldsymbol{w}$ and $\boldsymbol{d}$ on the null space of the input coupling matrix $\boldsymbol{B}^\perp(\boldsymbol{q}_s, \tilde{\boldsymbol{q}}_c + \boldsymbol{q}_{cr})$, resulting from the application of the nonlinear $\mathcal{W}_{2/\infty}$ and $\mathcal{H}_\infty$ controllers to the Quadrotor UAV, and the disturbance signals.

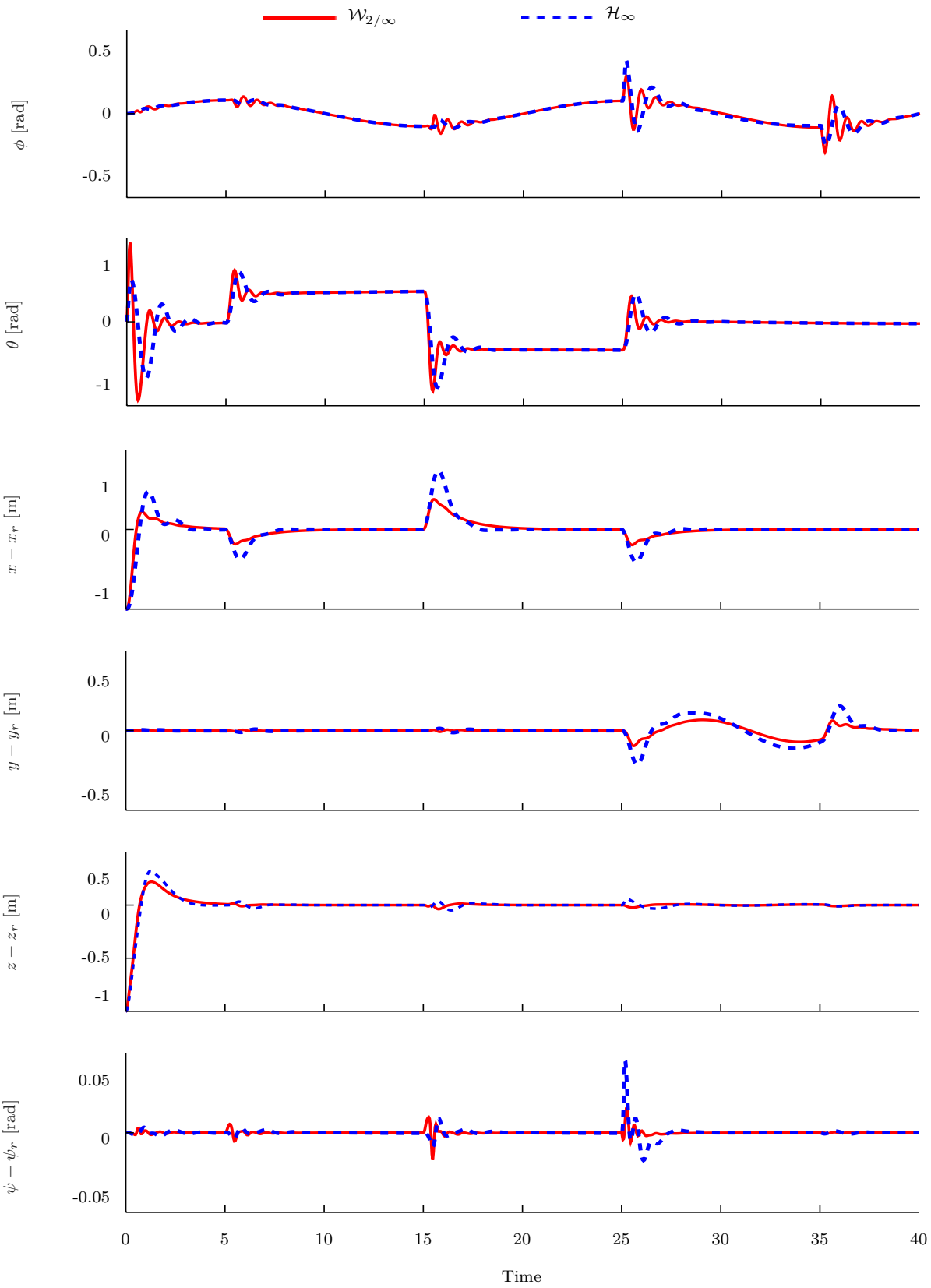

Figure 5.8: Time evolution of the stabilized DOF and tracking error of the controlled DOF, resulting from the application of the nonlinear $\mathcal{W}_{2/\infty}$ and $\mathcal{H}_\infty$ controllers to the Quadrotor UAV.

5.4 Final remarks

This section formulated the nonlinear $\mathcal{W}_2$ and $\mathcal{W}_\infty$ control approaches in the weighted Sobolev space for mechanical systems represented by the Euler-Lagrange equations. Analytical solutions were proposed to the classes of fully actuated and reduced underactuated mechanical systems, and underactuated mechanical systems with input coupling. Numerical experiments conducted with a fully actuated manipulator, a two-wheeled self-balanced vehicle, and a Quadrotor UAV corroborated the efficiency of the proposed control strategies and demonstrated that they provided better transient performance with faster reaction to external disturbances, in comparison with the $\mathcal{H}_\infty$ controller.

In the next chapter, the linear $\mathcal{W}_\infty$ control approach is developed via convex optimization problem with linear matrix inequality constraints. In addition, a new approach is introduced, in which the dynamic behavior of the disturbances is taken into consideration in the control design stage by means of a disturbance model.

6

Linear $\mathcal{W}_\infty$ control

This chapter formulates the full-state and dynamic output feedback linear $\mathcal{W}_\infty$ control problems in weighted Sobolev spaces. The control problems are developed and represented by semidefinite programming problems written as LMIs to simplify the process of achieving a solution. It also introduces a new approach in which the effects of the time derivative of the disturbances are taken into consideration in the control design stage by means of a disturbances model. Pole placement constraints are formulated in order to allow the synthesis of $\mathcal{W}_\infty$ controllers with the closed-loop poles allocated in a predefined region of the complex plane.

6.1 Full-state feedback linear $\mathcal{W}_\infty$ control approach

In this section, the full-state feedback $\mathcal{W}_\infty$ control problem is formulated for closed-loop time-invariant linear systems represented by the following standard form:

$$\mathcal{P}_1: \begin{cases} \dot{\boldsymbol{x}}(t) = \boldsymbol{A}\boldsymbol{x}(t) + \boldsymbol{B}\boldsymbol{u}(t) + \boldsymbol{D}\boldsymbol{w}(t), \\ \boldsymbol{u}(t) = \boldsymbol{K}\boldsymbol{x}(t), \\ \boldsymbol{z}(t) = \boldsymbol{x}(t), \end{cases} \tag{6.1}$$

where $t \in \mathbb{R}_{\geq 0}$ is the time variable, $\boldsymbol{A} \in \mathbb{R}^{n_x \times n_x}$, $\boldsymbol{B} \in \mathbb{R}^{n_x \times n_u}$, and $\boldsymbol{D} \in \mathbb{R}^{n_x \times n_w}$ are matrices that represent the dynamics of the system, $\boldsymbol{x}(t) : \mathbb{R}_{\geq 0} \to \mathbb{R}^{n_x}$ is the state vector, $\boldsymbol{u}(t) : \mathbb{R}_{\geq 0} \to \mathbb{R}^{n_u}$ is the input vector, $\boldsymbol{w}(t) : \mathbb{R}_{\geq 0} \to \mathbb{R}^{n_w}$ is the disturbance vector, $\boldsymbol{z}(t) : \mathbb{R}_{\geq 0} \to \mathbb{R}^{n_x}$ is the

cost variable, and $\boldsymbol{K} \in \mathbb{R}^{n_u \times n_x}$ is the state feedback gain to be designed, with $n_x, n_u, n_w \in \mathbb{N}$.

For the sake of formulating the control problem, the following assumptions are considered:

Assumption 9. *The pair* $(\boldsymbol{A}, \boldsymbol{B})$ *is controllable.*

Assumption 10. *The state vector* $\boldsymbol{x}(t)$ *is available for feedback.*

Assumption 11. *The disturbance vector belongs to the* $\mathcal{L}_2$*-space, i.e.* $\boldsymbol{w}(t) \in \mathcal{L}_2[0, \infty)$ *or, equivalently,* $||\boldsymbol{w}(t)||_{\mathcal{L}_2} < \infty$.

Assumption 12. *The matrix* $\boldsymbol{D}$ *has full column rank, i.e.* $rank(\boldsymbol{D}) = n_w$.

The $\mathcal{W}_\infty$ controller is designed in order to ensure the smallest $\gamma \in \mathbb{R}_{\geq 0}$ that satisfies the inequality

$$\gamma > \sup \frac{||\boldsymbol{z}(t)||_{\mathcal{W}_{1,2,\boldsymbol{\Gamma}}}}{||\boldsymbol{w}(t)||_{\mathcal{L}_2}} = \sup \frac{\left(||\boldsymbol{z}(t)||^2_{\mathcal{L}_{2,\boldsymbol{\Gamma}_0}} + ||\dot{\boldsymbol{z}}(t)||^2_{\mathcal{L}_{2,\boldsymbol{\Gamma}_1}}\right)^{\frac{1}{2}}}{||\boldsymbol{w}(t)||_{\mathcal{L}_2}}, \tag{6.2}$$

subject to $\mathcal{P}_1$, $\forall \boldsymbol{w}(t) \in \mathcal{L}_2[0, \infty)$ and $||\boldsymbol{w}(t)||_{\mathcal{L}_2} \neq 0$, where γ is the $\mathcal{W}_\infty$ attenuation level, and $\boldsymbol{\Gamma} = \{\boldsymbol{\Gamma}_0, \boldsymbol{\Gamma}_1\}$, where $\boldsymbol{\Gamma}_\alpha$, for $\alpha \in \{0, 1\}$ is a tuning matrix with appropriate dimension.

The control problem is posed based on inequality (6.2), as

$$\min_{\boldsymbol{K}, \gamma} \gamma, \tag{6.3}$$
$$s.t. : \begin{cases} \mathcal{P}_1, \\ ||\boldsymbol{z}(t)||^2_{\mathcal{W}_{1,2,\boldsymbol{\Gamma}}} - \gamma^2 ||\boldsymbol{w}(t)||^2_{\mathcal{L}_2} < 0. \end{cases}$$

Remark 37. *In contrast to the classic linear* $\mathcal{H}_\infty$ *controller, the linear* $\mathcal{W}_\infty$ *controller is designed by explicitly taking into account the time derivative of the cost variable. The aim is to achieve improved transient performance with a faster disturbances attenuation. The reason is that when minimizing* γ *in* (6.3)*, we are reducing the influence of the disturbances in the time evolution of the cost variable.*

In what follows, we perform some algebraic manipulations to (6.3), in order to represent this control problem by a semidefinite programming problem written as LMI.

Initially, aiming an asymptotic stable closed-loop system, i.e. $\lim_{t \to \infty} x(t) = 0$, assuming the origin as the initial condition, i.e. $x(0) = 0$, and considering the candidate Lyapunov function $\boldsymbol{V}(\boldsymbol{x}) = \boldsymbol{x}' \boldsymbol{P} \boldsymbol{x} > 0$, where the matrix $\boldsymbol{P}$ is a decision variable of the optimization problem, one can represent (6.3) as[1]

$$\min_{\boldsymbol{K}, \boldsymbol{P}, \gamma} \gamma, \tag{6.4}$$

[1]For the sake of simplicity, along this manuscript some function dependencies are omitted.

$$s.t.: \begin{cases} \mathcal{P}_1, \\ \boldsymbol{x}'\boldsymbol{P}\boldsymbol{x} > 0, \\ \dot{\boldsymbol{V}}(\boldsymbol{x}) + \boldsymbol{x}'\boldsymbol{\Gamma}_0\boldsymbol{x} + \dot{\boldsymbol{x}}'\boldsymbol{\Gamma}_1\dot{\boldsymbol{x}} - \gamma^2\boldsymbol{w}'\boldsymbol{w} < 0, \end{cases}$$

in which $\dot{\boldsymbol{V}}(\boldsymbol{x}) = \dot{\boldsymbol{x}}'\boldsymbol{P}\boldsymbol{x} + \boldsymbol{x}'\boldsymbol{P}\dot{\boldsymbol{x}}$.

Remark 38. *The last inequality in* (6.3) *can be obtained by integrating the last inequality in* (6.4) *in the time interval* $t \in [0, \infty)$ *and assuming the asymptotic stability condition, which implies that* $\lim_{t\to\infty} \boldsymbol{V}(x(t)) = 0$.

Taking into account system (6.1) and the candidate Lyapunov function $\boldsymbol{V}(\boldsymbol{x})$, the last inequality (6.4) results in

$$\begin{bmatrix} \boldsymbol{x} \\ \boldsymbol{w} \end{bmatrix}' \begin{bmatrix} \boldsymbol{M}_{11} & * \\ \boldsymbol{M}_{21} & \boldsymbol{M}_{22} \end{bmatrix} \begin{bmatrix} \boldsymbol{x} \\ \boldsymbol{w} \end{bmatrix} < 0, \tag{6.5}$$

where the $*$ term can be deduced by symmetry, $\boldsymbol{M}_{11} \triangleq \boldsymbol{A}'\boldsymbol{P} + \boldsymbol{P}\boldsymbol{A} + \boldsymbol{K}'\boldsymbol{B}'\boldsymbol{P} + \boldsymbol{P}\boldsymbol{B}\boldsymbol{K} + \boldsymbol{\Gamma}_0 + \boldsymbol{A}'\boldsymbol{\Gamma}_1\boldsymbol{A} + \boldsymbol{A}'\boldsymbol{\Gamma}_1\boldsymbol{B}\boldsymbol{K} + \boldsymbol{K}'\boldsymbol{B}'\boldsymbol{\Gamma}_1\boldsymbol{A} + \boldsymbol{K}'\boldsymbol{B}'\boldsymbol{\Gamma}_1\boldsymbol{B}\boldsymbol{K}$, $\boldsymbol{M}_{21} \triangleq \boldsymbol{P}\boldsymbol{D} + \boldsymbol{A}'\boldsymbol{\Gamma}_1\boldsymbol{D} + \boldsymbol{K}'\boldsymbol{B}'\boldsymbol{\Gamma}_1\boldsymbol{D}$, and $\boldsymbol{M}_{22} \triangleq \boldsymbol{D}'\boldsymbol{\Gamma}_1\boldsymbol{D} - \gamma^2\boldsymbol{I}$.

Thereafter, considering the similarity transformation $\boldsymbol{x} = \boldsymbol{P}^{-1}\boldsymbol{y}$ and the change of variables $\gamma^* \triangleq \gamma^2$, $\boldsymbol{R} \triangleq \boldsymbol{K}\boldsymbol{S}$ and $\boldsymbol{S} \triangleq \boldsymbol{P}^{-1}$, one can represent (6.4) as

$$\min_{\boldsymbol{R},\boldsymbol{S},\boldsymbol{P},\gamma^*} \gamma^*, \tag{6.6}$$
$$s.t.: \begin{cases} \gamma^* > 0, \\ \boldsymbol{S} > 0, \\ \begin{bmatrix} \bar{\boldsymbol{M}}_{11} & * \\ \bar{\boldsymbol{M}}_{21} & \bar{\boldsymbol{M}}_{22} \end{bmatrix} < 0, \end{cases}$$

where $\bar{\boldsymbol{M}}_{11} \triangleq \boldsymbol{S}\boldsymbol{A}' + \boldsymbol{A}\boldsymbol{S} + \boldsymbol{R}'\boldsymbol{B}' + \boldsymbol{B}\boldsymbol{R} + \boldsymbol{S}\boldsymbol{\Gamma}_0\boldsymbol{S} + \boldsymbol{S}\boldsymbol{A}'\boldsymbol{\Gamma}_1\boldsymbol{A}\boldsymbol{S}$
$+ \boldsymbol{S}\boldsymbol{A}'\boldsymbol{\Gamma}_1\boldsymbol{B}\boldsymbol{R} + \boldsymbol{R}'\boldsymbol{B}'\boldsymbol{\Gamma}_1\boldsymbol{A}\boldsymbol{S} + \boldsymbol{R}'\boldsymbol{B}'\boldsymbol{\Gamma}_1\boldsymbol{B}\boldsymbol{R}$, $\bar{\boldsymbol{M}}_{21} \triangleq \boldsymbol{D}' + \boldsymbol{D}'\boldsymbol{\Gamma}_1\boldsymbol{A}\boldsymbol{S} + \boldsymbol{D}'\boldsymbol{\Gamma}_1\boldsymbol{B}\boldsymbol{R}$, and $\bar{\boldsymbol{M}}_{22} \triangleq \boldsymbol{D}'\boldsymbol{\Gamma}_1\boldsymbol{D} - \gamma^*\boldsymbol{I}$.

Then, by applying the Schur complement in the last inequality of (6.6), the full-state feedback linear $\mathcal{W}_\infty$ control problem results in solving the following semidefinite programming problem written as LMIs:

$$\min_{\boldsymbol{R},\boldsymbol{S},\gamma^*} \gamma^*, \tag{6.7}$$

$$s.t.: \begin{cases} \gamma^* > 0, \\ \boldsymbol{S} > 0, \\ \begin{bmatrix} \Xi_1 & * & * & * \\ \boldsymbol{D}' & -\gamma^* \boldsymbol{I} & * & * \\ \boldsymbol{AS} + \boldsymbol{BR} & \boldsymbol{D} & -\boldsymbol{\Gamma}_1^{-1} & * \\ \boldsymbol{S} & \boldsymbol{0} & \boldsymbol{0} & -\boldsymbol{\Gamma}_0^{-1} \end{bmatrix} < 0, \end{cases}$$

in which $\Xi_1 \triangleq \boldsymbol{SA}' + \boldsymbol{AS} + \boldsymbol{R}'\boldsymbol{B}' + \boldsymbol{BR}$. After solving (6.7), the state feedback gain is computed by $\boldsymbol{K} = \boldsymbol{RS}^{-1}$, the matrix $\boldsymbol{P} = \boldsymbol{S}^{-1}$, and the $\mathcal{W}_\infty$ index by $\gamma = \sqrt{\gamma^*}$.

Theorem 7. *Let Assumptions 9-12 hold for system (6.1), and consider $\boldsymbol{x}(0) \in \mathbb{R}^{n_x}$. If $\boldsymbol{K} = \boldsymbol{RS}^{-1}$, $\boldsymbol{P} = \boldsymbol{S}^{-1}$, and $\gamma = \sqrt{\gamma^*}$ are obtained by solving the semidefinite programming problem (6.7), then the closed-loop system (6.1) is asymptotically stable.*

Proof. Note that after solving the semi definite programming problem (6.7), the parameters $\boldsymbol{K}$, $\boldsymbol{P}$, and γ satisfy the related LMIs, consequently,

$$\boldsymbol{V}(\boldsymbol{x}) = \boldsymbol{x}'\boldsymbol{P}\boldsymbol{x} > 0, \quad \forall \boldsymbol{x} \neq \boldsymbol{0}. \tag{6.8}$$

In addition, from the last LMI in (6.4), and assuming $\boldsymbol{w}(t) = 0$, we have that

$$\dot{\boldsymbol{V}}(\boldsymbol{x}) < -\begin{bmatrix} \boldsymbol{x} \\ \dot{\boldsymbol{x}} \end{bmatrix}' \begin{bmatrix} \boldsymbol{\Gamma}_0 & \boldsymbol{0} \\ \boldsymbol{0} & \boldsymbol{\Gamma}_1 \end{bmatrix} \begin{bmatrix} \boldsymbol{x} \\ \dot{\boldsymbol{x}} \end{bmatrix} < 0, \quad \forall (\boldsymbol{x}, \dot{\boldsymbol{x}}) \neq \boldsymbol{0}, \tag{6.9}$$

where $\boldsymbol{\Gamma}_0$ and $\boldsymbol{\Gamma}_1$ are positive definite matrices. Accordingly, the closed-loop system (6.1) is asymptotically stable in the sense of Lyapunov, and $\boldsymbol{V}(\boldsymbol{x})$ is a Lyapunov function. □

Definition 7 also applies to the linear $\mathcal{W}_\infty$ controller. Note that by integrating both sides of the last inequality in (6.4) in the time interval $t \in [0, \infty)$, and considering that $\boldsymbol{x}(0) \in \mathbb{R}$ and Assumption 11 hold, with a few algebraic manipulations, one can obtain

$$||\boldsymbol{z}(t)||^2_{\mathcal{W}_{1,2,\boldsymbol{\Gamma}}} < \gamma^2 ||\boldsymbol{w}(t)||^2_{\mathcal{L}_2} + \boldsymbol{V}(\boldsymbol{x}(0)) = \gamma^2 c_2 + c_1, \tag{6.10}$$

for some $c_1, c_2 \in \mathbb{R}_{\geq 0}$. Therefore, according to Definition 7, and considering that $\boldsymbol{K}$, $\boldsymbol{P}$, and γ is a solution of (6.7), the closed-loop system (6.1) is $\mathcal{W}_{1,2,\boldsymbol{\Gamma}}$-stable, with γ being the $\mathcal{W}_{1,2,\boldsymbol{\Gamma}}$-gain.

6.2 The linear $\mathcal{W}_\infty$ control approach with dynamic output feedback

The control strategy presented in the previous section is designed based on the assumption that all states of the system are available. However, this is not usually the case. Therefore, in this section, the dynamic output feedback $\mathcal{W}_\infty$ control problem is formulated for time-invariant linear systems represented by

$$\mathcal{P}_2: \begin{cases} \dot{\boldsymbol{x}}(t) = \boldsymbol{A}\boldsymbol{x}(t) + \boldsymbol{B}\boldsymbol{u}(t) + \boldsymbol{D}\boldsymbol{w}(t), \\ \boldsymbol{y}(t) = \boldsymbol{C}\boldsymbol{x}(t), \\ \boldsymbol{z}(t) = \boldsymbol{x}(t), \end{cases} \tag{6.11}$$

in closed-loop with the dynamic controller

$$\mathcal{K}_1: \begin{cases} \dot{\boldsymbol{x}}_f(t) = \boldsymbol{A}_f\boldsymbol{x}_f(t) + \boldsymbol{B}_f\boldsymbol{y}(t), \\ \boldsymbol{u}(t) = \boldsymbol{C}_f\boldsymbol{x}_f(t) + \boldsymbol{D}_f\boldsymbol{y}(t), \end{cases} \tag{6.12}$$

where $\boldsymbol{A}$, $\boldsymbol{B}$, $\boldsymbol{D}$, $\boldsymbol{x}(t)$, $\boldsymbol{u}(t)$, $\boldsymbol{w}(t)$, and $\boldsymbol{z}(t)$ are defined as in (6.1), and $\boldsymbol{y}(t) : \mathbb{R}_{\geq 0} \to \mathbb{R}^{n_y}$ is the vector of measured outputs, with $\boldsymbol{C} \in \mathbb{R}^{n_y \times n_x}$. Besides, $\boldsymbol{x}_f(t) \in \mathbb{R}^{n_x}$ represents the states of the dynamic controller, and $\boldsymbol{A}_f$, $\boldsymbol{B}_f$, $\boldsymbol{C}_f$ and $\boldsymbol{D}_f$, are real matrices with appropriate dimension to be determined.

In addition to Assumptions 9, 11, and 12 that hold for (6.11), the following ones are considered to formulate the control problem:

Assumption 13. *The pair $(\boldsymbol{A}, \boldsymbol{C})$ is observable.*

Assumption 14. *The vector $\boldsymbol{y}(t)$ is available.*

The closed-loop system resulting from $\mathcal{P}_2$ and $\mathcal{K}_1$ is denoted by $\mathcal{P}_2(\mathcal{K}_1)$ and is written as

$$\mathcal{P}_2(\mathcal{K}_1): \begin{cases} \dot{\boldsymbol{\mathcal{X}}}_a(t) = \boldsymbol{A}_a\boldsymbol{\mathcal{X}}_a(t) + \boldsymbol{D}_a\boldsymbol{w}(t), \\ \boldsymbol{z}(t) = \boldsymbol{x}(t), \end{cases} \tag{6.13}$$

where $\boldsymbol{A}_a \triangleq \begin{bmatrix} \boldsymbol{A} + \boldsymbol{B}\boldsymbol{D}_f\boldsymbol{C} & \boldsymbol{B}\boldsymbol{C}_f \\ \boldsymbol{B}_f\boldsymbol{C} & \boldsymbol{A}_f \end{bmatrix}$, $\boldsymbol{D}_a \triangleq \begin{bmatrix} \boldsymbol{D} \\ \boldsymbol{0} \end{bmatrix}$, and $\boldsymbol{\mathcal{X}}_a(t) \triangleq \begin{bmatrix} \boldsymbol{x}'(t) & \boldsymbol{x}_f'(t) \end{bmatrix}'$.

Therefore, aiming asymptotic stability in closed-loop, i.e. $\lim_{t\to\infty} \boldsymbol{\mathcal{X}}_a(t) = 0$, assuming the origin of the state space as initial condition, i.e. $\boldsymbol{\mathcal{X}}_a(0) = 0$, and proposing the candidate Lyapunov function $\boldsymbol{V}(\boldsymbol{\mathcal{X}}_a) = \boldsymbol{\mathcal{X}}_a'\boldsymbol{P}\boldsymbol{\mathcal{X}}_a > 0$, where $\boldsymbol{P}$ is a matrix with appropriate dimension, the control problem is formulated in order to achieve the smallest γ that

satisfies the inequality (6.2), as follows:

$$\min_{\boldsymbol{A}_f,\boldsymbol{B}_f,\boldsymbol{C}_f,\boldsymbol{D}_f,\boldsymbol{P},\gamma} \gamma, \tag{6.14}$$
$$s.t.: \begin{cases} \mathcal{P}_2(\mathcal{K}_1), \\ \mathcal{X}_a'\boldsymbol{P}\mathcal{X}_a > 0, \\ \dot{V}(\mathcal{X}_a) + \boldsymbol{x}'\boldsymbol{\Gamma}_0\boldsymbol{x} + \dot{\boldsymbol{x}}'\boldsymbol{\Gamma}_1\dot{\boldsymbol{x}} - \gamma^2\boldsymbol{w}'\boldsymbol{w} < 0, \end{cases}$$

in which $\dot{V}(\mathcal{X}_a) = \dot{\mathcal{X}}_a{}'\boldsymbol{P}\mathcal{X}_a + \mathcal{X}_a'\boldsymbol{P}\dot{\mathcal{X}}_a$.

In order to represent (6.14) by a semidefinite programming problem written as Linear Matrix Inequalities (LMI), the last inequality in (6.14) is expanded, yielding

$$\begin{bmatrix} \mathcal{X}_a \\ \boldsymbol{w} \end{bmatrix}' \begin{bmatrix} \boldsymbol{A}_a'\boldsymbol{P} + \boldsymbol{P}\boldsymbol{A}_a + \boldsymbol{F} + \boldsymbol{U}'\boldsymbol{\Gamma}_1\boldsymbol{U} & * \\ \boldsymbol{D}_a'\boldsymbol{P} + \boldsymbol{D}'\boldsymbol{\Gamma}_1\boldsymbol{U} & \boldsymbol{D}'\boldsymbol{\Gamma}_1\boldsymbol{D} - \gamma^2\boldsymbol{I} \end{bmatrix} \begin{bmatrix} \mathcal{X}_a \\ \boldsymbol{w} \end{bmatrix} < 0, \tag{6.15}$$

where $\boldsymbol{F} \triangleq \begin{bmatrix} \boldsymbol{\Gamma}_0 & \boldsymbol{0} \\ \boldsymbol{0} & \boldsymbol{0} \end{bmatrix}$ and $\boldsymbol{U} \triangleq \begin{bmatrix} \boldsymbol{A} + \boldsymbol{B}\boldsymbol{D}_f\boldsymbol{C} & \boldsymbol{B}\boldsymbol{C}_f \end{bmatrix}$.

Then, by performing the similarity transformation $\mathcal{X}_a = \boldsymbol{P}^{-1}\boldsymbol{M}'\mathcal{Y}_a$, where $\boldsymbol{P}^{-1} \triangleq \begin{bmatrix} \boldsymbol{S} & \boldsymbol{T} \\ \boldsymbol{T}' & \boldsymbol{R} \end{bmatrix}$ and $\boldsymbol{M} \triangleq \begin{bmatrix} \boldsymbol{I} & \boldsymbol{0} \\ \boldsymbol{I} & -\boldsymbol{T}\boldsymbol{R}^{-1} \end{bmatrix}$, the first inequality in (6.14) and the inequality (6.15) result in

$$\mathcal{Y}_a'\boldsymbol{M}\boldsymbol{P}^{-1}\boldsymbol{M}'\mathcal{Y}_a = \begin{bmatrix} \boldsymbol{S} & \boldsymbol{S}-\boldsymbol{Q} \\ \boldsymbol{S}-\boldsymbol{Q} & \boldsymbol{S}-\boldsymbol{Q} \end{bmatrix} > 0, \tag{6.16}$$

$$\begin{bmatrix} \mathcal{Y}_a \\ \boldsymbol{w} \end{bmatrix}' \begin{bmatrix} \boldsymbol{M}\boldsymbol{P}^{-1}\left(\boldsymbol{A}_a'\boldsymbol{P}+\boldsymbol{P}\boldsymbol{A}_a+\boldsymbol{F}+\boldsymbol{U}'\boldsymbol{\Gamma}_1\boldsymbol{U}\right)\boldsymbol{P}^{-1}\boldsymbol{M}' & * \\ \left(\boldsymbol{D}_a'\boldsymbol{P}+\boldsymbol{D}'\boldsymbol{\Gamma}_1\boldsymbol{U}\right)\boldsymbol{P}^{-1}\boldsymbol{M}' & \boldsymbol{D}'\boldsymbol{\Gamma}_1\boldsymbol{D}-\gamma^2\boldsymbol{I} \end{bmatrix} \begin{bmatrix} \mathcal{Y}_a \\ \boldsymbol{w} \end{bmatrix} < 0, \tag{6.17}$$

where $\boldsymbol{Q} \triangleq \boldsymbol{T}'\boldsymbol{R}^{-1}\boldsymbol{T}$.

By applying the Schur complement in inequality (6.17), and defining $\boldsymbol{L} \triangleq \begin{bmatrix} \boldsymbol{S}' & \boldsymbol{S}'-\boldsymbol{Q}' \end{bmatrix}'$, one obtains

$$\begin{bmatrix} \boldsymbol{M}\boldsymbol{P}^{-1}\left(\boldsymbol{A}_a'\boldsymbol{P}+\boldsymbol{P}\boldsymbol{A}_a\right)\boldsymbol{P}^{-1}\boldsymbol{M}' & * & * & * \\ \boldsymbol{D}_a'\boldsymbol{M}' & -\gamma^2\boldsymbol{I} & * & * \\ \boldsymbol{L}' & \boldsymbol{0} & -\boldsymbol{\Gamma}_0^{-1} & * \\ \boldsymbol{U}\boldsymbol{P}^{-1}\boldsymbol{M}' & \boldsymbol{D} & \boldsymbol{0} & -\boldsymbol{\Gamma}_1^{-1} \end{bmatrix} < 0 \tag{6.18}$$

Then, inequality (6.18) is represented by

$$\begin{bmatrix} \boldsymbol{\Psi}_1 & * & * \\ \boldsymbol{\Psi}_2 - \boldsymbol{A}_m & \boldsymbol{\Psi}_3 & * \\ \boldsymbol{\Psi}_4 & \boldsymbol{\Psi}_5 & \boldsymbol{\Psi}_6 \end{bmatrix} < 0, \tag{6.19}$$

where $\begin{bmatrix} \boldsymbol{\Psi}_1 & * \\ \boldsymbol{\Psi}_2 - \boldsymbol{A}_m & \boldsymbol{\Psi}_3 \end{bmatrix} \triangleq \boldsymbol{M}\boldsymbol{P}^{-1}\left(\boldsymbol{A}_a'\boldsymbol{P} + \boldsymbol{P}\boldsymbol{A}_a\right)\boldsymbol{P}^{-1}\boldsymbol{M}'$, with $\boldsymbol{\Psi}_1 \triangleq \boldsymbol{A}\boldsymbol{S}+\boldsymbol{B}(\boldsymbol{D}_f\boldsymbol{C}\boldsymbol{S}+\boldsymbol{C}_f\boldsymbol{T}')+(\boldsymbol{A}\boldsymbol{S}+\boldsymbol{B}(\boldsymbol{D}_f\boldsymbol{C}\boldsymbol{S}+\boldsymbol{C}_f\boldsymbol{T}))'$, $\boldsymbol{\Psi}_2 \triangleq (\boldsymbol{S}-\boldsymbol{Q})(\boldsymbol{A}+\boldsymbol{B}\boldsymbol{D}_f\boldsymbol{C})'+(\boldsymbol{A}+\boldsymbol{B}\boldsymbol{D}_f\boldsymbol{C})\boldsymbol{S}'+\boldsymbol{B}\boldsymbol{C}_f\boldsymbol{T}'-\boldsymbol{T}\boldsymbol{R}^{-1}\boldsymbol{B}_f\boldsymbol{C}\boldsymbol{S}'$, $\boldsymbol{A}_m \triangleq \boldsymbol{T}\boldsymbol{R}^{-1}\boldsymbol{A}_f\boldsymbol{T}'$, $\boldsymbol{\Psi}_3 = (\boldsymbol{S}-\boldsymbol{Q})\boldsymbol{A}' + \boldsymbol{A}(\boldsymbol{S}-\boldsymbol{Q})' + (\boldsymbol{S}-\boldsymbol{Q})\boldsymbol{C}'(\boldsymbol{D}_f\boldsymbol{B}' - \boldsymbol{B}_f'\boldsymbol{R}^{-1}\boldsymbol{T}') + (\boldsymbol{B}\boldsymbol{D}_f - \boldsymbol{T}\boldsymbol{R}^{-1}\boldsymbol{B}_f)\boldsymbol{C}(\boldsymbol{S}-\boldsymbol{Q})'$, $\begin{bmatrix} \boldsymbol{\Psi}_4 & \boldsymbol{\Psi}_5 \end{bmatrix} \triangleq \begin{bmatrix} \boldsymbol{D}_a'\boldsymbol{M}' \\ \boldsymbol{L}' \\ \boldsymbol{U}\boldsymbol{P}^{-1}\boldsymbol{M}' \end{bmatrix}$, $\boldsymbol{\Psi}_6 \triangleq \begin{bmatrix} -\gamma^2\boldsymbol{I} & * & * \\ \boldsymbol{0} & -\boldsymbol{\Gamma}_0^{-1} & * \\ \boldsymbol{D} & \boldsymbol{0} & -\boldsymbol{\Gamma}_1^{-1} \end{bmatrix}$.

In addition, choosing $\boldsymbol{A}_m = \boldsymbol{\Psi}_2$, considering $\gamma^2 = \gamma^*$, $\boldsymbol{C}_s \triangleq \boldsymbol{D}_f\boldsymbol{C}\boldsymbol{S} + \boldsymbol{C}_f\boldsymbol{T}$, $\boldsymbol{B}_s \triangleq \boldsymbol{W}(\boldsymbol{B}\boldsymbol{D}_f - \boldsymbol{T}'\boldsymbol{R}^{-1}\boldsymbol{B}_f)$, with $\boldsymbol{W} \triangleq (\boldsymbol{S}-\boldsymbol{Q})^{-1}$, and applying the following congruent transformations to the inequalities (6.16) and (6.19),

$$\begin{bmatrix} \boldsymbol{I} & \boldsymbol{0} \\ \boldsymbol{0} & \boldsymbol{W} \end{bmatrix} \begin{bmatrix} \boldsymbol{S} & \boldsymbol{S}-\boldsymbol{Q} \\ \boldsymbol{S}-\boldsymbol{Q} & \boldsymbol{S}-\boldsymbol{Q} \end{bmatrix} \begin{bmatrix} \boldsymbol{I} & \boldsymbol{0} \\ \boldsymbol{0} & \boldsymbol{W}' \end{bmatrix} > 0, \tag{6.20}$$

$$\begin{bmatrix} \boldsymbol{I} & \boldsymbol{0} & \boldsymbol{0} \\ \boldsymbol{0} & \boldsymbol{W} & \boldsymbol{0} \\ \boldsymbol{0} & \boldsymbol{0} & \boldsymbol{I} \end{bmatrix} \begin{bmatrix} \boldsymbol{\Psi}_1 & * & * \\ \boldsymbol{0} & \boldsymbol{\Psi}_3 & * \\ \boldsymbol{\Psi}_4 & \boldsymbol{\Psi}_5 & \boldsymbol{\Psi}_6 \end{bmatrix} \begin{bmatrix} \boldsymbol{I} & \boldsymbol{0} & \boldsymbol{0} \\ \boldsymbol{0} & \boldsymbol{W}' & \boldsymbol{0} \\ \boldsymbol{0} & \boldsymbol{0} & \boldsymbol{I} \end{bmatrix} < 0, \tag{6.21}$$

these become linear in the parameters. Therefore, the dynamic output feedback linear $\mathcal{W}_\infty$ controller can be designed by solving the following semidefinite programing problem written as LMIs:

$$\min_{\gamma^*, \boldsymbol{S}, \boldsymbol{W}, \boldsymbol{B}_s, \boldsymbol{C}_s, \boldsymbol{D}_f} \gamma^*, \tag{6.22}$$

$$s.t.: \begin{cases} \gamma^* > 0, \\ \begin{bmatrix} \boldsymbol{S} & \boldsymbol{I} \\ \boldsymbol{I} & \boldsymbol{W}' \end{bmatrix} > 0, \\ \begin{bmatrix} \boldsymbol{\Psi}_1 & * & * \\ \boldsymbol{0} & \boldsymbol{W}\boldsymbol{\Psi}_3\boldsymbol{W}' & * \\ \boldsymbol{\Psi}_4 & \boldsymbol{\Psi}_5\boldsymbol{W}' & \boldsymbol{\Psi}_6 \end{bmatrix} < 0, \end{cases}$$

where $\boldsymbol{\Psi}_1 \triangleq \boldsymbol{A}\boldsymbol{S} + \boldsymbol{B}\boldsymbol{C}_s + (\boldsymbol{A}\boldsymbol{S} + \boldsymbol{B}\boldsymbol{C}_s)'$, $\boldsymbol{W}\boldsymbol{\Psi}_3\boldsymbol{W}' \triangleq \boldsymbol{A}'\boldsymbol{W} + \boldsymbol{C}'\boldsymbol{B}_s' + \boldsymbol{W}\boldsymbol{A} + \boldsymbol{B}_s\boldsymbol{C}$, $\boldsymbol{\Psi}_4' \triangleq \begin{bmatrix} \boldsymbol{D} & \boldsymbol{S} & \boldsymbol{S}\boldsymbol{A}' + \boldsymbol{C}_s'\boldsymbol{B}' \end{bmatrix}$, $\boldsymbol{W}\boldsymbol{\Psi}_5' \triangleq \begin{bmatrix} \boldsymbol{W}\boldsymbol{D} & \boldsymbol{I} & \boldsymbol{A}' + \boldsymbol{C}'\boldsymbol{D}_f'\boldsymbol{B}' \end{bmatrix}$, $\boldsymbol{\Psi}_6 \triangleq \begin{bmatrix} -\gamma^*\boldsymbol{I} & \boldsymbol{0} & \boldsymbol{D}' \\ \boldsymbol{0} & -\boldsymbol{\Gamma}_0^{-1} & \boldsymbol{0} \\ \boldsymbol{D} & \boldsymbol{0} & -\boldsymbol{\Gamma}_1^{-1} \end{bmatrix}$. After solving (6.22), the $\mathcal{W}_\infty$-index is obtained as $\gamma = \sqrt{\gamma^*}$, and the controller variables as

$$\boldsymbol{R} = \boldsymbol{T}(\boldsymbol{S} - \boldsymbol{W}^{-1})^{-1}\boldsymbol{T}', \tag{6.23}$$

$$\boldsymbol{A}_f = \boldsymbol{T}(\boldsymbol{S} - \boldsymbol{W}^{-1})^{-1}(\boldsymbol{A}\boldsymbol{S} + \boldsymbol{B}\boldsymbol{C}_s - (\boldsymbol{B}\boldsymbol{D}_f - \boldsymbol{W}^{-1}\boldsymbol{B}_s)\boldsymbol{C}\boldsymbol{S} \tag{6.24}$$

$$+ (\boldsymbol{W}^{-1})'(\boldsymbol{A} + \boldsymbol{B}\boldsymbol{D}_f\boldsymbol{C})')\boldsymbol{T}^{-1} \tag{6.25}$$

$$\boldsymbol{B}_f = \boldsymbol{T}(\boldsymbol{S} - \boldsymbol{W}^{-1})^{-1}\left(\boldsymbol{B}\boldsymbol{D}_f - \boldsymbol{W}^{-1}\boldsymbol{B}_s\right), \tag{6.26}$$

$$\boldsymbol{C}_f = \left(\boldsymbol{C}_s - \boldsymbol{D}_f\boldsymbol{C}\boldsymbol{S}\right)\boldsymbol{T}^{-1}, \tag{6.27}$$

where $\boldsymbol{T}$ is a symmetric and positive definite matrix that can be arbitrarily chosen.

Remark 39. *The invertible matrix $\boldsymbol{T}$ defines a similarity transformation over the state of the dynamic controller, $\boldsymbol{x}_f$, therefore, does not affect the closed-loop transfer function.*

Theorem 8. *Let Assumptions 9, 11, 12, 13, and 14 hold, and consider $\boldsymbol{x}(0) \in \mathbb{R}^{n_x}$. If $\boldsymbol{A}_f$, $\boldsymbol{B}_f$, $\boldsymbol{C}_f$, $\boldsymbol{D}_f$, $\boldsymbol{S}$, $\boldsymbol{T}$, $\boldsymbol{R}$, and γ are obtained by solving the semidefinite programming problem (6.22), then the closed-loop system (6.13) is asymptotically stable.*

Proof. The proof follows the same steps of the proof of Theorem 7. □

With a few manipulations, one can demonstrate that Definition 7 applies to the dynamic output feedback $\mathcal{W}_\infty$ controller, therefore, the closed-loop system (6.13) is $\mathcal{W}_{1,2,\mathbf{\Gamma}}$-stable, with γ being the $\mathcal{W}_{1,2,\mathbf{\Gamma}}$-gain of the system.

6.3 The linear $\mathcal{W}_\infty$ control approach formulated considering the dynamics of the disturbance

The control approaches addressed in the previous sections are useful for a wide variety of linear systems. Nevertheless, when a disturbance model is available, it can be used in the cost functional to improve the results of the $\mathcal{W}_\infty$ controller. Therefore, in this section, the full-state and dynamic output feedback linear $\mathcal{W}_\infty$ control problems are formulated taking into account disturbance model.

6.3.1 Full-states feedback approach

In this subsection, the full-states feedback $\mathcal{W}_\infty$ controller is designed taking into account the linear time-invariant system (6.1) together with a disturbance dynamic model, as follows:

$$\mathcal{P}_3\colon \begin{cases} \dot{\boldsymbol{x}}(t) = \boldsymbol{A}\boldsymbol{x}(t) + \boldsymbol{B}\boldsymbol{u}(t) + \boldsymbol{D}\boldsymbol{w}(t), \\ \boldsymbol{u}(t) = \boldsymbol{K}\boldsymbol{x}(t), \\ \dot{\boldsymbol{d}}(t) = \boldsymbol{A}_d\boldsymbol{d}(t) + \boldsymbol{B}_d\boldsymbol{v}(t), \\ \boldsymbol{w}(t) = \boldsymbol{C}_d\boldsymbol{d}(t), \\ \boldsymbol{z}(t) = \boldsymbol{x}(t), \end{cases} \tag{6.28}$$

where $\boldsymbol{A}_d \in \mathbb{R}^{n_d \times n_d}$, $\boldsymbol{B}_d \in \mathbb{R}^{n_d \times n_v}$, and $\boldsymbol{C}_d \in \mathbb{R}^{n_w \times n_d}$ are matrices describing the disturbance dynamics, $\boldsymbol{d}(t) : \mathbb{R}_{\geq 0} \to \mathbb{R}^{n_d}$ is the disturbance states, and $\boldsymbol{v}(t) : \mathbb{R}_{\geq 0} \to \mathbb{R}^{n_v}$ is an exogenous signal that excites the disturbance behavior. In addition to Assumptions 9, 10 and 12 that hold for $\mathcal{P}_3$, the following ones are also considered to formulate the control problem:

Assumption 15. *The disturbance vector $\boldsymbol{w}(t)$ belongs to the Sobolev space, i.e. $\boldsymbol{w}(t) \in \mathcal{W}_{1,2}[0, \infty)$.*

Assumption 16. *$\boldsymbol{A}_d$ has negative eigenvalues.*

Assumption 17. *The matrix $\boldsymbol{B}_d$ has full column rank, i.e. rank$(\boldsymbol{B}_d) = \mathbb{R}^{n_v}$.*

Remark 40. *The vector of disturbances, $\boldsymbol{w}(t)$, and the disturbances states, $\boldsymbol{d}(t)$, are not measured.*

In this case, the $\mathcal{W}_\infty$ controller is designed in order to ensure the smallest γ such that

$$\gamma > \sup \frac{||\boldsymbol{z}(t)||_{\mathcal{W}_{1,2,\boldsymbol{\Gamma}}}}{||\boldsymbol{w}(t)||_{\mathcal{W}_{1,2,\boldsymbol{\Upsilon}}}} = \sup \frac{\left(||\boldsymbol{z}(t)||_{\mathcal{L}_{2,\boldsymbol{\Gamma}_0}} + ||\dot{\boldsymbol{z}}(t)||_{\mathcal{L}_{2,\boldsymbol{\Gamma}_1}}\right)^{\frac{1}{2}}}{\left(||\boldsymbol{w}(t)||_{\mathcal{L}_{2,\boldsymbol{\Upsilon}_0}} + ||\dot{\boldsymbol{w}}(t)||_{\mathcal{L}_{2,\boldsymbol{\Upsilon}_1}}\right)^{\frac{1}{2}}}, \tag{6.29}$$

with $||\boldsymbol{w}(t)||_{\mathcal{W}_{1,2}} \neq 0$, $\forall \boldsymbol{w}(t) \in \mathcal{W}_{1,2}[0, \infty)$, and subject to $\mathcal{P}_9$, where $\boldsymbol{\Gamma}$ is defined as in (6.2), and $\boldsymbol{\Upsilon} = \{\boldsymbol{\Upsilon}_0, \ \boldsymbol{\Upsilon}_1\}$.

Remark 41. *The $\mathcal{W}_\infty$ controller is now designed taking into account the time derivative of the disturbances, consequently, the minimization of γ in (6.29), implies in less influence of the disturbances and its time derivative in the closed-loop system (6.28).*

Similarly to Section 6.1, one can formulate the control problem as

$$\min_{\boldsymbol{K}, \boldsymbol{P}, \gamma} \quad \gamma, \tag{6.30}$$
$$s.t. : \begin{cases} \mathcal{P}_3, \\ \boldsymbol{x}'\boldsymbol{P}\boldsymbol{x} > 0, \\ \dot{\boldsymbol{V}}(\boldsymbol{x}) + \boldsymbol{x}'\boldsymbol{\Gamma}_0\boldsymbol{x} + \dot{\boldsymbol{x}}'\boldsymbol{\Gamma}_1\dot{\boldsymbol{x}} - \gamma^2\left(\boldsymbol{w}'\boldsymbol{\Upsilon}_0\boldsymbol{w} + \dot{\boldsymbol{w}}'\boldsymbol{\Upsilon}_1\dot{\boldsymbol{w}}\right) < 0. \end{cases}$$

Moreover, by employing the same transformations and change of variables that are considered in Section 6.1, with some manipulations and using the Schur complement, the full-state feedback $\mathcal{W}_\infty$ control problem results in solving the following semidefinite programming problem written as LMIs:

$$\min_{\boldsymbol{R}, \boldsymbol{S}, \gamma^*} \gamma^*, \tag{6.31}$$

$$s.t.: \begin{cases} \gamma^* > 0, \\ \boldsymbol{S} > 0, \\ \begin{bmatrix} \Xi_3 & * & * & * & * \\ \boldsymbol{C}_d'\boldsymbol{D}' & \Xi_4 & * & * & * \\ \boldsymbol{0} & \Xi_5 & \Xi_6 & * & * \\ \boldsymbol{A}\boldsymbol{S}+\boldsymbol{B}\boldsymbol{R} & \boldsymbol{D}\boldsymbol{C}_d & \boldsymbol{0} & -\boldsymbol{\Gamma}_1^{-1} & * \\ \boldsymbol{S} & \boldsymbol{0} & \boldsymbol{0} & \boldsymbol{0} & -\boldsymbol{\Gamma}_0^{-1} \end{bmatrix} < 0, \end{cases}$$

in which $\Xi_3 \triangleq \boldsymbol{S}\boldsymbol{A}'+\boldsymbol{A}\boldsymbol{S}+\boldsymbol{R}'\boldsymbol{B}'+\boldsymbol{B}\boldsymbol{R}$, $\Xi_4 \triangleq -\gamma^*(\boldsymbol{C}_d'\Upsilon_0\boldsymbol{C}_d'+\boldsymbol{A}_d'\boldsymbol{C}_d'\Upsilon_1\boldsymbol{C}_d\boldsymbol{A}_d)$, $\Xi_5 \triangleq -\gamma^*\boldsymbol{B}_d'\boldsymbol{C}_d'\Upsilon_1\boldsymbol{C}_d\boldsymbol{A}_d$, and $\Xi_6 \triangleq -\gamma^*\boldsymbol{B}_d'\boldsymbol{C}_d'\Upsilon_1\boldsymbol{C}_d\boldsymbol{B}_d$. After solving (6.31), the state feedback gain is computed by $\boldsymbol{K} = \boldsymbol{R}\boldsymbol{S}^{-1}$, the matrix $\boldsymbol{P} = \boldsymbol{S}^{-1}$, and the $\mathcal{W}_\infty$-index is given by $\gamma = \sqrt{\gamma^*}$.

Theorem 9. *Let Assumptions 9,10, 12-17 hold for (6.28), and consider $\boldsymbol{x}(0) \in \mathbb{R}^{n_x}$. If $\boldsymbol{K} = \boldsymbol{R}\boldsymbol{S}^{-1}$, $\boldsymbol{P} = \boldsymbol{S}^{-1}$, and $\gamma = \sqrt{\gamma^*}$ are obtained by solving the semidefinite programming problem (6.31), then the closed-loop system (6.28) is asymptotically stable.*

Proof. The proof follows similar to the proof of Theorem (7). □

In the following, Definition 7 is extended to a more general case.

Definition 8. *Suppose $\boldsymbol{w}(t) : \mathbb{R}_{\geq 0} \to \mathbb{R}^{n_w}$, $\boldsymbol{z}(t) : \mathbb{R}_{\geq 0} \to \mathbb{R}^{n_x}$, for some $n_w, n_x \in \mathbb{N}$, and $\boldsymbol{z}(t) = \boldsymbol{G}(\boldsymbol{w}(t))$, with $\boldsymbol{G} : \mathbb{R}^{n_w} \to \mathbb{R}^{n_x}$. The map $\boldsymbol{G}$ is said to be $\mathcal{W}_{n,q,\boldsymbol{\Upsilon}}^{m,p,\boldsymbol{\Gamma}}$-stable if there exist finite constants $\gamma, v \in \mathbb{R}_{\geq 0}$, such that the inequality*

$$||\boldsymbol{z}(t)||^2_{\mathcal{W}_{m,p,\boldsymbol{\Gamma}}} \leq \gamma^2 ||\boldsymbol{w}(t)||^2_{\mathcal{W}_{n,q,\boldsymbol{\Upsilon}}} + v \tag{6.32}$$

holds for any $\boldsymbol{w}(t) \in \mathcal{W}_{n,q}[0,\infty)$ and some matrices $\Gamma = \{\Gamma_0, \ldots \Gamma_p\}$ and $\boldsymbol{\Upsilon} = \{\boldsymbol{\Upsilon}_0, \ldots \boldsymbol{\Upsilon}_n\}$, where $m, n \in \mathbb{N} \cup \{0\}$ and $p, q \in \mathbb{N} \cup \{\infty\}$. Moreover, if $\gamma = \inf S$ in which $S = \{\gamma \in \mathbb{R}_{\geq 0} : ||\boldsymbol{z}(t)||^2_{\mathcal{W}_{m,p,\boldsymbol{\Gamma}}} \leq \gamma^2 ||\boldsymbol{w}(t)||^2_{\mathcal{W}_{n,q,\boldsymbol{\Upsilon}}} + v,\ \forall \boldsymbol{w}(t) \in \mathcal{W}_{n,q}[0,\infty),\ v \in \mathbb{R}_{\geq 0}\}$, then γ is called the $\mathcal{W}_{n,q,\boldsymbol{\Upsilon}}^{m,p,\boldsymbol{\Gamma}}$-gain of the system.

Remark 42. *Definition 7 is a particular case of Definition 8, in which $n = 0$, $q = p$, and $\boldsymbol{\Upsilon} = \{\boldsymbol{I}\}$.*

Regarding the control problem (6.31), with a few manipulations, one can show that

$$||\boldsymbol{z}(t)||^2_{\mathcal{W}_{1,2,\boldsymbol{\Gamma}}} < \gamma^2 ||\boldsymbol{w}(t)||^2_{\mathcal{W}_{1,2,\boldsymbol{\Upsilon}}} + \boldsymbol{V}(\boldsymbol{x}(0)) = \gamma^2 c_2 + c_1, \tag{6.33}$$

$\forall \boldsymbol{w}(t) \in \mathcal{W}_{1,2}[0,\infty)$, for some $c_1, c_2 \in \mathbb{R}_{\geq 0}$. Therefore, according to Definition 8, one can conclude that the closed-loop system (6.28) is $\mathcal{W}$-stable with the $\mathcal{W}_{1,2,\boldsymbol{\Gamma}}^{1,2,\boldsymbol{\Upsilon}}$-gain γ.

6.3.2 Output feedback approach

This subsection considers linear time-invariant systems represented by

$$\mathcal{P}_{10}: \begin{cases} \dot{\boldsymbol{x}}(t) = \boldsymbol{A}\boldsymbol{x}(t) + \boldsymbol{B}\boldsymbol{u}(t) + \boldsymbol{D}\boldsymbol{w}(t), \\ \boldsymbol{y}(t) = \boldsymbol{C}\boldsymbol{x}(t), \\ \dot{\boldsymbol{d}}(t) = \boldsymbol{A}_d\boldsymbol{d}(t) + \boldsymbol{B}_d\boldsymbol{v}(t), \\ \boldsymbol{w}(t) = \boldsymbol{C}_d\boldsymbol{d}(t), \\ \boldsymbol{z}(t) = \boldsymbol{x}(t), \end{cases} \tag{6.34}$$

in closed-loop with the dynamic controller $\mathcal{K}_1$ given by (6.12), where $\boldsymbol{A}$, $\boldsymbol{B}$, $\boldsymbol{C}$, $\boldsymbol{D}$, $\boldsymbol{x}(t)$, $\boldsymbol{u}(t)$, $\boldsymbol{w}(t)$, $\boldsymbol{y}(t)$ and $\boldsymbol{z}(t)$ are defined as in (6.11), and $\boldsymbol{A}_d$, $\boldsymbol{B}_d$, $\boldsymbol{C}_d$, $\boldsymbol{d}(t)$, and $\boldsymbol{v}(t)$ are defined as in (6.28). Additionally, Assumptions 9, 12-14 hold for (6.34).

Accordingly, aiming to achieve the condition (6.29), the control problem is posed as

$$\min_{\boldsymbol{A}_f,\boldsymbol{B}_f,\boldsymbol{C}_f,\boldsymbol{D}_f,\boldsymbol{P},\gamma} \gamma, \tag{6.35}$$
$$s.t.: \begin{cases} \mathcal{P}_{10}(\mathcal{K}_1), \\ \mathcal{X}_a'\boldsymbol{P}\mathcal{X}_a > 0, \\ \dot{V}(\mathcal{X}_a) + \boldsymbol{x}'\boldsymbol{\Gamma}_0\boldsymbol{x} + \dot{\boldsymbol{x}}'\boldsymbol{\Gamma}_1\dot{\boldsymbol{x}} - \gamma^2\left(\boldsymbol{w}'\boldsymbol{\Upsilon}_0\boldsymbol{w} + \dot{\boldsymbol{w}}'\boldsymbol{\Upsilon}_1\dot{\boldsymbol{w}}\right) < 0, \end{cases}$$

where $\mathcal{P}_{10}(\mathcal{K}_1)$ denotes the closed-loop dynamics of system (6.34) with the dynamic controller (6.12).

Thereafter, regarding the same transformations and change of variables considered in Section (6.2), and using the Schur complement, with some algebraic manipulations, the optimal control problem results in solving

$$\min_{\gamma^*,\boldsymbol{S},\boldsymbol{W},\boldsymbol{B}_s,\boldsymbol{C}_s,\boldsymbol{D}_f} \gamma^*, \tag{6.36}$$
$$s.t.: \begin{cases} \gamma^* > 0, \\ \begin{bmatrix} \boldsymbol{S} & \boldsymbol{I} \\ \boldsymbol{I} & \boldsymbol{W}' \end{bmatrix} > 0, \\ \begin{bmatrix} \boldsymbol{\Psi}_1 & * & * \\ \boldsymbol{0} & \boldsymbol{W}\boldsymbol{\Psi}_3\boldsymbol{W}' & * \\ \boldsymbol{\Psi}_7 & \boldsymbol{\Psi}_8\boldsymbol{W}' & \boldsymbol{\Psi}_9 \end{bmatrix} < 0, \end{cases}$$

where $\boldsymbol{\Psi}_1 \triangleq \boldsymbol{A}\boldsymbol{S} + \boldsymbol{B}\boldsymbol{C}_s + (\boldsymbol{A}\boldsymbol{S} + \boldsymbol{B}\boldsymbol{C}_s)'$, $\boldsymbol{W}\boldsymbol{\Psi}_3\boldsymbol{W}' \triangleq \boldsymbol{A}'\boldsymbol{W} + \boldsymbol{C}'\boldsymbol{B}_s' + \boldsymbol{W}\boldsymbol{A} + \boldsymbol{B}_s\boldsymbol{C}$, $\boldsymbol{\Psi}_7' \triangleq$

$[\boldsymbol{D}\boldsymbol{C}_d\ \mathbf{0}\ \ \boldsymbol{S}\ \ \boldsymbol{S}\boldsymbol{A}'+\boldsymbol{C}_s'\boldsymbol{B}']$, $\boldsymbol{W}\boldsymbol{\Psi}_8' \triangleq [\boldsymbol{W}\boldsymbol{D}\boldsymbol{C}_d\ \ \mathbf{0}\ \boldsymbol{I}\ \ \boldsymbol{A}'+\boldsymbol{C}'\boldsymbol{D}_f'\boldsymbol{B}']$, and

$$\boldsymbol{\Psi}_9 \triangleq \begin{bmatrix} \Xi_8 & * & * & * \\ -\gamma^*\boldsymbol{B}_d'\boldsymbol{C}_d'\boldsymbol{\Upsilon}_1\boldsymbol{C}_d'\boldsymbol{A}_d & -\gamma^*\boldsymbol{B}_d'\boldsymbol{C}_d'\boldsymbol{\Upsilon}_1\boldsymbol{C}_d\boldsymbol{B}_d & * & * \\ \boldsymbol{D}\boldsymbol{C}_d & \mathbf{0} & -\boldsymbol{\Gamma}_1^{-1} & \mathbf{0} \\ \mathbf{0} & \mathbf{0} & \mathbf{0} & -\boldsymbol{\Gamma}_0^{-1} \end{bmatrix},$$

in which $\Xi_8 \triangleq -\gamma^*(\boldsymbol{C}_d'\boldsymbol{\Upsilon}_0\boldsymbol{C}_d' + \boldsymbol{A}_d'\boldsymbol{C}_d'\boldsymbol{\Upsilon}_1\boldsymbol{C}_d\boldsymbol{A}_d)$. After solving (6.36), the controller parameters are computed as in (6.23)-(6.27).

Theorem 10. *Let Assumptions 9, 12-14 hold for the system (6.34), and consider $\boldsymbol{x}(0) \in \mathbb{R}^{n_x}$. If $\boldsymbol{A}_f$, $\boldsymbol{B}_f$, $\boldsymbol{C}_f$, $\boldsymbol{D}_f$, $\boldsymbol{S}$, $\boldsymbol{T}$, $\boldsymbol{R}$, and γ are obtained by solving the convex optimization problem with LMI constraints (6.36), then the closed-loop system (6.34) with the dynamic controller (6.12) is asymptotically stable.*

Proof. The proof follows the same steps of the proof of Theorem 7. □

Regarding Definition 8, with a few manipulations, it is possible to demonstrate that after solving the control problem (6.36), the closed-loop system achieve inequality (6.33).

6.4 Linear $\mathcal{W}_\infty$ control synthesis with pole placement constraints

It is well known that the behavior of a linear system can be characterized by the location of its poles and zeros. Therefore, this section incorporates the pole placement constraints that allows to synthesize a $\mathcal{W}_\infty$ controller with the closed-loop poles allocated in a predefined region $\mathcal{D}$ of the complex plane.

We begin by recalling the following definitions and theorem from Chilali and Gahinet (1996).

Definition 9. *(Adapted from Chilali and Gahinet (1996)) Let $\mathcal{D}$ be a subregion of the complex plane. The dynamic system $\dot{\boldsymbol{x}}(t) = \boldsymbol{A}\boldsymbol{x}(t)$ is called $\mathcal{D}$-stable if all poles of $\boldsymbol{A}$ lie in $\mathcal{D}$.*

Definition 10. *(Adapted from Chilali and Gahinet (1996)) A subset $\mathcal{D}$ of the complex plane is called an LMI region if there exist symmetric matrices $\boldsymbol{\alpha} \in \mathbb{R}^{n_i \times n_i}$ and $\boldsymbol{\beta} \in \mathbb{R}^{n_i \times n_i}$ such that*

$$\mathcal{D} = \{s \in \mathbb{C} : \boldsymbol{\alpha} + s\boldsymbol{\beta} + s^*\boldsymbol{\beta}' < 0\}. \tag{6.37}$$

Theorem 11. *(Adapted from Chilali and Gahinet (1996)) The matrix* $\boldsymbol{A} \in \mathbb{R}^{n_x \times n_x}$ *is* $\mathcal{D}$*-stable if and only if there exists a symmetric matrix* $\boldsymbol{P} \in \mathbb{R}^{n_x \times n_x}$ *such that*

$$\boldsymbol{\alpha} \otimes \boldsymbol{P} + \boldsymbol{\beta} \otimes (\boldsymbol{P}\boldsymbol{A}) + \boldsymbol{\beta}' \otimes (\boldsymbol{P}\boldsymbol{A})' < 0, \quad \boldsymbol{P} > 0, \tag{6.38}$$

where $\otimes$ *stands for the Kronecker product.*

Accordingly, regarding Theorem 11 and the change of variables $\boldsymbol{R} \triangleq \boldsymbol{K}\boldsymbol{S}$ and $\boldsymbol{S} \triangleq \boldsymbol{P}^{-1}$, a pole placement constraint can be considered by adding the following LMI into the convex optimization problems (6.7) or (6.31):

$$\begin{aligned} (\boldsymbol{I} \otimes \boldsymbol{P}^{-1}) \left(\boldsymbol{\alpha} \otimes \boldsymbol{P} + \boldsymbol{\beta} \otimes \boldsymbol{P}(\boldsymbol{A} + \boldsymbol{B}\boldsymbol{K}) + \boldsymbol{\beta}' \otimes (\boldsymbol{A} + \boldsymbol{B}\boldsymbol{K})' \boldsymbol{P}\right) (\boldsymbol{I} \otimes \boldsymbol{P}^{-1}) < 0, \\ \boldsymbol{\alpha} \otimes \boldsymbol{S} + \boldsymbol{\beta} \otimes (\boldsymbol{A}\boldsymbol{S} + \boldsymbol{B}\boldsymbol{R}) + \boldsymbol{\beta}' \otimes (\boldsymbol{A}\boldsymbol{S} + \boldsymbol{B}\boldsymbol{R})' < 0. \end{aligned} \tag{6.39}$$

If inequality (6.39) is satisfied, the poles of $\boldsymbol{A} + \boldsymbol{B}\boldsymbol{K}$ belongs to a sub-region $\mathcal{D}$ of the complex plane determined by the matrices $\boldsymbol{\beta}$ and $\boldsymbol{\alpha}$ (See Definitions 9 and 10).

Also, from Theorem 11, Definition 10, the output feedback controllers can be synthesized with the closed-loop poles allocated in a predefined region $\mathcal{D}$ of the complex plane by adding the following LMI into the convex optimization problems (6.22) and (6.36):

$$\begin{aligned} \Psi\Big(\boldsymbol{\alpha} \otimes \boldsymbol{P} + \boldsymbol{\beta} \otimes \boldsymbol{P}\boldsymbol{A}_a + \boldsymbol{\beta}' \otimes (\boldsymbol{P}\boldsymbol{A}_a)'\Big)\Psi' < 0, \\ \boldsymbol{\alpha} \otimes \begin{bmatrix} \boldsymbol{S} & \boldsymbol{I} \\ \boldsymbol{I} & \boldsymbol{W}' \end{bmatrix} + \boldsymbol{\beta} \otimes \boldsymbol{A}_k + \boldsymbol{\beta}' \otimes \boldsymbol{A}_k' < 0, \end{aligned} \tag{6.40}$$

where $\Psi \triangleq \left(\boldsymbol{I} \otimes \begin{bmatrix} \boldsymbol{I} & \boldsymbol{0} \\ \boldsymbol{0} & \boldsymbol{W} \end{bmatrix} \boldsymbol{M}\boldsymbol{P}^{-1}\right)$, and $\boldsymbol{A}_k \triangleq \begin{bmatrix} \boldsymbol{I} & \boldsymbol{0} \\ \boldsymbol{0} & \boldsymbol{W} \end{bmatrix} \boldsymbol{M}\boldsymbol{A}_a\boldsymbol{P}^{-1}\boldsymbol{M}' \begin{bmatrix} \boldsymbol{I} & \boldsymbol{0} \\ \boldsymbol{0} & \boldsymbol{W}' \end{bmatrix}$
$= \begin{bmatrix} \boldsymbol{A}\boldsymbol{S} + \boldsymbol{B}\boldsymbol{C}_s & \boldsymbol{A} + \boldsymbol{B}\boldsymbol{D}_f\boldsymbol{C} \\ -\boldsymbol{A}' - \boldsymbol{C}'\boldsymbol{D}_f'\boldsymbol{B}' & \boldsymbol{W}\boldsymbol{A} + \boldsymbol{B}_s\boldsymbol{C} \end{bmatrix}$, which was computed using the equality $\boldsymbol{A}_m = \boldsymbol{\Psi}_2$.

6.5 Numerical examples

This section presents numerical results of three experiments. In the first experiment, the linear $\mathcal{W}_\infty$ controllers are synthesized for a simple linear system. The aim is to corroborate the efficiency of these controllers and to demonstrate the advantages of approaches in which the dynamics of the disturbance are considered in the controller formulation (proposed in Section 6.3). In the second experiment, full-state and dynamic output feedback linear $\mathcal{W}_\infty$ controllers are synthesized for a Two-wheeled Self-balanced vehicle considering pole placement constraints, and a comparative analysis with classic linear $\mathcal{H}_\infty$ controllers is presented. Finally, in the third experiment, a state feedback linear $\mathcal{W}_\infty$ controller is synthesized for a Quadrotor UAV considering uncertainties in the system's parameters.

As in the previous experiment, a comparative analysis with the classic linear $\mathcal{H}_\infty$ controller is presented.

6.5.1 Simple example

This subsection corroborates the effectiveness of the proposed linear $\mathcal{W}_\infty$ controllers with numerical experiments conducted with the following linear system:

$$\mathcal{P}_{13}: \begin{cases} \dot{\boldsymbol{x}}(t) = \begin{bmatrix} 0 & 50 \\ -50 & -50 \end{bmatrix} \boldsymbol{x}(t) + \begin{bmatrix} 0 \\ 1 \end{bmatrix} \boldsymbol{u}(t) + \begin{bmatrix} 0 \\ 1 \end{bmatrix} \boldsymbol{w}(t), \\ \dot{\boldsymbol{d}}(t) = \begin{bmatrix} 0 & 100 \\ -100 & -100 \end{bmatrix} \boldsymbol{d}(t) + \begin{bmatrix} 0 \\ 100 \end{bmatrix} \boldsymbol{v}(t), \\ \boldsymbol{w}(t) = \begin{bmatrix} 10 & 10 \end{bmatrix} \boldsymbol{d}(t), \\ \boldsymbol{y}(t) = \begin{bmatrix} 1 & 1 \end{bmatrix} \boldsymbol{x}(t). \end{cases} \tag{6.41}$$

The linear $\mathcal{W}_\infty$ controllers were synthesized by solving (6.7), (6.22), (6.31), and (6.36). For the sake of comparison analysis, all the controllers were tuned with the same tuning matrices, with $\boldsymbol{\Gamma}_0 = \text{diag}(10,\ 10)$, $\boldsymbol{\Gamma}_1 = \text{diag}(1,\ 1)$ and $\boldsymbol{\Upsilon}_0 = \text{diag}(1)$. Nevertheless, the $\mathcal{W}_\infty$ controllers addressed in Section 6.3, that consider the disturbance dynamic model, were also tuned with $\boldsymbol{\Upsilon}_1 = \text{diag}(1000)$ for the state feedback approach and $\boldsymbol{\Upsilon}_1 = \text{diag}(500)$ for the output feedback approach.

In the numerical experiments, the system starts with the initial condition $\boldsymbol{x}(0) = [3\ 1]'$. Besides, a white noise Gaussian signal $\boldsymbol{v}(t)$ with zero mean and unitary variance is applied during $1 \leq t \leq 9$ s. The results are shown in Figure 6.1, and a quantitative analysis of these results is presented in Table 6.1.

As can be observed in Figure 6.1, the system starts displaced from the origin of the state-space and asymptotically converges to it. Along the experiment, all the controllers were able to provide stability to the system. However, the $\mathcal{W}_\infty$ controllers that were formulated considering the disturbance dynamic model in the cost functional achieved better disturbance attenuation with faster transient response and smaller control effort. These controllers achieved better performance for all analyzed indexes in comparison with the linear $\mathcal{W}_\infty$ controllers without considering the disturbance dynamic behavior in their formulations, see Table 6.1.

6.5.2 Two-wheeled Self-balanced vehicle

This subsection synthesizes the state feedback and the output feedback $\mathcal{W}_\infty$ controllers, considering pole placement constraint for the Two-wheeled Self-balanced vehicle. In addition, a comparison analysis is performed with the classic linear $\mathcal{H}_\infty$ controller (Chilali

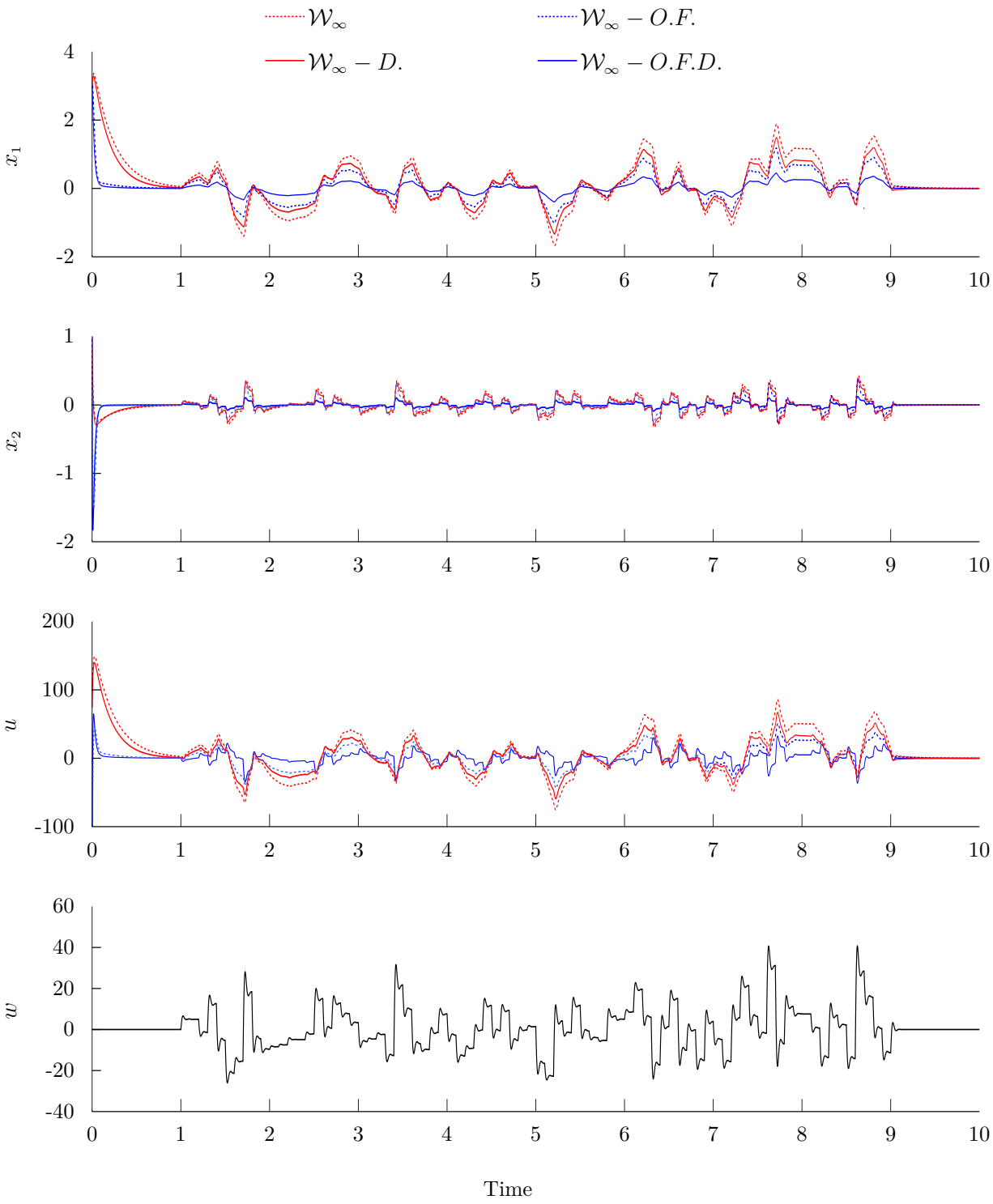

Figure 6.1: Time evolution of the states and control inputs, resulting from the application of the state feedback $\mathcal{W}_\infty$ and output feedback $\mathcal{W}_\infty$-O.F. controllers, and the state feedback $\mathcal{W}_\infty$-D. and output feedback $\mathcal{W}_\infty$-O.F.D. controllers with the disturbance model, and the disturbance signal.

and Gahinet, 1996).

In order to design the linear controllers, initially, the Two-wheeled Self-balanced vehicle equations of motion, which are described by the Euler-Lagrange equations (4.30) given in

Table 6.1: Table of performance indexes computed from the results of the state feedback $\mathcal{W}_\infty$ and output feedback $\mathcal{W}_\infty$-O.F. controllers, and the state feedback $\mathcal{W}_\infty$-D. and output feedback $\mathcal{W}_\infty$-O.F.D. controllers with the disturbance model.

P. Index	computed by	$\mathcal{W}_\infty$	$\mathcal{W}_\infty - D.$	$\mathcal{W}_\infty - O.F.$	$\mathcal{W}_\infty - O.F.D.$
ISE	$\int_0^\tau x_1^2(t)dt$	5.4(100%)	**3.4**(**64**%)	1.5(100%)	**0.3**(**21**%)
	$\int_0^\tau x_2^2(t)dt$	0.13(100%)	**0.10**(**74**%)	0.12(100%)	**0.07**(**63**%)
IADU$\times 10^3$	$\int_0^t \lvert\frac{d\boldsymbol{u}(\tau)}{d\tau}\rvert d\tau$	2.0(100%)	**1.8**(**90**%)	1.5(100%)	**1.1**(**77**%)
$\mathcal{H}_\infty \times 10^{-3}$	$\lvert\lvert\boldsymbol{x}(t)\rvert\rvert_{\mathcal{L}_2}/\lvert\lvert\boldsymbol{w}(t)\rvert\rvert_{\mathcal{L}_2}$	5.2(100%)	**4.1**(**77**%)	2.8(100%)	**1.1**(**40**%)

Section 4.4, are represented in the state-space,

$$\dot{\boldsymbol{x}}(t) = \boldsymbol{f}(\boldsymbol{x}) + \boldsymbol{g}(\boldsymbol{x})\boldsymbol{u}(t) + \boldsymbol{k}(\boldsymbol{x})\boldsymbol{w}(t), \tag{6.42}$$

with

$$\boldsymbol{f}(\boldsymbol{x}) = \begin{bmatrix} \dot{\theta} \\ -\boldsymbol{M}^{-1}(\boldsymbol{q})\left[\boldsymbol{C}(\boldsymbol{q},\dot{\boldsymbol{q}})\dot{\boldsymbol{q}} + \boldsymbol{K}(\dot{\boldsymbol{q}}) + \boldsymbol{G}(\boldsymbol{q})\right] \end{bmatrix}, \boldsymbol{g}(\boldsymbol{x}) = \begin{bmatrix} 0 \\ \boldsymbol{M}^{-1}(\boldsymbol{q})\boldsymbol{F}(\boldsymbol{q}) \end{bmatrix}, \boldsymbol{k}(\boldsymbol{x}) = \begin{bmatrix} 0 & 0 \\ \boldsymbol{M}^{-1}(\boldsymbol{q}) \end{bmatrix},$$

and $\boldsymbol{x}(t) = \begin{bmatrix}\theta(t) & \dot{\phi}(t) & \dot{\theta}(t)\end{bmatrix}'$. Then, the state-space system (6.42) is linearized around the equilibrium point $\boldsymbol{x} = \boldsymbol{0}$ and represented by the standard forms (6.1) and (6.13). The state feedback and output feedback $\mathcal{W}_\infty$ controllers are synthesized through (6.7) and (6.22).

For the sake of comparison analysis, the $\mathcal{W}_\infty$ and the classic $\mathcal{H}_\infty$ controllers are designed to achieve, similar settling time for the pendulum angular position when the closed-loop system starts from the initial condition $\boldsymbol{x}(0) = [\frac{\pi}{4}\ 0\ 0]'$ (it was used the criteria of 2%), as shown in Figure 6.2. With this objective, the state feedback $\mathcal{W}_\infty$ controller is tuned with $\boldsymbol{\Gamma}_0 = \text{diag}(0.2,\ 2,\ 0.3)$, $\boldsymbol{\Gamma}_1 = \text{diag}(2.6,\ 0.25,\ 0.625)$, and $\boldsymbol{\Upsilon}_0 = \text{diag}(1,\ 1)$, while the output feedback $\mathcal{W}_\infty$ controller is tuned with $\boldsymbol{\Gamma}_0 = \text{diag}(10,\ 1,\ 10)$, and $\boldsymbol{\Gamma}_1 = \text{diag}(0.66,\ 0.35,\ 0.3355)$.

In order to design the output feedback controllers, it was considered that the pendulum angular velocity is not available, which implies that $\boldsymbol{C} = \begin{bmatrix} 1 & 0 & 0 \\ 0 & 1 & 0 \end{bmatrix}$ in (6.11).

All the controllers are designed with the poles allocation region constrained by a ball with radius r centered at the origin of the complex plane. This region is defined by (6.37), with

$$\boldsymbol{\alpha} = \begin{bmatrix} -r & 0 \\ 0 & r \end{bmatrix}, \qquad \boldsymbol{\beta} = \begin{bmatrix} 0 & 1 \\ 0 & 0 \end{bmatrix}. \tag{6.43}$$

From (6.43), the LMIs (6.39) and (6.40) are added, respectively, to (6.7) and (6.22). The state feedback $\mathcal{W}_\infty$ and $\mathcal{H}_\infty$ controllers are synthesized with $r = 40$ and the output feedback controllers with an enlarged radius $r = 150$. This allows the poles related to the dynamic controller be faster than the poles related to the physical system.

In the numerical experiment, the system starts with the pendulum inclined in the initial condition $\boldsymbol{x}(0) = [\frac{\pi}{4}\ 0\ 0]'$, and is subjected to the disturbances $w_\phi(t) = 2$ N·m, for $5 \leq t \leq 10$ s, and $w_\theta(t) = 2\sin(\frac{2\pi t}{5})$ N·m, for $15 < t \leq 20$ s. The results are shown in Figure 6.3, and a quantitative analysis is presented in Table 6.2.

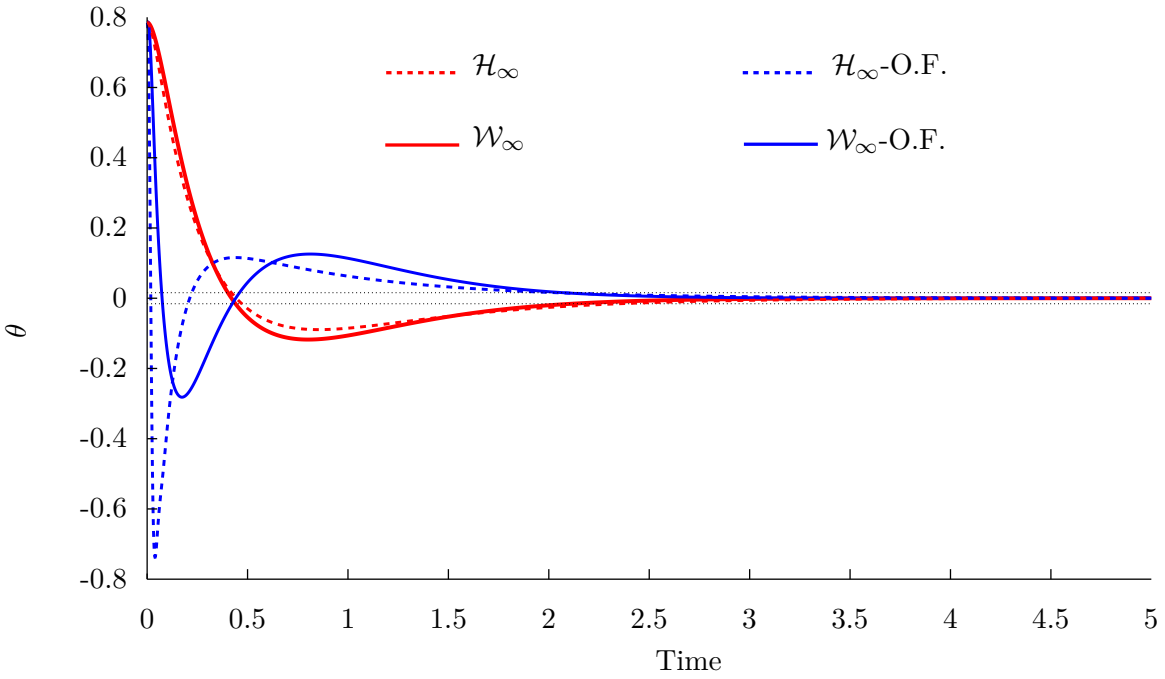

Figure 6.2: Settling time of the pendulum angular position resulting from the application of the state feedback $\mathcal{H}_\infty$ and $\mathcal{W}_\infty$ controllers, and the output feedback $\mathcal{H}_\infty$-O.F. and $\mathcal{W}_\infty$-O.F. controllers to the Two-wheeled Self-balanced vehicle.

It is noteworthy that, since the $\mathcal{W}_\infty$ and $\mathcal{H}_\infty$ controllers were tuned to achieve similar settling time of the pendulum angular position, they achieved a similar results with respect to the ISE index computed for this variable. However, the former achieved faster transient response with improved ISE index of the wheels' velocity, and a better $\mathcal{H}_\infty$ performance index, in addition to less control effort.

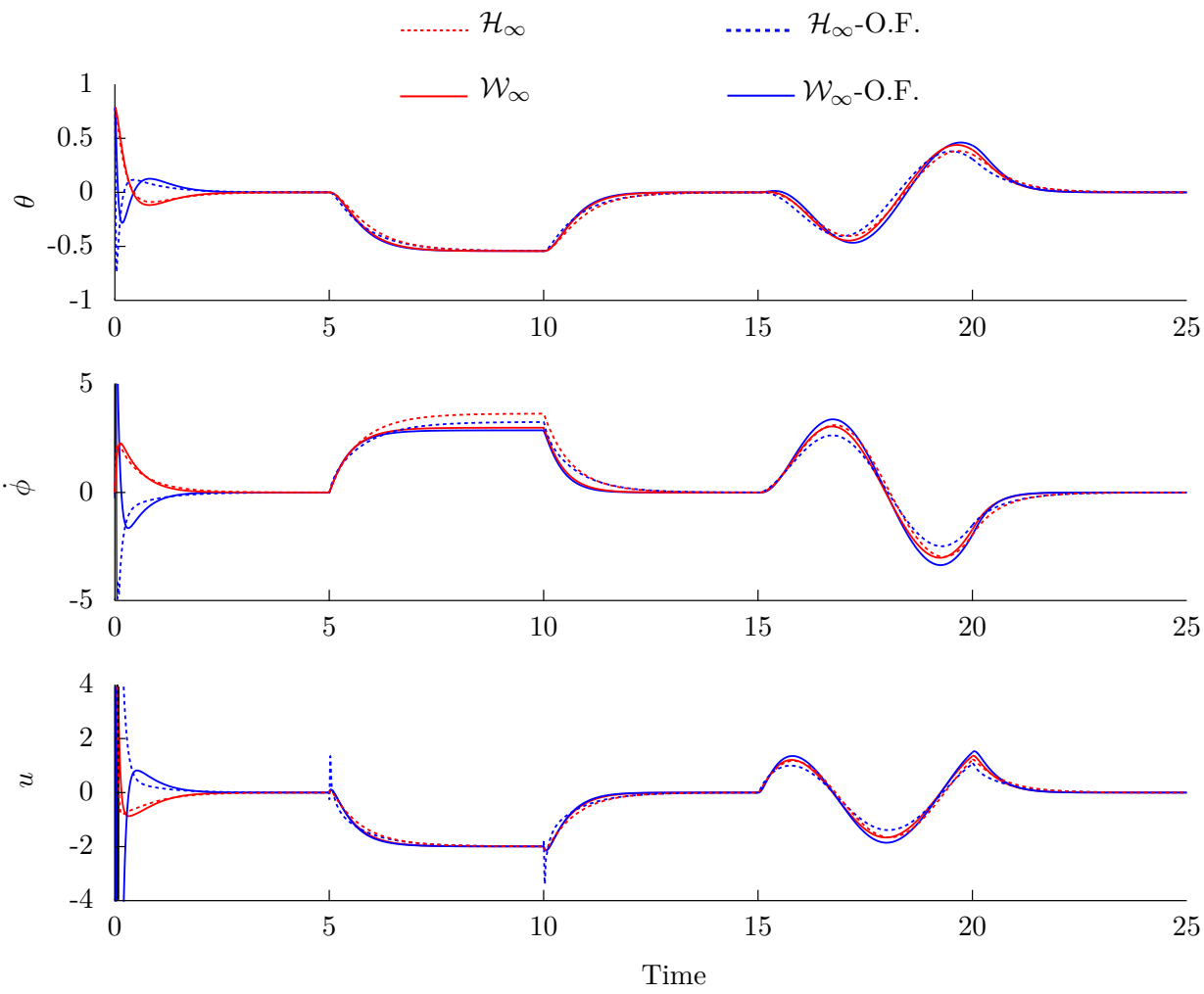

Figure 6.3: Time evolution of the pendulum angular position, wheels velocity, and control inputs signals resulting from the application of the state feedback $\mathcal{H}_\infty$ and $\mathcal{W}_\infty$ controllers, and the output feedback $\mathcal{H}_\infty$-O.F. and $\mathcal{W}_\infty$-O.F. controllers to the Two-wheeled Self-balanced vehicle.

Table 6.2: Table of performance indexes computed from the results of the state feedback $\mathcal{H}_\infty$ and $\mathcal{W}_\infty$ controllers, and output feedback $\mathcal{H}_\infty$-O.F. and $\mathcal{W}_\infty$-O.F. controllers applied to the Two-wheeled Self-balanced vehicle.

P. Index	computed by	$\mathcal{H}_\infty$	$\mathcal{W}_\infty$	$\mathcal{H}_\infty - O.F.$	$\mathcal{W}_\infty - O.F.$
ISE	$\int_0^\tau \theta^2(t)dt$	**1.7**(**100**%)	1.8(109.5%)	**1.6**(**100**%)	1.8(112.5%)
	$\int_0^\tau \dot{\phi}^2(t)dt$	82.9(100%)	**65.8**(**79.4**%)	96.1(100%)	**71.6**(**74.5**%)
IADU	$\int_0^t \lvert\frac{d\boldsymbol{u}(\tau)}{d\tau}\rvert d\tau$	48.2(100%)	**33.5**(**69.6**%)	4544(100%)	**682**(**15.0**%)
$\mathcal{H}_\infty$	$\lvert\lvert\boldsymbol{x}(t)\rvert\rvert_{\mathcal{L}_2}/\lvert\lvert\boldsymbol{w}(t)\rvert\rvert_{\mathcal{L}_2}$	1.47 (100%)	**1.32** (**90**%)	13.5 (100%)	**9.2** (**68**%)

6.5.3 Quadrotor UAV

This subsection synthesizes the linear state feedback $\mathcal{W}_\infty$ controller for a Quadrotor UAV, considering parametric uncertainties. In addition, a comparative analysis with respect to the classic $\mathcal{H}_\infty$ controller is presented. The aim is to evaluate the performance of these control strategies under the effects of parametric uncertainties.

In order to design the controller, initially, the Quadrotor UAV equations of motion, which are given in Section 5.3 and described by the Euler-Lagrange equations (5.123), are represented in the state-space

$$\dot{\hat{\boldsymbol{x}}}(t) = \boldsymbol{f}(\hat{\boldsymbol{x}}) + \boldsymbol{g}(\hat{\boldsymbol{x}})\boldsymbol{\tau}(t) + \boldsymbol{k}(\hat{\boldsymbol{x}})\boldsymbol{w}(t), \tag{6.44}$$

with

$$\boldsymbol{f}(\hat{\boldsymbol{x}}) = \begin{bmatrix} \dot{\theta} \\ -\boldsymbol{M}^{-1}(\boldsymbol{q})\left[\boldsymbol{C}(\boldsymbol{q},\dot{\boldsymbol{q}})\dot{\boldsymbol{q}} + \boldsymbol{G}(\boldsymbol{q})\right] \end{bmatrix}, \boldsymbol{g}(\hat{\boldsymbol{x}}) = \begin{bmatrix} 0 \\ \boldsymbol{M}^{-1}(\boldsymbol{q})\boldsymbol{B}(\boldsymbol{q}) \end{bmatrix}, \boldsymbol{k}(\hat{\boldsymbol{x}}) = \begin{bmatrix} 0 & 0 \\ \boldsymbol{M}^{-1}(\boldsymbol{q}) \end{bmatrix},$$

and $\hat{\boldsymbol{x}}(t) = [\phi\ \theta\ \psi\ x\ y\ z\ \dot{\phi}\ \dot{\theta}\ \dot{\psi}\ \dot{x}\ \dot{y}\ \dot{z}]'$.

Then, the state-space system (6.44) is linearized around the equilibrium point with $\phi = \theta = \psi = 0$, and represented by the Linear Parameter Varying (LPV) system

$$\mathcal{P}_{11}: \begin{cases} \dot{\boldsymbol{x}}(t) = \boldsymbol{A}(\epsilon)\boldsymbol{x}(t) + \boldsymbol{B}(\epsilon)\boldsymbol{u}(t) + \boldsymbol{D}(\epsilon)\boldsymbol{w}(t), \\ \boldsymbol{u}(t) = \boldsymbol{K}\boldsymbol{x}(t), \\ \boldsymbol{z}(t) = \boldsymbol{x}(t), \end{cases} \tag{6.45}$$

with $\boldsymbol{K} = \boldsymbol{R}\boldsymbol{S}^{-1}$, in which it is assumed the Quadrotor UAV mass and inertia tensors as uncertain parameters, $\epsilon = [m\ Ixx\ Iyy\ Izz]'$, with 10% of uncertainty. Consequently, $\epsilon \in \Omega$, such that $m \in [2.0160, 2.4640]$, $Ixx \in [0.0346, 0.0422]$, $Iyy \in [0.0346, 0.0422]$, and $Izz \in [0.0554, 0.0677]$.

The linear $\mathcal{W}_\infty$ controller is designed taking into account the following theorem.

Corollary 1. *Consider the LPV system (6.45) in which ϵ is an affine uncertain parameter that belongs to a known compact convex set*

$$\Omega = \{\epsilon \in \mathbb{R}^{n_\epsilon} : \epsilon_{\min} \leq \epsilon \leq \epsilon_{\max}\}. \tag{6.46}$$

Suppose that matrices $\boldsymbol{R}$ and $\boldsymbol{S}$, and the $\mathcal{W}_\infty$-index γ^* satisfy

$$\begin{aligned} &\min_{\boldsymbol{R},\boldsymbol{S},\gamma^*} \gamma^*, \\ &s.t.: \Psi(\boldsymbol{R},\boldsymbol{S},\gamma^*,\boldsymbol{A}_j,\boldsymbol{B}_j,\boldsymbol{D}_j) < 0, \quad \textit{for } j = 1,\cdots,q, \end{aligned} \tag{6.47}$$

in which $\Psi(\cdot) < 0$ is a compact representation of all inequalities in (6.7), and $\boldsymbol{A}_j$, $\boldsymbol{B}_j$, $\boldsymbol{D}_j$

represent the dynamics of (6.45) *evaluated at the* $j-th$ *vertex of* Ω. *Then, the system* (6.45) *is asymptotically stable for any* $\epsilon \in \Omega$.

Proof. Since Ω is a known compact convex set, the system (6.45) can be precisely represented by the convex polytopic representation (Boyd et al., 1994; Hamdi et al., 2009)

$$\mathcal{P}_{12}: \begin{cases} \dot{\boldsymbol{x}}(t) = \boldsymbol{A}(\delta)\boldsymbol{x}(t) + \boldsymbol{B}(\delta)\boldsymbol{u}(t) + \boldsymbol{D}(\delta)\boldsymbol{w}(t), \\ \boldsymbol{u}(t) = \boldsymbol{K}\boldsymbol{x}(t), \\ \boldsymbol{z}(t) = \boldsymbol{x}(t), \end{cases} \tag{6.48}$$

where $\boldsymbol{A}(\delta) \triangleq \sum_{j=1}^{q} \delta_j \boldsymbol{A}_j$, $\boldsymbol{B}(\delta) \triangleq \sum_{j=1}^{q} \delta_j \boldsymbol{B}_j$, $\boldsymbol{D}(\delta) \triangleq \sum_{j=1}^{q} \delta_j \boldsymbol{D}_j$, in which the matrices $\boldsymbol{A}_j$, $\boldsymbol{B}_j$, $\boldsymbol{D}_j$ represent the dynamics of (6.45) evaluated at the j-th vertex of Ω, and δ_j is the j-th element of the vector $\boldsymbol{\delta} \in \mathbb{R}^q$ satisfying $0 \leq \delta_j \leq 1$ and $\sum_{j=1}^{q} \delta_j = 1$. In addition, $n_\epsilon = 2^q$ is the number of vertices of the convex set Ω.

Taking into account the similarity transformation $\boldsymbol{x} = \boldsymbol{S}\boldsymbol{y}$ and the change of variables $\boldsymbol{R} = \boldsymbol{K}\boldsymbol{S}$, in which $\boldsymbol{S} = \boldsymbol{P}^{-1}$, one can propose the following candidate Lyapunov function for (6.48):

$$\boldsymbol{V}(\boldsymbol{x}) = \boldsymbol{x}'\boldsymbol{P}\boldsymbol{x} = \boldsymbol{y}'\boldsymbol{S}\boldsymbol{y} > 0, \tag{6.49}$$

whose time derivative is given by

$$\begin{aligned} \dot{\boldsymbol{V}}(\boldsymbol{x}) &= \frac{\partial \boldsymbol{V}(\boldsymbol{x})}{\partial \boldsymbol{x}}\dot{\boldsymbol{x}} = \frac{\partial \boldsymbol{V}(\boldsymbol{x})}{\partial \boldsymbol{x}}\left(\left(\boldsymbol{A}(\delta) + \boldsymbol{B}(\delta)\boldsymbol{K}\right)\boldsymbol{x}(t) + \boldsymbol{D}(\delta)\boldsymbol{w}(t)\right), \\ &= \sum_{j=1}^{q} \delta_j \frac{\partial \boldsymbol{V}(\boldsymbol{x})}{\partial \boldsymbol{x}}\left(\left(\boldsymbol{A}_j + \boldsymbol{B}_j\boldsymbol{K}\right)\boldsymbol{x}(t) + \boldsymbol{D}_j\boldsymbol{w}(t)\right). \end{aligned} \tag{6.50}$$

Therefore, regarding Theorem 7, if $\boldsymbol{R}$, $\boldsymbol{S}$ and γ^* satisfy (6.47) for all the vertices of Ω, we have that

$$\frac{\partial \boldsymbol{V}(\boldsymbol{x})}{\partial \boldsymbol{x}}\left(\left(\boldsymbol{A}_j + \boldsymbol{B}_j\boldsymbol{K}\right)\boldsymbol{x}(t) + \boldsymbol{D}_j\boldsymbol{w}(t)\right) < 0, \quad \text{for } j = 1, \cdots, q. \tag{6.51}$$

Consequently, since $0 \leq \delta_j \leq 1$ and $\sum_{j=1}^{q} \delta_j = 1$, the equation (6.49) is a Lyapunov function for (6.48) and, consequently, for (6.45). □

To perform the numerical experiments, the linear $\mathcal{W}_\infty$ controller is tuned with $\boldsymbol{\Gamma}_0 = \text{diag}(0.3183\ 0.3183\ 5.093\ 10\ 10\ 10.159\ 0.159\ \ 1.91\ 0.05\ 0.05\ 0.5)$, $\boldsymbol{\Gamma}_1 = \text{diag}(0.159\ 0.159\ 1.91\ 0.05\ 0.05\ 0.5\ 7.194\ 7.194\ 0.248\ 0.0327\ 0.0327\ \ 0.3597)$, and $\boldsymbol{\Upsilon}_0 = \text{diag}(1\ 1\ 1\ 1\ 1\ 1)$. In addition, aiming to bound the fastest poles, this controller is designed considering (6.43) with $r = 100$.

A linear $\mathcal{H}_\infty$ controller is also designed for the Quadrotor UAV (Chilali and Gahinet, 1996). For comparison analysis purposes, this controller is also synthesized to be robust

Table 6.3: Desired trajectory for the Quadrotor UAV translational position.

	$x_r(t)$	$y_r(t)$	$z_r(t)$
$t \geq 0$	$8\cos\left(\frac{\pi t}{20}\right)$	$8\sin\left(\frac{\pi t}{10}\right)$	$3-\cos\left(\frac{\pi t}{20}\right)$

for $\epsilon \in \Omega$, with the same pole placement constraints as the $\mathcal{W}_\infty$ controller. In addition, the linear $\mathcal{H}_\infty$ controller is tuned to achieve similar ISE performance index to the $\mathcal{W}_\infty$ controller, as shown in Table 6.4.

The simulation is conducted with the Quadrotor UAV starting from the initial condition $\dot{\boldsymbol{q}}(0) = \mathbf{0}$ and $\boldsymbol{q}(0) = [0\ 0\ 0\ 4\ 0\ 1]'$, and designated to track the desired trajectory present in Table 6.3. Along the numerical experiments, the disturbances $\delta_y(t) = 10$ N, for $10 < t < 15$ s, and $\delta_z(t) = 10\sin(0.4\pi t)$ N, for $25 < t < 30$ s, are applied to the system. The results are shown in Figures 6.4-6.6.

As can ben observed, in this experiment, the $\mathcal{W}_\infty$ controller achieved again better disturbance attenuation with faster transient response. In addition, although both controllers presented similar ISE, the proposed linear state feedback $\mathcal{W}_\infty$ controller demanded less control effort. It achieved the same performance with respect to the ISE index, but with a smaller control effort.

Table 6.4: Table of performance indexes computed with the results of the linear $\mathcal{H}_\infty$ and $\mathcal{W}_\infty$ controllers applied to the Quadrotor UAV.

P. Index	computed as	$\mathcal{H}_\infty$	$\mathcal{W}_\infty$
ISE	$\int_0^\tau \boldsymbol{x}'(t)\boldsymbol{x}(t)dt$	68.3 (100%)	**67.9** (**99.4**%)
IADU	$\int_0^t \sum_{i=1}^4 \lvert\frac{d\boldsymbol{\Omega}_i(\tau)}{d\tau}\rvert d\tau$	22635 (100%)	**10025** (**44.29**%)

6.6 Final remarks

This section proposed linear $\mathcal{W}_\infty$ controllers in weighted Sobolev spaces for linear time-invariant systems via semidefinite programming problems written as LMIs. They were designed considering full-state and dynamic output feedback. In addition, a new approach in which the disturbance dynamic behavior is taken into consideration in the control design stage by means of a disturbance model was presented, and pole placement constraints were formulated to allow the synthesis of $\mathcal{W}_\infty$ controllers with the closed-loop poles allocated in a predefined region of the complex plane.

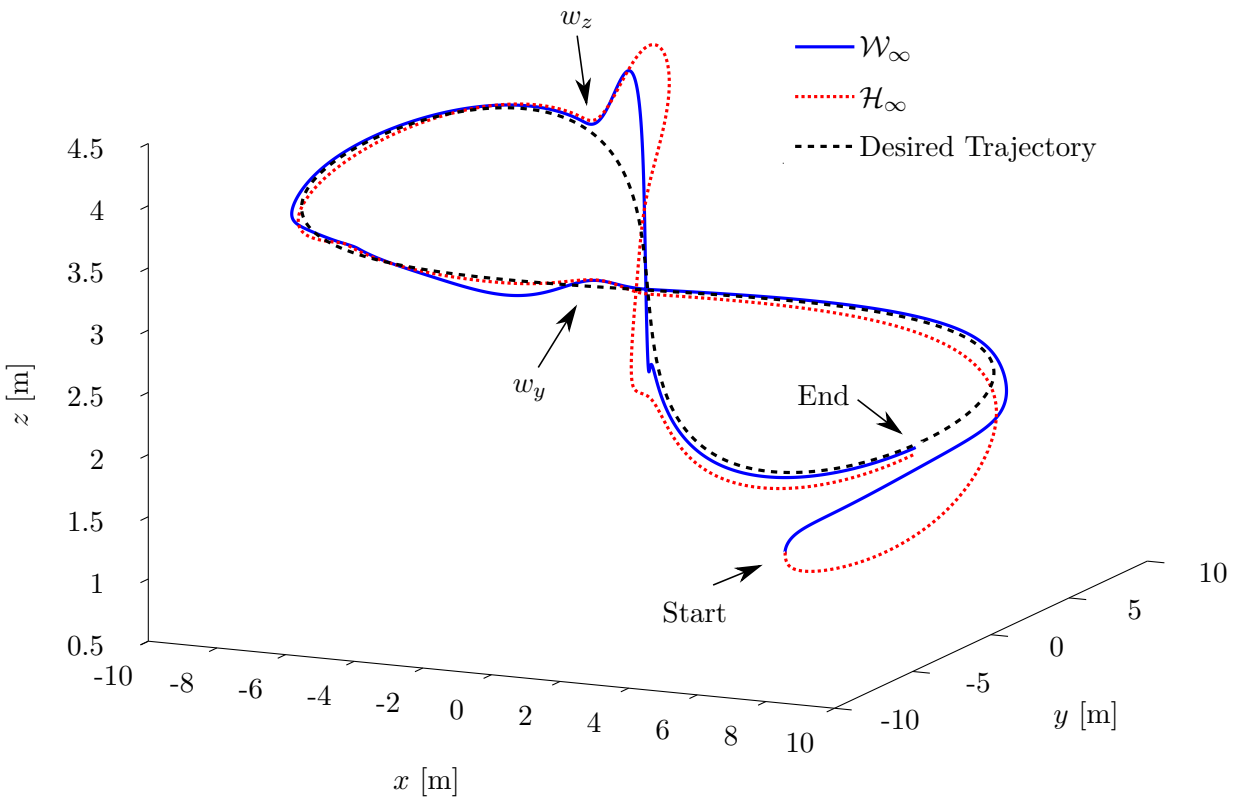

Figure 6.4: Three dimensional view of the trajectory performed by the Quadrotor UAV, resulting from the application of the $\mathcal{W}_\infty$ and $\mathcal{H}_\infty$ controllers.

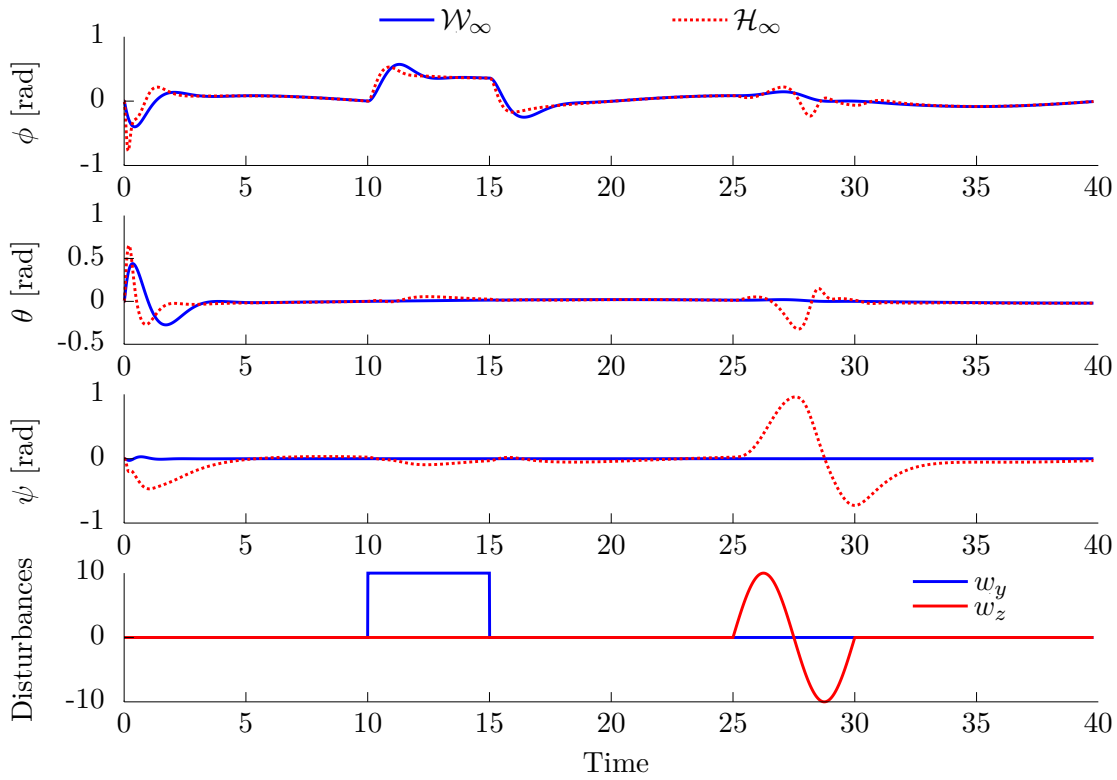

Figure 6.5: Time evolution of the Quadrotor UAV attitude, resulting from the application of the linear $\mathcal{W}_\infty$ and $\mathcal{H}_\infty$ controllers, and the disturbance signals.

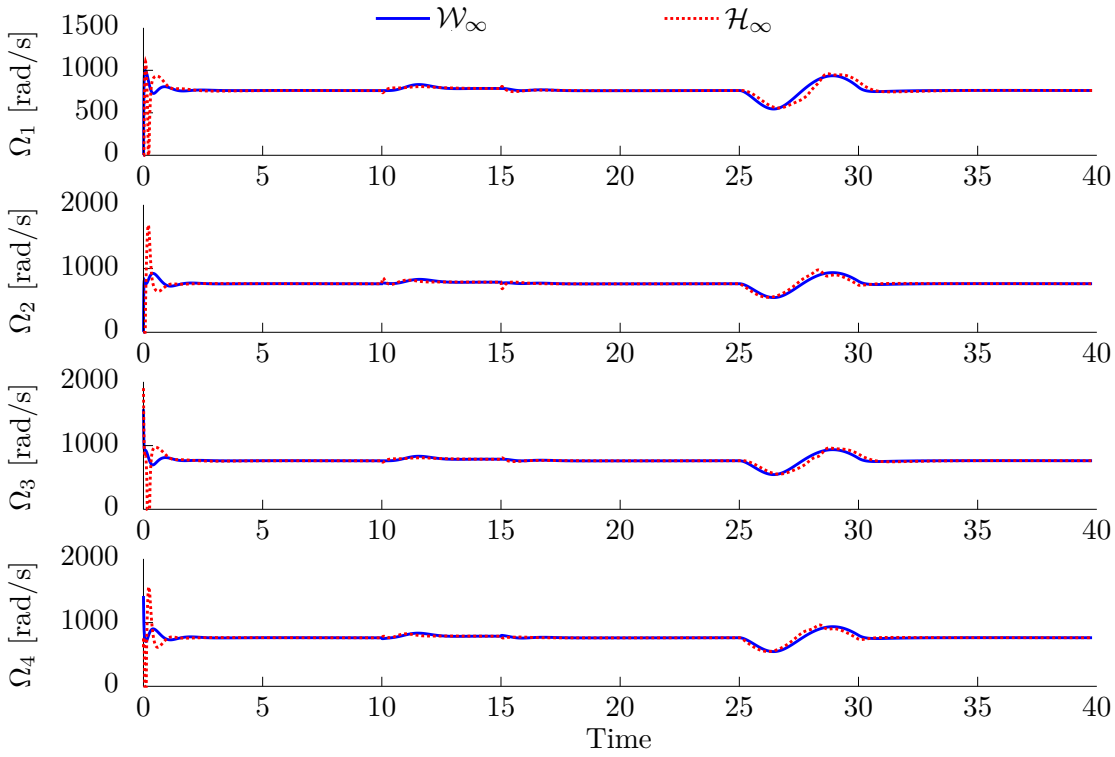

Figure 6.6: Time evolution of the Quadrotor UAV control inputs, resulting from the application of the $\mathcal{W}_\infty$ and $\mathcal{H}_\infty$ controllers.

Numerical experiments were conducted with a simple linear system, a Two-wheeled Self-balanced vehicle, and a Quadrotor UAV which corroborated the efficacy of the linear $\mathcal{W}_\infty$ control framework, proposed in this chapter. In addition, it was demonstrated that the proposed controllers achieved better results when compared with a linear $\mathcal{H}_\infty$ controller.

The next chapter concerns a case study with tilt-rotor UAV. Initially, it employs linear $\mathcal{W}_\infty$ control techniques to design controllers for a tilt-rotor UAV operating in the helicopter-flight mode. Then, the nonlinear $\mathcal{W}_\infty$ controller is incremented with a control allocation to handle the tilt-rotor UAV full flight envelope trajectory tracking problem.

7

Case study: convertible Tilt-rotor UAV

This chapter designs $\mathcal{W}_\infty$ controllers for a convertible Tilt-rotor UAV. Initially, the equations of motion of the convertible Tilt-rotor UAV are derived through the Euler-Lagrange approach. The full-state and dynamic output feedback linear $\mathcal{W}_\infty$ controllers addressed in Chapter 6 are synthesized in order to perform trajectory tracking in the helicopter-flight mode. Then, a nonlinear $\mathcal{W}_\infty$ controller is proposed to solve the full flight envelope trajectory tracking problem of the Tilt-rotor UAV. The nonlinear controller is designed regarding the nonlinear $\mathcal{W}_\infty$ control approach for mechanical system with input coupling, addressed in Section 5.2, but in this case, the vector of generalized coordinates is divided into controlled, regulated, and stabilized degrees of freedom. A control allocation scheme is also proposed to map the optimal control law to the appropriated control inputs signals according to the magnitude of the relative wind speed.

7.1 Introduction

Designing Unmanned Aerial Vehicles (UAVs) is among the most active fields of research. Lately results achieved on related areas, like sensors fusion, state estimation, robotics, aeronautics, and control, have improved UAVs performance and their reliability, making them attractive to several civilian applications such as search and rescue (Ryan and Hedrick, 2005), remote inspection (Metni and Hamel, 2007), load transportation (Rego and Raffo, 2019), public security (Daniel and Wietfeld, 2011), mapping (Zongjian, 2008), agriculture (Saari et al., 2011), among others. The increasing demand of applica-

tions has required UAVs with the capability of accomplishing long-range missions with rapid deployment, higher flight endurance, and able to perform hovering and Vertical Take-off and Landing (VTOL). To comply with these tasks, convertible UAVs such as the Quad-tilting rotor (Flores et al., 2012), the Tail-sitter (Verling et al., 2016), the Tilt-wing (Dickeson et al., 2005), and the Tilt-rotor (Maisel et al., 2000) have gained considerable attention. A review about convertible UAVs can be found in Morin (2015).

Besides the aforementioned advantages, the design of control laws to successfully execute tasks of convertible UAVs is challenging, since the relative wind generated by the aircraft's motion substantially changes the vehicle dynamic behavior between helicopter and cruise flight modes (Morin, 2015; Yuksek et al., 2016). In helicopter flight mode (VTOL and hovering), the aerodynamic surfaces do not produce significant forces and moments, whereas, in cruise flight mode, the wing generates significant aerodynamic forces that sustain forward flight, enabling conversion to the airplane mode, and small deflections of the aerodynamic control surfaces (aileron, rudder, and elevator) produce forces and moments that allow control and guidance. This fact poses some challenges for the control design of convertible UAVs, which cannot usually be solved using classical linear controllers when it is required to achieve good performance throughout the full flight envelope trajectory tracking. Furthermore, nonlinear control techniques designed for mechanical systems, such as Johansson (1990); Raffo et al. (2011a), cannot be directly applied to solve the problem since they were developed for systems whose input coupling matrix rank does not vary with time. In addition, convertible UAVs are usually subjected to uncertainties from many sources as wind gusts, unmodeled dynamics, and parametric uncertainties, which make the design of controllers for these systems even less trivial.

This chapter deals with the full flight envelope trajectory tracking problem of convertible UAVs through the Tilt-rotor configuration. A review about Tilt-rotor UAVs can be found in Liu et al. (2017); Hegde et al. (2019). This kind of vehicle is a multi-body, highly-coupled underactuated mechanical system that is often modeled as a single-body (Kendoul et al., 2005; Papachristos et al., 2011; Sanchez et al., 2008). Although the resulting dynamic model is simpler to handle, it is based on questionable simplifications. The single-body model neglects the coupling between the thrusters' groups and the main body, including the servomotors' dynamics (tilting mechanism dynamics), assuming that it can reach any inclination instantaneously. Besides, these simplified dynamics result in non-affine models with respect to the control inputs that make control design difficult. To overcome such simplification, works such as Rego and Raffo (2019); Almeida and Raffo (2015); Raffo and Almeida (2018) have proposed the modeling of the Tilt-rotor UAV as a multi-body mechanical system. The corresponding model is more accurate and takes into account the dynamics of servomotors. In the present work, the Tilt-rotor UAV equations of motion are obtained through the Euler-Lagrange formalism considering it as a multi-body mechanical system. Nevertheless, different from Rego and Raffo (2019); Almeida

and Raffo (2015); Raffo and Almeida (2018), here we take into account the aerodynamics effects generated by the fuselage, wings, tail-surfaces and propellers.

Concerning the control design of Tilt-rotor UAVs, due to the rank of the input coupling matrix that varies according to the flight mode, some works limit the control problem to the helicopter-flight mode and propose linear controllers. In Donadel et al. (2014) and Donadel (2015), for example, linear $\mathcal{H}_\infty$ and mixed $\mathcal{H}_2/\mathcal{H}_\infty$ controllers are designed to perform trajectory tracking of the Tilt-rotor UAV. The authors in, Papachristos et al. (2013) propose a proportional-integral-derivative (PID) controller in order to stabilize the Tilt-rotor UAV attitude dynamics. Papachristos et al. (2012) synthesize a Proportional-Derivative (PD) controller for the Tilt-rotor UAV altitude and attitude dynamics, presenting experimental results. Almeida et al. (2014) address the trajectory tracking problem of the Tilt-rotor UAV carrying a suspended load. A linear $\mathcal{H}_\infty$ controller with D-stability constraints is designed in order to guide the aircraft through the trajectory, maintaining stabilized the load. Santos and Raffo (2016) and Rego and Raffo (2016) propose a Model Predictive Controller (MPC) and a discrete-time linear quadratic regulator (DLQR), respectively, to solve the trajectory tracking problem of a Tilt-rotor UAV carrying a suspended load.

Another common strategy used to design controllers for Tilt-rotor UAVs operating in the helicopter-flight mode is the cascade approach. However, since the dynamics of the Tilt-rotor UAV are highly-coupled, the development of such controllers usually relies on mathematical model simplifications in order to decouple it. In Sanchez et al. (2008), a cascade controller is designed based on the Lyapunov theory aiming to perform hover flight. The control strategy is validated through experimental results. Additionally, Small et al. (2016) propose a cascaded P-PI and PID based control structure to achieve hover flight of a tilt-wing UAV. Chen et al. (2017) design a cascade control strategy to achieve trajectory tracking of a tricopter tiltrotor UAV. The inner loop is designed for attitude control based on a PID control strategy, while the outer loop is designed to control the translational position, which generates the desired references to be executed by the inner loop.

The first nonlinear controller designed to deal with the multi-body dynamics of the Tilt-rotor UAV in helicopter-flight mode was proposed by Almeida and Raffo (2015). As the aforementioned works, a cascade control strategy is designed based on simplifications on the mathematical model that aim of decoupling it. The control system is partitioned in three loops: the inner loop, that controls the servos' angles, roll motion and the altitude; the middle loop that controls the pitch and yaw angles; and the outer loop controls the x and y motions while stabilizes the load dynamics. For each loop a nonlinear controller is designed based on feedback linearization. This control strategy is improved in Raffo and Almeida (2018), by applying feedback linearization with dynamic extension, which reduces the number of cascade loops to two.

In Gress (2002), an alternative mechanical structure to the Tilt-rotor UAV is presented to improve the controllability of the system in helicopter-flight mode. This mechanical structure allows the thrusters to tilt in two degrees of freedom. The works of Kendoul et al. (2005) and Amiri et al. (2011) are developed based on the same Tilt-rotor UAV structure. In these works, the controllers are designed via backstepping. The first one aims to regulate the position and yaw dynamics and stabilize the remaining degrees of freedom, while the second one regulates the attitude dynamics. In both works, simplifications are performed over the mathematical model in order to decouple the dynamics of the system.

In addition to the literature dealing with helicopter-flight mode, there are few works concerning the cruise flight mode. In Calise and Rysdyk (1998), an attitude controller is proposed for the Tilt-rotor XV-15 aircraft (Nasa, 1975). The model is linearized around the equilibrium point by the first order Taylor series, from which a neural network is applied to estimate the unmodelled dynamics generated by the linearization. The controller uses information given by the neural network to improve its efficiency. In Mehra et al. (2001), the same mathematical model is considered in order to design a Model Predictive Controller (MPC) based on Linear Parameter Varying (LPV) model representation of the system. Numerical results are presented.

Regarding the difficulty to accomplish the transition between helicopter and cruise flight modes, some works focus on the problem of computing the optimal transition maneuvers. In Naldi and Marconi (2011), the minimum-time and minimum-energy optimal transition problems are formulated and solved numerically in order to compute reference maneuvers to be executed by the UAV. Just a few works consider the full flight envelope of Tilt-rotor UAVs, which are often based on gain-scheduling strategies. In Peng et al. (2010), for example, the V-22 Osprey aircraft (Norton, 2004) is controlled assuming a simplified single-body model of the x and z dynamics of the aircraft. Twenty controllers are synthesized to cover the entire aircraft flight envelope, being a gain-scheduling performed by combining the Optimum Preemptive Static Algorithm and the Optimum Preemptive Dynamic Scheduling Algorithms. In Lee et al. (2007), a Tilt-rotor UAV developed by the Korea Airspace Research Institute - (KARI) is presented. They explore the use of a gain-scheduling strategy to design a controller for the roll and pitch dynamics of the Tilt-rotor UAV, solving online an optimization problem by means of the Particle Swarm Optimization (PSO).

Still concerning the control of Tilt-rotor UAV throughout the full flight envelope, in Papachristos et al. (2013), a model predictive controller is proposed for a quad-tiltrotor UAV. The conversion control problem is solved by representing the system as a Linear Parameter Varying (LPV) and designing an LMPC (Linear Model Predictive Controller). Cardoso et al. (2016a) design linear state feedback mixed $\mathcal{H}_2/\mathcal{H}_\infty$ controllers to cover the Tilt-rotor UAV full flight envelope. In this work, a gain-scheduling scheme is performed by means of a neural network, applied in order to accomplish forward flight. This control

strategy is improved in Cardoso et al. (2016b), replacing the neural network by a robust adaptive mixing scheme. References Czyba et al. (2018); Kong and Lu (2018) perform gain-scheduling of controllers especially designed to cope with each flight mode. The classical PID method was used during the phase of VTOL, while a nonlinear control law based on backstepping was proposed to achieve a stable transition from vertical flight to horizontal flight. Although good experimental and numerical results have been obtained in these works, they do not present stability analysis of the proposed strategies. From the best knowledge of the author and as commented in Morin (2015), the design of a controller for convertible Tilt-rotor UAVs to accomplish transition between hover and cruise flight modes fully exploiting the aircraft multi-body nonlinear dynamics is an open field for researches.

In this context, this chapter designs a nonlinear $\mathcal{W}_\infty$ controller to solve the full flight envelope trajectory tracking problem of the Tilt-rotor UAV. In order to design this controller, the approach addressed in Section 5.2 is extended to the case in which the vector of generalized coordinates is divided into controlled, regulated, and stabilized degrees of freedom. In addition, a control allocation scheme is proposed to map the optimal control law to the appropriated control inputs signals according to the magnitude of the relative wind speed. Control allocation (Durham, 1993) has been widely used to handle actuators redundancy (Harkegard and Glad, 2005) and fault tolerant control (Temiz et al., 2018) in over actuated mechanical systems. Regarding applications to convertible UAVs, the readers are directed to Fuhrer et al. (2019); Chen et al. (2017); Shi et al. (2018). This technique comprehends in mapping the vector of generalized forces to the control inputs via predefined rules. A survey about control allocation is found in Johansen and Fossen (2013). Here, the control allocation is designed via the solution of an optimization problem with dynamic constraints.

7.2 Tilt-rotor UAV modeling

This section derives the equations of motion of a Tilt-rotor UAV using the Euler-Lagrange formulation. The aircraft is depicted in Figure 7.1 and is composed of: (i) the fuselage, where electronic components like battery, sensors, microprocessors, and others are assembled; (ii) two groups of thrusters, one at each side of the aircraft, that include propellers, DC brushless motors, and servomotors; (iii) the wings; and (iii) the V-tail surfaces.

7.2.1 Forward kinematics and generalized coordinates

In this work, the Tilt-rotor UAV is considered as a multi-body mechanical system composed of three rigid bodies, the main body, that includes the fuselage, wings and V-

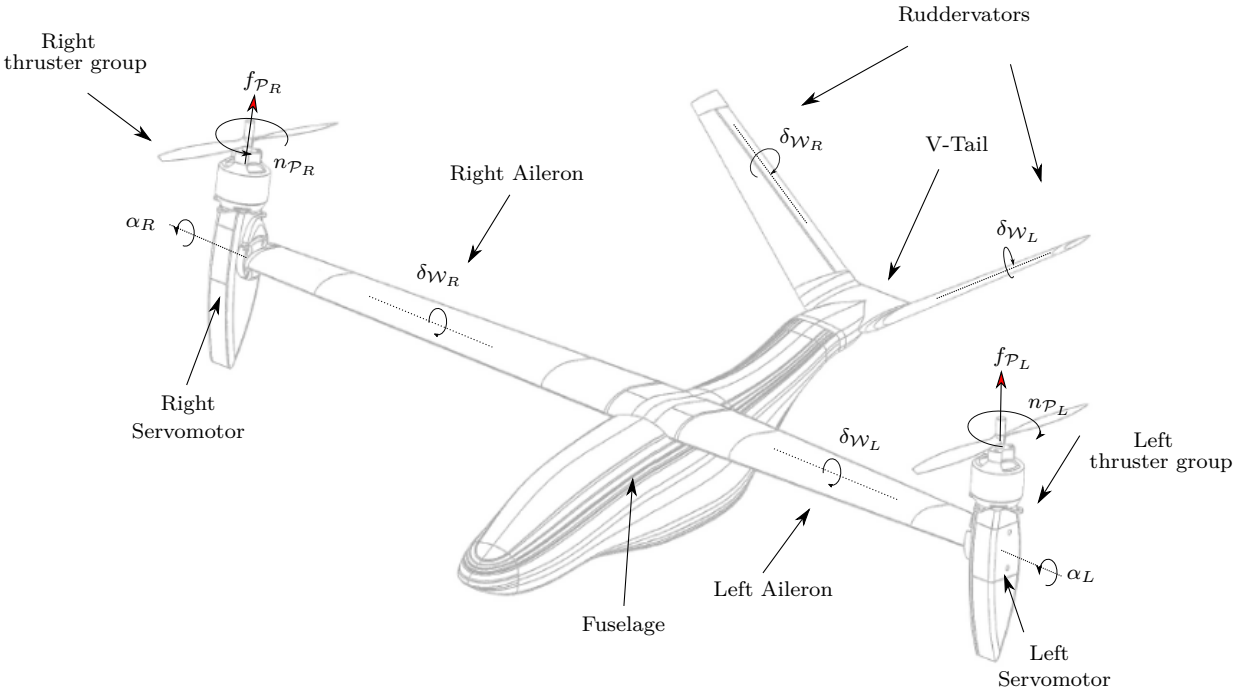

Figure 7.1: The Tilt-rotor UAV details.

tail surfaces, and the two groups of thrusters. Accordingly, in order to obtain the forward kinematics, seven reference frames are rigidly attached to the system (as depicted in Figure 7.2): the inertial reference frame $\mathcal{I}$; the aircraft's reference frame $\mathcal{B}$; frame $\mathcal{C}_1$, which is attached to the main body center of mass; frames $\mathcal{C}_2$ and $\mathcal{C}_3$ which are attached, respectively, to the right and left thruster's groups centers of mass; and two auxiliary frames, $\mathcal{A}_2$ and $\mathcal{A}_3$, placed at the axes of rotation of the right and left servomotors, respectively.

The Tilt-rotor UAV has eight degrees of freedom and is described by the vector of generalized coordinates $\boldsymbol{q}(t) : \mathbb{R}_{\geq 0} \to \mathbb{R}^8$ with $\boldsymbol{q}(t) \triangleq [\boldsymbol{\alpha}'(t)\ \boldsymbol{\eta}'(t)\ \boldsymbol{\xi}'(t)]'$, where $\boldsymbol{\alpha}(t) \triangleq [\alpha_R(t)\ \alpha_L(t)]'$ is the vector of the tilting mechanisms' angles, which are measured from the tilting axis of each servomotor[1]; $\boldsymbol{\eta}(t) \triangleq [\phi(t)\ \theta(t)\ \psi(t)]'$ is the orientation vector of $\mathcal{B}$ with respect to $\mathcal{I}$, described by the Euler angles with ZYX convention about the local axes; and $\boldsymbol{\xi}(t) \triangleq [x(t)\ y(t)\ z(t)]'$ is the position of $\mathcal{B}$ with respect to $\mathcal{I}$.

Accordingly, the position and orientation of frames $\mathcal{C}_1$, $\mathcal{C}_2$, and $\mathcal{C}_3$ with respect to the inertial frame are computed by[2]

$$\boldsymbol{p}^{\mathcal{I}}_{\mathcal{I},\mathcal{C}_1} = \boldsymbol{R}^{\mathcal{I}}_{\mathcal{B}} \boldsymbol{d}^{\mathcal{B}}_{\mathcal{B},\mathcal{C}_1} + \boldsymbol{\xi}, \tag{7.1}$$

$$\boldsymbol{R}^{\mathcal{I}}_{\mathcal{C}_1} = \boldsymbol{R}^{\mathcal{I}}_{\mathcal{B}}, \tag{7.2}$$

$$\boldsymbol{p}^{\mathcal{I}}_{\mathcal{I},\mathcal{C}_2} = \boldsymbol{R}^{\mathcal{I}}_{\mathcal{B}} \left(\boldsymbol{R}^{\mathcal{B}}_{\mathcal{A}_2} \boldsymbol{d}^{\mathcal{A}_2}_{\mathcal{A}_2,\mathcal{C}_2} + \boldsymbol{d}^{\mathcal{B}}_{\mathcal{B},\mathcal{A}_2} \right) + \boldsymbol{\xi}, \tag{7.3}$$

[1] Throughout the manuscript the subscripts R and L will be used to differentiate between the right and left components of the aircraft.

[2] For the sake of simplicity, throughout the manuscript some time dependencies are omitted.

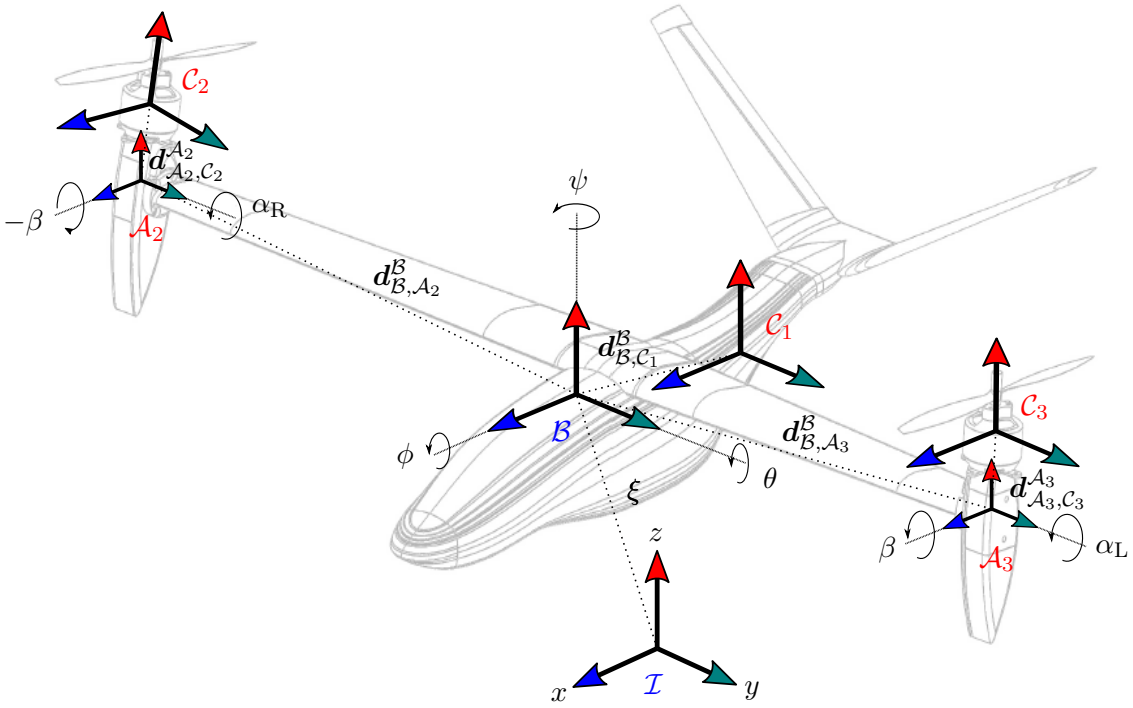

Figure 7.2: The Tilt-rotor UAV kinematic definitions.

$$\boldsymbol{R}^{\mathcal{I}}_{\mathcal{C}_2} = \boldsymbol{R}^{\mathcal{I}}_{\mathcal{B}} \boldsymbol{R}^{\mathcal{B}}_{\mathcal{A}_2}, \tag{7.4}$$

$$\boldsymbol{p}^{\mathcal{I}}_{\mathcal{I},\mathcal{C}_3} = \boldsymbol{R}^{\mathcal{I}}_{\mathcal{B}} \left(\boldsymbol{R}^{\mathcal{B}}_{\mathcal{A}_3} \boldsymbol{d}^{\mathcal{A}_3}_{\mathcal{A}_3,\mathcal{C}_3} + \boldsymbol{d}^{\mathcal{B}}_{\mathcal{B},\mathcal{A}_3} \right) + \boldsymbol{\xi}. \tag{7.5}$$

$$\boldsymbol{R}^{\mathcal{I}}_{\mathcal{C}_3} = \boldsymbol{R}^{\mathcal{I}}_{\mathcal{B}} \boldsymbol{R}^{\mathcal{B}}_{\mathcal{A}_3}, \tag{7.6}$$

where $\boldsymbol{p}^{p}_{n,m}(\boldsymbol{q}) : \mathbb{R}^8 \to \mathbb{R}^3$ and $\boldsymbol{d}^{p}_{n,m} \in \mathbb{R}^3$ are the position of the origin of the frame m w.r.t n, expressed in p, and $\boldsymbol{R}^{n}_{m} \in \mathrm{SO}(3)$ is the rotation matrix from frame m to n, for $m, n, p \in \{\mathcal{I}, \mathcal{B}, \mathcal{C}_1, \mathcal{C}_2, \mathcal{C}_3, \mathcal{A}_2, \mathcal{A}_3\}$. Moreover, $\boldsymbol{R}^{\mathcal{I}}_{\mathcal{B}}(\boldsymbol{q}) \triangleq \boldsymbol{R}_{z,\psi} \boldsymbol{R}_{y,\theta} \boldsymbol{R}_{x,\phi}$, $\boldsymbol{R}^{\mathcal{B}}_{\mathcal{A}_2}(\boldsymbol{q}) \triangleq \boldsymbol{R}_{y,\alpha_R} \boldsymbol{R}_{x,-\beta}$, and $\boldsymbol{R}^{\mathcal{B}}_{\mathcal{A}_3}(\boldsymbol{q}) \triangleq \boldsymbol{R}_{y,\alpha_L} \boldsymbol{R}_{x,\beta}$, where $\beta \in \mathbb{R}_{\geq 0}$ is a small inclination angle of the thrusters groups toward the fuselage, added during the mechanical design in order to improve the system controllability (Raffo et al., 2011a).

The linear velocity[3] $\boldsymbol{v}^{\mathcal{I}}_{\mathcal{I},i}(\boldsymbol{q}, \dot{\boldsymbol{q}}) : (\mathbb{R}^8 \times \mathbb{R}^8) \to \mathbb{R}^3$ of each center of mass is computed by the time derivative of its position $\boldsymbol{p}^{\mathcal{I}}_{\mathcal{I},i}(\boldsymbol{q})$, for $i \in \{\mathcal{C}_1, \mathcal{C}_2, \mathcal{C}_3\}$, as follows

$$\begin{aligned}
\boldsymbol{v}^{\mathcal{I}}_{\mathcal{I},\mathcal{C}_1} &= \dot{\boldsymbol{p}}^{\mathcal{I}}_{\mathcal{I},\mathcal{C}_1} = \boldsymbol{R}^{\mathcal{I}}_{\mathcal{B}} \boldsymbol{S}(\boldsymbol{w}^{\mathcal{B}}_{\mathcal{I},\mathcal{B}}) \boldsymbol{d}^{\mathcal{B}}_{\mathcal{B},\mathcal{C}_1} + \dot{\boldsymbol{\xi}}, \\
&= \begin{bmatrix} \boldsymbol{0} & \boldsymbol{0} & -\boldsymbol{R}^{\mathcal{I}}_{\mathcal{B}} \boldsymbol{S}(\boldsymbol{d}^{\mathcal{B}}_{\mathcal{B},\mathcal{C}_1}) \boldsymbol{W}_{\eta} & \boldsymbol{I} \end{bmatrix} \dot{\boldsymbol{q}}, \\
&= \boldsymbol{J}_{\mathcal{C}_1}(\boldsymbol{q}) \dot{\boldsymbol{q}},
\end{aligned} \tag{7.7}$$

$$\begin{aligned}
\boldsymbol{v}^{\mathcal{I}}_{\mathcal{I},\mathcal{C}_2} &= \dot{\boldsymbol{p}}^{\mathcal{I}}_{\mathcal{I},\mathcal{C}_2} = \boldsymbol{R}^{\mathcal{I}}_{\mathcal{C}_2} \boldsymbol{S}(\boldsymbol{w}^{\mathcal{C}_2}_{\mathcal{I},\mathcal{C}_2}) \boldsymbol{d}^{\mathcal{A}_2}_{\mathcal{A}_2,\mathcal{C}_2} + \boldsymbol{R}^{\mathcal{I}}_{\mathcal{B}} \boldsymbol{S}(\boldsymbol{w}^{\mathcal{B}}_{\mathcal{I},\mathcal{B}}) \boldsymbol{d}^{\mathcal{B}}_{\mathcal{B},\mathcal{A}_2} + \dot{\boldsymbol{\xi}}, \\
&= [-\boldsymbol{R}^{\mathcal{I}}_{\mathcal{C}_2} \boldsymbol{S}(\boldsymbol{d}^{\mathcal{A}_2}_{\mathcal{A}_2,\mathcal{C}_2}) \boldsymbol{a}_{y_R} \;\; \boldsymbol{0} \;\; -\boldsymbol{R}^{\mathcal{I}}_{\mathcal{B}} \boldsymbol{S}(\boldsymbol{R}^{\mathcal{B}}_{\mathcal{A}_2} \boldsymbol{d}^{\mathcal{A}_2}_{\mathcal{A}_2,\mathcal{C}_2} + \boldsymbol{d}^{\mathcal{B}}_{\mathcal{B},\mathcal{A}_2}) \boldsymbol{W}_{\eta} \;\; \boldsymbol{I}] \dot{\boldsymbol{q}}, \\
&= \boldsymbol{J}_{\mathcal{C}_2}(\boldsymbol{q}) \dot{\boldsymbol{q}},
\end{aligned} \tag{7.8}$$

[3]Throughout the text the notations $\boldsymbol{v}^{l}_{n,m}$ and $\boldsymbol{w}^{l}_{n,m}$ are used to represent, respectively, the linear and angular velocities of frame m with respect to n, expressed in l.

$$\begin{aligned}\boldsymbol{v}^{\mathcal{I}}_{\mathcal{I},\mathcal{C}_3} &= \dot{\boldsymbol{p}}^{\mathcal{I}}_{\mathcal{I},\mathcal{C}_3} = \boldsymbol{R}^{\mathcal{I}}_{\mathcal{C}_3}\boldsymbol{S}(\boldsymbol{w}^{\mathcal{C}_3}_{\mathcal{I},\mathcal{C}_3})\boldsymbol{d}^{\mathcal{A}_3}_{\mathcal{A}_3,\mathcal{C}_3} + \boldsymbol{R}^{\mathcal{I}}_{\mathcal{B}}\boldsymbol{S}(\boldsymbol{w}^{\mathcal{B}}_{\mathcal{I},\mathcal{B}})\boldsymbol{d}^{\mathcal{B}}_{\mathcal{B},\mathcal{A}_3} + \dot{\boldsymbol{\xi}},\\ &= [\boldsymbol{0} \;\; -\boldsymbol{R}^{\mathcal{I}}_{\mathcal{C}_3}\boldsymbol{S}(\boldsymbol{d}^{\mathcal{A}_3}_{\mathcal{A}_3,\mathcal{C}_3})\boldsymbol{a}_{y_L} \;\; -\boldsymbol{R}^{\mathcal{I}}_{\mathcal{B}}\boldsymbol{S}(\boldsymbol{R}^{\mathcal{B}}_{\mathcal{A}_3}\boldsymbol{d}^{\mathcal{A}_3}_{\mathcal{A}_3,\mathcal{C}_3} + \boldsymbol{d}^{\mathcal{B}}_{\mathcal{B},\mathcal{A}_3})\boldsymbol{W}_{\boldsymbol{\eta}} \;\; \boldsymbol{I}]\dot{\boldsymbol{q}},\\ &= \boldsymbol{J}_{\mathcal{C}_3}(\boldsymbol{q})\dot{\boldsymbol{q}}, \end{aligned} \tag{7.9}$$

where $\boldsymbol{R}^{\mathcal{I}}_{\mathcal{A}_2} = \boldsymbol{R}^{\mathcal{I}}_{\mathcal{C}_2}$, $\boldsymbol{R}^{\mathcal{I}}_{\mathcal{A}_3} = \boldsymbol{R}^{\mathcal{I}}_{\mathcal{C}_3}$, $\boldsymbol{a}_{y_R} \triangleq (\boldsymbol{R}_{x,-\beta})'\boldsymbol{a}_y$ and $\boldsymbol{a}_{y_L} \triangleq (\boldsymbol{R}_{x,\beta})'\boldsymbol{a}_y$, with $\boldsymbol{a}_y \triangleq [0\ 1\ 0]'$, $\boldsymbol{J}_i(\boldsymbol{q}) : \mathbb{R}^8 \to \mathbb{R}^{3\times 8}$ is the linear velocity Jacobian, and

$$\boldsymbol{W}_{\boldsymbol{\eta}} \triangleq \begin{bmatrix} 1 & 0 & -\sin(\theta) \\ 0 & \cos(\phi) & \cos(\theta)\sin(\phi) \\ 0 & -\sin(\phi) & \cos(\phi)\cos(\theta) \end{bmatrix}. \tag{7.10}$$

Besides, it was used the property $\dot{\boldsymbol{R}}^j_i = \boldsymbol{R}^j_i\boldsymbol{S}(\boldsymbol{w}^i_{j,i})$, where $\boldsymbol{S}(\cdot) : \mathbb{R}^3 \to \mathbb{R}^{3\times 3}$ denotes a skew-symmetric matrix (Spong et al., 2006).

In addition, the angular velocities of the centers of mass are given by

$$\begin{aligned}\boldsymbol{w}^{\mathcal{I}}_{\mathcal{I},\mathcal{C}_1} &= \boldsymbol{R}^{\mathcal{I}}_{\mathcal{C}_1}\boldsymbol{w}^{\mathcal{C}_1}_{\mathcal{I},\mathcal{C}_1} = \boldsymbol{R}^{\mathcal{I}}_{\mathcal{B}}\boldsymbol{W}_{\boldsymbol{\eta}}\dot{\boldsymbol{\eta}},\\ &= \begin{bmatrix}\boldsymbol{0} & \boldsymbol{0} & \boldsymbol{R}^{\mathcal{I}}_{\mathcal{B}}\boldsymbol{W}_{\boldsymbol{\eta}} & \boldsymbol{0}\end{bmatrix}\dot{\boldsymbol{q}},\\ &= \boldsymbol{W}_{\mathcal{C}_1}(\boldsymbol{q})\dot{\boldsymbol{q}}, \end{aligned} \tag{7.11}$$

$$\begin{aligned}\boldsymbol{w}^{\mathcal{I}}_{\mathcal{I},\mathcal{C}_2} &= \boldsymbol{w}^{\mathcal{I}}_{\mathcal{I},\mathcal{B}} + \boldsymbol{w}^{\mathcal{I}}_{\mathcal{B},\mathcal{C}_2} = \boldsymbol{R}^{\mathcal{I}}_{\mathcal{B}}\boldsymbol{w}^{\mathcal{B}}_{\mathcal{I},\mathcal{B}} + \boldsymbol{R}^{\mathcal{I}}_{\mathcal{C}_2}\boldsymbol{w}^{\mathcal{C}_2}_{\mathcal{B},\mathcal{C}_2},\\ &= \begin{bmatrix}\boldsymbol{R}^{\mathcal{I}}_{\mathcal{C}_2}\boldsymbol{a}_{y_R} & \boldsymbol{0} & \boldsymbol{R}^{\mathcal{I}}_{\mathcal{B}}\boldsymbol{W}_{\boldsymbol{\eta}} & \boldsymbol{0}\end{bmatrix}\dot{\boldsymbol{q}},\\ &= \boldsymbol{W}_{\mathcal{C}_2}(\boldsymbol{q})\dot{\boldsymbol{q}}, \end{aligned} \tag{7.12}$$

$$\begin{aligned}\boldsymbol{w}^{\mathcal{I}}_{\mathcal{I},\mathcal{C}_3} &= \boldsymbol{w}^{\mathcal{I}}_{\mathcal{I},\mathcal{B}} + \boldsymbol{w}^{\mathcal{I}}_{\mathcal{B},\mathcal{C}_3} = \boldsymbol{R}^{\mathcal{I}}_{\mathcal{B}}\boldsymbol{w}^{\mathcal{B}}_{\mathcal{I},\mathcal{B}} + \boldsymbol{R}^{\mathcal{I}}_{\mathcal{C}_3}\boldsymbol{w}^{\mathcal{C}_3}_{\mathcal{B},\mathcal{C}_3},\\ &= \begin{bmatrix}\boldsymbol{0} & \boldsymbol{R}^{\mathcal{I}}_{\mathcal{C}_3}\boldsymbol{a}_{y_L} & \boldsymbol{R}^{\mathcal{I}}_{\mathcal{B}}\boldsymbol{W}_{\boldsymbol{\eta}} & \boldsymbol{0}\end{bmatrix}\dot{\boldsymbol{q}},\\ &= \boldsymbol{W}_{\mathcal{C}_3}(\boldsymbol{q})\dot{\boldsymbol{q}}, \end{aligned} \tag{7.13}$$

where $\boldsymbol{W}_i(\boldsymbol{q}) : \mathbb{R}^8 \to \mathbb{R}^{3\times 8}$ is the angular velocity Jacobian.

7.2.2 Equations of motion

The equations of motion of the Tilt-rotor UAV illustrated in Figures 7.1 and 7.2 are written in the Euler-Lagrange canonical form

$$\boldsymbol{M}(\boldsymbol{q})\ddot{\boldsymbol{q}}(t) + \boldsymbol{C}(\boldsymbol{q},\dot{\boldsymbol{q}})\dot{\boldsymbol{q}}(t) + \boldsymbol{g}(\boldsymbol{q}) = \boldsymbol{\vartheta}(\boldsymbol{q},\dot{\boldsymbol{q}},\boldsymbol{\tau},\boldsymbol{\zeta}), \tag{7.14}$$

where $\boldsymbol{M}(\boldsymbol{q}) : \mathbb{R}^8 \to \mathbb{R}^{8\times 8}$ is the inertia matrix, $\boldsymbol{C}(\boldsymbol{q},\dot{\boldsymbol{q}}) : (\mathbb{R}^8 \times \mathbb{R}^8) \to \mathbb{R}^{8\times 8}$ is the Coriolis and centripetal forces matrix, $\boldsymbol{g}(\boldsymbol{q}) : \mathbb{R}^8 \to \mathbb{R}^8$ is the gravitational force vector, and $\boldsymbol{\vartheta}(\boldsymbol{q},\dot{\boldsymbol{q}},\boldsymbol{\tau},\boldsymbol{\zeta}) : (\mathbb{R}^8 \times \mathbb{R}^8 \times \mathbb{R}^{n_\tau} \times \mathbb{R}^{n_\zeta}) \to \mathbb{R}^8$ is the vector of generalized forces that actuate on the system. For details of the Euler-Lagrange formulation, see Section 3.5.

The inertia matrix is obtained from the Tilt-rotor UAV total kinetic energy, which is

computed as

$$\mathcal{K}(\boldsymbol{q},\dot{\boldsymbol{q}}) \triangleq \frac{1}{2}\sum_i \left(m_i(\boldsymbol{v}^{\mathcal{I}}_{\mathcal{I},i})'\boldsymbol{v}^{\mathcal{I}}_{\mathcal{I},i} + (\boldsymbol{w}^{\mathcal{I}}_{\mathcal{I},i})'\boldsymbol{R}^{\mathcal{I}}_i\mathbb{I}_i(\boldsymbol{R}^{\mathcal{I}}_i)'\boldsymbol{w}^{\mathcal{I}}_{\mathcal{I},i}\right) = \frac{1}{2}\dot{\boldsymbol{q}}'\boldsymbol{M}(\boldsymbol{q})\dot{\boldsymbol{q}}, \tag{7.15}$$

where $i \in \{\mathcal{C}_1,\mathcal{C}_2,\mathcal{C}_3\}$, $m_i \in \mathbb{R}_{\geq 0}$ is the i-th body mass, and $\mathbb{I}_i \in \mathbb{R}^{3\times 3}$ is the inertia tensor matrix with respect to its respective center of mass attached frame.

Thus, by manipulating (7.15) algebraically, yields

$$\boldsymbol{M}(\boldsymbol{q}) = \begin{bmatrix} \boldsymbol{M}_{11} & * & * & * \\ \boldsymbol{M}_{21} & \boldsymbol{M}_{22} & * & * \\ \boldsymbol{M}_{31} & \boldsymbol{M}_{32} & \boldsymbol{M}_{33} & * \\ \boldsymbol{M}_{41} & \boldsymbol{M}_{42} & \boldsymbol{M}_{43} & \boldsymbol{M}_{44} \end{bmatrix}, \tag{7.16}$$

where the * term indicates symmetry, and

$$\begin{aligned}
\boldsymbol{M}_{11} &= \boldsymbol{a}'_{y_R}\left[\mathbb{I}_{\mathcal{C}_2} - m_{\mathcal{C}_2}\boldsymbol{S}(\boldsymbol{d}^{\mathcal{A}_2}_{\mathcal{A}_2,\mathcal{C}_2})\boldsymbol{S}(\boldsymbol{d}^{\mathcal{A}_2}_{\mathcal{A}_2,\mathcal{C}_2})\right]\boldsymbol{a}_{y_R},\\
\boldsymbol{M}_{21} &= 0,\\
\boldsymbol{M}_{22} &= \boldsymbol{a}'_{y_L}\left[\mathbb{I}_{\mathcal{C}_3} - m_{\mathcal{C}_3}\boldsymbol{S}(\boldsymbol{d}^{\mathcal{A}_3}_{\mathcal{A}_3,\mathcal{C}_3})\boldsymbol{S}(\boldsymbol{d}^{\mathcal{A}_3}_{\mathcal{A}_3,\mathcal{C}_3})\right]\boldsymbol{a}_{y_L},\\
\boldsymbol{M}_{31} &= \boldsymbol{W}'_\eta\left[\boldsymbol{R}^{\mathcal{B}}_{\mathcal{C}_2}\mathbb{I}_{\mathcal{C}_2} - m_{\mathcal{C}_2}\boldsymbol{S}(\boldsymbol{d}^{\mathcal{B}}_{\mathcal{B},\mathcal{A}_2} + \boldsymbol{R}^{\mathcal{B}}_{\mathcal{A}_2}\boldsymbol{d}^{\mathcal{A}_2}_{\mathcal{A}_2,\mathcal{C}_2})\boldsymbol{R}^{\mathcal{B}}_{\mathcal{A}_2}\boldsymbol{S}(\boldsymbol{d}^{\mathcal{A}_2}_{\mathcal{A}_2,\mathcal{C}_2})\right]\boldsymbol{a}_{y_R},\\
\boldsymbol{M}_{32} &= \boldsymbol{W}'_\eta\left[\boldsymbol{R}^{\mathcal{B}}_{\mathcal{C}_3}\mathbb{I}_{\mathcal{C}_3} - m_{\mathcal{C}_3}\boldsymbol{S}(\boldsymbol{d}^{\mathcal{B}}_{\mathcal{B},\mathcal{A}_3} + \boldsymbol{R}^{\mathcal{B}}_{\mathcal{A}_3}\boldsymbol{d}^{\mathcal{A}_3}_{\mathcal{A}_3,\mathcal{C}_3})\boldsymbol{R}^{\mathcal{B}}_{\mathcal{A}_3}\boldsymbol{S}(\boldsymbol{d}^{\mathcal{A}_3}_{\mathcal{A}_3,\mathcal{C}_3})\right]\boldsymbol{a}_{y_L},\\
\boldsymbol{M}_{33} &= \boldsymbol{W}'_\eta\Big[\mathbb{I}_{\mathcal{C}_1} + \boldsymbol{R}^{\mathcal{B}}_{\mathcal{C}_2}\mathbb{I}_{\mathcal{C}_2}(\boldsymbol{R}^{\mathcal{B}}_{\mathcal{C}_2})' + \boldsymbol{R}^{\mathcal{B}}_{\mathcal{C}_3}\mathbb{I}_{\mathcal{C}_3}(\boldsymbol{R}^{\mathcal{B}}_{\mathcal{C}_3})' - m_{\mathcal{C}_1}\boldsymbol{S}(\boldsymbol{d}^{\mathcal{B}}_{\mathcal{B},\mathcal{C}_1})\boldsymbol{S}(\boldsymbol{d}^{\mathcal{B}}_{\mathcal{B},\mathcal{C}_1})\\
&\quad - m_{\mathcal{C}_2}\boldsymbol{S}(\boldsymbol{d}^{\mathcal{B}}_{\mathcal{B},\mathcal{A}_2} + \boldsymbol{R}^{\mathcal{B}}_{\mathcal{A}_2}\boldsymbol{d}^{\mathcal{A}_2}_{\mathcal{A}_2,\mathcal{C}_2})\boldsymbol{S}(\boldsymbol{d}^{\mathcal{B}}_{\mathcal{B},\mathcal{A}_2} + \boldsymbol{R}^{\mathcal{B}}_{\mathcal{A}_2}\boldsymbol{d}^{\mathcal{A}_2}_{\mathcal{A}_2,\mathcal{C}_2}),\\
&\quad - m_{\mathcal{C}_3}\boldsymbol{S}(\boldsymbol{d}^{\mathcal{B}}_{\mathcal{B},\mathcal{A}_2} + \boldsymbol{R}^{\mathcal{B}}_{\mathcal{A}_2}\boldsymbol{d}^{\mathcal{A}_3}_{\mathcal{A}_3,\mathcal{C}_3})\boldsymbol{S}(\boldsymbol{d}^{\mathcal{B}}_{\mathcal{B},\mathcal{A}_3} + \boldsymbol{R}^{\mathcal{B}}_{\mathcal{A}_3}\boldsymbol{d}^{\mathcal{A}_3}_{\mathcal{A}_3,\mathcal{C}_3})\Big]\boldsymbol{W}_\eta\\
\boldsymbol{M}_{41} &= -m_{\mathcal{C}_2}\boldsymbol{R}^{\mathcal{I}}_{\mathcal{C}_2}\boldsymbol{S}(\boldsymbol{d}^{\mathcal{A}_2}_{\mathcal{A}_2,\mathcal{C}_2})\boldsymbol{a}_{y_R},\\
\boldsymbol{M}_{42} &= -m_{\mathcal{C}_3}\boldsymbol{R}^{\mathcal{I}}_{\mathcal{C}_3}\boldsymbol{S}(\boldsymbol{d}^{\mathcal{A}_3}_{\mathcal{A}_3,\mathcal{C}_3})\boldsymbol{a}_{y_L},\\
\boldsymbol{M}_{43} &= -\boldsymbol{R}^{\mathcal{I}}_{\mathcal{B}}\left[m_{\mathcal{C}_1}\boldsymbol{S}(\boldsymbol{d}^{\mathcal{B}}_{\mathcal{B},\mathcal{C}_1}) + m_{\mathcal{C}_2}\boldsymbol{S}(\boldsymbol{d}^{\mathcal{B}}_{\mathcal{B},\mathcal{A}_2} + \boldsymbol{R}^{\mathcal{B}}_{\mathcal{A}_2}\boldsymbol{d}^{\mathcal{A}_2}_{\mathcal{A}_2,\mathcal{C}_2}) + m_{\mathcal{C}_3}\boldsymbol{S}(\boldsymbol{d}^{\mathcal{B}}_{\mathcal{B},\mathcal{A}_3} + \boldsymbol{R}^{\mathcal{B}}_{\mathcal{A}_3}\boldsymbol{d}^{\mathcal{A}_3}_{\mathcal{A}_3,\mathcal{C}_3})\right]\boldsymbol{W}_\eta,\\
\boldsymbol{M}_{44} &= (m_{\mathcal{C}_1} + m_{\mathcal{C}_2} + m_{\mathcal{C}_3})\boldsymbol{I}.
\end{aligned}$$

The Coriolis and centripetal forces matrix is obtained from the inertia matrix (7.16) by computing the Christoffel symbols of first kind (see section 3.5, equation (3.40)). In addition, the gravitational force vector is obtained through the potential energy of the system

$$\mathcal{P}(\boldsymbol{q}) = -\sum_i m_i\boldsymbol{g}'_{\boldsymbol{r}}\boldsymbol{p}^{\mathcal{I}}_{\mathcal{I},i}, \tag{7.17}$$

where $\boldsymbol{g}(\boldsymbol{q}) = \partial\mathcal{P}(\boldsymbol{q})/\partial\boldsymbol{q}$, in which $\boldsymbol{g}_{\boldsymbol{r}} = [0\ 0\ -9.8]'(m/s^2)$ is the gravity acceleration vector, given with respect to $\mathcal{I}$.

7.2.3 Generalized forces

The vector of generalized forces $\boldsymbol{\vartheta}(\boldsymbol{q},\dot{\boldsymbol{q}},\boldsymbol{\tau},\boldsymbol{\zeta})$ in (7.14) is composed of non-conservative forces and torques that actuate on the Tilt-rotor UAV. It is a function of the vector of

generalized coordinates $\boldsymbol{q}(t)$, the vector of generalized velocities $\dot{\boldsymbol{q}}(t)$, the control input vector $\boldsymbol{\tau}(t) : \mathbb{R}_{\geq 0} \to \mathbb{R}^8$, and the environment wind speed vector $\boldsymbol{\zeta}(t) : \mathbb{R}_{\geq 0} \to \mathbb{R}^3$.

As illustrated in Figure 7.1, the control input vector is given by $\boldsymbol{\tau}(t) = [n_{\mathcal{P}_R}(t)\ n_{\mathcal{P}_L}(t)\ \tau_{s_R}(t)\ \tau_{s_L}(t)\ \delta_{\mathcal{W}_R}(t)\ \delta_{\mathcal{W}_L}(t)\ \delta_{\mathcal{T}_R}(t)\ \delta_{\mathcal{T}_L}(t)]'$, where $n_{\mathcal{P}_R}(t)$ and $n_{\mathcal{P}_L}(t)$ are the angular velocities of the propellers, $\tau_{s_R}(t)$ and $\tau_{s_L}(t)$ are the torques applied by the servomotors, $\delta_{\mathcal{W}_R}(t)$ and $\delta_{\mathcal{W}_L}(t)$ are the right and left aileron deflections, respectively, and $\delta_{\mathcal{T}_R}(t)$ and $\delta_{\mathcal{T}_L}(t)$ are the right and left ruddervator deflections, respectively. In addition, the environment wind speed vector is given by $\boldsymbol{\zeta}(t) = \begin{bmatrix}\zeta_x(t) & \zeta_y(t) & \zeta_z(t)\end{bmatrix}'$, in which the elements are the magnitude of the environment wind speed on the axes of $\mathcal{I}$.

In order to compute the vector of generalized forces, this work splits this vector into terms related to the contribution of the propellers, servomotors, fuselage, wings, tail surfaces, and aerodynamic interference, as follows

$$\boldsymbol{\vartheta}(\dot{\boldsymbol{q}}, \boldsymbol{q}, \boldsymbol{\tau}, \boldsymbol{\zeta}) = \boldsymbol{\vartheta}_{\mathcal{P}} + \boldsymbol{\vartheta}_{s} + \boldsymbol{\vartheta}_{\mathcal{F}} + \boldsymbol{\vartheta}_{\mathcal{W}} + \boldsymbol{\vartheta}_{\mathcal{T}} + \boldsymbol{\vartheta}_{I}. \tag{7.18}$$

In the following the terms in (7.18) are computed.

Propellers

In order to compute the term in (7.18) related to the right and left propellers, initially, the reference frames $\mathcal{P}_R$ and $\mathcal{P}_L$ are rigidly attached to the center of rotation of the propellers, as depicted in Figure 7.3. The position of $\mathcal{P}_R$ and $\mathcal{P}_L$ with respect to the inertial frame are described by

$$\boldsymbol{p}^{\mathcal{I}}_{\mathcal{I},\mathcal{P}_R} = \boldsymbol{R}^{\mathcal{I}}_{\mathcal{B}} \left(\boldsymbol{R}^{\mathcal{B}}_{\mathcal{A}_2} \boldsymbol{d}^{\mathcal{A}_2}_{\mathcal{A}_2,\mathcal{P}_R} + \boldsymbol{d}^{\mathcal{B}}_{\mathcal{B},\mathcal{A}_2} \right) + \boldsymbol{\xi}, \tag{7.19}$$

$$\boldsymbol{p}^{\mathcal{I}}_{\mathcal{I},\mathcal{P}_L} = \boldsymbol{R}^{\mathcal{I}}_{\mathcal{B}} \left(\boldsymbol{R}^{\mathcal{B}}_{\mathcal{A}_3} \boldsymbol{d}^{\mathcal{A}_3}_{\mathcal{A}_3,\mathcal{P}_L} + \boldsymbol{d}^{\mathcal{B}}_{\mathcal{B},\mathcal{A}_3} \right) + \boldsymbol{\xi}. \tag{7.20}$$

where $\boldsymbol{d}^{\mathcal{A}_2}_{\mathcal{A}_2,\mathcal{P}_R}, \boldsymbol{d}^{\mathcal{A}_3}_{\mathcal{A}_3,\mathcal{P}_L} \in \mathbb{R}^3$ are the distances between frames $\mathcal{A}_2$ and $\mathcal{A}_3$ and the center of rotation of the right and left propellers, respectively.

Consequently, the linear and angular velocities of $\mathcal{P}_R$ and $\mathcal{P}_L$ are given by

$$\begin{aligned}
\boldsymbol{v}^{\mathcal{I}}_{\mathcal{I},\mathcal{P}_R} &= \dot{\boldsymbol{p}}^{\mathcal{I}}_{\mathcal{I},\mathcal{P}_R} = \boldsymbol{R}^{\mathcal{I}}_{\mathcal{P}_R} \boldsymbol{S}(\boldsymbol{w}^{\mathcal{P}_R}_{\mathcal{I},\mathcal{P}_R}) \boldsymbol{d}^{\mathcal{A}_2}_{\mathcal{A}_2,\mathcal{P}_R} + \boldsymbol{R}^{\mathcal{I}}_{\mathcal{B}} \boldsymbol{S}(\boldsymbol{w}^{\mathcal{B}}_{\mathcal{I},\mathcal{B}}) \boldsymbol{d}^{\mathcal{B}}_{\mathcal{B},\mathcal{A}_2} + \dot{\boldsymbol{\xi}}, \\
&= \begin{bmatrix} -\boldsymbol{R}^{\mathcal{I}}_{\mathcal{A}_2} \boldsymbol{S}(\boldsymbol{d}^{\mathcal{A}_2}_{\mathcal{A}_2,\mathcal{P}_R}) \boldsymbol{a}_{y_R} & \boldsymbol{0} & -\boldsymbol{R}^{\mathcal{I}}_{\mathcal{B}} \boldsymbol{S}(\boldsymbol{R}^{\mathcal{B}}_{\mathcal{A}_2} \boldsymbol{d}^{\mathcal{A}_2}_{\mathcal{A}_2,\mathcal{P}_R} + \boldsymbol{d}^{\mathcal{B}}_{\mathcal{B},\mathcal{A}_2}) \boldsymbol{W}_{\boldsymbol{\eta}} & \boldsymbol{I} \end{bmatrix} \dot{\boldsymbol{q}}, \\
&= \boldsymbol{J}_{\mathcal{P}_R}(\boldsymbol{q}) \dot{\boldsymbol{q}},
\end{aligned} \tag{7.21}$$

$$\begin{aligned}
\boldsymbol{v}^{\mathcal{I}}_{\mathcal{I},\mathcal{P}_L} &= \dot{\boldsymbol{p}}^{\mathcal{I}}_{\mathcal{I},\mathcal{P}_L} = \boldsymbol{R}^{\mathcal{I}}_{\mathcal{P}_L} \boldsymbol{S}(\boldsymbol{w}^{\mathcal{P}_L}_{\mathcal{I},\mathcal{P}_L}) \boldsymbol{d}^{\mathcal{A}_3}_{\mathcal{A}_3,\mathcal{P}_L} + \boldsymbol{R}^{\mathcal{I}}_{\mathcal{B}} \boldsymbol{S}(\boldsymbol{w}^{\mathcal{B}}_{\mathcal{I},\mathcal{B}}) \boldsymbol{d}^{\mathcal{B}}_{\mathcal{B},\mathcal{A}_3} + \dot{\boldsymbol{\xi}}, \\
&= \begin{bmatrix} \boldsymbol{0} & -\boldsymbol{R}^{\mathcal{I}}_{\mathcal{A}_3} \boldsymbol{S}(\boldsymbol{d}^{\mathcal{A}_3}_{\mathcal{A}_3,\mathcal{P}_L}) \boldsymbol{a}_{y_L} & -\boldsymbol{R}^{\mathcal{I}}_{\mathcal{B}} \boldsymbol{S}(\boldsymbol{R}^{\mathcal{B}}_{\mathcal{A}_3} \boldsymbol{d}^{\mathcal{A}_3}_{\mathcal{A}_3,\mathcal{P}_L} + \boldsymbol{d}^{\mathcal{B}}_{\mathcal{B},\mathcal{A}_3}) \boldsymbol{W}_{\boldsymbol{\eta}} & \boldsymbol{I} \end{bmatrix} \dot{\boldsymbol{q}}, \\
&= \boldsymbol{J}_{\mathcal{P}_L}(\boldsymbol{q}) \dot{\boldsymbol{q}},
\end{aligned} \tag{7.22}$$

$$\begin{aligned}
\boldsymbol{w}^{\mathcal{I}}_{\mathcal{I},\mathcal{P}_R} &= \boldsymbol{w}^{\mathcal{I}}_{\mathcal{I},\mathcal{B}} + \boldsymbol{w}^{\mathcal{I}}_{\mathcal{B},\mathcal{P}_R} = \boldsymbol{R}^{\mathcal{I}}_{\mathcal{B}} \boldsymbol{w}^{\mathcal{B}}_{\mathcal{I},\mathcal{B}} + \boldsymbol{R}^{\mathcal{I}}_{\mathcal{P}_R} \boldsymbol{w}^{\mathcal{P}_R}_{\mathcal{B},\mathcal{P}_R}, \\
&= \begin{bmatrix} \boldsymbol{R}^{\mathcal{I}}_{\mathcal{A}_2} \boldsymbol{a}_{y_R} & \boldsymbol{0} & \boldsymbol{R}^{\mathcal{I}}_{\mathcal{B}} \boldsymbol{W}_{\boldsymbol{\eta}} & \boldsymbol{0} \end{bmatrix} \dot{\boldsymbol{q}},
\end{aligned}$$

$$= \boldsymbol{W}_{\mathcal{P}_R}(\boldsymbol{q})\dot{\boldsymbol{q}}, \tag{7.23}$$

$$\begin{aligned} \boldsymbol{w}^{\mathcal{I}}_{\mathcal{I},\mathcal{P}_L} &= \boldsymbol{w}^{\mathcal{I}}_{\mathcal{I},\mathcal{B}} + \boldsymbol{w}^{\mathcal{I}}_{\mathcal{B},\mathcal{P}_L} = \boldsymbol{R}^{\mathcal{I}}_{\mathcal{B}}\boldsymbol{w}^{\mathcal{B}}_{\mathcal{I},\mathcal{B}} + \boldsymbol{R}^{\mathcal{I}}_{\mathcal{P}_L}\boldsymbol{w}^{\mathcal{P}_L}_{\mathcal{B},\mathcal{P}_L}, \\ &= \begin{bmatrix} \boldsymbol{0} & \boldsymbol{R}^{\mathcal{I}}_{\mathcal{A}_3}\boldsymbol{a}_{y_L} & \boldsymbol{R}^{\mathcal{I}}_{\mathcal{B}}\boldsymbol{W}_{\boldsymbol{\eta}} & \boldsymbol{0} \end{bmatrix}\dot{\boldsymbol{q}}, \\ &= \boldsymbol{W}_{\mathcal{P}_L}(\boldsymbol{q})\dot{\boldsymbol{q}}. \end{aligned} \tag{7.24}$$

in which $\boldsymbol{R}^{\mathcal{I}}_{\mathcal{P}_R} \triangleq \boldsymbol{R}^{\mathcal{I}}_{\mathcal{C}_2} = \boldsymbol{R}^{\mathcal{I}}_{\mathcal{A}_2}$ and $\boldsymbol{R}^{\mathcal{I}}_{\mathcal{P}_L} \triangleq \boldsymbol{R}^{\mathcal{I}}_{\mathcal{C}_3} = \boldsymbol{R}^{\mathcal{I}}_{\mathcal{A}_3}$.

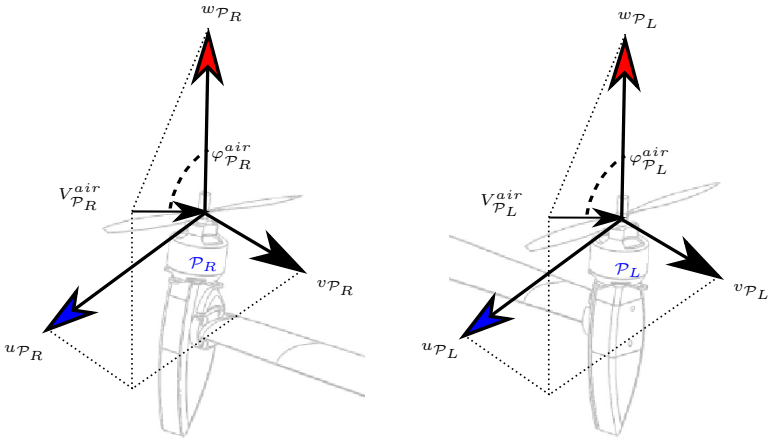

Figure 7.3: Angle of attack, $\varphi^{air}_{\mathcal{P}_R}$, $\varphi^{air}_{\mathcal{P}_L}$, and magnitude of the relative wind speed, $V^{air}_{\mathcal{P}_R}$, $V^{air}_{\mathcal{P}_L}$, actuating on the right and left propellers.

The thrusts and torques generated by the propellers are computed by (Ortega et al., 2021)

$$f_{\mathcal{P}_R} = \rho d^4 n^2_{\mathcal{P}_R} c_t \left(J_{\mathcal{P}_R}, \varphi^{air}_{\mathcal{P}_R}\right), \tag{7.25}$$

$$t_{\mathcal{P}_R} = \lambda_{\mathcal{P}_R} \rho d^5 n^2_{\mathcal{P}_R} c_q \left(J_{\mathcal{P}_R}, \varphi^{air}_{\mathcal{P}_R}\right), \tag{7.26}$$

$$f_{\mathcal{P}_L} = \rho d^4 n^2_{\mathcal{P}_L} c_t \left(J_{\mathcal{P}_L}, \varphi^{air}_{\mathcal{P}_L}\right), \tag{7.27}$$

$$t_{\mathcal{P}_L} = \lambda_{\mathcal{P}_L} \rho d^5 n^2_{\mathcal{P}_L} c_q \left(J_{\mathcal{P}_L}, \varphi^{air}_{\mathcal{P}_L}\right), \tag{7.28}$$

where $\rho \in \mathbb{R}_{\geq 0}$ is the air density, $d \in \mathbb{R}_{\geq 0}$ is the diameter of the propeller, and $\lambda_{\mathcal{P}_R}, \lambda_{\mathcal{P}_L} \in \{1, -1\}$ are given according to the direction of rotation of the corresponding propeller: if clockwise, -1, if counter-clockwise, 1. In order to cancel the gyroscope effect generated by the propellers, it is considered $\lambda_R = 1$, and $\lambda_L = -1$. In addition, $c_t, c_q : (\mathbb{R}_{\geq 0} \times \mathbb{R}_{\geq 0}) \to \mathbb{R}$ are estimated thrust and torque coefficients. These are functions of $J_{\mathcal{P}}(V^{air}_{\mathcal{P}}, n_{\mathcal{P}}) = \dfrac{V^{air}_{\mathcal{P}}}{d\ n_{\mathcal{P}}}$, in which $V^{air}_{\mathcal{P}}$ is the magnitude of the relative wind speed actuating on the propeller $\mathcal{P}$, and $\varphi^{air}_{\mathcal{P}}$ is the angle of attack of the propeller $\mathcal{P}$, for $\mathcal{P} \in \{\mathcal{P}_R, \mathcal{P}_L\}$, as illustrated in Figure 7.3.

Remark 43. *For control purposes, the dynamics of the rotors are neglected. The thrusts and torques applied by the propellers* (7.25)-(7.28) *are computed assuming the rotors in steady-state.*

The magnitude of the relative wind speed actuating on the propeller $\mathcal{P}$ is computed as

$$V_{\mathcal{P}}^{air} = \sqrt{u_{\mathcal{P}}^2 + v_{\mathcal{P}}^2 + w_{\mathcal{P}}^2}, \tag{7.29}$$

and the angle of attack is given by

$$\varphi_{\mathcal{P}}^{air} = \operatorname{acos}\left(\frac{w_{\mathcal{P}}}{V_{\mathcal{P}}^{air}}\right), \tag{7.30}$$

where

$$\begin{bmatrix} u_{\mathcal{P}} \\ v_{\mathcal{P}} \\ w_{\mathcal{P}} \end{bmatrix} = \left(\boldsymbol{R}_{\mathcal{P}}^{\mathcal{I}}\right)' \left(\dot{\boldsymbol{p}}_{\mathcal{I},\mathcal{P}}^{\mathcal{I}} - \boldsymbol{\zeta}\right), \tag{7.31}$$

with $\dot{\boldsymbol{p}}_{\mathcal{I},\mathcal{P}}^{\mathcal{I}} = \boldsymbol{J}_{\mathcal{P}}(\boldsymbol{q})\dot{\boldsymbol{q}}$, $\boldsymbol{R}_{\mathcal{P}_R}^{\mathcal{I}} \triangleq \boldsymbol{R}_{\mathcal{C}_2}^{\mathcal{I}}$, and $\boldsymbol{R}_{\mathcal{P}_L}^{\mathcal{I}} \triangleq \boldsymbol{R}_{\mathcal{C}_3}^{\mathcal{I}}$.

Thus, regarding the mappings (3.41) and (3.43), the terms in the vector of generalized forces (7.18) related to the propellers are computed as follows

$$\boldsymbol{\vartheta}_{\mathcal{P}} = \overbrace{\boldsymbol{J}_{\mathcal{P}_R}' \boldsymbol{R}_{\mathcal{P}_R}^{\mathcal{I}} \begin{bmatrix} 0 \\ f_{\mathcal{P}_R} \end{bmatrix}}^{\text{right prop. force}} + \overbrace{\boldsymbol{W}_{\mathcal{P}_R}' \boldsymbol{R}_{\mathcal{P}_R}^{\mathcal{I}} \begin{bmatrix} 0 \\ \lambda_{\mathcal{P}_R} t_{\mathcal{P}_R} \end{bmatrix}}^{\text{right prop. drag torque}} + \overbrace{\boldsymbol{J}_{\mathcal{P}_L}' \boldsymbol{R}_{\mathcal{P}_L}^{\mathcal{I}} \begin{bmatrix} 0 \\ f_{\mathcal{P}_L} \end{bmatrix}}^{\text{left prop. force}} + \overbrace{\boldsymbol{W}_{\mathcal{P}_L}' \boldsymbol{R}_{\mathcal{P}_L}^{\mathcal{I}} \begin{bmatrix} 0 \\ \lambda_{\mathcal{P}_L} t_{\mathcal{P}_L} \end{bmatrix}}^{\text{left prop. drag torque}}. \tag{7.32}$$

Servomotors

The vector of generalized forces generated by the servomotors are computed through the law of action and reaction, and is given by

$$\boldsymbol{\vartheta}_s = \overbrace{\boldsymbol{W}_{\mathcal{C}_2}' \boldsymbol{R}_{\mathcal{C}_2}^{\mathcal{I}} \begin{bmatrix} 0 \\ \tau_{s_R} \\ 0 \end{bmatrix}}^{\text{Right serv. action}} - \overbrace{\boldsymbol{W}_{\mathcal{C}_1}' \boldsymbol{R}_{\mathcal{C}_2}^{\mathcal{I}} \begin{bmatrix} 0 \\ \tau_{s_R} \\ 0 \end{bmatrix}}^{\text{Body's reaction}} + \overbrace{\boldsymbol{W}_{\mathcal{C}_3}' \boldsymbol{R}_{\mathcal{C}_3}^{\mathcal{I}} \begin{bmatrix} 0 \\ \tau_{s_L} \\ 0 \end{bmatrix}}^{\text{Left serv. action}} - \overbrace{\boldsymbol{W}_{\mathcal{C}_1}' \boldsymbol{R}_{\mathcal{C}_3}^{\mathcal{I}} \begin{bmatrix} 0 \\ \tau_{s_L} \\ 0 \end{bmatrix}}^{\text{Body's reaction}} - \overbrace{\begin{bmatrix} \nu \boldsymbol{I} & \boldsymbol{0} \\ \boldsymbol{0} & \boldsymbol{0} \end{bmatrix}}^{\text{Friction}} \dot{\boldsymbol{q}}, \tag{7.33}$$

where the last term concerns the friction, in which $\nu \in \mathbb{R}_{\geq 0}$ is the coefficient of viscosity of the servomotors.

Fuselage, wings, and tail-surfaces

In order to compute the vectors of generalized forces generated by the fuselage, wings, the tail-surfaces, the Tilt-rotor UAV is split into five aerodynamic surfaces and five frames are rigidly attached to the system, one at each aerodynamic center. These are given by $\mathcal{S} \in \{\mathcal{F},\ \mathcal{W}_R,\ \mathcal{W}_L,\ \mathcal{T}_R,\ \mathcal{T}_L\}$, in which $\mathcal{F}$ denotes the fuselage, $\mathcal{W}_R$ and $\mathcal{W}_L$ the right and left wings, and $\mathcal{T}_R$ and $\mathcal{T}_L$ the right and left tail-surfaces.

Accordingly, the position of the aerodynamic center $\mathcal{S}$ with respect to $\mathcal{I}$ is computed as

$$\boldsymbol{p}_{\mathcal{I},\mathcal{S}}^{\mathcal{I}} = \boldsymbol{R}_{\mathcal{B}}^{\mathcal{I}} \boldsymbol{d}_{\mathcal{B},\mathcal{S}}^{\mathcal{B}} + \boldsymbol{\xi}, \tag{7.34}$$

where $\boldsymbol{d}_{\mathcal{B},\mathcal{S}}^{\mathcal{B}} \in \mathbb{R}^3$ is the position of the aerodynamic center $\mathcal{S}$ with respect to $\mathcal{B}$, expressed in $\mathcal{B}$.

The velocity of the aerodynamic center $\mathcal{S}$ is computed as the time derivative of its position (7.34), as follows

$$\begin{aligned} \boldsymbol{v}_{\mathcal{I},\mathcal{S}}^{\mathcal{I}} = \dot{\boldsymbol{p}}_{\mathcal{I},\mathcal{S}}^{\mathcal{I}} &= \boldsymbol{R}_{\mathcal{B}}^{\mathcal{I}} \boldsymbol{S}(\boldsymbol{w}_{\mathcal{I},\mathcal{B}}^{\mathcal{B}}) \boldsymbol{d}_{\mathcal{B},\mathcal{S}}^{\mathcal{B}} + \dot{\boldsymbol{\xi}} = -\boldsymbol{R}_{\mathcal{B}}^{\mathcal{I}} \boldsymbol{S}(\boldsymbol{d}_{\mathcal{B},\mathcal{S}}^{\mathcal{B}}) \boldsymbol{W}_{\eta} \dot{\boldsymbol{\eta}} + \dot{\boldsymbol{\xi}} \\ &= \begin{bmatrix} \boldsymbol{0} & \boldsymbol{0} & -\boldsymbol{R}_{\mathcal{B}}^{\mathcal{I}} \boldsymbol{S}(\boldsymbol{d}_{\mathcal{B},\mathcal{S}}^{\mathcal{B}}) \boldsymbol{W}_{\eta} & \boldsymbol{I} \end{bmatrix} \dot{\boldsymbol{q}} = \boldsymbol{J}_{\mathcal{S}} \dot{\boldsymbol{q}}, \end{aligned} \tag{7.35}$$

where $\boldsymbol{J}_{\mathcal{S}}(\boldsymbol{q}) : \mathbb{R}^8 \to \mathbb{R}^{3\times 8}$ is the linear velocity Jacobian of the aerodynamic center $\mathcal{S}$. The angular velocity of the aerodynamic center $\mathcal{S}$ with respect to $\mathcal{I}$ is given by

$$\begin{aligned} \boldsymbol{w}_{\mathcal{I},\mathcal{S}}^{\mathcal{I}} &= \boldsymbol{R}_{\mathcal{B}}^{\mathcal{I}} \boldsymbol{w}_{\mathcal{I},\mathcal{S}}^{\mathcal{S}} = \boldsymbol{R}_{\mathcal{B}}^{\mathcal{I}} \boldsymbol{W}_{\eta} \dot{\boldsymbol{\eta}}, \\ &= \begin{bmatrix} \boldsymbol{0} & \boldsymbol{0} & \boldsymbol{R}_{\mathcal{B}}^{\mathcal{I}} \boldsymbol{W}_{\eta} & \boldsymbol{0} \end{bmatrix} \dot{\boldsymbol{q}} = \boldsymbol{W}_{\mathcal{S}}(\boldsymbol{q}) \dot{\boldsymbol{q}}, \end{aligned} \tag{7.36}$$

where $\boldsymbol{W}_{\mathcal{S}}(\boldsymbol{q}) : \mathbb{R}^8 \to \mathbb{R}^{3\times 8}$ is the angular velocity Jacobian.

Assumption 18. *The positions of aerodynamic centers remain constant with respect to $\mathcal{B}$ during the flight.*

In addition, before computing the aerodynamic forces and torques, the magnitude and orientation of the relative wind speed must be computed for every aerodynamic surface. Similarly to (7.31), the relative wind speed vector actuating on the aerodynamic center $\mathcal{S}$ is given by

$$\begin{bmatrix} u_{\mathcal{S}} \\ v_{\mathcal{S}} \\ w_{\mathcal{S}} \end{bmatrix} = \left(\boldsymbol{R}_{\mathcal{S}}^{\mathcal{I}}\right)' \left(\dot{\boldsymbol{p}}_{\mathcal{I},\mathcal{S}}^{\mathcal{I}} - \boldsymbol{\zeta}\right), \tag{7.37}$$

where the rotation matrices $\boldsymbol{R}_{\mathcal{F}}^{\mathcal{I}}$, $\boldsymbol{R}_{\mathcal{W}_R}^{\mathcal{I}}$, $\boldsymbol{R}_{\mathcal{W}_L}^{\mathcal{I}}$, $\boldsymbol{R}_{\mathcal{T}_R}^{\mathcal{I}}$, $\boldsymbol{R}_{\mathcal{T}_L}^{\mathcal{I}} \in \mathrm{SO}(3)$ are given according to the orientation of each aerodynamic center frame[4]. In the particular case in which these frames are oriented according to the aerodynamic surface, these matrices are given by $\boldsymbol{R}_{\mathcal{F}}^{\mathcal{I}} \triangleq \boldsymbol{R}_{\mathcal{B}}^{\mathcal{I}}$, $\boldsymbol{R}_{\mathcal{W}_R}^{\mathcal{I}} \triangleq \boldsymbol{R}_{\mathcal{B}}^{\mathcal{I}} \boldsymbol{R}_{x,-\epsilon}$, $\boldsymbol{R}_{\mathcal{W}_L}^{\mathcal{I}} \triangleq \boldsymbol{R}_{\mathcal{B}}^{\mathcal{I}} \boldsymbol{R}_{x,\epsilon}$, $\boldsymbol{R}_{\mathcal{T}_R}^{\mathcal{I}} \triangleq \boldsymbol{R}_{\mathcal{B}}^{\mathcal{I}} \boldsymbol{R}_{x,-\mu}$, and $\boldsymbol{R}_{\mathcal{T}_L}^{\mathcal{I}} \triangleq \boldsymbol{R}_{\mathcal{B}}^{\mathcal{I}} \boldsymbol{R}_{x,\mu}$, where $\epsilon, \mu \in \mathbb{R}$ are the dihedral angles of the wings and tail-surfaces, respectively, with respect to the aircraft reference frame $\mathcal{B}$.

[4]The frame of the aerodynamic center must be oriented taking into account the wind tunnel experiments, and are related to the aerodynamic coefficients.

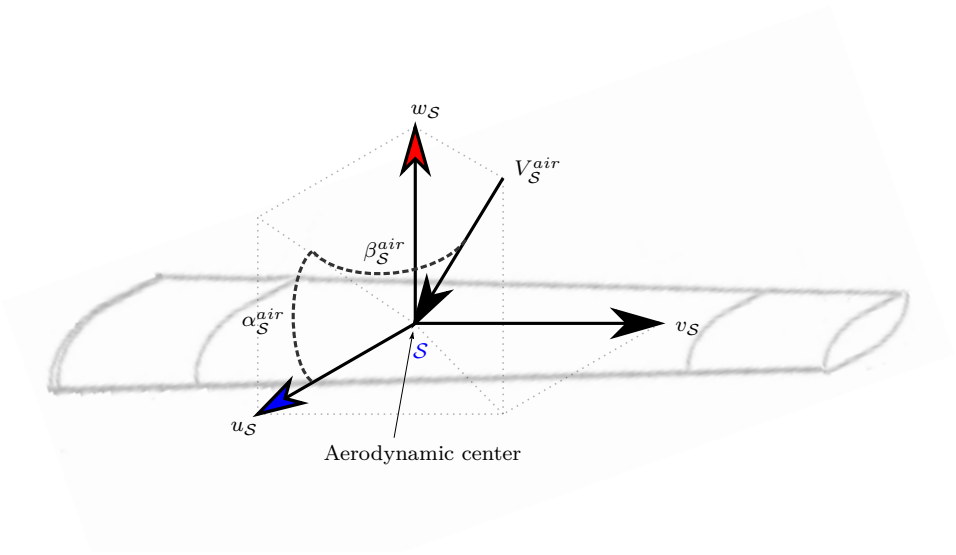

Figure 7.4: Illustration of the relative wind speed vector and its orientation for a generic aerodynamic surface.

From (7.37), the magnitude of the relative wind speed actuating at the aerodynamic center $\mathcal{S}$ is given by

$$V_{\mathcal{S}}^{air} = \sqrt{w_{\mathcal{S}}^2 + v_{\mathcal{S}}^2 + u_{\mathcal{S}}^2}. \tag{7.38}$$

In addition, the orientation of the relative wind speed actuating at the aerodynamic centers $\mathcal{S}$ is given by the angle of attack and the side-slip angle, which are compute, respectively, by[5]

$$\alpha_{\mathcal{S}}^{air} = \text{atan}\Big(\frac{w_{\mathcal{S}}}{u_{\mathcal{S}}}\Big), \tag{7.39}$$

$$\beta_{\mathcal{S}}^{air} = \text{asin}\Big(\frac{v_{\mathcal{S}}}{V_{\mathcal{S}}}\Big). \tag{7.40}$$

The relative wind speed vector, angle of attack, and side-slip angle are illustrated in Figure 7.4.

Taking into account the expressions (7.34)-(7.40), the aerodynamic forces and moments generated by each surface $\mathcal{S}$ are then computed as

$$f_{\mathcal{S}}^{d} = -\kappa_{\mathcal{S}}^{air}\ s_{\mathcal{S}}\ c_{\mathcal{S}}^{d}, \tag{7.41}$$

$$f_{\mathcal{S}}^{y} = \ \ \kappa_{\mathcal{S}}^{air}\ s_{\mathcal{S}}\ c_{\mathcal{S}}^{y}, \tag{7.42}$$

$$f_{\mathcal{S}}^{l} = \ \ \kappa_{\mathcal{S}}^{air}\ s_{\mathcal{S}}\ c_{\mathcal{S}}^{l}, \tag{7.43}$$

$$L_{\mathcal{S}} = \ \ \kappa_{\mathcal{S}}^{air}\ s_{\mathcal{S}}\ c_{\mathcal{S}}^{L}, \tag{7.44}$$

$$M_{\mathcal{S}} = \ \ \kappa_{\mathcal{S}}^{air}\ s_{\mathcal{S}}\ c_{\mathcal{S}}^{M}, \tag{7.45}$$

[5]In this work, the angle of attack and side-slip angle do not follow the North-East-Down (NED) aerodynamic convention.

$$N_{\mathcal{S}} = \quad \kappa_{\mathcal{S}}^{air} \; s_{\mathcal{S}} \; c_{\mathcal{S}}^{N}, \tag{7.46}$$

where $\kappa_{\mathcal{S}}^{air} = \frac{1}{2}\rho\,(V_{\mathcal{S}}^{air})^2$, $f_{\mathcal{S}}^{d}$ is the drag force, $f_{\mathcal{S}}^{y}$ is the side force, $f_{\mathcal{S}}^{l}$ is the lift force, $L_{\mathcal{S}}$ is the rolling moment, $M_{\mathcal{S}}$ is the pitching moment, and $N_{\mathcal{S}}$ is the yawing moment. In addition, $c_{\mathcal{S}}^{d}, c_{\mathcal{S}}^{y}, c_{\mathcal{S}}^{l}, c_{\mathcal{S}}^{L}, c_{\mathcal{S}}^{M}, c_{\mathcal{S}}^{N}$ are estimated aerodynamic coefficients of the surface $\mathcal{S}$. These are functions of the angle of attack, side-slip angle, and may also be function of the deflection of the aerodynamic control surfaces, depending on the considered surface. In addition, these coefficients are assumed adimensionalized with respect to the surface area $s_{\mathcal{S}} \in \mathbb{R}$. The aerodynamic coefficients of the fuselage, wings, and tail-surfaces are presented in Appendix B. Figure 7.5 illustrates the aerodynamic forces and moments actuating on a generic aerodynamic surface $\mathcal{S}$.

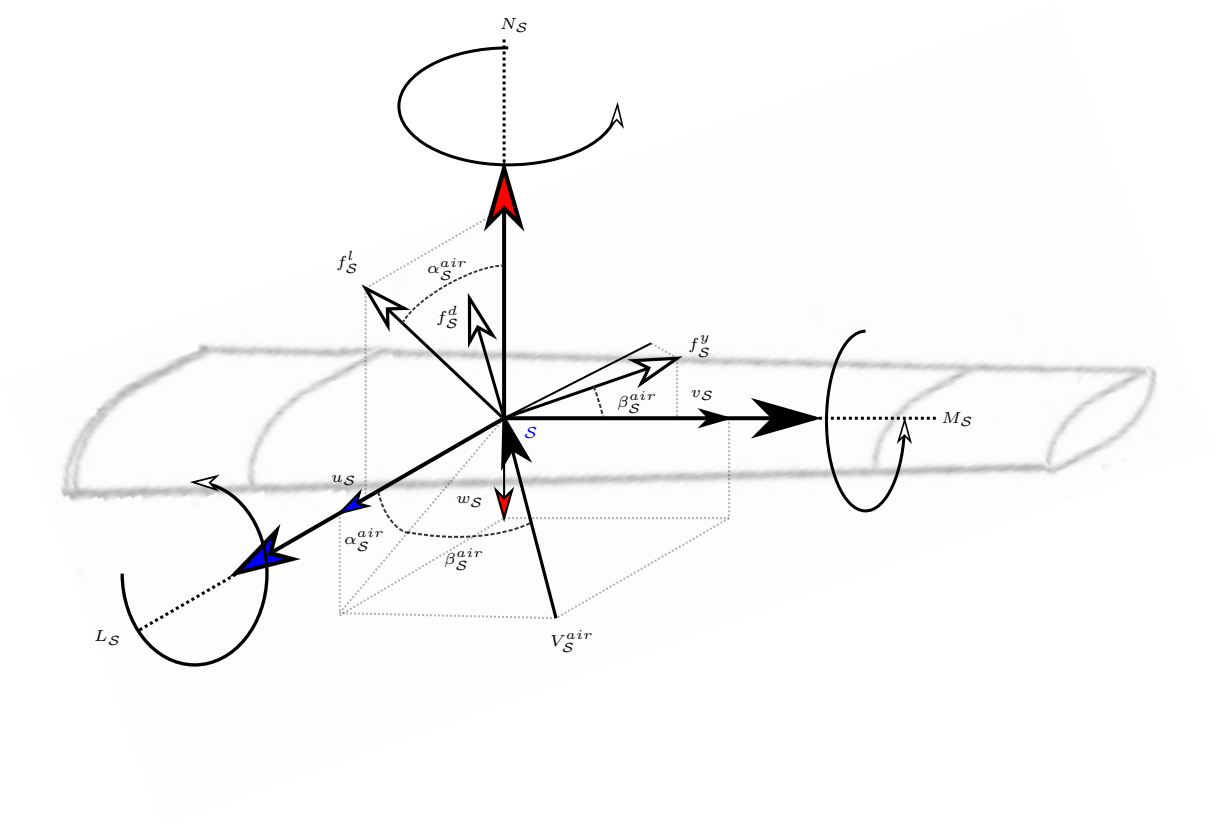

Figure 7.5: Forces and moments actuating on a generic aerodynamic surface due to the relative wind speed. The drag force is parallel with the relative wind speed vector, the lift and the side forces are oriented according to the angle of attack and side-slip angle, respectively.

Concerning the mappings (3.41) and (3.43), and (7.41)-(7.46), the vector of generalized forces generated by the aerodynamic forces and moments due to the fuselage, wings, and

tail surfaces, are computed as follows

$$\boldsymbol{\vartheta}_{\mathcal{F}} = \boldsymbol{J}'_{\mathcal{F}}\boldsymbol{R}^{\mathcal{I}}_{\mathcal{F}}\left(\boldsymbol{R}^{\mathcal{F}}_{\mathcal{W}_{\mathcal{F}}}\begin{bmatrix} f^d_{\mathcal{F}} \\ f^y_{\mathcal{F}} \\ f^l_{\mathcal{F}} \end{bmatrix}\right) + \boldsymbol{W}'_{\mathcal{F}}\boldsymbol{R}^{\mathcal{I}}_{\mathcal{F}}\begin{bmatrix} L_{\mathcal{F}} \\ M_{\mathcal{F}} \\ N_{\mathcal{F}} \end{bmatrix}, \tag{7.47}$$

$$\begin{aligned}\boldsymbol{\vartheta}_{\mathcal{W}} = {} & \boldsymbol{J}'_{\mathcal{W}_R}\boldsymbol{R}^{\mathcal{I}}_{\mathcal{W}_R}\left(\boldsymbol{R}^{\mathcal{W}_R}_{\mathcal{W}_{\mathcal{W}_R}}\begin{bmatrix} f^d_{\mathcal{W}_R} \\ f^y_{\mathcal{W}_R} \\ f^l_{\mathcal{W}_R} \end{bmatrix}\right) + \boldsymbol{W}'_{\mathcal{W}_R}\boldsymbol{R}^{\mathcal{I}}_{\mathcal{W}_R}\begin{bmatrix} L_{\mathcal{W}_R} \\ M_{\mathcal{W}_R} \\ N_{\mathcal{W}_R} \end{bmatrix} \\ & + \boldsymbol{J}'_{\mathcal{W}_L}\boldsymbol{R}^{\mathcal{I}}_{\mathcal{W}_L}\left(\boldsymbol{R}^{\mathcal{W}_L}_{\mathcal{W}_{\mathcal{W}_L}}\begin{bmatrix} f^d_{\mathcal{W}_L} \\ f^y_{\mathcal{W}_L} \\ f^l_{\mathcal{W}_L} \end{bmatrix}\right) + \boldsymbol{W}'_{\mathcal{W}_L}\boldsymbol{R}^{\mathcal{I}}_{\mathcal{W}_L}\begin{bmatrix} L_{\mathcal{W}_L} \\ M_{\mathcal{W}_L} \\ N_{\mathcal{W}_L} \end{bmatrix},\end{aligned} \tag{7.48}$$

$$\begin{aligned}\boldsymbol{\vartheta}_{\mathcal{T}} = {} & \boldsymbol{J}'_{\mathcal{T}_R}\boldsymbol{R}^{\mathcal{I}}_{\mathcal{T}_R}\left(\boldsymbol{R}^{\mathcal{T}_R}_{\mathcal{W}_{\mathcal{T}_R}}\begin{bmatrix} f^d_{\mathcal{T}_R} \\ f^y_{\mathcal{T}_R} \\ f^l_{\mathcal{T}_R} \end{bmatrix}\right) + \boldsymbol{W}'_{\mathcal{T}_R}\boldsymbol{R}^{\mathcal{I}}_{\mathcal{T}_R}\begin{bmatrix} L_{\mathcal{T}_R} \\ M_{\mathcal{T}_R} \\ N_{\mathcal{T}_R} \end{bmatrix} \\ & + \boldsymbol{J}'_{\mathcal{T}_L}\boldsymbol{R}^{\mathcal{I}}_{\mathcal{T}_L}\left(\boldsymbol{R}^{\mathcal{T}_L}_{\mathcal{W}_{\mathcal{T}_L}}\begin{bmatrix} f^d_{\mathcal{T}_L} \\ f^y_{\mathcal{T}_L} \\ f^l_{\mathcal{T}_L} \end{bmatrix}\right) + \boldsymbol{W}'_{\mathcal{T}_L}\boldsymbol{R}^{\mathcal{I}}_{\mathcal{T}_L}\begin{bmatrix} L_{\mathcal{T}_L} \\ M_{\mathcal{T}_L} \\ N_{\mathcal{T}_L} \end{bmatrix},\end{aligned} \tag{7.49}$$

where the rotation matrix $\boldsymbol{R}^{\mathcal{S}}_{\mathcal{W}_{\mathcal{S}}} \triangleq \boldsymbol{R}_{y,-\alpha^{air}_{\mathcal{S}}}\boldsymbol{R}_{z,-\beta^{air}_{\mathcal{S}}}$ is used to express the lift, drag, and side forces from the wind orientation to the aerodynamic center frame. Also, the linear and angular velocity Jacobians $\boldsymbol{J}_{\mathcal{S}}$ and $\boldsymbol{W}_{\mathcal{S}}$ are computed according to (7.35) and (7.36).

It is noteworthy that the forces and moments generated by the aerodynamic surfaces (7.41)-(7.46) are dependent on the dynamic pressure $\kappa^{air}_{\mathcal{S}}$, which increases with the square of the magnitude of the relative wind speed. When performing VTOL and hovering, the magnitude of the relative wind speed is very small. Consequently, the thrusters' groups must provide the moments and forces necessary to perform the flight maneuvers. On the other side, during the transition and while performing cruise flight, the aircraft can take advantage of the lift generated by the wings, and the roll, pitch, and yaw moments generated by the aerodynamic control surfaces. These forces and moments, added to the ones generated by the propulsion system, allow the Tilt-rotor UAV to tilt the rotors towards the horizontal position and convert to the airplane mode.

Aerodynamic interference

The vectors of generalized forces (7.47)-(7.49) take into account forces and moments generated by each aerodynamic surface individually and disregard the coupling effects between these surfaces, as well as the wind interference generated by one surface on the others. On one hand, these interferences can be assumed as external disturbances, which must be compensated by the controller. On the other hand, the vector of generalized

forces generated by aerodynamic interferences can be modeled and considered into the vector of generalized forces. In the latter case, this vector can be computed as

$$\boldsymbol{\vartheta}_I = \boldsymbol{J}_I' \boldsymbol{R}_I^{\mathcal{I}} \left(\boldsymbol{R}_{\mathcal{W}_{\mathcal{I}}}^{I} \begin{bmatrix} f_I^d \\ f_I^y \\ f_I^l \end{bmatrix} \right) + \boldsymbol{W}_I' \boldsymbol{R}_I^{\mathcal{I}} \begin{bmatrix} L_I \\ M_I \\ N_I \end{bmatrix}, \tag{7.50}$$

with

$$f_I^d = -\kappa_I^{air}\ s_I\ c_I^d, \tag{7.51}$$
$$f_I^y = \ \ \kappa_I^{air}\ s_I\ c_I^y, \tag{7.52}$$
$$f_I^l = \ \ \kappa_I^{air}\ s_I\ c_I^l, \tag{7.53}$$
$$L_I = \ \ \kappa_I^{air}\ s_I\ c_I^L, \tag{7.54}$$
$$M_I = \ \ \kappa_I^{air}\ s_I\ c_I^M, \tag{7.55}$$
$$N_I = \ \ \kappa_I^{air}\ s_I\ c_I^N, \tag{7.56}$$

where $c_I^d, c_I^y, c_I^l, c_I^L, c_I^M, c_I^N$ are aerodynamic coefficients of the interference, adimensionalized with respect to the surface area $s_I \in \mathbb{R}$. These coefficients may be estimated via wind-tunnel experiments or in flight and, then, can complement the aerodynamic model.

The forces and moments generated by the aerodynamic interference can be assumed applied at the center of gravity of the aircraft. In this case, the magnitude and orientation of the relative wind speed for the aerodynamic interference is computed through (7.37), (7.38), (7.39) and (7.40), considering $\mathcal{S} = \mathcal{C}_1$ and $\boldsymbol{R}_I^{\mathcal{I}} = \boldsymbol{R}_{\mathcal{C}_1}^{\mathcal{I}}$.

Remark 44. *The modeling presented in this work is general enough for Tilt-rotor UAVs. Any forces and moments resulting from additional effects can be considered in the model by adding their contributions to the generalized forces vector* (7.18).

7.2.4 The ProVANT Simulator

The Tilt-rotor UAV used to perform the numerical experiments in this chapter is the ProVANT-Emergentia Tilt-rotor UAV (see Figure 7.6). This aircraft is currently being built in the ProVANT Emergentia research project, whose goal is developing Tilt-rotor UAVs for load transportation and search-and-rescue missions with rapid deployment, which is available on the ProVANT Simulator[6]. The ProVANT Simulator is a software developed at Federal University of Minas Gerais (UFMG) and released under the MIT open-source license (Lara et al., 2019, 2017). This software was created with the primary goal of providing high-fidelity simulations with visual feedback of control strategies designed for UAVs.

[6] https://github.com/Guiraffo/ProVANT-Simulator

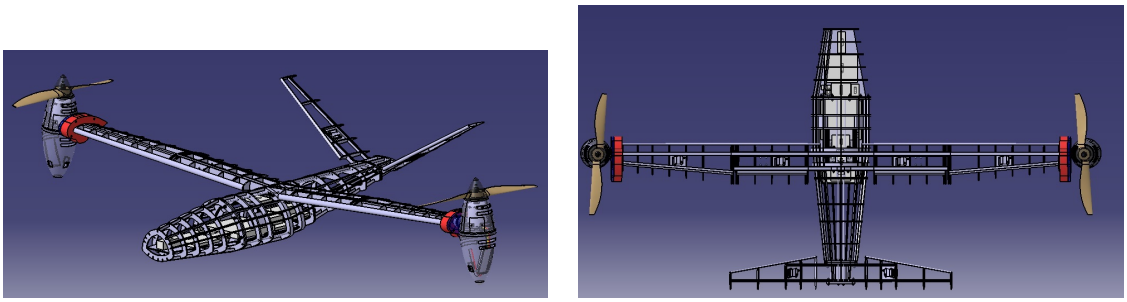

Figure 7.6: The ProVANT-Emergentia Tilt-rotor UAV mechanical structure.

The mechanical design of the ProVANT-Emergentia Tilt-rotor UAV was developed in the Computer-Aided Three-Dimensional Interactive Application (CATIA) software and exported to the ProVANT simulator, which was developed using ROS (Quigley et al., 2009) and Gazebo (Koenig and Howard, 2004) platforms. The simulator has a set of plugins that provide the states of the system for the controller and receive the control input signals. A schematic of the simulator is presented in Figure 7.7.

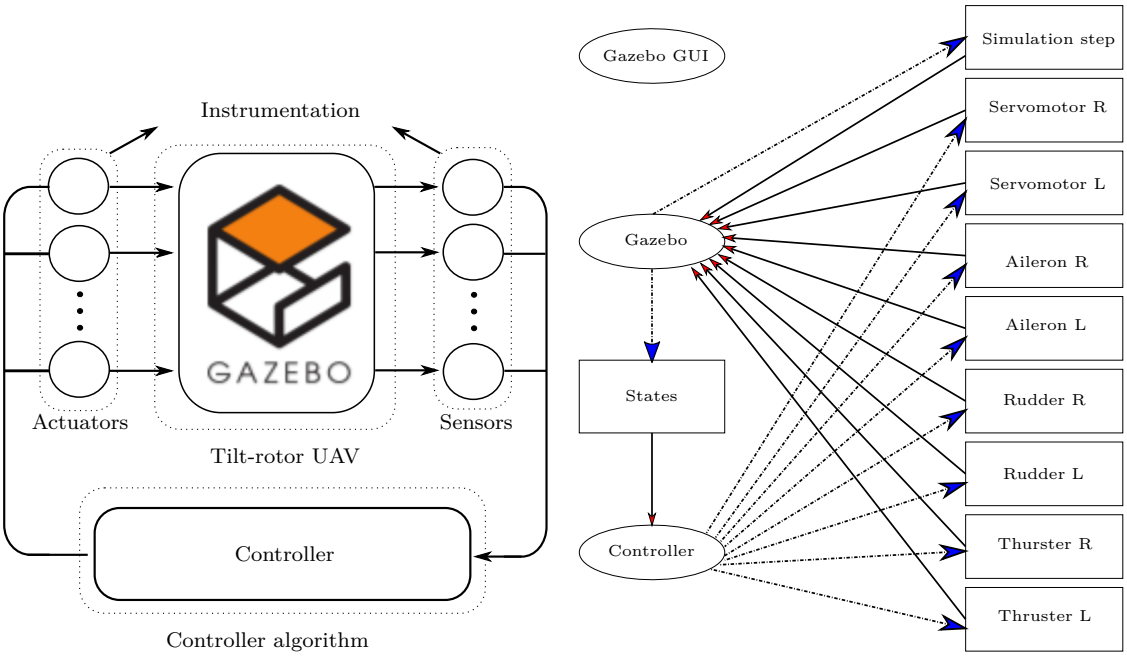

(a) Information flow in the ProVANT Simulator.

(b) Communication between the simulation elements.

Figure 7.7: Schematic of the ProVANT Simulator.

As Gazebo platform does not allow electronic circuit and fluid simulation, the electrical dynamics of the brushless motors are neglected, the thrust and torques applied by the propellers are computed through (7.25)-(7.28), and the aerodynamic forces and moments generated by the fuselage, wings, tail-surfaces, and aerodynamic interference, are computed through (7.41)-(7.46) and (7.51)-(7.56).

The nonlinear aerodynamic coefficients used to compute the forces and moments generated by the propellers, fuselage, wings, and tail-surfaces, were obtained via wind tunnel experiments and are presented in Appendix B.

7.3 Robust control design for the Tilt-rotor UAV

This section proposes robust controllers for the ProVANT-Emergentia Tilt-rotor UAV.

Initially, the state-feedback and output feedback linear $\mathcal{W}_\infty$ controllers addressed in Chapter 6 are synthesized for the Tilt-rotor UAV, in order to achieve trajectory tracking in the helicopter-flight mode. These controllers are synthesized by assuming the environment wind as disturbance, and the Von Kàrmàn wind turbulence model is used as disturbance model. A comparative analysis of the controllers are presented.

In addition, a nonlinear $\mathcal{W}_\infty$ controller is also proposed to solve the full flight envelope trajectory tracking problem of the Tilt-rotor UAV. To design this controller, the nonlinear $\mathcal{W}_\infty$ control approach addressed in Section 5.2 is extended to the case in which the vector of generalized coordinates is divided into controlled, regulated, and stabilized degrees of freedom. Besides, a control allocation scheme is proposed to map the optimal control law to the appropriated control inputs signals according to the magnitude of the relative wind speed.

7.3.1 Linear $\mathcal{W}_\infty$ control design for helicopter-flight mode

This section verifies the efficacy of the full-state and dynamic output feedback linear $\mathcal{W}_\infty$ controllers proposed in Chapter 6 in the case study of Tilt-rotor UAV.

In order to design the linear $\mathcal{W}_\infty$ controllers, the nonlinear dynamic equations (7.14) are linearized around the generic trajectory $x_r(t)$, $y_r(t)$, $z_r(t)$, which results in the following trimming point of system (7.14), $\boldsymbol{q}_r = [-0.137 \;\; -0.137 \;\; 0 \; 0.137 \; 0 \; x_r(t) \;\; y_r(t) \; z_r(t)]'$, $\dot{\boldsymbol{q}}_r = \mathbf{0}$, and $\boldsymbol{\tau}_r = [51.9 \; 51.9 \; -0.127 \; -0.127 \; 0 \; 0 \;\; 0 \; 0]$, assuming $\boldsymbol{\zeta}_r = \mathbf{0}$. The linearized state-space model is given by

$$\Delta\dot{\boldsymbol{x}}(t) = \boldsymbol{A}\Delta\boldsymbol{x}(t) + \boldsymbol{B}\Delta\boldsymbol{u}(t) + \boldsymbol{D}\Delta\boldsymbol{\zeta}(t), \tag{7.57}$$

where $\Delta\boldsymbol{x} = [\Delta\boldsymbol{q}'(t) \;\; \Delta\dot{\boldsymbol{q}}'(t) \;\; \int_0^t \Delta\psi(\tau)d\tau \;\; \int_0^t \Delta x(\tau)d\tau \;\; \int_0^t \Delta y(\tau)d\tau \;\; \int_0^t \Delta z(\tau)d\tau]'$, in which $\Delta(\cdot) \triangleq (\cdot) - (\cdot)_r$. The linear $\mathcal{W}_\infty$ controllers are designed to handle with the Tilt-rotor UAV operating in the helicopter-flight mode. Therefore, due to the low magnitude of the relative wind speed in this flight mode, the deflection of the aerodynamic control surfaces are assumed as fixed and removed from the control input vector, yielding $\Delta\boldsymbol{u}(t) = [\Delta n_{\mathcal{P}_R} \;\; \Delta n_{\mathcal{P}_L} \;\; \Delta\tau_{s_R} \;\; \Delta\tau_{s_L}]'$.

In this section, the environment wind is simulated through the von Kàrmàn wind turbulence model (Tatom et al., 1982). In this turbulence model, the linear velocities

of the wind gusts are characterized by power spectral densities, that are implemented through the following transfer functions:

$$\frac{\zeta_x(s)}{v_1(s)} = \frac{\sigma_u\sqrt{\frac{2L_u}{\pi V}}\left(1+0.25\frac{L_u}{V}s\right)}{1+1.357\frac{L_u}{V}s+0.1987\left(\frac{L_u}{V}s\right)^2} \tag{7.58}$$

$$\frac{\zeta_y(s)}{v_2(s)} = \frac{\sigma_v\sqrt{\frac{2L_v}{\pi V}}\left(1+2.7478\frac{2L_v}{V}s+0.3398\left(\frac{2L_v}{V}s\right)^2\right)}{1+2.9958\frac{2L_v}{V}s+1.9754\left(\frac{2L_v}{V}s\right)^2+0.1539\left(\frac{2L_v}{V}s\right)^3} \tag{7.59}$$

$$\frac{\zeta_z(s)}{v_3(s)} = \frac{\sigma_w\sqrt{\frac{2L_w}{\pi V}}\left(1+2.7478\frac{2L_w}{V}s+0.3398\left(\frac{2L_w}{V}s\right)^2\right)}{1+2.9958\frac{2L_w}{V}s+1.9754\left(\frac{2L_w}{V}s\right)^2+0.1539\left(\frac{2L_w}{V}s\right)^3} \tag{7.60}$$

in which $v_1(s)$, $v_2(s)$, and $v_3(s)$ are white Gaussian noise signals with zero mean, unitary variance, and the sampling time 0.01 seconds. In addition, $\sigma_u = 1$, $\sigma_v = 5$, and $\sigma_w = 3$ are the turbulence intensity, $L_u, L_v, L_w = 20$ are the scale length, and $V = 5.1$ is the speed with which the vehicle is moving through the gust field.

For the sake of control design, the linear system (7.57) is represented in the standard forms (6.1) and (6.11), and the controllers addressed in Sections 6.1 and 6.2, are synthesized for this system by solving the convex optimization problems with LMI constraints (6.7) and (6.22), respectively. The output feedback controller is designed over the assumption that the Tilt-rotor UAV velocities $\dot{\boldsymbol{x}}$ and $\dot{\boldsymbol{y}}$ are not measured, which results in the output vector $\boldsymbol{y}(t) = [\Delta\boldsymbol{q}'(t) \;\; \Delta\dot{\alpha}_R(t) \;\; \Delta\dot{\alpha}_L(t) \;\; \Delta\dot{\phi}(t) \;\; \Delta\dot{\theta}(t) \;\; \Delta\dot{\psi}(t) \;\; \Delta\dot{z}(t) \;\; \int_0^t \Delta x(\tau)d\tau \;\; \int_0^t \Delta y(\tau)d\tau \;\; \int_0^t \Delta z(\tau)d\tau \;\; \int_0^t \Delta\psi(\tau)]'$. Both the state and output feedback controllers, are tuned via trial-and-error with $\boldsymbol{\Gamma}_0 = \text{diag}(4.77,\ 4.77,\ 0.47,\ 3.82,\ 1.27,\ 5,\ 10,\ 10,\ 7.32,\ 7.32,\ 1.91,\ 6.36,\ 2.54,\ 1.66,\ 1.66,\ 1.66,\ 100,\ 100,\ 100,\ 100)$, $\boldsymbol{\Gamma}_1 = \text{diag}(6.59,\ 6.59,\ 1.72,\ 5.73,\ 2.29,\ 1.5,\ 1.5,\ 1.5,\ 0.57,\ 0.57,\ 2.86,\ 0.57,\ 4.58,\ 9,\ 9,\ 18,\ 1.14,\ 4.5,\ 9,\ 9)$, and $\boldsymbol{\Upsilon}_0 = \text{diag}(5, 5, 5)$.

Moreover, in order to synthesize the state and output feedback $\mathcal{W}_\infty$-D controllers[7] proposed in Section 6.3, the von Kàrmàn wind turbulence model (7.58)-(7.60) is represented in the state-space and, together with system (7.57), rewritten in the standard forms (6.28) and (6.34). For the sake of comparison analysis, the $\mathcal{W}_\infty$-D controllers are tuned with the same tuning matrices as the $\mathcal{W}_\infty$ controllers, but considering $\boldsymbol{\Upsilon}_1 = diag(16, 9.5, 14.7)$ for the state feedback controller, and $\boldsymbol{\Upsilon}_1 = diag(0.1, 0.1, 0.1)$ for the output feedback controller. The $\mathcal{W}_\infty$-D controllers are obtained by solving the convex optimization problems with LMI constraints (6.31) and (6.36).

In the particular case of the Tilt-rotor UAV, the design of the output feedback $\mathcal{W}_\infty$ controller leads to undesired fast poles of the closed-loop system. Thus, the LMI (6.40)

[7] In this section the controllers that are designed assuming the knowledge of the dynamics of the disturbance will be called $\mathcal{W}_\infty$-D controllers

is added into the convex optimization problems (6.22) and (6.36), considering

$$\boldsymbol{\alpha} = \begin{bmatrix} -r & 0 \\ 0 & r \end{bmatrix}, \qquad \boldsymbol{\beta} = \begin{bmatrix} 0 & 1 \\ 0 & 0 \end{bmatrix}, \tag{7.61}$$

with $r = 250$ which limits the poles allocation space to a ball with radius r centered at the origin of the complex plane.

In the numerical experiment, the Tilt-rotor UAV starts displaced from the desired trajectory, with the initial conditions $\boldsymbol{q}(0) = [0\ 0\ 0\ 0\ 0\ \ -1\ 20\ 0]'$ and $\dot{\boldsymbol{q}}(0) = \mathbf{0}$, and is designated to track the desired trajectory given in Table 7.1, with $\psi_r = \phi_r = 0$, $\alpha_{R_r} = \alpha_{L_r} = -0.137$, and $\theta_r = 0.137$. The results of the numerical experiment are presented in Figures 7.8-7.12, and a quantitative analysis of the results is presented in Table 7.2.

As shown in Figure 7.10, the von Kàrmàn wind turbulence model (7.58)-(7.60) is applied to emulate the environment wind vector $\boldsymbol{\zeta}(t) = [\zeta_x(t)\ \ \zeta_y\ \ \zeta_z(t)]'$ during the time interval $30 \leq t \leq 170$ s. In addition, in order to satisfy the range $\alpha_S^{air}, \beta_S^{air} \in [-\frac{\pi}{2}, \frac{\pi}{2}]$ rad, for which the aerodynamic coefficients are valid, the component $\zeta_x(t)$ of the environment wind speed vector is decremented by 3 [m/s].

From the results of Figures 7.8-7.12, one can observe that all the controllers ($\mathcal{W}_\infty$, $\mathcal{W}_\infty$-D, $\mathcal{W}_\infty$-O.F., $\mathcal{W}_\infty$-O.F.D) are able to track the desired trajectory and reach the final destination. Nevertheless, the controllers that are designed considering the dynamics of the disturbance in the cost functional achieved a less oscillatory behavior and a better disturbance attenuation, with a smaller control effort, which can also be verified though the ISE and IAVU indexes, shown in Table 7.2.

Table 7.1: Desired trajectory for the Tilt-rotor UAV translational position.

	$x_r(t)$	$y_r(t)$	$z_r(t)$
$t \leq 105$	$20\sin(\frac{2\pi t}{35})$	$20\cos(\frac{2\pi t}{35})$	$\frac{2t}{5} + 1$
$105 < t \leq 125$	$3.59(t-105) - \frac{1}{2}0.1795(t-105)^2$	20	43
$125 < t \leq 186.5$	35.9	20	$43 - 0.7(t-125)$
$t \geq 186.5$	35.9	20	0

Table 7.2: Table of performance indexes.

P. Index	computed by	$\mathcal{W}_\infty$	$\mathcal{W}_\infty - D.$	$\mathcal{W}_\infty - O.F.$	$\mathcal{W}_\infty - O.F.D.$
ISE	$\int_0^\tau (\Delta\boldsymbol{x}(t))'\Delta\boldsymbol{x}(t)dt$	21.4 (100%)	**10.9** (**51**%)	60.7 (100%)	**39.2** (**64**%)
IADU	$\int_0^t \sum_{i=1}^4 \lvert\frac{d\Delta\boldsymbol{u_i}(\tau)}{d\tau}\rvert d\tau$	2182 (100%)	**1541.8** (**70**%)	1376.2 (100%)	**1317.3** (**95**%)

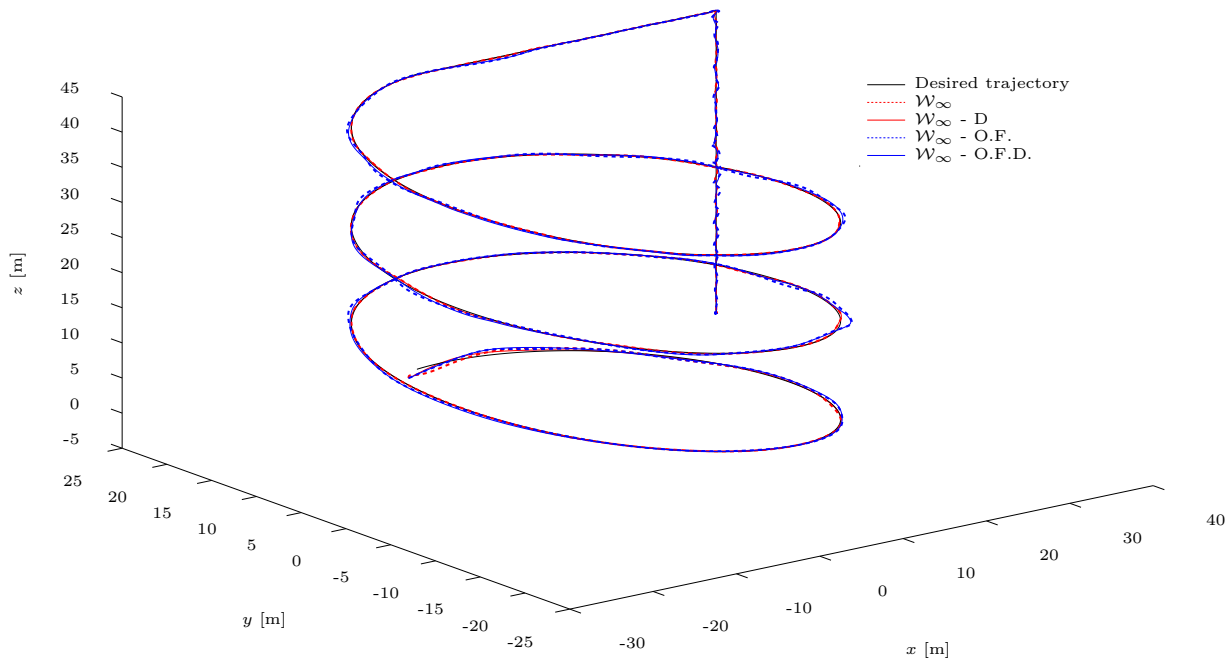

Figure 7.8: 3D view of the Tilt-rotor UAV trajectory resulting from the application of the state feedback $\mathcal{W}_\infty$, output feedback $\mathcal{W}_\infty$-O.F., state feedback with disturbance model $\mathcal{W}_\infty$-D., and output feedback with disturbance model $\mathcal{W}_\infty$-O.F.D. controllers.

7.3.2 Nonlinear $\mathcal{W}_\infty$ control design with control allocation

In this subsection, a nonlinear $\mathcal{W}_\infty$ controller is proposed to achieve robust trajectory tracking throughout the full flight envelope of the Tilt-rotor UAV.

For control design purposes, initially, the vector of generalized forces (7.18) is manipulated and represented by the input-affine representation

$$\boldsymbol{\vartheta}(\dot{\boldsymbol{q}}, \boldsymbol{q}, \boldsymbol{\tau}, \boldsymbol{\zeta}) = \boldsymbol{B}(\boldsymbol{q}, \dot{\boldsymbol{q}}, \boldsymbol{\zeta})\bar{\boldsymbol{\tau}}(t) + \boldsymbol{\vartheta}_{passive}(\boldsymbol{q}, \dot{\boldsymbol{q}}, \boldsymbol{\zeta}) + \boldsymbol{w}(t), \tag{7.62}$$

where $\bar{\boldsymbol{\tau}} \triangleq [f_{\mathcal{P}_R}\ f_{\mathcal{P}_L}\ \tau_{s_R}\ \tau_{s_L}\ \delta_{\mathcal{W}_R}\ \delta_{\mathcal{W}_L}\ \delta_{\mathcal{T}_R}\ \delta_{\mathcal{T}_L}]'$ is the vector of control inputs, $\boldsymbol{w}(t) : \mathbb{R}_{\geq 0} \to \mathbb{R}^8$ represents the total effects of unmodeled dynamics and external disturbances, and $\boldsymbol{\vartheta}_{passive}(\boldsymbol{q}, \dot{\boldsymbol{q}}, \boldsymbol{\zeta})$ comprehends all the terms in $\boldsymbol{\vartheta}_{\mathcal{P}}$, $\boldsymbol{\vartheta}_s$, $\boldsymbol{\vartheta}_{\mathcal{F}}$, $\boldsymbol{\vartheta}_{\mathcal{W}}$, $\boldsymbol{\vartheta}_{\mathcal{T}}$ and $\boldsymbol{\vartheta}_I$ not influenced by the control inputs. The algebraic manipulation of the generalized forces (7.18) to represented in the input affine form (7.62) is presented in Appendix C.

Assumption 19. *The environment wind speed vector, $\boldsymbol{\zeta}$, is available.*

Remark 45. *The control input vector $\bar{\boldsymbol{\tau}}$ considers the forces applied by the propellers as control inputs and $\bar{\boldsymbol{\tau}} \neq \boldsymbol{\tau}$ (See (7.25) and (7.27)).*

As commented previously, when the Tilt-rotor UAV operates in the helicopter-flight mode, i.e. $V_S^{air} \approx 0$, the thrusters' groups are in charge of providing the forces and moments necessary to guide the aircraft, and the deflection of the aerodynamic surfaces does not generate enough forces and moments to be used by the control system, therefore,

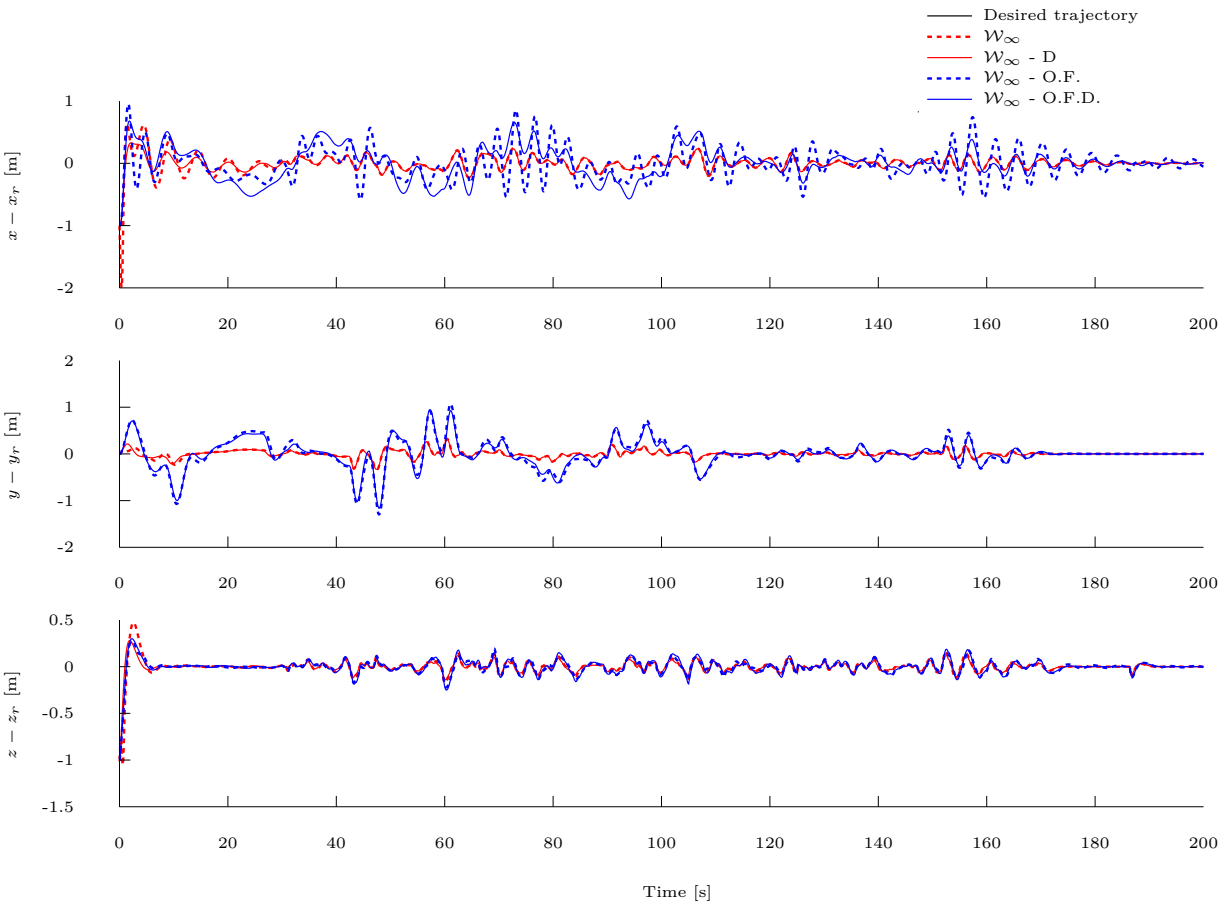

Figure 7.9: Tilt-rotor UAV tracking error, resulting from the application of the state feedback $\mathcal{W}_\infty$, output feedback $\mathcal{W}_\infty$-O.F., state feedback with disturbance model $\mathcal{W}_\infty$-D., and output feedback with disturbance model $\mathcal{W}_\infty$-O.F.D. controllers.

$\text{rank}(\boldsymbol{B}(\boldsymbol{q}, \dot{\boldsymbol{q}})) = 4$. On the other hand, when the aircraft is cruising and transitioning, the aerodynamic control surfaces can be used to improve the control system performance, therefore, $\text{rank}(\boldsymbol{B}(\boldsymbol{q}, \dot{\boldsymbol{q}})) \geq 4$. Consequently, one can verify that the relative wind speed affects the rank of the input coupling matrix. It is noteworthy that, in order to design the nonlinear $\mathcal{W}_\infty$ controllers proposed in Chapter 5, one must choose the number of controlled DOF taking into account the $\inf\{\text{rank}(\boldsymbol{B}(\boldsymbol{q}, \dot{\boldsymbol{q}}))\}, \forall(\boldsymbol{q}, \dot{\boldsymbol{q}}) \in \Omega$, such that Ω concerns all the flight envelope of the Tilt-rotor UAV, complying with Assumptions 5 and 6. Nevertheless, in the case of the nonlinear $\mathcal{W}_\infty$ controller formulated considering the whole dynamical model of the mechanical system, proposed in Section 5.2, this implies in several feasible choices to manipulate the stabilized DOF such that Assumption 8 holds when transitioning and cruising, which may lead to undesired values for the stabilized degrees of freedom. One undesired situation, for instance, is when the tilting angles of the servomotors are selected as stabilized DOF, then the controller can choose to point the group of thrusters down in cruising. To handle these issues, this section proposes a new nonlinear $\mathcal{W}_\infty$ controller with the generalized coordinates vector partitioned in stabilized, regulated, and controlled DOF, allowing also to set references for the regulated DOF.

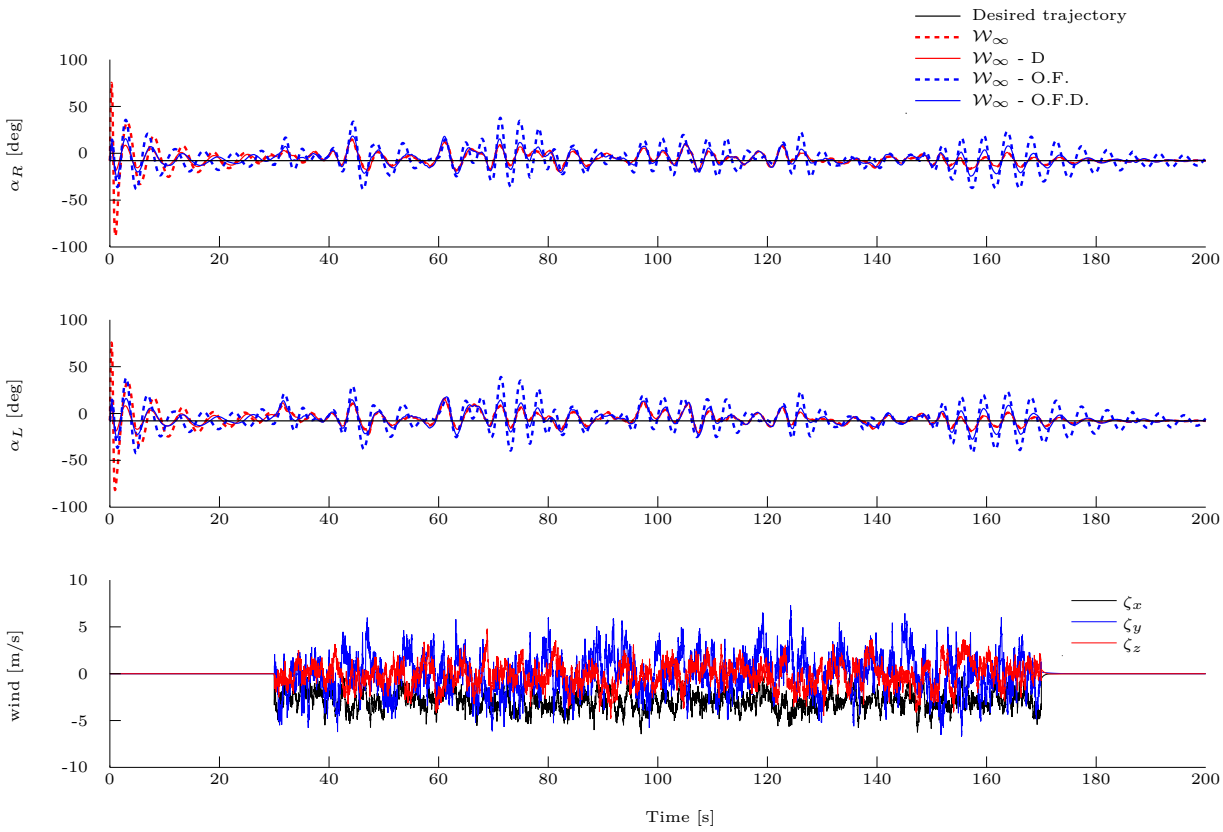

Figure 7.10: Tilt-rotor UAV tilting angles of the servomotors, resulting from the application of the state feedback $\mathcal{W}_\infty$, output feedback $\mathcal{W}_\infty$-O.F., state feedback with disturbance model $\mathcal{W}_\infty$-D., and output feedback with disturbance model $\mathcal{W}_\infty$-O.F.D. controllers, and the environment wind.

Note that in the previous controllers, the vector of generalized coordinates is partitioned in stabilized and controlled DOF.

Accordingly, in order to design the nonlinear $\mathcal{W}_\infty$ controller, and taking into account the input-affine representation of the vector of generalized forces (7.62), the Tilt-rotor UAV equations of motion (7.14) are partitioned in stabilized, regulated, and controlled DOF, as follows

$$\underbrace{\begin{bmatrix} \boldsymbol{M}_{ss}(\boldsymbol{q}) & \boldsymbol{M}_{sr}(\boldsymbol{q}) & \boldsymbol{M}_{sc}(\boldsymbol{q}) \\ \boldsymbol{M}_{rs}(\boldsymbol{q}) & \boldsymbol{M}_{rr}(\boldsymbol{q}) & \boldsymbol{M}_{rc}(\boldsymbol{q}) \\ \boldsymbol{M}_{cs}(\boldsymbol{q}) & \boldsymbol{M}_{cr}(\boldsymbol{q}) & \boldsymbol{M}_{cc}(\boldsymbol{q}) \end{bmatrix}}_{\boldsymbol{M}(\boldsymbol{q})} \underbrace{\begin{bmatrix} \ddot{\boldsymbol{q}}_s \\ \ddot{\boldsymbol{q}}_r \\ \ddot{\boldsymbol{q}}_c \end{bmatrix}}_{\ddot{\boldsymbol{q}}(t)} + \underbrace{\begin{bmatrix} \boldsymbol{C}_{ss}(\boldsymbol{q},\dot{\boldsymbol{q}}) & \boldsymbol{C}_{sr}(\boldsymbol{q},\dot{\boldsymbol{q}}) & \boldsymbol{C}_{sc}(\boldsymbol{q},\dot{\boldsymbol{q}}) \\ \boldsymbol{C}_{rs}(\boldsymbol{q},\dot{\boldsymbol{q}}) & \boldsymbol{C}_{rr}(\boldsymbol{q},\dot{\boldsymbol{q}}) & \boldsymbol{C}_{rc}(\boldsymbol{q},\dot{\boldsymbol{q}}) \\ \boldsymbol{C}_{cs}(\boldsymbol{q},\dot{\boldsymbol{q}}) & \boldsymbol{C}_{cr}(\boldsymbol{q},\dot{\boldsymbol{q}}) & \boldsymbol{C}_{cc}(\boldsymbol{q},\dot{\boldsymbol{q}}) \end{bmatrix}}_{\boldsymbol{C}(\boldsymbol{q},\dot{\boldsymbol{q}})} \underbrace{\begin{bmatrix} \dot{\boldsymbol{q}}_s \\ \dot{\boldsymbol{q}}_r \\ \dot{\boldsymbol{q}}_c \end{bmatrix}}_{\dot{\boldsymbol{q}}(t)}$$
$$+ \underbrace{\begin{bmatrix} \boldsymbol{g}_s(\boldsymbol{q}) \\ \boldsymbol{g}_r(\boldsymbol{q}) \\ \boldsymbol{g}_c(\boldsymbol{q}) \end{bmatrix}}_{\boldsymbol{g}(\boldsymbol{q})} = \underbrace{\begin{bmatrix} \boldsymbol{B}_s(\boldsymbol{q},\dot{\boldsymbol{q}},\boldsymbol{\zeta}) \\ \boldsymbol{B}_r(\boldsymbol{q},\dot{\boldsymbol{q}},\boldsymbol{\zeta}) \\ \boldsymbol{B}_c(\boldsymbol{q},\dot{\boldsymbol{q}},\boldsymbol{\zeta}) \end{bmatrix}}_{\boldsymbol{B}(\boldsymbol{q},\dot{\boldsymbol{q}})} \bar{\boldsymbol{\tau}}(t) + \boldsymbol{\vartheta}_{passive}(\boldsymbol{q},\dot{\boldsymbol{q}},\boldsymbol{\zeta}) + \boldsymbol{w}(t), \tag{7.63}$$

with $\boldsymbol{q}(t) = [\boldsymbol{q}_s'(t)\ \boldsymbol{q}_r'(t)\ \boldsymbol{q}_c'(t)]'$, in which $\boldsymbol{q}_s(t) = [\phi(t)\ \ \theta(t)]'$ corresponds to the stabilized

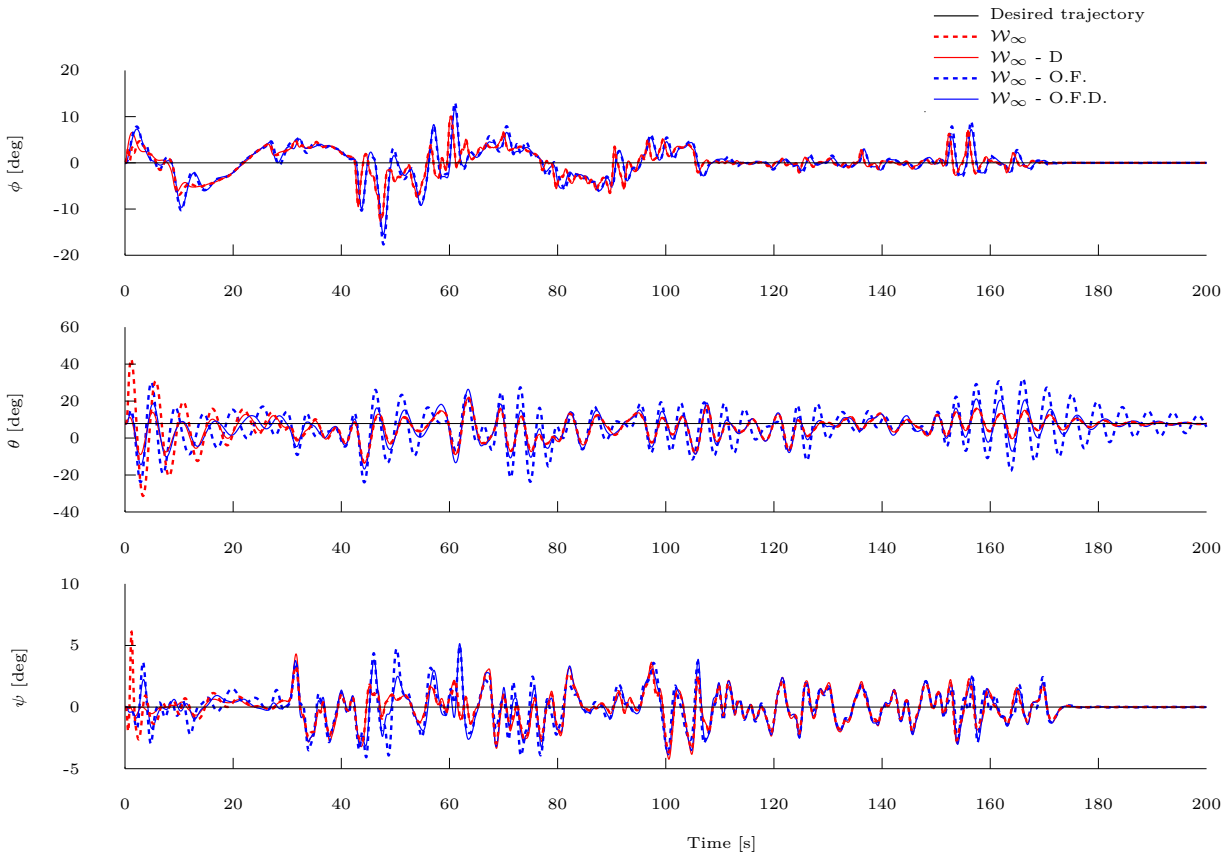

Figure 7.11: Tilt-rotor UAV attitude in the Euler angles, resulting from the application of the state feedback $\mathcal{W}_\infty$, output feedback $\mathcal{W}_\infty$-O.F., state feedback with disturbance model $\mathcal{W}_\infty$-D., and output feedback with disturbance model $\mathcal{W}_\infty$-O.F.D. controllers.

DOF, $\boldsymbol{q}_r(t) = [\psi(t) \;\; \alpha_R(t) \;\; \alpha_L(t)]'$ the regulated DOF, and $\boldsymbol{q}_c(t) = [x(t) \;\; y(t) \;\; z(t)]$ the controlled ones. The aim is to achieve trajectory tracking of the Tilt-rotor UAV translational position (controlled DOF) and set references for the tilting angles of the servomotors and yaw angle (regulated DOF) while stabilizing the roll and pitch dynamics (Stabilized DOF).

Accordingly, the tracking error dynamics are written as

$$\begin{aligned}\boldsymbol{M}\left(\begin{bmatrix}\boldsymbol{q}_s\\ \tilde{\boldsymbol{q}}_r+\boldsymbol{q}_{r_r}\\ \tilde{\boldsymbol{q}}_c+\boldsymbol{q}_{c_r}\end{bmatrix}\right)\begin{bmatrix}\ddot{\boldsymbol{q}}_s\\ \ddot{\tilde{\boldsymbol{q}}}_r+\ddot{\boldsymbol{q}}_{r_r}\\ \ddot{\tilde{\boldsymbol{q}}}_c+\ddot{\boldsymbol{q}}_{c_r}\end{bmatrix}+\boldsymbol{C}\left(\begin{bmatrix}\boldsymbol{q}_s\\ \tilde{\boldsymbol{q}}_r+\boldsymbol{q}_{r_r}\\ \tilde{\boldsymbol{q}}_c+\boldsymbol{q}_{c_r}\end{bmatrix},\begin{bmatrix}\dot{\boldsymbol{q}}_s\\ \dot{\tilde{\boldsymbol{q}}}_r+\dot{\boldsymbol{q}}_{r_r}\\ \dot{\tilde{\boldsymbol{q}}}_c+\dot{\boldsymbol{q}}_{c_r}\end{bmatrix}\right)\begin{bmatrix}\dot{\boldsymbol{q}}_s\\ \dot{\tilde{\boldsymbol{q}}}_r+\dot{\boldsymbol{q}}_{r_r}\\ \dot{\tilde{\boldsymbol{q}}}_c+\dot{\boldsymbol{q}}_{c_r}\end{bmatrix}\\ +\boldsymbol{g}\left(\begin{bmatrix}\boldsymbol{q}_s\\ \tilde{\boldsymbol{q}}_r+\boldsymbol{q}_{r_r}\\ \tilde{\boldsymbol{q}}_c+\boldsymbol{q}_{c_r}\end{bmatrix}\right)=\boldsymbol{B}\left(\begin{bmatrix}\boldsymbol{q}_s\\ \tilde{\boldsymbol{q}}_r+\boldsymbol{q}_{r_r}\\ \tilde{\boldsymbol{q}}_c+\boldsymbol{q}_{c_r}\end{bmatrix},\begin{bmatrix}\dot{\boldsymbol{q}}_s\\ \dot{\tilde{\boldsymbol{q}}}_r+\dot{\boldsymbol{q}}_{r_r}\\ \dot{\tilde{\boldsymbol{q}}}_c+\dot{\boldsymbol{q}}_{c_r}\end{bmatrix},\boldsymbol{\zeta}\right)\bar{\boldsymbol{\tau}}(t)+\boldsymbol{w}(t),\end{aligned}\tag{7.64}$$

with $\tilde{\boldsymbol{q}}_c(t) \triangleq \boldsymbol{q}_c(t) - \boldsymbol{q}_{c_r}(t)$ and $\tilde{\boldsymbol{q}}_r(t) \triangleq \boldsymbol{q}_r(t) - \boldsymbol{q}_{r_r}(t)$, where $\boldsymbol{q}_{cr}(t)$, $\dot{\boldsymbol{q}}_{cr}(t)$, $\ddot{\boldsymbol{q}}_{cr}(t)$, $\boldsymbol{q}_{r_r}(t)$, $\dot{\boldsymbol{q}}_{r_r}(t)$ and $\ddot{\boldsymbol{q}}_{r_r}(t)$ are the desired values of the controlled and regulated DOF and their time derivatives, in which $\boldsymbol{q}_{c_r}(t), \boldsymbol{q}_{r_r}(t) \in \mathcal{C}^2$.

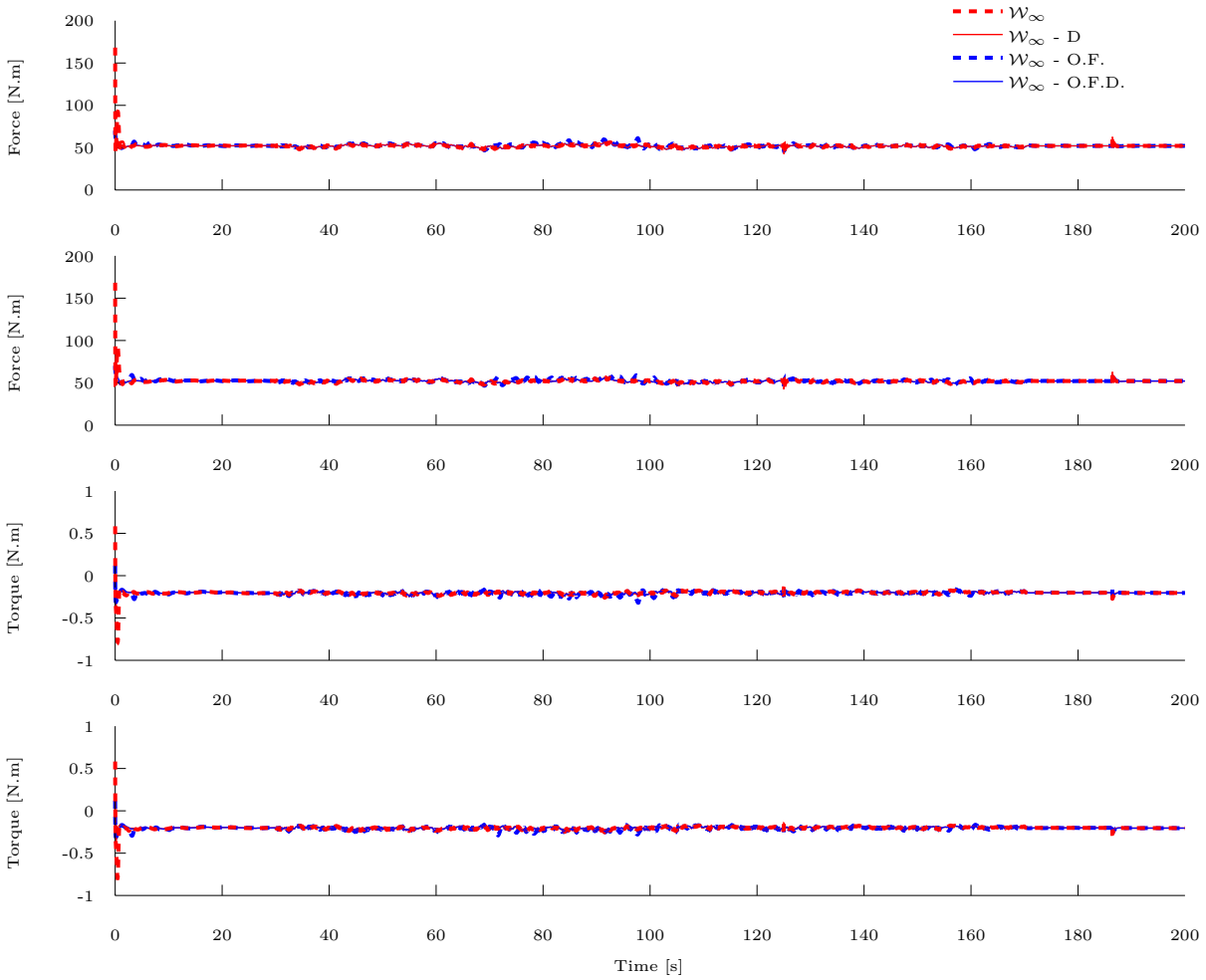

Figure 7.12: Tilt-rotor UAV control inputs signal resulting from the application of the state feedback $\mathcal{W}_\infty$, output feedback $\mathcal{W}_\infty$-O.F., state feedback with disturbance model $\mathcal{W}_\infty$-D., and output feedback with disturbance model $\mathcal{W}_\infty$-O.F.D. controllers.

Similarly to Section 5.2, by defining the state vector $\boldsymbol{x}(t) \triangleq [\dot{\boldsymbol{q}}_s'(t)\ \dot{\tilde{\boldsymbol{q}}}_r'(t)\ \dot{\tilde{\boldsymbol{q}}}_c'(t)\ \tilde{\boldsymbol{q}}_c'(t)\ \tilde{\boldsymbol{q}}_r'(t)\ \int_0^t \tilde{\boldsymbol{q}}_c'(\tau)d\tau]'$, equation (7.64) is manipulated in order to obtain the following state space representation:

$$\dot{\boldsymbol{x}}(t) = \underbrace{\left[\begin{array}{ccc|ccc} & & & \boldsymbol{0} & \boldsymbol{0} & \boldsymbol{0} \\ & -\boldsymbol{M}^{-1}\boldsymbol{C} & & \boldsymbol{0} & \boldsymbol{0} & \boldsymbol{0} \\ & & & \boldsymbol{0} & \boldsymbol{0} & \boldsymbol{0} \\ \hline \boldsymbol{0} & \boldsymbol{I} & \boldsymbol{0} & \boldsymbol{0} & \boldsymbol{0} & \boldsymbol{0} \\ \boldsymbol{0} & \boldsymbol{0} & \boldsymbol{I} & \boldsymbol{0} & \boldsymbol{0} & \boldsymbol{0} \\ \boldsymbol{0} & \boldsymbol{0} & \boldsymbol{0} & \boldsymbol{0} & \boldsymbol{I} & \boldsymbol{0} \end{array}\right]}_{\boldsymbol{f}(\boldsymbol{x},\boldsymbol{q}_S)} \boldsymbol{x}(t) - \underbrace{\begin{bmatrix} \boldsymbol{M}^{-1}\boldsymbol{d} \\ \boldsymbol{0} \\ \boldsymbol{0} \\ \boldsymbol{0} \end{bmatrix}}_{\bar{\boldsymbol{f}}(\boldsymbol{x},\boldsymbol{q}_S,\boldsymbol{\zeta},t)} + \underbrace{\begin{bmatrix} \boldsymbol{M}^{-1} \\ \boldsymbol{0} \\ \boldsymbol{0} \\ \boldsymbol{0} \end{bmatrix}}_{\boldsymbol{g}(\boldsymbol{x},\boldsymbol{q}_S)} \boldsymbol{u}(t) + \underbrace{\begin{bmatrix} \boldsymbol{M}^{-1} \\ \boldsymbol{0} \\ \boldsymbol{0} \\ \boldsymbol{0} \end{bmatrix}}_{\boldsymbol{k}(\boldsymbol{x},\boldsymbol{q}_S)} \boldsymbol{w}(t), \qquad (7.65)$$

with $\boldsymbol{d} \triangleq \boldsymbol{g}(\boldsymbol{q}) - \boldsymbol{\vartheta}_{passive}(\boldsymbol{q}, \dot{\boldsymbol{q}}, \boldsymbol{\zeta}) + \boldsymbol{M}(\boldsymbol{q}) \begin{bmatrix} \boldsymbol{0} \\ \ddot{\boldsymbol{q}}_{r_r} \\ \ddot{\boldsymbol{q}}_{c_r} \end{bmatrix} + \boldsymbol{C}(\boldsymbol{q}, \dot{\boldsymbol{q}}) \begin{bmatrix} \boldsymbol{0} \\ \ddot{\boldsymbol{q}}_{r_r} \\ \dot{\boldsymbol{q}}_{c_r} \end{bmatrix}$, and $\boldsymbol{u}(t) = \boldsymbol{B}(\boldsymbol{q}, \dot{\boldsymbol{q}}, \boldsymbol{\zeta})\bar{\boldsymbol{\tau}}(t)$ is the generalized input vector.

Then, the system (7.65) is represented in the standard form

$$\mathcal{P}_{14} : \begin{cases} \dot{\boldsymbol{x}}(t) & = \boldsymbol{f}(\boldsymbol{x}, \boldsymbol{q}_s) + \bar{\boldsymbol{f}}(\boldsymbol{x}, \boldsymbol{q}_s, t) + \boldsymbol{g}(\boldsymbol{x}, \boldsymbol{q}_s)\boldsymbol{u}(t) + \boldsymbol{k}(\boldsymbol{x}, \boldsymbol{q}_s)\boldsymbol{w}(t), \\ \boldsymbol{z}_c(t) & = \int_0^t \tilde{\boldsymbol{q}}_c(\tau) d\tau, \\ \boldsymbol{z}_r(t) & = \boldsymbol{q}_r(t), \\ \boldsymbol{z}_s(t) & = \dot{\boldsymbol{q}}_s(t), \end{cases} \tag{7.66}$$

where the cost variable $\boldsymbol{z}_c(t)$ is related to the trajectory tracking of the controlled DOF with disturbance rejection capability, $\boldsymbol{z}_r(t)$ is related to set-point tracking of the regulated DOF, and $\boldsymbol{z}_s(t)$ is defined in order to ensure remaining DOF are stabilized in some equilibrium point.

The nonlinear $\mathcal{W}_\infty$ control problem for full flight envelope trajectory tracking of the Tilt-rotor UAV, based on plant $\mathcal{P}_1$, is posed as finding the control law $\boldsymbol{u}(\boldsymbol{x}, \boldsymbol{q}_s, \boldsymbol{\zeta}, t) \in \mathcal{U}$ that minimizes the cost functional

$$\mathcal{J}_\infty = \frac{1}{2}\left(||\boldsymbol{z}_c(t)||^2_{\mathcal{W}_{3,2,\boldsymbol{\Gamma}}} + ||\boldsymbol{z}_r(t)||^2_{\mathcal{W}_{2,2,\boldsymbol{\Sigma}}} + ||\boldsymbol{z}_s(t)||^2_{\mathcal{W}_{1,2,\boldsymbol{\Upsilon}}} - \gamma^2 ||\boldsymbol{w}(t)||^2_{\mathcal{L}_2} \right), \tag{7.67}$$

for the worst case of the disturbances $\boldsymbol{w}(t) \in \mathcal{L}_2[0, \infty)$, considering a given sufficiently large $\gamma \in \mathbb{R}_{\geq 0}$. The optimal control problem is written as

$$\begin{aligned} \boldsymbol{V}_\infty = & \min_{\boldsymbol{u} \in \mathcal{U}} \max_{\boldsymbol{w} \in \mathcal{D}} \mathcal{J}_\infty \\ & \text{s.t.} \quad \mathcal{P}_1. \end{aligned} \tag{7.68}$$

with $\mathcal{U} : (\mathbb{R}^{n_x} \times \mathbb{R}^{n_s} \times \mathbb{R}^{n_\zeta} \times \mathbb{R}_{\geq 0}) \to \mathbb{R}^{n_u}$ and $\mathcal{D} = \mathcal{L}_2[0, \infty)$, where n_x, n_s, n_ζ. and n_u are the dimensions of the vectors $\boldsymbol{x}$, $\boldsymbol{q}_s$, $\boldsymbol{\zeta}$, and $\boldsymbol{u}$, respectively.

Remark 46. *In (7.67), the number of derivatives taken by the weighted Sobolev norm is different for each cost variable. The objective is to include the dynamics of the system, i.e. $\ddot{\boldsymbol{q}}_s$, $\ddot{\tilde{\boldsymbol{q}}}_r$, $\ddot{\tilde{\boldsymbol{q}}}_c$, in the cost functional.*

Remark 47. *In the optimal control problem (7.68), the time derivatives of the stabilized DOF are required to converge to zero, but there are no references for the stabilized DOF. This allows the controller to manipulate the roll and pitch angles to achieve trajectory tracking and attenuate disturbances.*

Remark 48. *The cost variable $\boldsymbol{z}_r(t)$ is chosen to allow setting references for the regulated DOF without forcing null steady-state error when the system is subjected to constant dis-*

turbances. This gives the controller the capability of manipulating these variables around their desired references to attenuate the effects of disturbances.

A particular solution to (7.68) is proposed in the following theorem.

Theorem 12. *Let $\boldsymbol{V}_\infty$ be the parametrized scalar function*

$$\boldsymbol{V}_\infty(\boldsymbol{x},t)=\frac{1}{2}\boldsymbol{x}'\begin{bmatrix}\boldsymbol{U}&\boldsymbol{0}&\boldsymbol{0}&\boldsymbol{0}&\boldsymbol{0}&\boldsymbol{0}\\ \boldsymbol{0}&\boldsymbol{A}&\boldsymbol{0}&\boldsymbol{B}&\boldsymbol{0}&\boldsymbol{0}\\ \boldsymbol{0}&\boldsymbol{0}&\boldsymbol{Q}&\boldsymbol{0}&\boldsymbol{K}&\boldsymbol{T}\\ \boldsymbol{0}&\boldsymbol{B}&\boldsymbol{0}&\boldsymbol{C}&\boldsymbol{0}&\boldsymbol{0}\\ \boldsymbol{0}&\boldsymbol{0}&\boldsymbol{K}&\boldsymbol{0}&\boldsymbol{R}&\boldsymbol{S}\\ \boldsymbol{0}&\boldsymbol{0}&\boldsymbol{T}&\boldsymbol{0}&\boldsymbol{S}&\boldsymbol{P}\end{bmatrix}\boldsymbol{x}>0, \tag{7.69}$$

such that $\boldsymbol{U}$, $\boldsymbol{A}$, $\boldsymbol{B}$, $\boldsymbol{Q}$, $\boldsymbol{K}$, $\boldsymbol{T}$, $\boldsymbol{R}$, $\boldsymbol{S}$, and $\boldsymbol{P}$ are positive definite matrices and verify $\boldsymbol{Q}-\boldsymbol{K}\boldsymbol{R}^{-1}\boldsymbol{K}>0$, $\boldsymbol{A}-\boldsymbol{B}\boldsymbol{C}^{-1}\boldsymbol{B}>0$, and $\begin{bmatrix}\boldsymbol{Q}&\boldsymbol{K}\\ \boldsymbol{K}&\boldsymbol{R}\end{bmatrix}-\begin{bmatrix}\boldsymbol{T}\\ \boldsymbol{S}\end{bmatrix}\boldsymbol{P}^{-1}\begin{bmatrix}\boldsymbol{T}&\boldsymbol{S}\end{bmatrix}>0$, with $\boldsymbol{U}$, $\boldsymbol{B}$, $\boldsymbol{T}$, $\boldsymbol{A}$, $\boldsymbol{K}$, and $\boldsymbol{Q}$ obtained from the following Riccati equations

$$-\boldsymbol{U}\boldsymbol{\Upsilon}_1^{-1}\boldsymbol{U}+\boldsymbol{\Upsilon}_0=\boldsymbol{0}, \tag{7.70}$$
$$-\boldsymbol{B}\boldsymbol{\Sigma}_2^{-1}\boldsymbol{B}+\boldsymbol{\Sigma}_0=\boldsymbol{0}, \tag{7.71}$$
$$-\boldsymbol{T}\boldsymbol{\Gamma}_3^{-1}\boldsymbol{T}+\boldsymbol{\Gamma}_0=\boldsymbol{0}, \tag{7.72}$$
$$-\boldsymbol{A}\boldsymbol{\Sigma}_2^{-1}\boldsymbol{A}+2\boldsymbol{B}+\boldsymbol{\Sigma}_1=\boldsymbol{0}, \tag{7.73}$$
$$-\boldsymbol{K}\boldsymbol{\Gamma}_3^{-1}\boldsymbol{K}+\boldsymbol{\Gamma}_1+2\boldsymbol{T}\boldsymbol{\Gamma}_3^{-1}\boldsymbol{Q}=\boldsymbol{0}, \tag{7.74}$$
$$-\boldsymbol{Q}\boldsymbol{\Gamma}_3^{-1}\boldsymbol{Q}+2\boldsymbol{K}+\boldsymbol{\Gamma}_2=\boldsymbol{0}, \tag{7.75}$$

Besides, $\boldsymbol{C}$, $\boldsymbol{S}$, $\boldsymbol{P}$, and $\boldsymbol{R}$ are given by

$$\boldsymbol{C}=\boldsymbol{B}\boldsymbol{\Gamma}_2^{-1}\boldsymbol{A}, \tag{7.76}$$
$$\boldsymbol{S}=\boldsymbol{Q}\boldsymbol{\Gamma}_3^{-1}\boldsymbol{T}, \tag{7.77}$$
$$\boldsymbol{P}=\boldsymbol{T}\boldsymbol{\Gamma}_3^{-1}\boldsymbol{K}, \tag{7.78}$$
$$\boldsymbol{R}=\boldsymbol{K}\boldsymbol{\Gamma}_3^{-1}\boldsymbol{Q}-\boldsymbol{T}, \tag{7.79}$$
$$\tag{7.80}$$

Then, function $\boldsymbol{V}_\infty(\boldsymbol{x},t)$ is a solution to the HJ equation (7.68).

Proof. The proof follows similar to one of Theorem 4. □

From (7.68) and (7.69), the optimal control law is given by

$$\boldsymbol{u}^*=-\boldsymbol{\Pi}^{-1}\boldsymbol{g}(\boldsymbol{x},\boldsymbol{q}_s)'\frac{\partial \boldsymbol{V}_\infty}{\partial \boldsymbol{x}}+\boldsymbol{C}\dot{\tilde{\boldsymbol{q}}}+\boldsymbol{d}-\boldsymbol{w}^*, \tag{7.81}$$

(7.82)

with $\boldsymbol{\Pi} \triangleq \boldsymbol{M}^{-1}\boldsymbol{E}\boldsymbol{M}^{-1}$ and $\boldsymbol{E} \triangleq blkdiag(\boldsymbol{\Upsilon}_1, \boldsymbol{\Sigma}_2, \boldsymbol{\Gamma}_3)$, with the worst case of the disturbances given by

$$\boldsymbol{w}^* = \frac{1}{\gamma^2}\left(\boldsymbol{k}' - \boldsymbol{g}'\right)\frac{\partial \boldsymbol{V}_\infty}{\partial \boldsymbol{x}}. \tag{7.83}$$

In order to handle the varying rank of the input coupling matrix, the $\mathcal{W}_\infty$ controller is implemented taking into account the control allocation scheme

$$\begin{aligned} \min_{\bar{\boldsymbol{\tau}} \in \mathcal{T}} \; & \left(\boldsymbol{u}^*(t) - \boldsymbol{B}(\boldsymbol{q}, \dot{\boldsymbol{q}}, \boldsymbol{\zeta})\bar{\boldsymbol{\tau}}(t)\right)' \left(\boldsymbol{u}^*(t) - \boldsymbol{B}(\boldsymbol{q}, \dot{\boldsymbol{q}}, \boldsymbol{\zeta})\bar{\boldsymbol{\tau}}(t)\right), \\ \text{s.t.} \quad & \boldsymbol{lo}(t) \leq \bar{\boldsymbol{\tau}}(t) \leq \boldsymbol{up}(t), \end{aligned} \tag{7.84}$$

where $\mathcal{T} : \mathbb{R}_{\geq 0} \to \mathbb{R}^{n_{\bar{\tau}}}$, and

$$\boldsymbol{up}(t) \triangleq \begin{bmatrix} f_{\mathcal{P}_R}^{max} & f_{\mathcal{P}_L}^{max} & \tau_{s_R}^{max} & \tau_{s_L}^{max} & \delta_{\mathcal{W}_R}^{max} & \delta_{\mathcal{W}_L}^{max} & \delta_{\mathcal{T}_R}^{max} & \delta_{\mathcal{T}_L}^{max} \end{bmatrix}', \tag{7.85}$$

$$\boldsymbol{lo}(t) \triangleq \begin{bmatrix} f_{\mathcal{P}_R}^{min} & f_{\mathcal{P}_L}^{min} & \tau_{s_R}^{min} & \tau_{s_L}^{min} & \delta_{\mathcal{W}_R}^{min} & \delta_{\mathcal{W}_L}^{min} & \delta_{\mathcal{T}_R}^{min} & \delta_{\mathcal{T}_L}^{min} \end{bmatrix}', \tag{7.86}$$

in which $f_{\mathcal{P}_R}^{min}, f_{\mathcal{P}_R}^{max}, f_{\mathcal{P}_L}^{min}, f_{\mathcal{P}_L}^{max}, \tau_{s_R}^{min}, \tau_{s_R}^{max}, \tau_{s_L}^{min}, \tau_{s_L}^{max} \in \mathbb{R}$ are the minimum and maximum values of thrust and torque, which can be applied by the propellers and servomotors, respectively, and $\delta_{\mathcal{W}_R}^{min}, \delta_{\mathcal{W}_R}^{max}, \delta_{\mathcal{W}_L}^{min}, \delta_{\mathcal{W}_L}^{max}, \delta_{\mathcal{T}_R}^{min}, \delta_{\mathcal{T}_R}^{max}, \delta_{\mathcal{T}_L}^{min}, \delta_{\mathcal{T}_L}^{max} : \mathbb{R} \to \mathbb{R}$ are functions that determine the maximum and minimum deflection of the aerodynamic control surfaces, they are computed taking into account the magnitude of the relative wind-speed, as follows,

$$\delta_{\mathcal{A}}^{min} = \delta^{min}\text{sigmf}(V_{\mathcal{A}}^{air}), \tag{7.87}$$

$$\delta_{\mathcal{A}}^{max} = \delta^{max}\text{sigmf}(V_{\mathcal{A}}^{air}), \tag{7.88}$$

for $\mathcal{A} \in \{\mathcal{W}_R, \mathcal{W}_L, \mathcal{T}_R, \mathcal{T}_L\}$, where $\delta^{min}, \delta^{max} \in \mathbb{R}$ are the maximum and minimum deflection of the ailerons and ruddervators, and

$$\text{sigmf}(V_{\mathcal{A}}^{air}) = \frac{1}{1 + e^{-s\left(V_{\mathcal{A}}^{air} - c\right)}}, \tag{7.89}$$

in which $c, s \in \mathbb{R}$ are tuning parameters that determine the magnitude and interval of the relative wind-speed in which the transition occurs, as illustrated in Figure 7.13.

Remark 49. *The control allocation scheme (7.84) can be seen as a pseudo-inverse mapping with parameter varying saturation constraints. These constraints adapt the mapping according to the magnitude of the relative wind speed allowing to use the control aerodynamic surfaces when they are effective.*

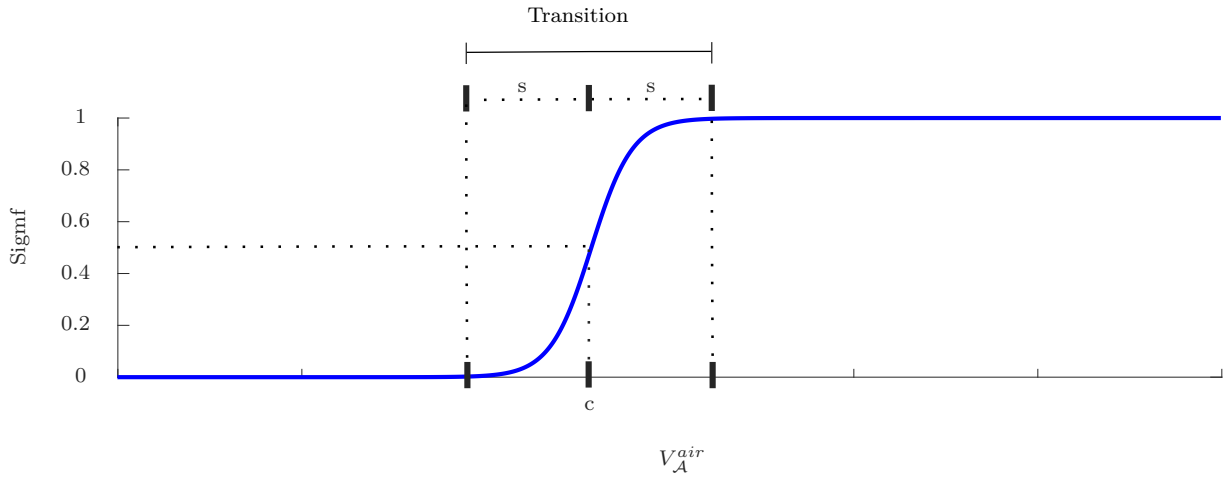

Figure 7.13: Illustration of the sigmf function.

The control input $f_{\mathcal{P}}$, for $\mathcal{P} \in \{\mathcal{P}_R, \mathcal{P}_L\}$, generated by the control allocation (7.84) is then mapped to the angular velocity of the propeller by solving the nonlinear function:

$$f_{\mathcal{P}} - \rho d^4 n_{\mathcal{P}}^2 c_t \left(J_{\mathcal{P}}, \alpha_{\mathcal{P}}\right) = 0, \tag{7.90}$$

for $n_{\mathcal{P}} > 0$.

Remark 50. *Equation* (7.90) *comes from* (7.25) *and* (7.27).

In order to verify the efficacy of the proposed nonlinear $\mathcal{W}_\infty$ controller, numerical experiments are conducted considering two different kind of scenarios. The first scenario devotes to verify the capabilities of the Tilt-rotor UAV to operate in the helicopter-flight mode. The second scenario concerns a more general case in which the Tilt-rotor UAV must take-off from a home base, accelerate in forward motion while transitioning from helicopter to cruise flight mode, perform a circular trajectory, then decelerate while transitioning from cruise to helicopter-flight mode, and land at the final destination.

To perform the numerical experiments, the $\mathcal{W}_\infty$ controller is tuned via trial-and-error with $\boldsymbol{\Upsilon}_0 = \text{diag}(180,\ 10)$, $\boldsymbol{\Upsilon}_1 = \text{diag}(2,\ 0.02)$, $\boldsymbol{\Sigma}_0 = \text{diag}(20,\ 20,\ 0.01)$, $\boldsymbol{\Sigma}_1 = \text{diag}(15, 15, 400)$, $\boldsymbol{\Sigma}_2 = \text{diag}(0.1, 0.1, 15)$, $\boldsymbol{\Gamma}_0 = \text{diag}(0.05,\ 0.05,\ 0.5)$, $\boldsymbol{\Gamma}_1 = \text{diag}(1,\ 1,\ 1)$, $\boldsymbol{\Gamma}_2 = \text{diag}(400,\ 400,\ 200)$, $\boldsymbol{\Gamma}_3 = \text{diag}(500,\ 500,\ 50)$, and the generalized inputs (7.81) are computed taking into account the solution (7.69), which is given in Theorem (12), of the HJBI equation (5.104). The control signals are computed from the generalized inputs (7.81) by solving the control allocation problem (7.84), with $f_{\mathcal{P}_R}^{max} = f_{\mathcal{P}_L}^{max} = 100$, $f_{\mathcal{P}_R}^{min} = f_{\mathcal{P}_L}^{min} = 0$, $\tau_{s_R}^{max} = \tau_{s_L}^{max} = 2$, $\tau_{s_R}^{min} = \tau_{s_L}^{min} = -2$, $\delta^{max} = \dfrac{5\pi}{36}$, $\delta^{min} = -\dfrac{5\pi}{36}$, and with the parameters $s = 2$ and $c = 12$ in (7.89), then solving the nonlinear function (7.90).

In the first experiment, the Tilt-rotor UAV is designated to track the desired trajectory present in Table 7.1. The experiment is conducted with the aircraft starting displaced from the desired trajectory, with initial conditions $\boldsymbol{q}(0) = \dot{\boldsymbol{q}}(0) = \mathbf{0}$. Along the experiment, a constant environment wind with magnitude $\boldsymbol{\zeta} = [0 \quad 3 \quad 0]'$ affects the system.

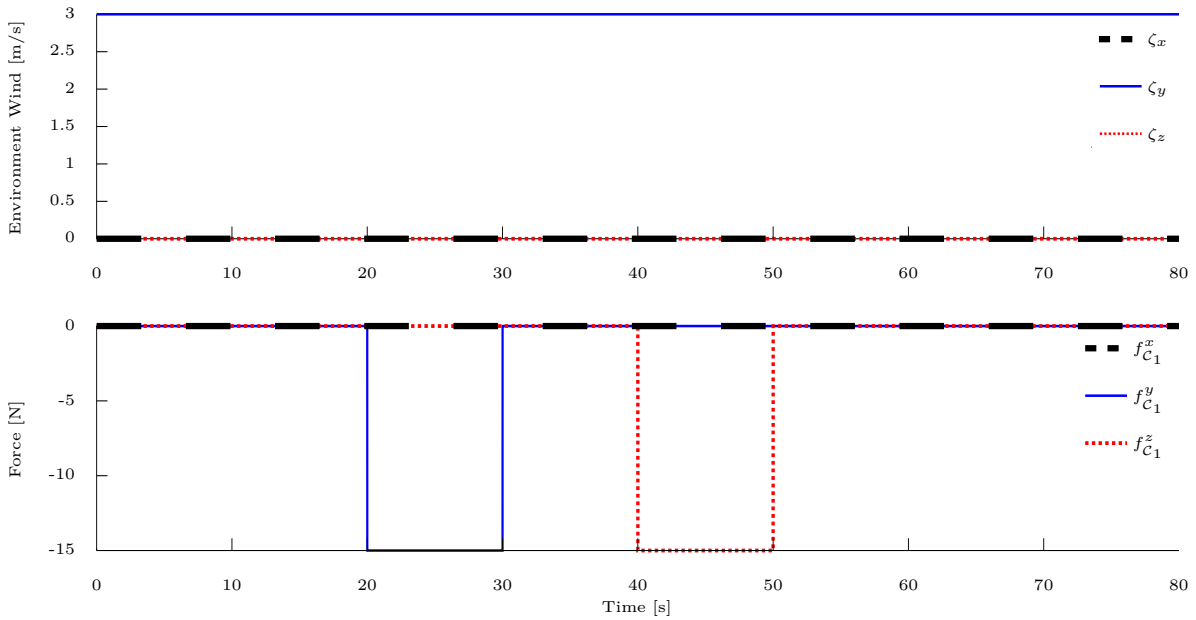

Figure 7.14: Environment wind and external disturbances applied in the first scenario.

In addition, the external disturbance $\boldsymbol{w}(t) = \boldsymbol{J}'_{\mathcal{C}_1}(\boldsymbol{q}) f^{\mathcal{C}_1}_{\mathcal{I}}(t)$ is applied to the system, with $f^{\mathcal{I}}_{\mathcal{C}_1}(t) = [f^x_{\mathcal{C}_1}(t) \quad f^y_{\mathcal{C}_1}(t) \quad f^z_{\mathcal{C}_1}(t)]'$, in which $f^x_{\mathcal{C}_1}, f^y_{\mathcal{C}_1}, f^z_{\mathcal{C}_1} \in \mathbb{R}_{\geq 0} \rightarrow \mathbb{R}$ are forces applied to the center of mass of the aircraft and oriented according to the inertial frame, $\mathcal{I}$, whose magnitudes are given in Figure 7.14. The results of the experiment are shown in Figures 7.15-7.20.

As can be observed, at the beginning of the experiment, the Tilt-rotor UAV starts far from the desired trajectory and converges to it. From 20 to 30 seconds, and 40 to 50 seconds, external forces with magnitude -15 N, given according to the $\vec{y} - axis$ and $\vec{z} - axis$ of the inertial frame, respectively, are applied at the center of gravity of the aircraft. At these intervals, the aircraft is pushed out from the desired trajectory and the $\mathcal{W}_\infty$ controller manipulates the control signals together with the stabilized degrees of freedom to attenuate these disturbances.

It is noteworthy that to handle the lateral environmental wind, the Tilt-rotor UAV performs the experiment with a displacement in the yaw angle. Moreover, as illustrated in Figures 7.19 and 7.20, since the control aerodynamic surfaces are not employed by the control system, the experiment is carried out with the controller making use only of the group of thrusters and the servomotors. In the first experiment, the Tilt-rotor UAV accomplished the mission and reach the final destination.

In the second experiment, the Tilt-rotor UAV is designated to track the desired trajectory present in Table 7.3. This trajectory is composed of six stretches. In the first stretch, the UAV must take-off from a home point while accelerating in forward motion. In the second stretch, the UAV reaches the cruise speed (33 m/s) and performs forward flight with constant altitude. In the third stretch, it performs a circular path with constant altitude and cruise speed. At the end of this stretch, the UAV performs forward flight

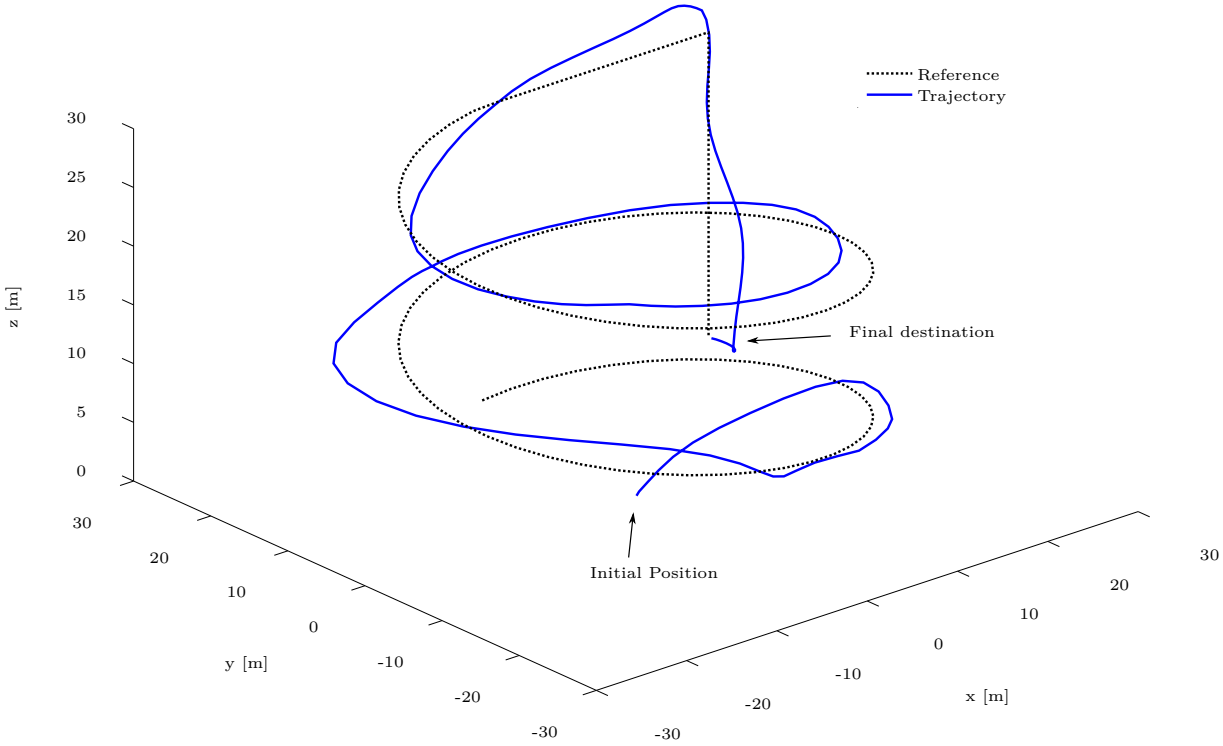

Figure 7.15: Tilt-rotor UAV trajectory in the 3D view, resulting from the application of the nonlinear $\mathcal{W}_\infty$ controller in the first scenario.

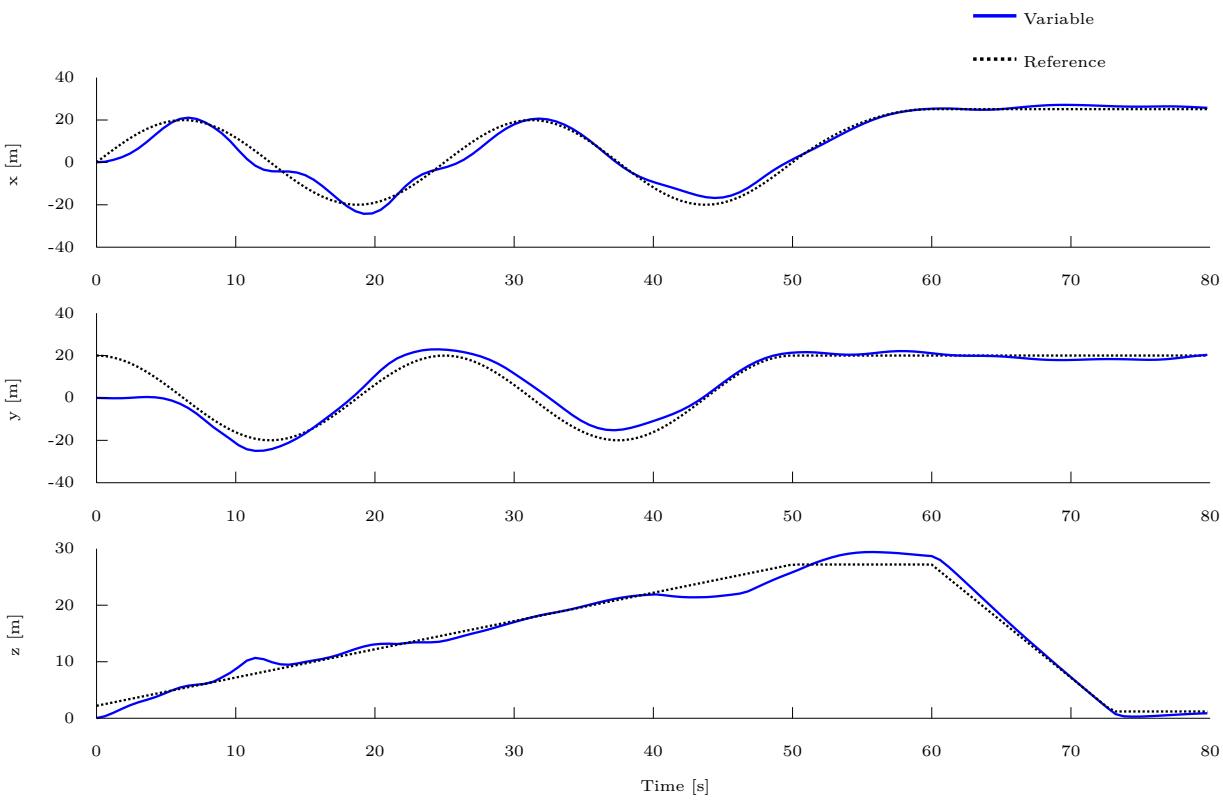

Figure 7.16: Tilt-rotor UAV translational position, resulting from the application of the nonlinear $\mathcal{W}_\infty$ controller in the first scenario.

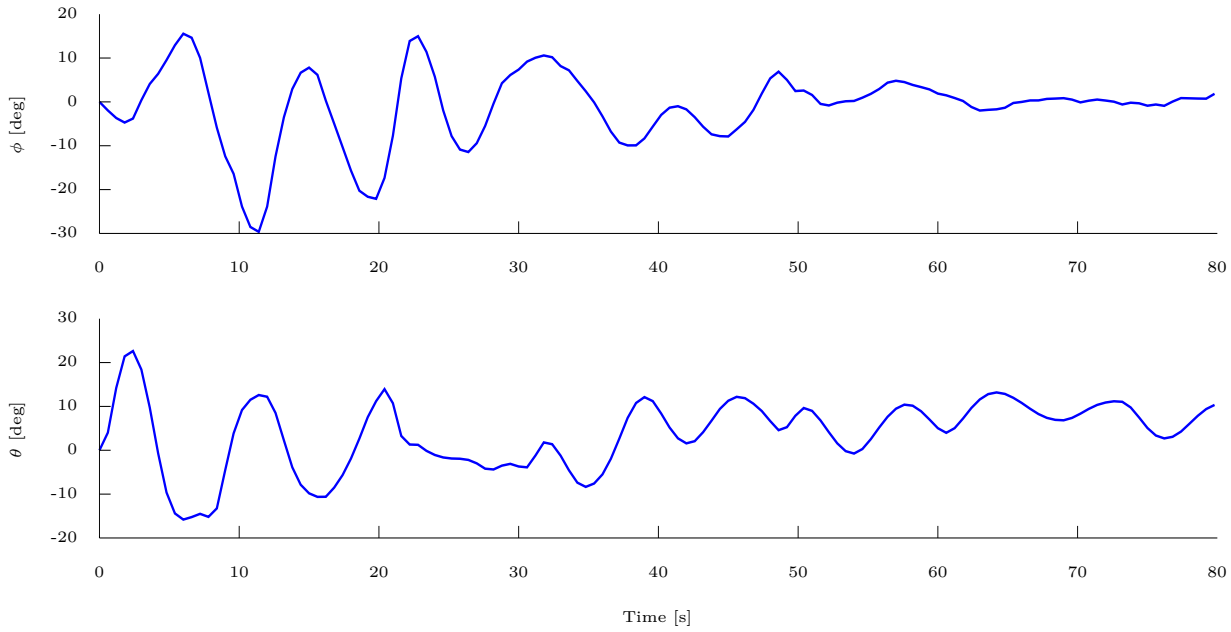

Figure 7.17: Tilt-rotor UAV roll and pitch angles, resulting from the application of the nonlinear $\mathcal{W}_\infty$ controller in the first scenario.

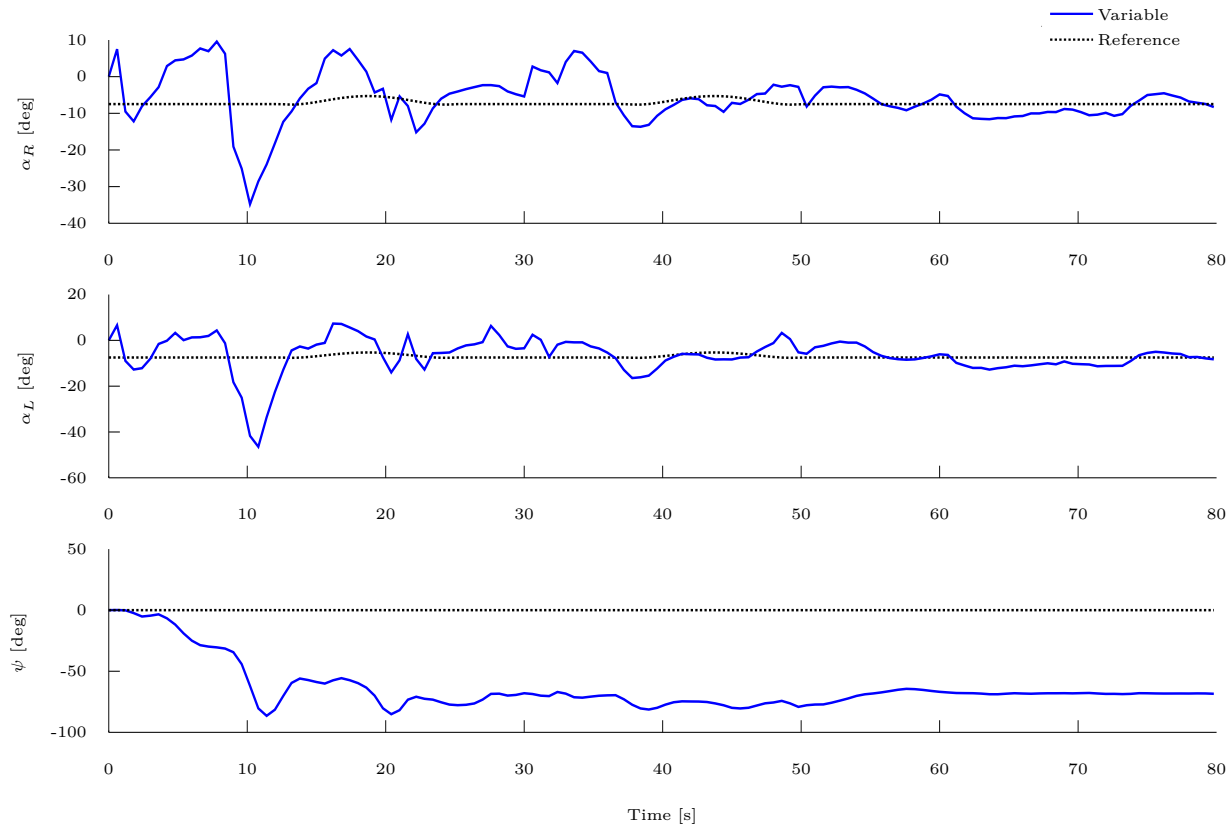

Figure 7.18: Tilt-rotor UAV tilting angles of the servomotors and yaw angle, resulting from the application of the nonlinear $\mathcal{W}_\infty$ controller in the first scenario.

again. Then, in the fifth and sixth stretches it decelerates and lands at a final destination, remaining at this position. In addition, during the experiment, the Tilt-rotor UAV

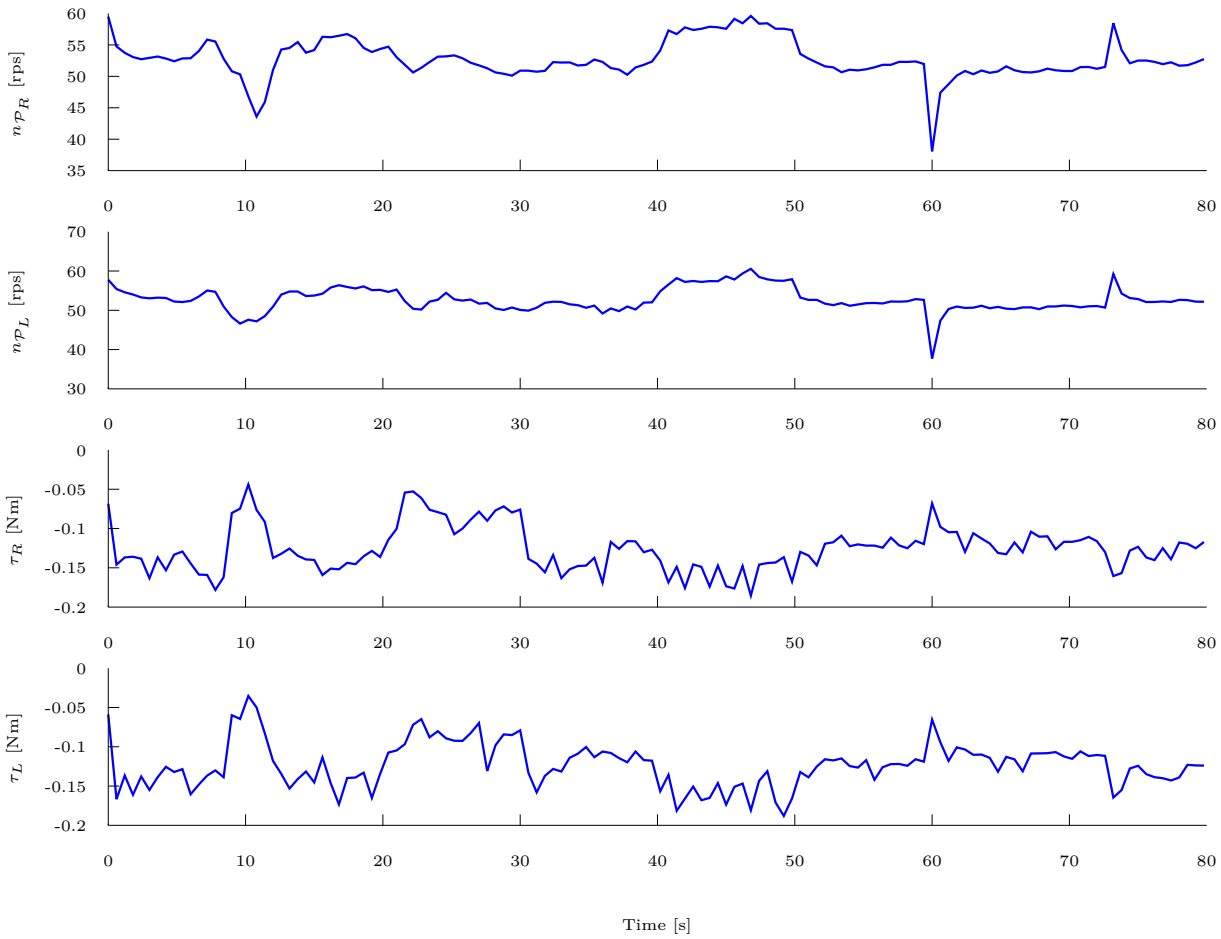

Figure 7.19: Tilt-rotor UAV propellers angular velocity and servomotor torques, resulting from the application of the nonlinear $\mathcal{W}_\infty$ controller in the first experiment.

is subjected to disturbances from wind gusts[8].

In the numerical experiments, the Tilt-rotor UAV starts with the initial condition $\boldsymbol{q}(0) = \dot{\boldsymbol{q}}(0) = \mathbf{0}$. Similarly to the previous experiment, the aircraft is subjected to a constant environment wind, with magnitude $\zeta_x = -3$ m/s, and also to wind gusts ζ_x, ζ_y with profile according to Figure 7.21. The results of the second numerical experiment are present in Figures 7.22-7.27.

Note that, at the beginning of the experiment, during the transition from helicopter to cruise flight mode, and also at the end of the experiment, during the transition from cruise to helicopter-flight mode, external disturbances and wind gusts are applied to the aircraft, as illustrated in Figure 7.21. All these disturbances were attenuated by the control system.

Observe that the circular path is performed with a roll angle. This behavior is physically necessary to project lift forces at the horizontal plane, allowing the Tilt-rotor UAV to perform turning flight. Moreover, as in the previous experiment, the yaw angle is

[8]In the numerical experiments, the changes in the magnitude of the relative wind speed, angle of attack, and side-slip angle originated from wind gusts are not measured, contradicting Assumption 19, so are considered as external disturbances by the control system.

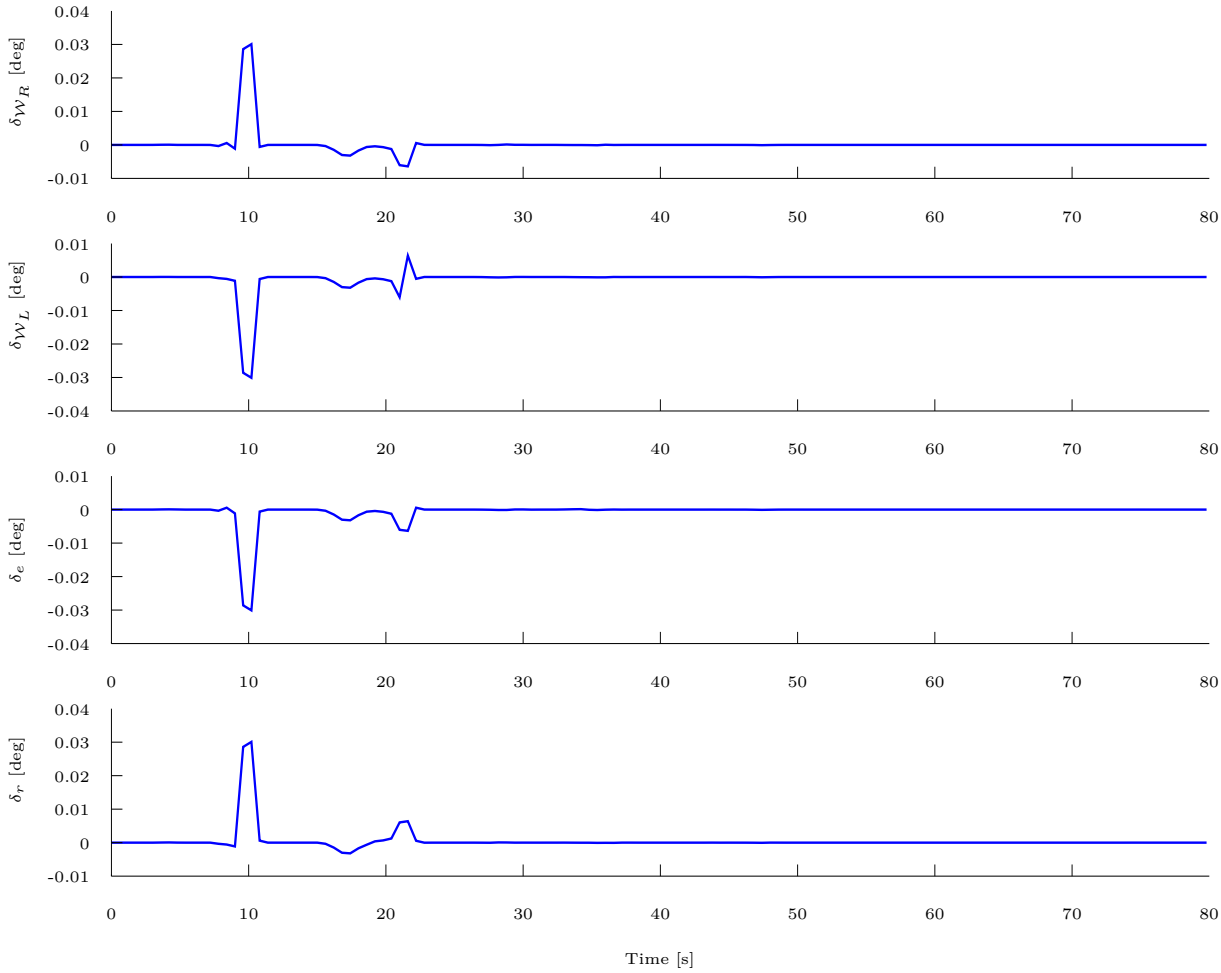

Figure 7.20: Tilt-rotor UAV deflection of the aerodynamic surfaces, resulting from the application of the nonlinear $\mathcal{W}_\infty$ controller in the first scenario. For the sake of simplicity, the tail control surfaces are represented by the equivalent deflection in the elevator and rudder, which are computed as $\delta_e = \frac{1}{2}(\delta_{\tau_R} + \delta_{\tau_L})$ and $\delta_r = \frac{1}{2}(\delta_{\tau_R} - \delta_{\tau_L})$.

displaced from the desired value due to the lateral wind affecting the system.

It is noteworthy that, due to the high magnitude of the relative wind speed, when the aircraft is in cruising, the propellers lose efficiency requiring a higher angular velocity (see Figure 7.26). Besides, the aerodynamic control surfaces are not employed when the Tilt-rotor UAV is in helicopter-flight mode (see Figure 7.27).

In the second experiment, the $\mathcal{W}_\infty$ controller was able to stabilize the stabilized DOF and manipulate the control inputs to attenuate the effects of the disturbances and track the desired trajectory. As in the previous experiment, the Tilt-rotor UAV attenuated disturbances and successfully reached the final destination.

Finally, it is worth highlighting that the Tilt-rotor UAV achieved better tracking performance in the second experiment, in comparison with the first. This is because the Tilt-rotor UAV have different dynamics in hovering, transition, and cruise flight modes, however, controller considers the same tuning for all the flight modes.

Table 7.3: Desired trajectory for the Tilt-rotor UAV translational position and yaw angle.

	$x_r(t)$	$y_r(t)$
$t \leq 66$	$\frac{t^2}{4}$	0
$66 < t \leq 86$	$33(t-66)+1089$	0
$86 < t \leq 146$	$420.17\cos(\frac{2\pi(t-86)}{80}-\frac{\pi}{2})+1749$	$420.17\sin(\frac{2\pi(t-86)}{80}-\frac{\pi}{2})+420.17$
$146 < t \leq 166$	1328.8	$420.17-33(t-146)$
$166 < t \leq 232$	1328.8	$-239.8-33(t-232)+\frac{(t-232)^2}{4}$
$232 < t$	1328.2	-1328.8
	$z_r(t)$	$\psi_r(t)$
$t \leq 66$	$\frac{115t^2}{1000}$	0
$66 < t \leq 86$	50	0
$86 < t \leq 146$	50	$\frac{2\pi(t-86)}{80}$
$146 < t \leq 166$	50	$\frac{3\pi}{2}$
$166 < t \leq 232$	$50-\frac{110(t-232)^2}{1000}$	$\frac{3\pi}{2}$
$232 < t$	1	$\frac{3\pi}{2}$

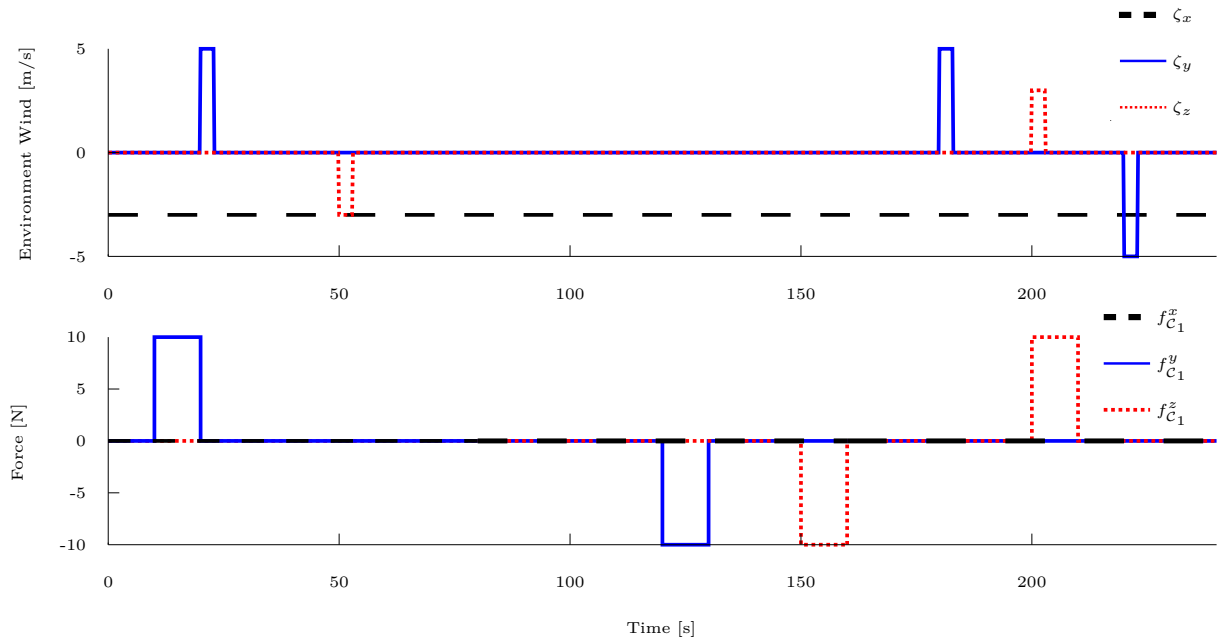

Figure 7.21: Environment wind and external disturbances applied in the second scenario.

7.4 Final Remarks

This chapter presented the modeling and the design of linear and nonlinear controllers for the Tilt-rotor UAV performing trajectory tracking when in hovering and for the full flight envelope.

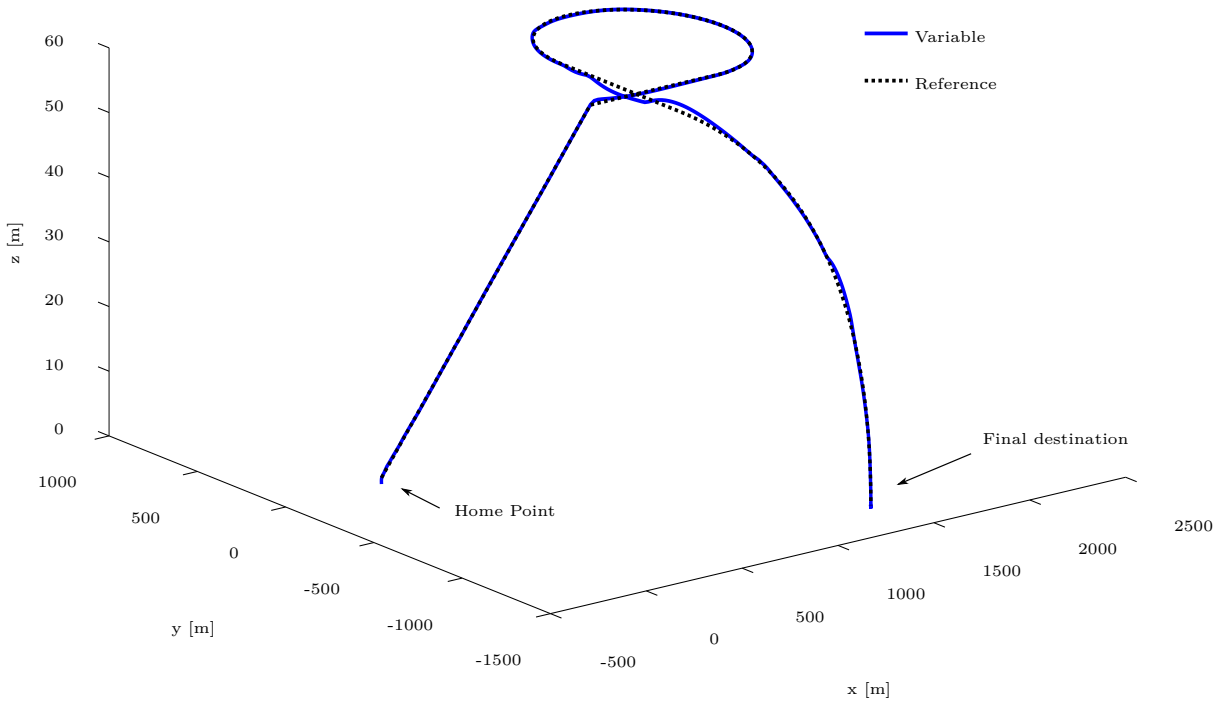

Figure 7.22: Tilt-rotor UAV trajectory in the 3D view, resulting from the application of the nonlinear $\mathcal{W}_\infty$ controller in the second scenario.

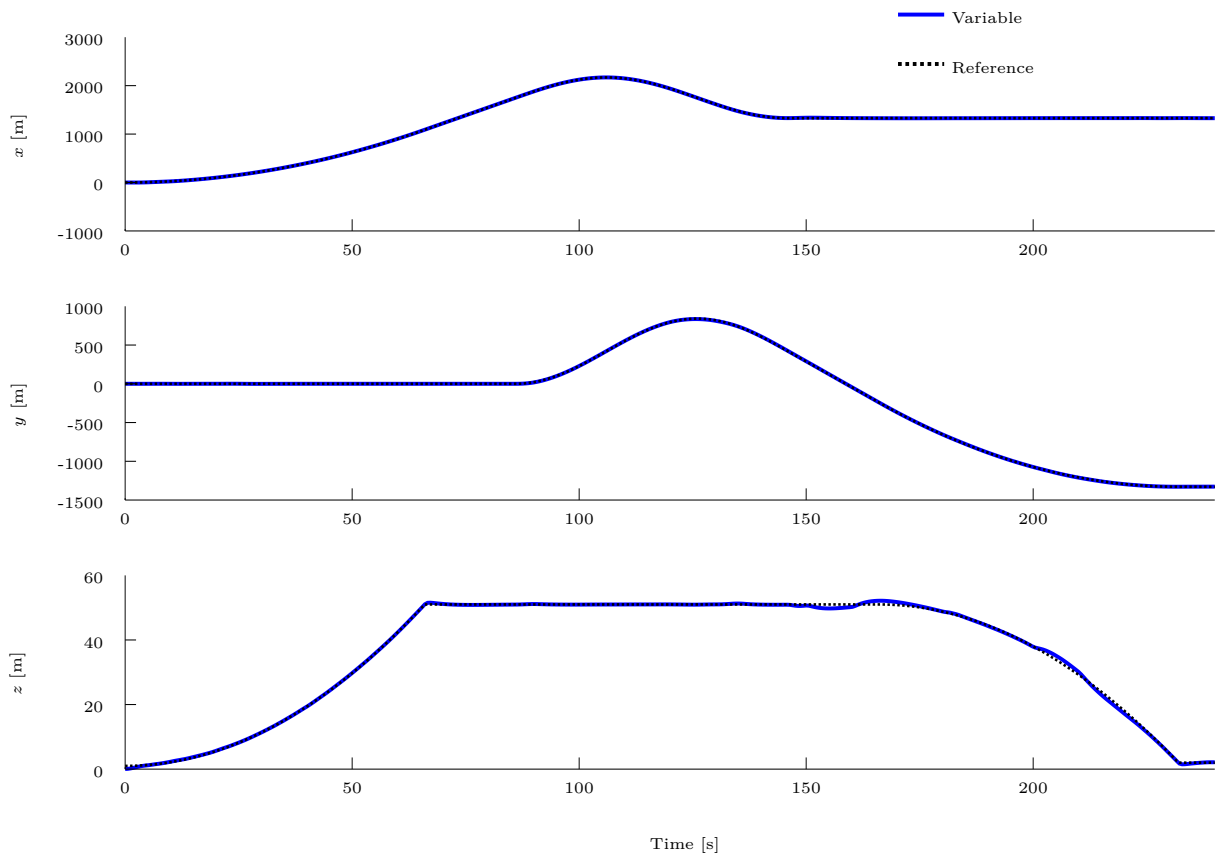

Figure 7.23: Tilt-rotor UAV translational position, resulting from the application of the nonlinear $\mathcal{W}_\infty$ controller in the second scenario.

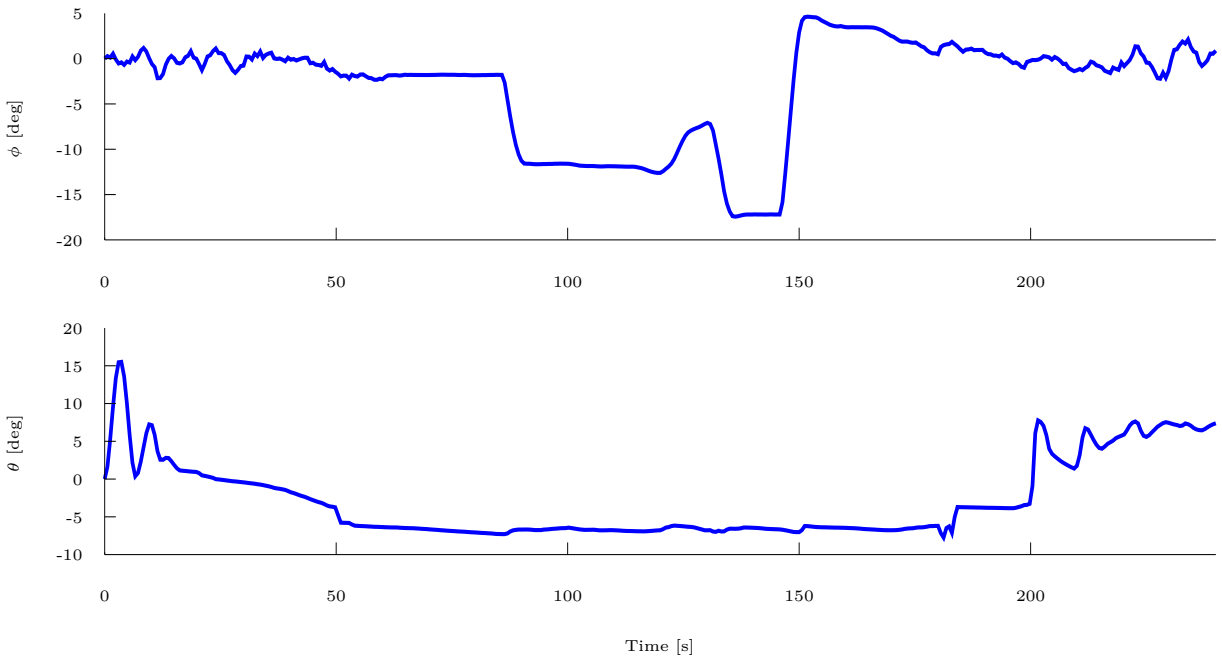

Figure 7.24: Tilt-rotor UAV roll and pitch angles, resulting from the application of the nonlinear $\mathcal{W}_\infty$ controller in the second scenario.

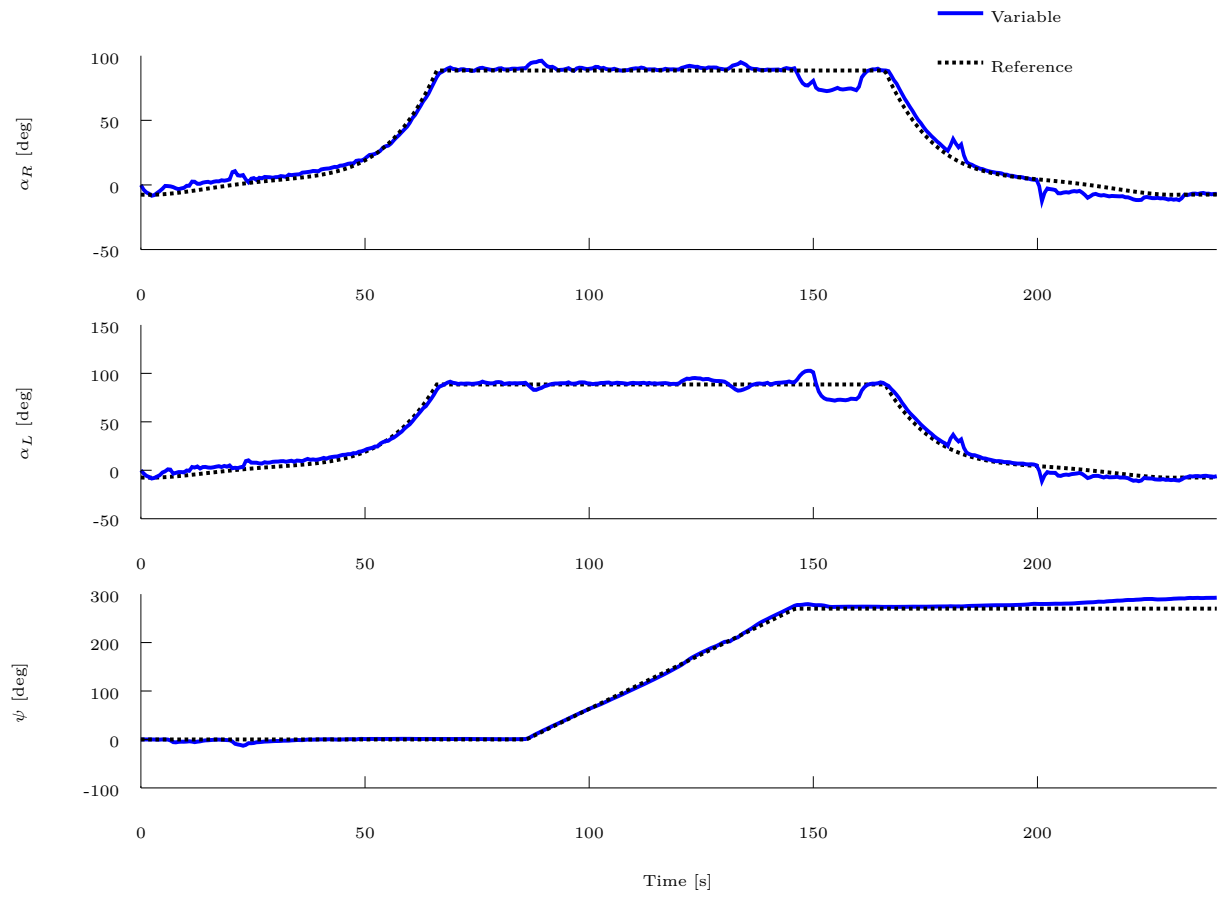

Figure 7.25: Tilt-rotor UAV tilting angles of the servomotors and yaw angle, resulting from the application of the nonlinear $\mathcal{W}_\infty$ controller in the second scenario.

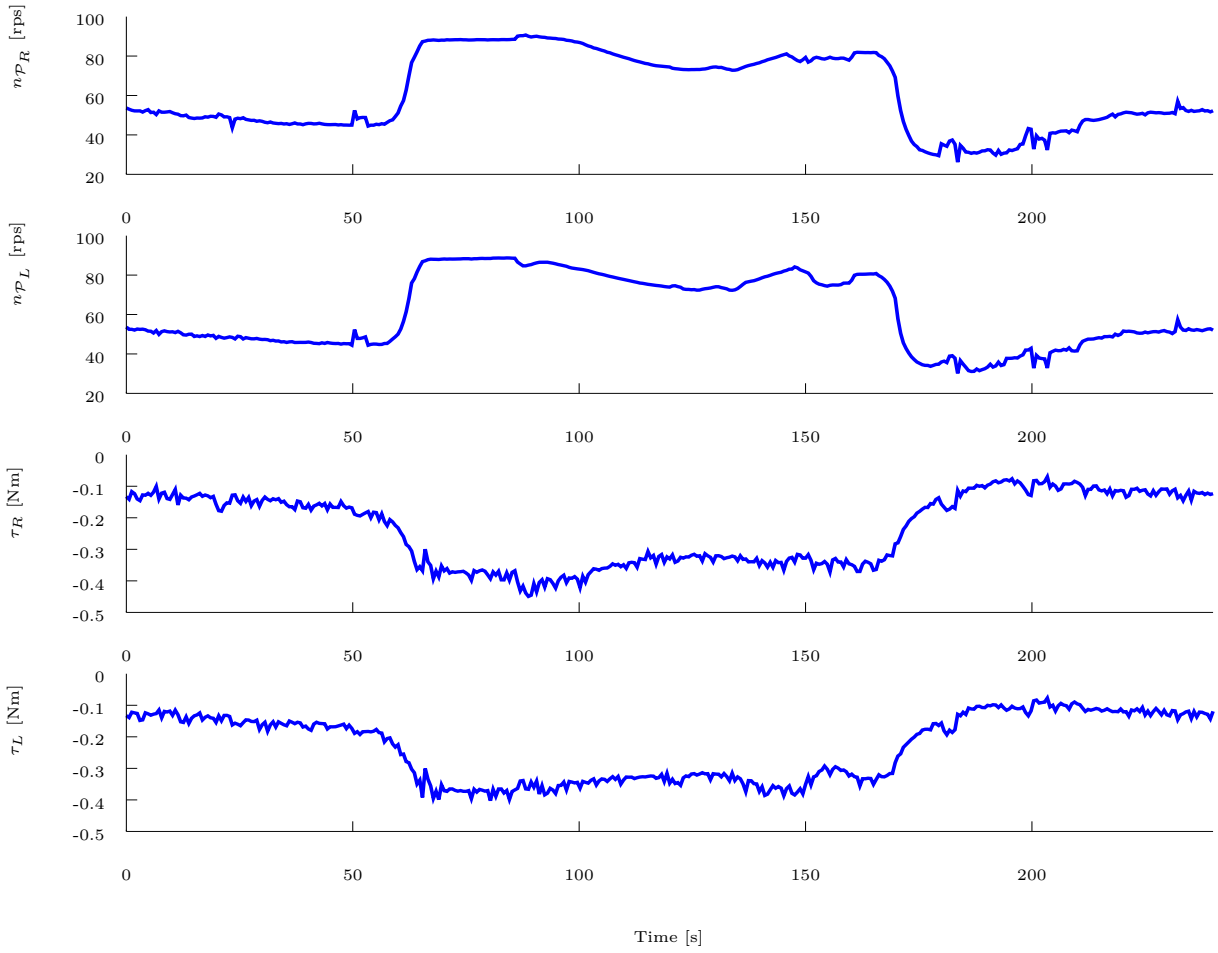

Figure 7.26: Tilt-rotor UAV propellers angular velocities and servomotor torques, resulting from the application of the nonlinear $\mathcal{W}_\infty$ controller in the second scenario.

A detailed modeling of the nonlinear multi-body dynamics of the Tilt-rotor UAV was conducted using the Euler-Lagrange formalism. Also, the non-conservative forces and torques generated by the propellers, servomotors, fuselage, wings, tail surfaces, and aerodynamic interference were computed and mapped to the vector of generalized forces. This aircraft was implement on the ProVANT Simulator using the CAD model and data from wind tunnel experiment, in which numerical experiments were conducted.

Initially, full-state and dynamic output feedback linear $\mathcal{W}_\infty$ controllers were synthesized for the Tilt-rotor UAV considering all the approaches addressed in Chapter 6. For the sake of control design, the Von Kàrmàn wind turbulence model was used to simulate the environment wind. The dynamics of this turbulence model was then used to design the controllers addressed in Section 6.3 (here called $\mathcal{W}_\infty$-D controllers). Comparison analysis was performed between the controllers, which verified that, although all the controllers achieved good results dealing with the helicopter-flight mode of the Tilt-rotor UAV, the $\mathcal{W}_\infty$-D controllers achieved a better disturbance attenuation with a smaller control effort.

Moreover, a nonlinear $\mathcal{W}_\infty$ controller was proposed to solve the full flight envelope

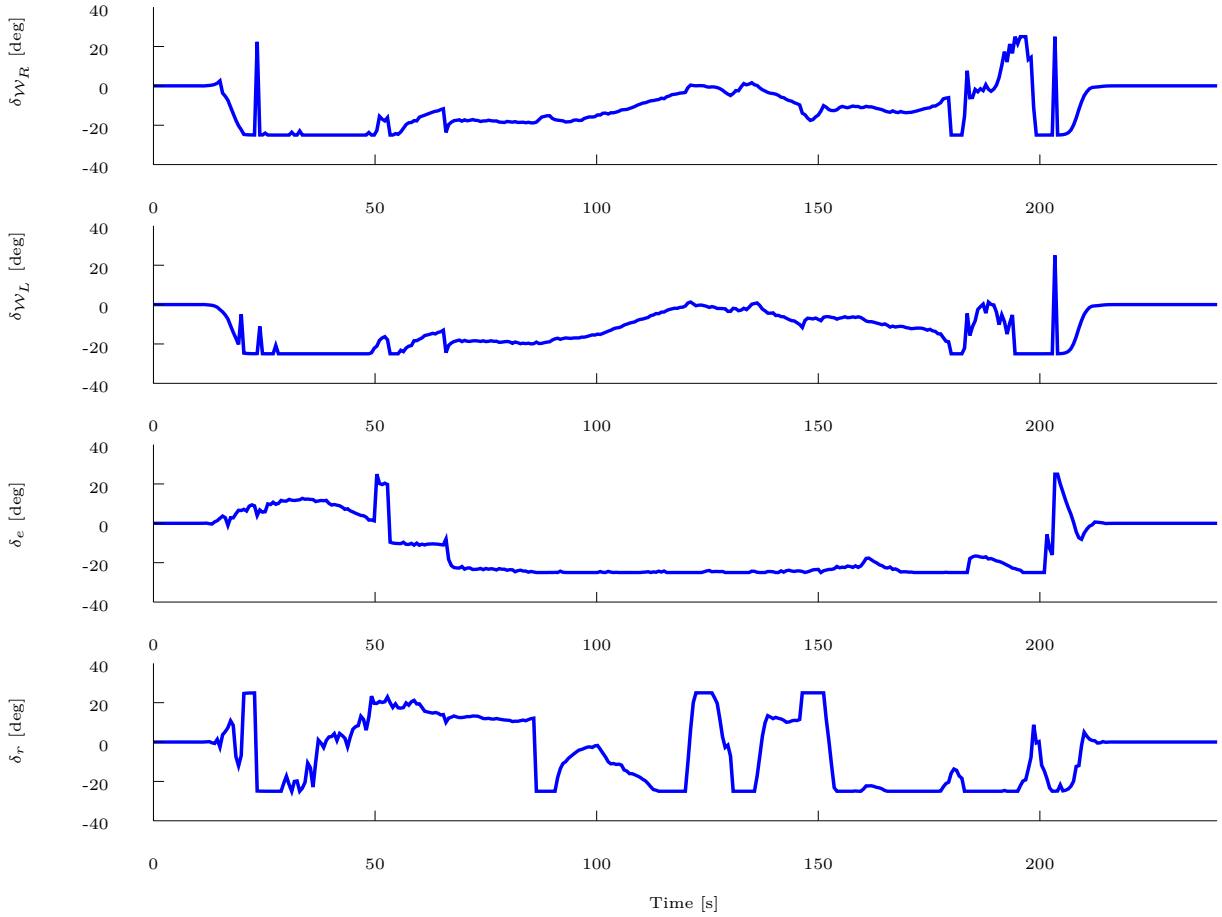

Figure 7.27: Tilt-rotor UAV deflection of the aerodynamic surfaces, resulting from the application of the nonlinear $\mathcal{W}_\infty$ controller in the second scenario. For the sake of simplicity, the tail control surfaces are represented by the equivalent deflection in the elevator and rudder, which are computed as $\delta_e = \frac{1}{2}(\delta_{\mathcal{T}_R} + \delta_{\mathcal{T}_L})$ and $\delta_r = \frac{1}{2}(\delta_{\mathcal{T}_R} - \delta_{\mathcal{T}_L})$.

trajectory tracking problem of the convertible Tilt-rotor UAV. In order to design this controller, the nonlinear control approach addressed in Section 5.2 was extended to the case in which the mechanical system is partitioned with respect to stabilized, regulated, and controlled DOF. Additionally, a control allocation scheme was also proposed to handle with the time-varying rank of the input coupling matrix, mapping the generalized optimal control law to the control inputs signals properly, by taking into account the magnitude of the relative wind speed. The efficiency of the nonlinear controller was verified in two different kind of scenarios. The first scenario concerns the operation of the Tilt-rotor UAV in the helicopter-flight mode, while the second scenario concerns the transition from hovering to cruise flight mode, and vice-versa, and turning flight level. The Tilt-rotor UAV was able to satisfactorily track the desired trajectory and attenuate the effects of external disturbances in both scenarios. From the best knowledge of the author, this is the first work that proposes a single nonlinear controller to cope with the full flight envelope of the Tilt-rotor UAV continuously, dealing with multi-body dynamics without

using any cascade strategy or simplifications on the mathematical model.

The next chapter concludes the thesis and presents some future work proposals.

8

Conclusions

This chapter summarizes the main contributions obtained in this doctoral thesis, and concludes the text. Future work proposals are also presented and detailed at the end of this chapter.

8.1 Overview and contributions

This doctoral thesis proposed new formulations of the $\mathcal{H}_2$ and $\mathcal{H}_\infty$ controllers in weighted Sobolev spaces with the aim of aggregating an improved transient performance to the closed-loop system. This manuscript was divided into eight chapters, whose content and contributions are detailed below.

Chapter 1 motivated the development of the $\mathcal{W}_2$ and $\mathcal{W}_\infty$ controllers and exposed the gap of the classic $\mathcal{H}_2$ and $\mathcal{H}_\infty$ controllers in providing little control over the transient performance of the closed-loop. Also, it presented the justification, and the objectives of this doctoral thesis.

Chapter 2 presented a detailed literature review on the main topics of interest in this doctoral thesis, namely the $\mathcal{H}_2$ and $\mathcal{H}_\infty$ control approaches, the Sobolev space and its applications in control theory, and approximate solutions to the Hamilton-Jacobi (HJ) equation. It was presented all the works used on the basis of this doctoral thesis.

Chapter 3 presented some preliminary concepts and definitions necessary to the development of this doctoral thesis. It was addressed the following topics: the Lebesgue and Sobolev spaces, interesting features of the $\mathcal{W}_2$ and $\mathcal{W}_\infty$ control formulations in the

weighted Sobolev space, the Hamilton-Jacobi-Bellman equation; the method of Galerkin; and the Euler-Lagrange formulation. In addition, this chapter highlighted interesting features of the $\mathcal{W}_2$ and $\mathcal{W}_\infty$ control formulation in the Sobolev space, such as the nonnecessity of the resulting control signal to belong on the $\mathcal{L}_2$-space, and gives the interpretation of the $\mathcal{W}_\infty$-attenuation level.

Chapter 4 introduced the nonlinear $\mathcal{W}_2$ and $\mathcal{W}_\infty$ control approaches in the weighted Sobolev space. The control problems were formulated for autonomous nonlinear systems and the control problems were developed via dynamic-programming, resulting in complex HJ equations to be solved. Due to the difficult to solve analytically these HJ equations, numerical algorithms were proposed to achieve solutions. Numerical experiments were performed with a Two-wheeled Self-balanced vehicle, and a comparative analysis with the classic $\mathcal{H}_\infty$ controller was presented. The results demonstrated that the controllers resulting from the weighted Sobolev approach achieved a better transient performance with a faster disturbance attenuation. The contributions of this chapter can be summarized as:

- The extension of the $\mathcal{W}_2$ and $\mathcal{W}_\infty$ control approaches proposed in Aliyu and Boukas (2011a) to the weighted Sobolev space;
- The extension of the Successive Galerkin Approximation Algorithm proposed in Beard and McLain (1998) to approximate solutions of the HJ equations resulting from the $\mathcal{W}_2$ and $\mathcal{W}_\infty$ control approaches;
- The design of the $\mathcal{W}_2$ and $\mathcal{W}_\infty$ controllers for a Two-wheeled Self-balanced vehicle with a comparative analysis with the classic $\mathcal{H}_\infty$ controller.

Chapter 5 proposed new formulations of the nonlinear $\mathcal{H}_2$ and $\mathcal{H}_\infty$ optimal control approaches in the weighted Sobolev space in order to handle two classes of underactuated mechanical systems: the class of reduced underactuated mechanical systems, with the objective of achieving trajectory tracking of a reduced number of degrees of freedom, called controlled DOF; and the class of underactuated mechanical systems with input coupling, with the objective of driving the controlled DOF along a desired trajectory while stabilizing the remaining ones. The optimal control problems were formulated via dynamic-programming, and particular solutions were presented for the resulting HJ equations with the corresponding stability analysis. The concepts of $\mathcal{W}_{m,p,\boldsymbol{\sigma}}$-gain and $\mathcal{W}_{m,p,\boldsymbol{\sigma}}$-stability were established and applied for the particular case of studies. Moreover, it was shown that for the particular class of underactuated mechanical systems, whose control inputs and the disturbances vector span the same space in the vector of generalized forces, the $\mathcal{W}_2$ and $\mathcal{W}_\infty$ controllers become equivalent. Numerical results obtained with a fully actuated manipulator, a Two-wheeled Self-balanced vehicle, and a Quadrotor UAV demonstrated the efficiency of the proposed control strategies, and that they provided better transient

performance with faster response against external disturbances in comparison with a classic nonlinear $\mathcal{H}_\infty$ controller, in addition to have a simple design. The contributions of this chapter are summarized as follows:

- The proposal of the nonlinear $\mathcal{W}_2$ and $\mathcal{W}_\infty$ control problems and their formulations via dynamic programming for reduced underactuated mechanical systems, and the analytical solutions for the resulting HJ equation with the corresponding stability analysis;
- The proposal of the nonlinear $\mathcal{W}_2$ and $\mathcal{W}_\infty$ control problems and their formulations via dynamic programming for underactuated mechanical systems with input coupling, and the analytical solutions for the resulting HJ equation with the corresponding stability analysis;
- The establishment of the concepts of $\mathcal{W}_{m,p,\boldsymbol{\sigma}}$-stability and $\mathcal{W}_{m,p,\boldsymbol{\sigma}}$-gain for a general class of systems, with the demonstration for the particular case of studies;
- The design of the nonlinear $\mathcal{W}_2$ and $\mathcal{W}_\infty$ controllers for a fully actuated manipulator, a Two-wheeled Self-balanced vehicle, and a Quadrotor UAV;
- A comparative analysis of the results with a classic nonlinear $\mathcal{H}_\infty$ controller.

Chapter 6 formulated the linear $\mathcal{W}_\infty$ controller in the weighted Sobolev space, for linear time-invariant systems, via convex optimization problem with Linear Matrix Inequality (LMI) constraints. It addressed the design of full-state and dynamic output feedback controllers and introduced a new approach in which the dynamic behavior of the disturbances is taken into consideration in the control design stage by means of a disturbance model. In addition, pole placement constraints were incorporated, allowing the synthesis of $\mathcal{W}_\infty$ controllers with the closed-loop poles allocated in a predefined region of the complex plane. Also, the linear $\mathcal{W}_\infty$ control approach was extended to deal with uncertain systems. Numerical experiments with a simple linear system, a Two-wheeled Self-balanced vehicle, and a quadrotor UAV corroborated the efficiency of the linear $\mathcal{W}_\infty$ control approaches and demonstrated that they achieved better performance in comparison with a linear $\mathcal{H}_\infty$ controller. The contributions of this chapter are summarized as follows:

- The formulation of the $\mathcal{W}_\infty$ control strategy in the weighted Sobolev space for linear systems via semi-definite programming with LMI constraints, considering state and output feedback approaches;
- The formulation of the $\mathcal{W}_\infty$ control strategy taken into account the dynamics of the disturbance;

- The development of pole placement constraints that allow the synthesis of $\mathcal{W}_\infty$ controllers with the closed-loop poles allocated in a predefined region $\mathcal{D}$ of the complex plane;

- The extension of these controllers to deal with uncertain systems.

Chapter 7 synthesized $\mathcal{W}_\infty$ controllers for the Tilt-rotor UAV. Initially, a detailed modeling of the nonlinear multi-body dynamics of this UAV was conducted using the Euler-Lagrange formalism, and the non-conservative forces and torques generated by the propellers, servomotors, fuselage, wings, tail surfaces, and aerodynamic interference were computed and mapped to the vector of generalized forces. Then, the state and output feedback linear $\mathcal{W}_\infty$ controllers proposed in Chapter 6 were synthesized for the Tilt-rotor UAV, with the Von Kármán wind turbulence model being considered as the disturbance model. Numerical experiments were conducted in a high fidelity simulator. Although all the controllers achieved good results when flying in the helicopter-flight mode, the controllers designed considering the disturbance model in the cost functional achieved better disturbance attenuation with a smaller control effort and improved IADU and ISE performance indexes.

Still in Chapter 7, a nonlinear $\mathcal{W}_\infty$ controller was proposed to solve the full flight envelope trajectory tracking problem of a convertible Tilt-rotor UAV. In order to design this controller, the nonlinear control approach addressed in Section 5.2 was extended to the case in which the mechanical system is partitioned with respect to stabilized, regulated, and controlled DOF. In addition, a control allocation scheme was proposed to handle the time-varying rank of the Tilt-rotor UAV input coupling matrix, mapping the generalized optimal control law to the control input signals properly, by taking into account the magnitude of the relative wind-speed. This controller was also implemented in a high fidelity simulator, and the performance was evaluated when the Tilt-rotor UAV is performing the following maneuvers: transition from hovering to cruise-flight mode, and vice-versa, turning flight level, and hovering. The Tilt-rotor UAV was able to satisfactorily track the desired trajectory and attenuate the effects of external disturbances. The contributions of this chapter are summarized as follows:

- A detailed modeling of the nonlinear multi-body dynamics of the Tilt-rotor UAV using the Euler-Lagrange formalism;

- The design of state and output feedback linear $\mathcal{W}_\infty$ controllers for the Tilt-rotor UAV to handle the helicopter-flight mode;

- The extension of the nonlinear $\mathcal{W}_\infty$ control approach addressed in Section 5.2 to the case in which the mechanical system is partitioned with respect to stabilized, regulated, and controlled DOF.

- The design of a nonlinear $\mathcal{W}_\infty$ controller for the Tilt-rotor UAV to achieve trajectory tracking through the full flight envelope;

8.2 Future work

This section describes some possible directions for future work derived from the contributions presented in this doctoral thesis.

- As commented in Chapter 7, the tilt-rotor UAV is being constructed at the Federal University of Minas Gerais. Therefore, an immediately goal is the implementation of the control strategies presented in this thesis in the real aircraft.

- The numerical algorithms proposed in Chapter 4 to approximate solutions of the HJ equations suffer from the curse of dimensionality, which may prevent their application for systems with several states, as for example the Tilt-rotor UAV. To circumvent this issue, an immediate future work is the implementation of the proposed algorithm using parallelization procedures in Graphics Processing Units (GPUs).

- Following the research line presented above, a future work is to approximate solutions of the HJ equations using Neural networks.

- The nonlinear $\mathcal{W}_2$ and $\mathcal{W}_\infty$ controllers proposed in Section 5.2 for underactuated mechanical systems with input coupling uses pseudo-inverse mapping to compute the control input vector. Therefore, future works include the reformulation of these controllers to avoid the use of pseudo-inverse mapping.

- One drawback when designing controllers for UAVs is whether all states are accessible. Therefore, a future work is the extension of the nonlinear $\mathcal{W}_2$ and $\mathcal{W}_\infty$ controllers to the output feedback case.

- Finally, another future work is the design of a Robust Adaptive Mixing Controller (RAMC) controller (Cardoso et al., 2021c) to solve the full fight envelope trajectory tracking problem of the convertible plane Tilt-rotor UAV. In this case, the candidate controllers can be synthesized through the linear $\mathcal{W}_\infty$ controllers proposed in Chapter 6, with the linear parameter-varying (LPV) model of the Tilt-rotor UAV obtained through Tensor Product (TP) transformations (Baranyi, 2004). In addition, the magnitude of the relative wind speed, the angle of attack, and the side-slip angle are taken into account in the design of the RAMC.

Bibliography

Adams, R. A. and Fournier, J. J. (2003). *Sobolev Spaces (Pure and Applied Mathematics; V. 140)*, Elsevier.

Aguilar, L. T., Orlov, Y. and Acho, L. (2003). Nonlinear $\mathcal{H}_\infty$-control of nonsmooth time-varying systems with application to friction mechanical manipulators, *Automatica* **39**(9): 1531–1542.

Alessandri, A. and Sanguineti, M. (2007). Input-output stability for optimal estimation problems, *Int'l Math. Forum*, Vol. 2, pp. 593–617.

Aliyu, M. and Boukas, E. K. (2011a). Extending nonlinear $\mathcal{H}_2$, $\mathcal{H}_\infty$ optimisation to $\mathcal{W}_{1,2}$, $\mathcal{W}_{1,\infty}$ spaces - part I: optimal control, *Int'l J. of Systems Science* **42**(5): 889–906.

Aliyu, M. and Boukas, E. K. (2011b). Extending nonlinear $\mathcal{H}_2$, $\mathcal{H}_\infty$ optimisation to $\mathcal{W}_2$ and $\mathcal{W}_\infty$ spaces-part II: optimal estimation and ouput-feedback control, *International Journal of Systems Science* **42**(5): 907–920.

Almeida, M., Donadel, R., Raffo, G. and Becker, L. (2014). Full control of a tiltrotor UAV for load transportation, *Proc. of XXth Congresso Brasileiro de Automatica, CBA*, pp. 2097–2104.

Almeida, M. M. and Raffo, G. V. (2015). Nonlinear control of a tiltrotor UAV for load transportation, *Proc. of the ACNAAV'15 IFAC*, pp. 232–237.

Amiri, N., Ramirez-Serrano, A. and Davies, R. (2011). Modelling of opposed lateral and longitudinal tilting dual-fan unmanned aerial vehicle, *18th International Federation of Automatic Control World Congress* **44**(1): 2054–2059.

Aquino, J. E. M., Cardoso, D. N. and Raffo, G. V. (2020). Robust optimal nonlinear control strategies for an aerial manipulator, *Anais do XXIII CONGRESSO BRASILEIRO DE AUTOMÁTICA (CBA2020)*, pp. 1–12.

Aquino, J. E. M., Cardoso, D. N. and Raffo, G. V. (2021a). Modeling and control of an aerial manipulator from the perspective of its end-effector, *Proc. of the Simpósio Brasileiro de Automação Inteligente 2021 (SBAI2021)*.

Aquino, J. E. M., Cardoso, D. N. and Raffo, G. V. (2021b). Robust nonlinear control of aerial manipulators, *Journal of Control, Automation and Electrical Systems* pp. 1–19. Submitted.

Baranyi, P. (2004). Tp model transformation as a way to LMI-based controller design, *IEEE Transactions on Industrial Electronics* **51**(2): 387–400.

Beard, R. W. (1995). *Improving the closed-looped performance of nonlinear systems*, PhD thesis, Rensselaer Polutechnic Institute.

Beard, R. W. and McLain, T. W. (1998). Successive galerkin approximation algorithms for nonlinear optimal and robust control, *International Journal of Control* **71**(5): 717–743.

Beard, R. W., Saridis, G. N. and Wen, J. T. (1997). Galerkin approximations of the generalized Hamilton-Jacobi-Bellman equation, *Automatica* **33**(12): 2159–2177.

Beard, R. W., Saridis, G. N. and Wen, J. T. (1998). Approximate solutions to the time-invariant Hamilton-Jacobi-Bellman equation, *Journal of Optimization theory and Applications* **96**(3): 589–626.

Beard, R. W., Saridis, G. and Wen, J. (1996). Improving the performance of stabilizing controls for nonlinear systems, *IEEE Control Systems Magazine* **16**(5): 27–35.

Bourles, H. and Colledani, F. (1995). W-stability and local input-output stability results, *IEEE Trans. Autom. Control* **40**(6): 1102–1108.

Boyd, S., El Ghaoui, L., Feron, E. and Balakrishnan, V. (1994). *Linear matrix inequalities in system and control theory*, SIAM.

Calise, A. J. and Rysdyk, R. T. (1998). Nonlinear adaptive flight control using neural networks, *IEEE control systems* **18**(6): 14–25.

Campos, J., Cardoso, D. N. and Raffo, G. V. (2021). Modeling and robust control for full-flight envelope trajectory tracking of a quadcp-vtol unmanned aerial vehicle, *In proc of The Vertical Flight Society's 77th Annual Forum & Technology Display (VFS2021)*, pp. 1–17.

Cardoso, D. N., Campos, J., Esteban, S., Normey-rico, J. E. and Raffo, G. V. (2019). Modelagem e simulação de um VANT convertível tilt-rotor, *Anais do II Congresso Aeroespacial Brasileiro.*, pp. 1–16.

Cardoso, D. N., Esteban, S. R. and Raffo, G. V. (2021a). A robust optimal control approach in the weighted sobolev space for underactuated mechanical systems, *Automatica* **125**: 1–11.

Cardoso, D. N., Esteban, S. and Raffo, G. V. (2018a). Nonlinear $\mathcal{H}_2$ and $\mathcal{H}_\infty$ control formulated in the sobolev space for mechanical systems, *In Proc. of 9th Symposium on Robust Control Design (ROCOND2018)*, pp. 3812–3817.

Cardoso, D. N., Esteban, S. and Raffo, G. V. (2018b). Nonlinear $\mathcal{H}_2$ and $\mathcal{H}_\infty$ control formulated in the weighted sobolev space for underactuated mechanical systems with input coupling, *In Proc. of 57th IEEE Conference on Decision and Control (CDC2018)*, IEEE, pp. 3812–3817.

Cardoso, D. N., Esteban, S. and Raffo, G. V. (2018c). Nonlinear $\mathcal{H}_\infty$ and $\mathcal{W}_\infty$ control approaches - a comparison analysis, *In Proc. of XXII Congresso Brasileiro de Automática (CBA2018)*, pp. 1–8.

Cardoso, D. N., Esteban, S. and Raffo, G. V. (2019). A nonlinear $\mathcal{W}_\infty$ controller of a tilt-rotor UAV for trajectory tracking, *Proc. of European Control Conference*, IEEE, pp. 928–934.

Cardoso, D. N., Esteban, S. and Raffo, G. V. (2021b). A linear robust control framework in the weighted sobolev space via LMIs, *To be submitted* pp. 1–14.

Cardoso, D. N., Esteban, S. and Raffo, G. V. (2021c). A new robust adaptive mixing control for trajectory tracking with improved forward flight of a tilt-rotor UAV, *ISA transactions* **110**: 86–104.

Cardoso, D. N., Esteban, S. and Raffo, G. V. (2021d). A robust nonlinear controller in the weighted sobolev space for trajectory tracking throughout the full flight envelope of a tilt-rotor UAV, *To be submitted* pp. 1–14.

Cardoso, D. N. and Raffo, G. V. (2018). Approximated solutions to the nonlinear $\mathcal{H}_2$ and $\mathcal{H}_\infty$ control approaches formulated in the sobolev space, *In Proc. of European Control Conference 2018 (ECC2018)*, pp. 3812–3817.

Cardoso, D. N., Raffo, G. V. and Esteban, S. (2016a). Modeling and control of a tilt-rotor UAV with improved forward flight, *In Proc. of XXIth Congresso Brasileiro de Automatica*, pp. 2473–2478.

Cardoso, D. N., Raffo, G. V. and Esteban, S. (2016b). A robust adaptive mixing control for improved forward flight of a tilt-rotor UAV, *Intelligent Transportation Systems (ITSC), 2016 IEEE 19th International Conference on*, IEEE, pp. 1432–1437.

Chen, B.-S., Lee, T.-S. and Chang, W.-S. (1996). A robust $\mathcal{H}_\infty$ model reference tracking design for non-holonomic mechanical control systems, *International Journal of Control* **63**(2): 283–306.

Chen, B. S., Lee, T. S. and Feng, J. H. (1994). A nonlinear $\mathcal{H}_\infty$ control design in robotic systems under parameter perturbation and external disturbance, *Int'l J. of Control* **59**(2): 439–461.

Chen, C.-T. and Chen, C.-T. (1984). *Linear system theory and design*, Vol. 301, Holt, Rinehart and Winston New York.

Chen, C., Zhang, J., Zhang, D. and Shen, L. (2017). Control and flight test of a tilt-rotor unmanned aerial vehicle, *International Journal of Advanced Robotic Systems* **14**(1): 1–12.

Cheng, Y. and Shu, C.-W. (2007). A discontinuous galerkin finite element method for directly solving the Hamilton-Jacobi equations, *Journal of Computational Physics* **223**(1): 398–415.

Cheng, Y. and Wang, Z. (2014). A new discontinuous galerkin finite element method for directly solving the hamilton-jacobi equations, *Journal of Computational Physics* **268**: 134–153.

Chilali, M. and Gahinet, P. (1996). $\mathcal{H}_\infty$ design with pole placement constraints: An LMI approach, *IEEE Transactions on automatic control* **41**(3): 358–367.

Curtis, J. W. and Beard, R. W. (2001). Successive collocation: An approximation to optimal nonlinear control, *Proceedings of the American Control Conference, 2001*, Vol. 5, IEEE, pp. 3481–3485.

Czyba, R., Lemanowicz, M., Simon, M., Kudala, T., Gorol, Z., Galeja, M., Hanke, K., Sikora, A., Grabowski, W., Ryczko, Ł. et al. (2018). Development of an unmanned vertical take-off and landing aircraft for medical express UAV challenge, *2018 23rd International Conference on Methods & Models in Automation & Robotics (MMAR)*, IEEE, pp. 461–466.

Daniel, K. and Wietfeld, C. (2011). Using public network infrastructures for UAV remote sensing in civilian security operations, *Technical report*, DORTMUND UNIV (GERMANY FR).

Dickeson, J. J., Mix, D. R., Koenig, J. S., Linda, K. M., Cifdaloz, O., Wells, V. L. and Rodriguez, A. A. (2005). h_∞ hover-to-cruise conversion for a tilt-wing rotorcraft, *Proceedings of the 44th IEEE Conference on Decision and Control*, IEEE, pp. 6486–6491.

Dlotko, T. (2014). Sobolev spaces and embedding theorems, *Technical report*, Citeseer.

Donadel, R. (2015). *Modeling and control of a tiltrotor unmanned aerial vehicle for path tracking*, Master's thesis, Federal University of Santa Catarina.

Donadel, R., Raffo, G. V. and Becker, L. (2014). Modeling and control of a tiltrotor UAV for path tracking, *IFAC Proceedings Volumes* **47**(3): 3839–3844.

Doyle, J. C., Francis, B. A. and Tannenbaum, A. R. (2013). *Feedback control theory*, Courier Corporation.

Doyle, J. C., Glover, K., Khargonekar, P. P. and Francis, B. A. (1989). State-space solutions to standard $\mathcal{H}_2$ and $\mathcal{H}_\infty$ control problems, *IEEE Trans. Autom. Control* **34**(8): 831–847.

Dullerud, G. E. and Paganini, F. (2013). *A course in robust control theory: a convex approach*, Vol. 36, Springer Science & Business Media.

Durham, W. C. (1993). Constrained control allocation, *Journal of Guidance, Control, and Dynamics* **16**(4): 717–725.

Feng, W. and Postlethwaite, I. (1993). Robust nonlinear $\mathcal{H}_\infty$/adaptative control of robot manipulator motion, *IFAC Proc. Vol.* **26**(2): 31–34.

Fleming, W. H. and Soner, H. M. (2006). *Controlled Markov processes and viscosity solutions*, Vol. 25, Springer Science & Business Media.

Flores, G. R., Escareño, J., Lozano, R. and Salazar, S. (2012). Quad-tilting rotor convertible mav: Modeling and real-time hover flight control, *Journal of Intelligent & Robotic Systems* **65**(1-4): 457–471.

Francis, B. A. and Doyle, J. C. (1987). Linear control theory with an $\mathcal{H}_\infty$ optimality criterion, *SIAM J. on Control and Optimization* **25**(4): 815–844.

Fuhrer, S., Verling, S., Stastny, T. and Siegwart, R. (2019). Fault-tolerant flight control of a vtol tailsitter UAV, *2019 International Conference on Robotics and Automation (ICRA)*, IEEE, pp. 4134–4140.

Gahinet, P. and Apkarian, P. (1994). A linear matrix inequality approach to $\mathcal{H}_\infty$ control, *Int'l J. of robust and nonlinear control* **4**(4): 421–448.

Geromel, J. C., Bernussou, J. and Oliveira, M. C. (1999). $\mathcal{H}_2$-norm optimization with constrained dynamic output feedback controllers: decentralized and reliable control, *IEEE Trans. Autom. Control* **44**(7): 1449–1454.

Goldshtein, V. and Ukhlov, A. (2009). Weighted sobolev spaces and embedding theorems, *Transactions of the American Mathematical Society* **361**(7): 3829–3850.

González De Paz, R. B. (2009). On a variational principle for shape optimization and elliptic free boundary problems, *Revista de Matemática: Teoría y Aplicaciones* **Vol. 6**(1).

Gress, G. R. (2002). Using dual propellers as gyroscopes for tilt-prop hover control, *Proc. of AIAA Biennial International Powered Lift Conference and Exhibit. Williamsburg, VA*, pp. 1–11.

Guillard, H. and Bourlès, H. (2000). Robust feedback linearization, *Proc. 14 th International Symposium on Mathematical Theory of Networks and Systems*.

Hamdi, H., Rodrigues, M., Mechmeche, C., Theilliol, D. and Braiek, N. B. (2009). State estimation for polytopic lpv descriptor systems: application to fault diagnosis, *IFAC Proceedings Volumes* **42**(8): 438–443.

Hardt, M., Helton, J. W. and Kreutz-Delgado, K. (2000). Numerical solution of nonlinear $\mathcal{H}_2$ and $\mathcal{H}_\infty$ control problems with application to jet engine compressors, *IEEE Transactions on Control Systems Technology* **8**(1): 98–111.

Harkegard, O. and Glad, S. T. (2005). Resolving actuator redundancy-optimal control vs control allocation, *Automatica* **41**(1): 137–144.

He, H. and Wang, Z. (2004). W-stability of nonlinear time-delay systems, *Proc. of Int'l Conf. on Information Acquisition.*, IEEE, pp. 23–25.

Hegde, N. T., George, V., Nayak, C. G. and Kumar, K. (2019). Design, dynamic modelling and control of tilt-rotor UAVs: a review, *International Journal of Intelligent Unmanned Systems* **8**(3): 143–161.

Hu, L.-S., Lam, J., Cao, Y.-Y. and Shao, H.-H. (2003). A linear matrix inequality (LMI) approach to robust $\mathcal{H}_2$ sampled-data control for linear uncertain systems, *IEEE Transactions on Systems, Man, and Cybernetics, Part B: Cybernetics* pp. 149–155.

Huang, J. and Lin, C.-F. (1995). Numerical approach to computing nonlinear $\mathcal{H}_\infty$ control laws, *Journal of Guidance, Control, and Dynamics* **18**(5): 989–994.

Johansen, T. A. and Fossen, T. I. (2013). Control allocation - a survey, *Automatica* **49**(5): 1087–1103.

Johansson, R. (1990). Quadratic optimization of motion coordination and control, *IEEE Trans. Autom. Control* **35**(11): 1197–1208.

Kane, T. R. and Levinson, D. A. (1985). *Dynamics: Theory and Applications*, Mcgraw-Hill College.

Kang, W., De, P. and Isidori, A. (1992). Flight control in a windshear via nonlinear $\mathcal{H}_\infty$ methods, *Decision and Control, 1992., Proceedings of the 31st IEEE Conference on*, IEEE, pp. 1135–1142.

Kendoul, F., Fantoni, I. and Lozano, R. (2005). Modeling and control of a small autonomous aircraft having two tilting rotors, *Proc. of the 44th IEEE Conference on CDC-ECC'05*, pp. 8144–8149.

Khalaf, M., Huang, J. and Lewis, F. (2006). Nonlinear $\mathcal{H}_2/\mathcal{H}_\infty$ constrained feedback control: a practical design approach using neural networks (advances in industrial control).

Khalil, H. K. and Grizzle, J. W. (2002). *Nonlinear systems*, Vol. 3, Prentice hall Upper Saddle River, NJ.

Khargonekar, P. P. and Rotea, M. A. (1991). Mixed $\mathcal{H}_2/\mathcal{H}_\infty$ control: a convex optimization approach, *IEEE Transactions on Automatic Control* **36**(7): 824–837.

Kilpeläinen, T. (1994). Weighted sobolev spaces and capacity, *Ann. Acad. Sci. Fenn. Ser. AI Math* **19**(1): 95–113.

Kirk, D. E. (2004). *Optimal control theory: an introduction*, Courier Corporation.

Koenig, N. and Howard, A. (2004). Design and use paradigms for gazebo, an open-source multi-robot simulator, *Intelligent Robots and Systems, 2004.(IROS 2004). Proceedings. 2004 IEEE/RSJ International Conference on*, Vol. 3, IEEE, pp. 2149–2154.

Kong, Z. and Lu, Q. (2018). Mathematical modeling and modal switching control of a novel tiltrotor UAV, *Journal of Robotics* **2018**.

Kufner, A. (1985). *Weighted sobolev spaces*, Vol. 31, John Wiley & Sons Incorporated.

Lara, A. V., Nascimento, I. B., Arias-Garcia, J., Becker, L. B. and Raffo, G. V. (2019). Hardware-in-the-loop simulation environment for testing of tilt-rotor UAV's control strategies, *Anais da Sociedade Brasileira de Automática* **1**(1).

Lara, A. V., Rego, B. S., Raffo, G. V. and Arias-Garcia, J. (2017). Desenvolvimento de um ambiente de simulação de vants tilt-rotor para testes de estratégias de controle, *Proc. of the XII Simpósio Brasileiro de Automação Inteligente* pp. 2135–2141.

Lee, J.-H., Min, B.-M. and Kim, E.-T. (2007). Autopilot design of tilt-rotor UAV using particle swarm optimization method, *Control, Automation and Systems, 2007. ICCAS'07. International Conference on*, IEEE, pp. 1629–1633.

Liu, Z., He, Y., Yang, L. and Han, J. (2017). Control techniques of tilt rotor unmanned aerial vehicle systems: A review, *Chinese Journal of Aeronautics* **30**(1): 135–148.

Lu, W.-M. and Doyle, J. C. (1995). $\mathcal{H}_\infty$ control of nonlinear systems: a convex characterization, *IEEE Transactions on Automatic Control* **40**(9): 1668–1675.

Lukes, D. L. (1969). Optimal regulation of nonlinear dynamical systems, *SIAM Journal on Control* **7**(1): 75–100.

Madero, V., Aracil, J. and Gordillo, F. (2010). A nonlinear control law for two-wheeled self-balanced vehicles, *15th IEEE Mediterranean Electrotechnical Conference*, IEEE, pp. 1557–1562.

Maisel, M. D., Giulianetti, D. J. and Dugan, D. C. (2000). The history of the XV-15 tilt rotor research aircraft from concept to flight.

Maz'ya, V. (2013). *Sobolev spaces*, Springer.

Mehra, R., Prasanth, R., Bennett, R., Neckels, D. and Wasikowski, M. (2001). Model predictive control design for XV-15 tilt rotor flight control, *AIAA Paper* **4331**: 1–11.

Metni, N. and Hamel, T. (2007). A UAV for bridge inspection: Visual servoing control law with orientation limits, *Automation in construction* **17**(1): 3–10.

Mikhlin, S. G. and Smolitskiy, K. L. (1967). *Approximate methods for solution of differential and integral equations*, American Elsevier New York.

Morin, P. (2015). Modeling and control of convertible micro air vehicles, *Robot Motion and Control (RoMoCo), 2015 10th International Workshop on*, IEEE, pp. 188–198.

Naldi, R. and Marconi, L. (2011). Optimal transition maneuvers for a class of V/STOL aircraft, *Automatica* **47**(5): 870–879.

Nasa (1975). Tilt rotor research aircraft familiarization document, http://ntrs.nasa.gov/archive/nasa/casi.ntrs.nasa.gov/19750016648.pdf.

Nichols, R. A., Reichert, R. T. and Rugh, W. J. (1993). Gain scheduling for H-infinity controllers: A flight control example, *IEEE Transactions on Control systems technology* **1**(2): 69–79.

Nielsen, M. (2012). On transference of multipliers on matrix weighted lp-spaces, *Journal of Geometric Analysis* **22**(1): 12–22.

Norton, B. (2004). *Bell Boeing V-22 Osprey: Tiltrotor Tactical Transport*, Aerofax.

Olfati-Saber, R. (2001). *Nonlinear control of underactuated mechanical systems with application to robotics and aerospace vehicles*, PhD thesis, Massachusetts Institute of Technology.

Ortega, F. J., Nunez, M. and Esteban, S. (2021). Aerodynamics and propulsive modeling of a bi-rotor convertible aircraft for the identification of trim conditions in longitudinal

flight, *In proc of The Vertical Flight Society's 77th Annual Forum & Technology Display (VFS2021)*, pp. 1–15.

Ortega, M. G., Vargas, M., Vivas, C. and Rubio, F. R. (2005). Robustness Improvement of a Nonlinear $\mathcal{H}_\infty$ Controller for Robot Manipulators via Saturation Functions, *Journal of Robotic Systems* **22**(8): 421–437.

Ortega, R., Spong, M. W., Gómez-Estern, F. and Blankenstein, G. (2002). Stabilization of a class of underactuated mechanical systems via interconnection and damping assignment, *IEEE Trans. Autom. Control* **47**(8): 1218–1233.

Papachristos, C., Alexis, K. and Tzes, A. (2011). Design and experimental attitude control of an unmanned tilt-rotor aerial vehicle, *Proc. of the 15th ICAR 2011*, pp. 465–470.

Papachristos, C., Alexis, K. and Tzes, A. (2012). Towards a high-end unmanned tri-tiltrotor: Design, modeling and hover control, *20th Mediterranean Conference on Control & Automation (MED), 2012*, IEEE, pp. 1579–1584.

Papachristos, C., Alexis, K. and Tzes, A. (2013). Hybrid model predictive flight mode conversion control of unmanned quad-tiltrotors, *Control Conference (ECC), 2013 European*, IEEE, pp. 1793–1798.

Patpong, L., Sampei, M., Koga, M. and Shimizu, E. (1996). A numerical computational approach of hamilton-jacobi-isaacs equation in nonlinear $\mathcal{H}_\infty$ control problems, *Decision and Control, 1996., Proceedings of the 35th IEEE Conference on*, Vol. 4, IEEE, pp. 3774–3779.

Pavel, L. (2013). Classical solutions in sobolev spaces for a class of hyperbolic lotka–volterra systems, *SIAM Journal on Control and Optimization* **51**(3): 2132–2151.

Peng, C.-C., Hwang, T.-S., Chen, S.-W., Chang, C.-Y., Lin, Y.-C., Wu, Y.-T., Lin, Y.-J. and Lai, W.-R. (2010). ZPETC path-tracking gain-scheduling design and real-time multi-task flight simulation for the automatic transition of tilt-rotor aircraft, *2010 IEEE Conference on Robotics, Automation and Mechatronics*, IEEE, pp. 118–123.

Quigley, M., Conley, K., Gerkey, B., Faust, J., Foote, T., Leibs, J., Wheeler, R. and Ng, A. Y. (2009). Ros: an open-source robot operating system, *ICRA workshop on open source software*, Vol. 3, Kobe, Japan, p. 5.

Raffo, G. V. (2011). *Robust control strategies for a quadrotor helicopter: An underactuated mechanical system*, PhD thesis, Univ. de Sevilla.

Raffo, G. V. and Almeida, M. (2018). A load transportation nonlinear control strategy using a tilt-rotor UAV, *Journal of Advanced Transportation* **2018**: 1–20.

Raffo, G. V., Ortega, M. G., Madero, V. and Rubio, F. R. (2015). Two-wheeled self-balanced pendulum workspace improvement via underactuated robust nonlinear control, *Control Eng. Practice* **44**: 231–242.

Raffo, G. V., Ortega, M. G. and Rubio, F. R. (2011a). Nonlinear $\mathcal{H}_\infty$ controller for the quad-rotor helicopter with input coupling, *IFAC Proc. Vol.* **44**(1): 13834–13839.

Raffo, G. V., Ortega, M. G. and Rubio, F. R. (2011b). Path Tracking of a UAV via an Underactuated $\mathcal{H}_\infty$ Control Strategy, *European J. of Control* **17**(2): 194–213.

Rego, B. S. and Raffo, G. V. (2016). Suspended load path tracking by a tilt-rotor UAV, *IFAC-PapersOnLine* **49**(32): 234–239.

Rego, B. S. and Raffo, G. V. (2019). Suspended load path tracking control using a tilt-rotor UAV based on zonotopic state estimation, *Journal of the Franklin Institute* **356**(4): 1695–1729.

Ryan, A. and Hedrick, J. K. (2005). A mode-switching path planner for UAV-assisted search and rescue, *Proc. of the 44th IEEE Conference on CDC-ECC'05*, pp. 1471–1476.

Saari, H., Pellikka, I., Pesonen, L., Tuominen, S., Heikkilä, J., Holmlund, C., Mäkynen, J., Ojala, K. and Antila, T. (2011). Unmanned aerial vehicle (UAV) operated spectral camera system for forest and agriculture applications, *In Proc. of SPIE 8174, Remote Sensing for Agriculture, Ecosystems, and Hydrology XIII*, Vol. 8174, International Society for Optics and Photonics, pp. 81740H–1 – 81740H–15.

Sage, H., De Mathelin, M. and Ostertag, E. (1999). Robust control of robot manipulators: a survey, *International Journal of control* **72**(16): 1498–1522.

Sanchez, A., Escareno, J., Garcia, O. and Lozano, R. (2008). Autonomous hovering of a noncyclic tiltrotor UAV: Modeling, control and implementation, *The International Federation of Automatic Control* **41**: 803–808.

Santos, M. A., Cardoso, D. N., Rego, B. S., Raffo, G. V. and Esteban, S. (2017). A discrete robust adaptive control of a tilt-rotor UAV for an enlarged flight envelope, *In proc of IEEE 56th Annual Conference on Decision and Control (CDC2017)*, IEEE, pp. 5208–5214.

Santos, M. A. and Raffo, G. V. (2016). Path tracking model predictive control of a tilt-rotor UAV carrying a suspended load, *IEEE 19th International Conference on Intelligent Transportation Systems (ITSC) 2016*, IEEE, pp. 1458–1463.

Sedhom, B. E., El-Saadawi, M. M., Hatata, A. Y. and Abd-Raboh, E. E. (2020). A multistage H-infinity-based controller for adjusting voltage and frequency and improving

power quality in islanded microgrids, *International Transactions on Electrical Energy Systems* **30**(1): e12143.

Shi, X., Kim, K., Rahili, S. and Chung, S.-J. (2018). Nonlinear control of autonomous flying cars with wings and distributed electric propulsion, *2018 IEEE Conference on Decision and Control (CDC)*, IEEE, pp. 5326–5333.

Simon, D. (2006). *Optimal state estimation: Kalman, $\mathcal{H}_\infty$, and nonlinear approaches*, John Wiley & Sons.

Sinha, P. K. and Pechev, A. N. (2004). Nonlinear $\mathcal{H}_\infty$ controllers for electromagnetic suspension systems, *IEEE Transactions on Automatic Control* **49**(4): 563–568.

Siqueira, A. A. and Terra, M. H. (2004). Nonlinear and markovian $\mathcal{H}_\infty$ controls of underactuated manipulators, *IEEE Transactions on Control Systems Technology* **12**(6): 811–826.

Siqueira, A. A., Terra, M. H. and Maciel, B. C. (2006). Nonlinear mixed $\mathcal{H}_2/\mathcal{H}_\infty$ control applied to manipulators via actuation, *Control engineering practice* **14**(4): 327–335.

Slotine, J.-J. E., Li, W. et al. (1991). *Applied nonlinear control*, Vol. 199, Prentice hall Englewood Cliffs, NJ.

Small, E., Fresk, E., Andrikopoulos, G. and Nikolakopoulos, G. (2016). Modelling and control of a tilt-wing unmanned aerial vehicle, *24th Mediterranean Conference on Control and Automation (MED) 2016*, IEEE, pp. 1254–1259.

Spong, M. W., Hutchinson, S., Vidyasagar, M. et al. (2006). *Robot modeling and control*, Vol. 3, Wiley New York.

Tatom, F. B., Smith, S. R., Fichtl, G. H. and Campbell, C. W. (1982). Simulation of atmospheric turbulent gusts and gust gradients, *Journal of Aircraft* **19**(4): 264–271.

Temiz, O., Cakmakci, M. and Yildiz, Y. (2018). A fault tolerant vehicle stability control using adaptive control allocation, *ASME 2018 Dynamic Systems and Control Conference*, American Society of Mechanical Engineers Digital Collection.

Treves, F. (2016). *Topological Vector Spaces, Distributions and Kernels: Pure and Applied Mathematics*, Vol. 25, Elsevier.

Trofino, A., Coutinho, D. and Barbosa, K. A. (2003). Sistemas multivariáveis: Uma abordagem via lmis, *Santa Catarina* .

Vamvoudakis, K. G. and Lewis, F. L. (2010). Online solution of nonlinear two-player zero-sum games using synchronous policy iteration, *49th IEEE Conference on Decision and Control (CDC)*, IEEE, pp. 3040–3047.

Van der Linden, G.-W. and Lambrechts, P. F. (1993). $\mathcal{H}_\infty$ control of an experimental inverted pendulum with dry friction, *IEEE Control Systems Magazine* **13**(4): 44–50.

Van der Schaft (1991). On a state space approach to nonlinear $\mathcal{H}_\infty$ control, *Systems & Control Letters* **16**(1): 1–8.

Van Der Schaft (1992). $\mathcal{L}_2$-gain analysis of nonlinear systems and nonlinear state-feedback $\mathcal{H}_\infty$ control, *IEEE Trans. Autom. Control* **37**(6): 770–784.

van der Schaft (2000). *L2-gain and passivity techniques in nonlinear control*, Vol. 2, Springer.

Verling, S., Weibel, B., Boosfeld, M., Alexis, K., Burri, M. and Siegwart, R. (2016). Full attitude control of a vtol tailsitter UAV, *2016 IEEE International Conference on Robotics and Automation (ICRA)*, IEEE, pp. 3006–3012.

Walters, P., Kamalapurkar, R., Voight, F., Schwartz, E. M. and Dixon, W. E. (2018). Online approximate optimal station keeping of a marine craft in the presence of an irrotational current, *IEEE Transactions on Robotics* **34**(2): 486–496.

Wernrud, A. and Rantzer, A. (2005). On approximate policy iteration for continuous-time systems, *44th IEEE Conference on Decision and Control and European Control Conference, 2005.*, IEEE, pp. 1453–1458.

Willems, J. C. (2007). Dissipative dynamical systems, *European Journal of Control* **13**(2-3): 134–151.

Wise, K. A. and Sedwick, J. L. (1994). Successive approximation solution of the hji equation, *Decision and Control, 1994., Proceedings of the 33rd IEEE Conference on*, Vol. 2, IEEE, pp. 1387–1391.

Wise, K. A. and Sedwick, J. L. (1996). Nonlinear $\mathcal{H}_\infty$ optimal control for agile missiles, *Journal of guidance, control, and dynamics* **19**(1): 157–165.

Xiao, G., Zhang, H., Zhang, K. and Wen, Y. (2018). Value iteration based integral reinforcement learning approach for $\mathcal{H}_\infty$ controller design of continuous-time nonlinear systems, *Neurocomputing* **285**: 51–59.

Xiao, M. and Basar, T. (1997). Viscosity supersolutions of a class of Hamilton-Jacobi-Isaacs equations arising in nonlinear $\mathcal{H}_\infty$ control, *Decision and Control, 1997., Proceedings of the 36th IEEE Conference on*, Vol. 2, IEEE, pp. 1761–1766.

Yazdanpanah, M., Khorasani, K. and Patel, R. (1998). Uncertainty compensation for a flexible-link manipulator using nonlinear $\mathcal{H}_\infty$ control, *International Journal of Control* **69**(6): 753–771.

Yazdanpanah, M., Khorasani, K. and Patel, R. (1999). On the estimate of the domain of validity of non-linear $\mathcal{H}_\infty$ control, *International Journal of Control* **72**(12): 1097–1105.

Yuksek, B., Vuruskan, A., Ozdemir, U., Yukselen, M. and Inalhan, G. (2016). Transition flight modeling of a fixed-wing vtol UAV, *Journal of Intelligent & Robotic Systems* **84**(1-4): 83–105.

Zemouche, A. and Boutayeb, M. (2008). Unknown input observer synthesis method with modified $\mathcal{H}_\infty$ criteria for nonlinear systems using sobolev norms, *IFAC Proc. Vol.* **41**(2): 8588–8593.

Zhu, Y. and Zhao, D. (2018). Comprehensive comparison of online adp algorithms for continuous-time optimal control, *Artificial Intelligence Review* **49**(4): 531–547.

Zongjian, L. (2008). UAV for mapping low altitude photogrammetric survey, *International Archives of Photogrammetry and Remote Sensing, Beijing, China* **37**: 1183–1186.

Appendices

A

Linear systems theory

This Appendix presents some preliminary concepts and definitions necessary into the development of the state and output feedback linear $\mathcal{W}_\infty$ controllers proposed in Chapter 6. The content of this section was adapted from Chen and Chen (1984); Trofino et al. (2003).

Consider the linear system

$$\mathcal{S}: \begin{cases} \dot{\boldsymbol{x}}(t) = \boldsymbol{A}\boldsymbol{x}(t) + \boldsymbol{B}\boldsymbol{u}(t) + \boldsymbol{D}\boldsymbol{w}(t), & \boldsymbol{x}(0) = \boldsymbol{x}_0 \\ \boldsymbol{u}(t) = \boldsymbol{K}\boldsymbol{x}(t), \\ \boldsymbol{y}(t) = \boldsymbol{C}\boldsymbol{x}(t). \end{cases} \tag{A.1}$$

where $\boldsymbol{x}(t) : \mathbb{R}_{\geq 0} \to \mathbb{R}^{n_x}$ is the state vector with $\boldsymbol{x}_0 \in \mathbb{R}^{n_x}$, $\boldsymbol{u}(t) : \mathbb{R}_{\geq 0} \to \mathbb{R}^{n_u}$ is the input vector, $\boldsymbol{w}(t) : \mathbb{R}_{\geq 0} \to \mathbb{R}^{n_w}$ is the disturbance vector, $\boldsymbol{y}(t) : \mathbb{R}_{\geq 0} \to \mathbb{R}^{n_y}$ is the output vector, and $\boldsymbol{A} \in \mathbb{R}^{n_x \times n_x}$, $\boldsymbol{B} \in \mathbb{R}^{n_x \times n_u}$, $\boldsymbol{D} \in \mathbb{R}^{n_x \times n_w}$,$\boldsymbol{K} \in \mathbb{R}^{n_u \times n_x}$, $\boldsymbol{C} \in \mathbb{R}^{n_y \times n_x}$ are constant matrices that represents the closed-loop dynamics of this system.

A fundamental tool to the analysis of linear systems is the eigenvalues and eigenvectors. A real or complex number $\lambda \in \mathbb{C}$ is called an eigenvalue of the matrix $\boldsymbol{A}$ if there exists a nonzero vector $\boldsymbol{x}$ such that $\boldsymbol{A}\boldsymbol{x} = \lambda\boldsymbol{x}$. Any nonzero vector $\boldsymbol{x}$ satisfying $\boldsymbol{A}\boldsymbol{x} = \lambda\boldsymbol{x}$ is called a right eigenvector of $\boldsymbol{A}$ associated with the eigenvalue λ. Consequently, the eigenvalues of matrix $\boldsymbol{A}$ are all λ that satisfy

$$det(\lambda\boldsymbol{I} - \boldsymbol{A}) = 0. \tag{A.2}$$

Another fundamental tool into the linear system's analysis is the notion of asymptotic stability in the sense of Lyapunov, as established by the following definition.

Definition 11. *The closed-loop system* (A.1) *is asymptotically stable if and only if all eigenvalues of* $(\boldsymbol{A}+\boldsymbol{BK})$ *have negative real parts.*

The asymptotic stability of a linear system can be verified through the Lyapunov equation. For the closed-loop system (A.1), all eigenvalues of $(\boldsymbol{A}+\boldsymbol{BK})$ have negative real parts if and only if the Lyapunov equation

$$(\boldsymbol{A}+\boldsymbol{BK})'\boldsymbol{P}+\boldsymbol{P}(\boldsymbol{A}+\boldsymbol{BK})=-\boldsymbol{N} \tag{A.3}$$

has a unique symmetric solution $\boldsymbol{P}>0$, for any given positive definite symmetric matrix $\boldsymbol{N}$, with $\boldsymbol{P},\boldsymbol{N}\in\mathbb{R}^{n_x\times n_x}$.

A higher restrictive concept of stability is the exponential stability, which is defined as follows.

Definition 12. *(Adapted from Khalil and Grizzle (2002)) The closed-loop system* (A.1) *is exponentially stable if it is asymptotically stable and there exist constants* $\boldsymbol{c},\boldsymbol{k},\boldsymbol{b}\in\mathbb{R}_{\geq 0}$ *such that*

$$||\boldsymbol{x}(t)||\leq k||\boldsymbol{x}(0)||e^{-bt},\qquad \forall||\boldsymbol{x}(0)||<c. \tag{A.4}$$

In addition, this system is globally exponentially stable if (A.4) *holds for any finite initial condition* $\boldsymbol{x}(0)\in\mathbb{R}^{n_x}$.

The solution of the linear time-invariant closed-loop system (A.1) is computed by (Chen and Chen, 1984)

$$\boldsymbol{x}(t)=e^{(\boldsymbol{A}+\boldsymbol{BK})t}\boldsymbol{x}(0)+\int_0^t e^{(\boldsymbol{A}+\boldsymbol{BK})(t-\tau)}\boldsymbol{D}\boldsymbol{w}(\tau)d\tau. \tag{A.5}$$

Therefore, according to Definition 12 and by assuming no disturbances actuating on the system, if all eigenvalues of $(\boldsymbol{A}+\boldsymbol{BK})$ have negative real part, the closed-loop system (A.1) is exponentially stable with $\boldsymbol{x}(t)=e^{(\boldsymbol{A}+\boldsymbol{BK})t}\boldsymbol{x}(0)$.

The following definition introduce the notion of controllability for linear systems.

Definition 13. *(Adapted from Chen and Chen (1984)) A state-space system is locally controllable in the space* Ω *if for any initial state* $\boldsymbol{x}_0\in\Omega$ *and any final state* $\boldsymbol{x}_f\in\Omega$, *there exists a control input signal that transfers* $\boldsymbol{x}_0$ *to* $\boldsymbol{x}_f$ *in a finite time. Otherwise, the system is locally uncontrollable. If* Ω *concerns all the state space, these terms change to controllable and uncontrollable, respectively.*

Regarding the open-loop system from (A.1), one can state that the pair $(\boldsymbol{A}, \boldsymbol{B})$ is controllable if the controllability matrix

$$\mathcal{C}(\boldsymbol{B}, \boldsymbol{A}) = [\boldsymbol{B} \quad \boldsymbol{AB} \quad \boldsymbol{A}^2\boldsymbol{B} \quad \cdots \quad \boldsymbol{A}^{n_x-1}\boldsymbol{B}] \tag{A.6}$$

has full row rank, i.e. $\text{rank}(\mathcal{C}) = n_x$.

Moreover, the following definition introduces the notion of observability.

Definition 14. *The state space system* (A.1) *is said to be observable if for any unknown initial state* $\boldsymbol{x}(0) = \boldsymbol{x}_0$*, there exists a finite time instant* $t_1 > 0$ *such that the knowledge of the input* $\boldsymbol{u}(t)$ *and the output* $\boldsymbol{y}(t)$ *over* $t \in [0, t_1]$ *suffices to determine uniquely the initial state* $x(0)$*. Otherwise, the system is said to be unobservable.*

Regarding the open-loop system from (A.1), one can state that the pair $(\boldsymbol{A}, \boldsymbol{C})$ is observable if the observability matrix

$$\mathcal{O}(\boldsymbol{C}, \boldsymbol{A}) = \begin{bmatrix} \boldsymbol{C} \\ \boldsymbol{CA} \\ \vdots \\ \boldsymbol{CA}^{n_x-1} \end{bmatrix}, \tag{A.7}$$

has full column rank, i.e. $\text{rank}(\mathcal{O}) = n_x$.

Another concept important for this doctoral thesis is the, similarity transformation, which is performed to transform a matrix inequality into a linear matrix inequality. In order to present this transformation, consider the system

$$\dot{\boldsymbol{x}}(t) = \boldsymbol{A}\boldsymbol{x}(t), \tag{A.8}$$

and the transformation

$$\bar{\boldsymbol{x}}(t) = \boldsymbol{P}\boldsymbol{x}(t), \tag{A.9}$$

where $\boldsymbol{x}(t)$ and $\boldsymbol{A}$ are defined as in (A.1) and $\boldsymbol{P} > 0$. In (A.9) the matrix $\boldsymbol{P}$ maps $\boldsymbol{x}(t)$ into $\bar{\boldsymbol{x}}(t)$ with respect to the orthonormal basis composed of the columns of $\boldsymbol{P}$. In the new basis, the system (A.8) is represented by

$$\dot{\bar{\boldsymbol{x}}}(t) = \underbrace{\boldsymbol{P}\boldsymbol{A}\boldsymbol{P}^{-1}}_{\bar{\boldsymbol{A}}}\bar{\boldsymbol{x}}(t) = \bar{\boldsymbol{A}}\bar{\boldsymbol{x}}(t). \tag{A.10}$$

This is the so-called similarity transformation, and matrices $\boldsymbol{A}$ and $\bar{\boldsymbol{A}}$ are said to be similar. It is noteworthy that using (A.9), one can go from (A.10) to (A.8).

Also, to transform matrix inequalities into linear matrix inequalities, the Schur complement can be used. According to the Schur complement, the following inequalities are

equivalents:

$$\begin{bmatrix} \boldsymbol{U} & \boldsymbol{E}' \\ \boldsymbol{E} & \boldsymbol{F} \end{bmatrix} > 0, \tag{A.11}$$

$$\boldsymbol{F} - \boldsymbol{E}\boldsymbol{U}^{-1}\boldsymbol{E}' > 0, \tag{A.12}$$

$$\boldsymbol{U} - \boldsymbol{E}'\boldsymbol{F}^{-1}\boldsymbol{E} > 0, \tag{A.13}$$

where $\boldsymbol{U} \in \mathbb{R}^{n_u \times n_u}$, $\boldsymbol{E} \in \mathbb{R}^{n_f \times n_u}$, $\boldsymbol{F} \in \mathbb{R}^{n_f \times n_f}$, with $\boldsymbol{U}, \boldsymbol{F} > 0$. Then, from the Schur complement, one can transform the nonlinear inequalities (A.12) and (A.13), with respect to the variables $\boldsymbol{U}$, $\boldsymbol{E}$ and $\boldsymbol{F}$, into the linear inequality (A.11).

B

ProVANT-Emergentia Tilt-rotor UAV physical parameters

This appendix presents the physical parameters and aerodynamic coefficients used into the dynamic model of the ProVANT-Emergentia Tilt-rotor UAV to obtain the numerical experiments of Chapter 7. All the coefficients used to computed the aerodynamic forces and moments were obtained via wind tunnel experiments conducted at the University of Seville (See Figure B.1). For more details about the experiments, the readers may refer to Ortega et al. (2021). In addition, the physical parameters of the ProVANT-Emergentia Tilt-rotor UAV were obtained from the CAD model.

The thrust and torque coefficients of the propellers, that are used to compute (7.25)-(7.28), are presented in Figure B.2.

In order to obtain the aerodynamic coefficients of the fuselage, wings, tail-surfaces and aerodynamic interference, the aerodynamic surfaces illustrated in Figure B.3 were experimented in wind tunnel. Experiments were conducted for each surface considering the longitudinal and the lateral wind, as illustrated in Figure B.4. The coefficients were obtained considering the North-East-Down (NED) axes convention, and are presented in Figures B.5 and B.6.

The NED axes convention differs from the axes convention employed into the Tilt-rotor UAV modeling presented in Chapter 7 by rotating the aerodynamic forces and moments in 180 degrees around the $\vec{x}$-axis. Therefore, by conducting the procedure illustrated in Figure (B.7), the aerodynamic forces and moments are computed through the following

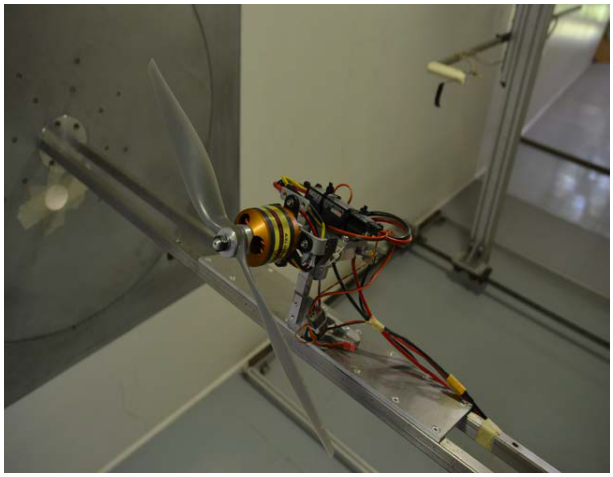

Figure B.1: Illustration of the wind tunnel experiment conducted to obtain the thrust and torque coefficients of the propellers.

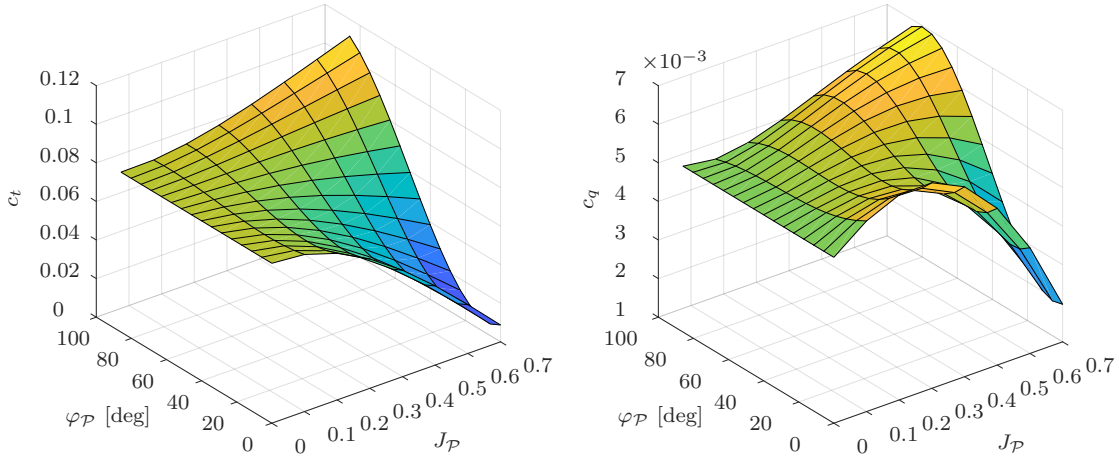

Figure B.2: Thrust and torque coefficients of the propellers.

equations:

$$\begin{bmatrix} f^d_{\mathcal{F}} \\ f^y_{\mathcal{F}} \\ f^l_{\mathcal{F}} \end{bmatrix} = \boldsymbol{R}^{\mathcal{W}_{\mathcal{F}}}_{NED} \begin{bmatrix} -\kappa^{air}_{\mathcal{F}} \; s_{\mathcal{F}} \; \left(c^d_{\mathcal{F}_{xy}}(\beta^{NED}_{\mathcal{F}}) + c^d_{\mathcal{F}_{xz}}(\alpha^{NED}_{\mathcal{F}}) \right) \\ -\kappa^{air}_{\mathcal{F}} \; s_{\mathcal{F}} \; c^y_{\mathcal{F}}(\beta^{NED}_{\mathcal{F}}) \\ -\kappa^{air}_{\mathcal{F}} \; s_{\mathcal{F}} \; c^l_{\mathcal{F}}(\alpha^{NED}_{\mathcal{F}}) \end{bmatrix}, \tag{B.1}$$

$$\begin{bmatrix} f^d_{\mathcal{W}_R} \\ f^y_{\mathcal{W}_R} \\ f^l_{\mathcal{W}_R} \end{bmatrix} = \boldsymbol{R}^{\mathcal{W}_{\mathcal{W}_R}}_{NED} \begin{bmatrix} -\kappa^{air}_{\mathcal{W}_R} \; s_{\mathcal{W}_R} \; \left(c^d_{\mathcal{W}_{Rxy}}(\beta^{NED}_{\mathcal{W}_R}) + c^d_{\mathcal{W}_{Rxz}}(\alpha^{NED}_{\mathcal{W}_R}) \right) \\ -\kappa^{air}_{\mathcal{W}_R} \; s_{\mathcal{W}_R} \; c^y_{\mathcal{W}_R}(\beta^{NED}_{\mathcal{W}_R}) \\ -\kappa^{air}_{\mathcal{W}_R} \; s_{\mathcal{W}_R} \; \left(c^l_{\mathcal{W}_R}(\alpha^{NED}_{\mathcal{W}_R}) + c^{\delta_a} \delta_{\mathcal{W}_R} \right) \end{bmatrix}, \tag{B.2}$$

$$\begin{bmatrix} f^d_{\mathcal{W}_L} \\ f^y_{\mathcal{W}_L} \\ f^l_{\mathcal{W}_L} \end{bmatrix} = \boldsymbol{R}^{\mathcal{W}_{\mathcal{W}_L}}_{NED} \begin{bmatrix} -\kappa^{air}_{\mathcal{W}_L} \; s_{\mathcal{W}_L} \; \left(c^d_{\mathcal{W}_{Lxy}}(\beta^{NED}_{\mathcal{W}_L}) + c^d_{\mathcal{W}_{Lxz}}(\alpha^{NED}_{\mathcal{W}_L}) \right) \\ -\kappa^{air}_{\mathcal{W}_L} \; s_{\mathcal{W}_L} \; c^y_{\mathcal{W}_L}(\beta^{NED}_{\mathcal{W}_L}) \\ -\kappa^{air}_{\mathcal{W}_L} \; s_{\mathcal{W}_L} \; \left(c^l_{\mathcal{W}_L}(\alpha^{NED}_{\mathcal{W}_L}) + c^{\delta_a} \delta_{\mathcal{W}_L} \right) \end{bmatrix}, \tag{B.3}$$

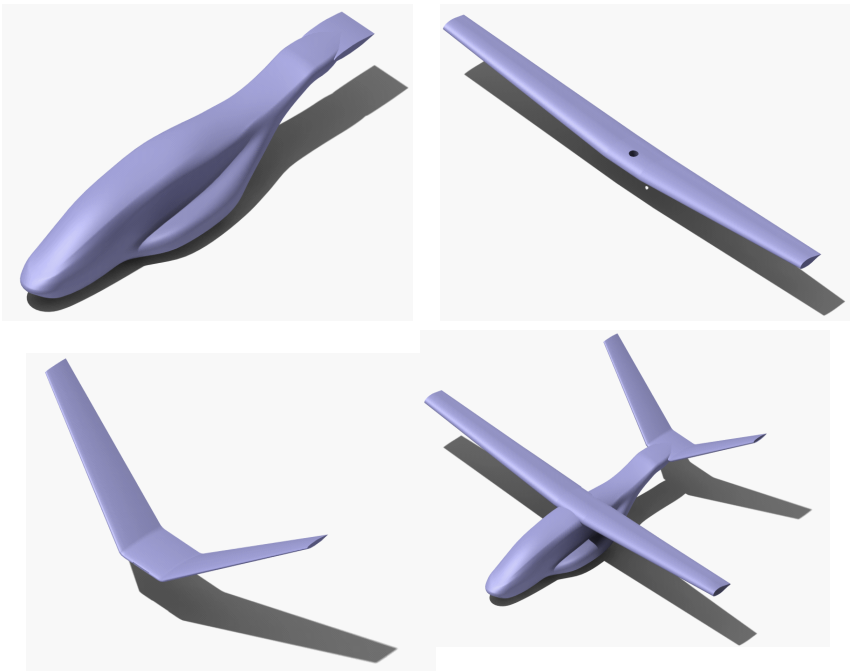

Figure B.3: Aerodynamic surfaces experimented in wind tunnel .

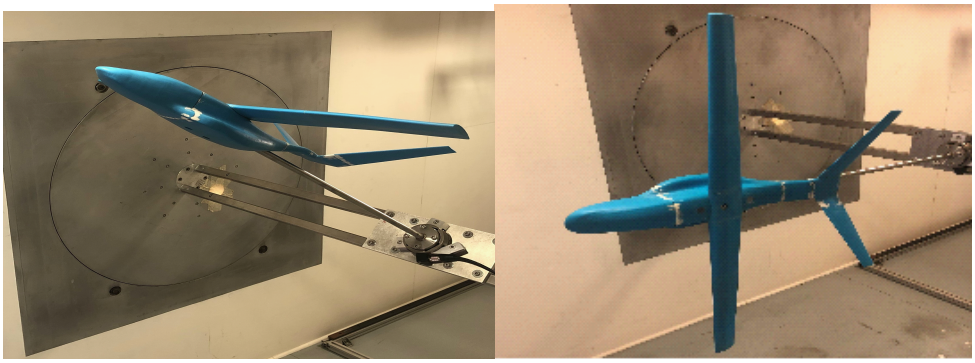

Figure B.4: Wind tunnel experiment with the connected parts, for the longitudinal and lateral dynamics.

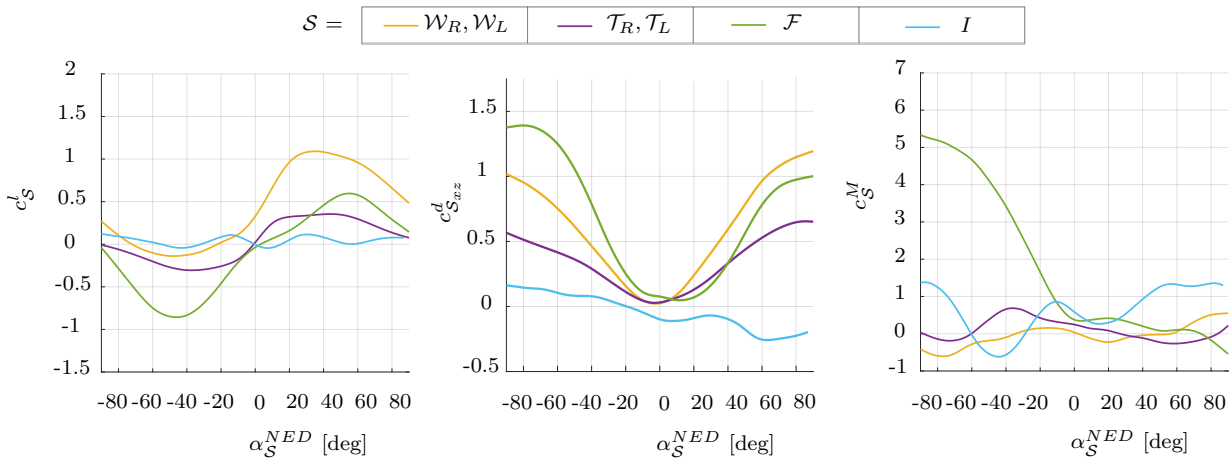

Figure B.5: Aerodynamic coefficients obtained from the wind tunnel experiments for the longitudinal wind dynamics.

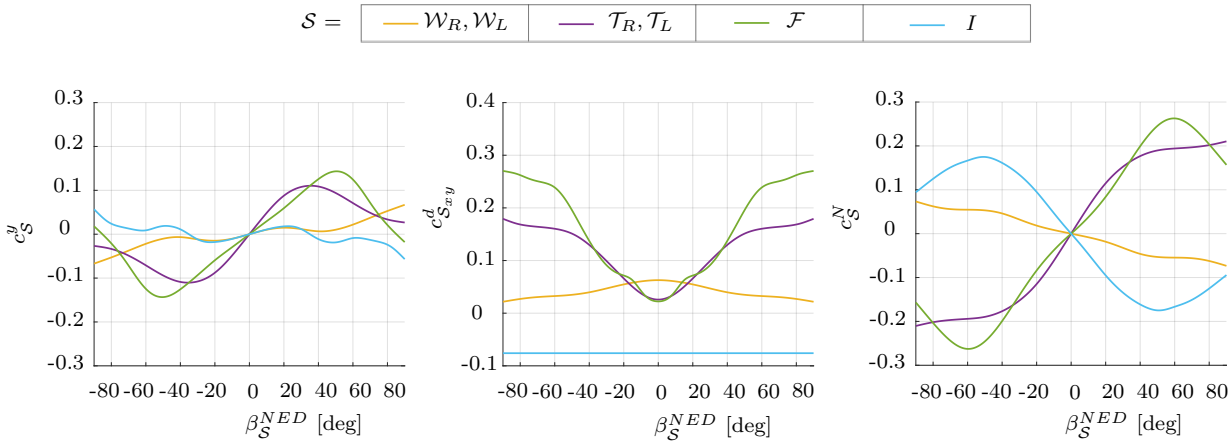

Figure B.6: Aerodynamic coefficients obtained from the wind tunnel experiments for the lateral wind dynamics.

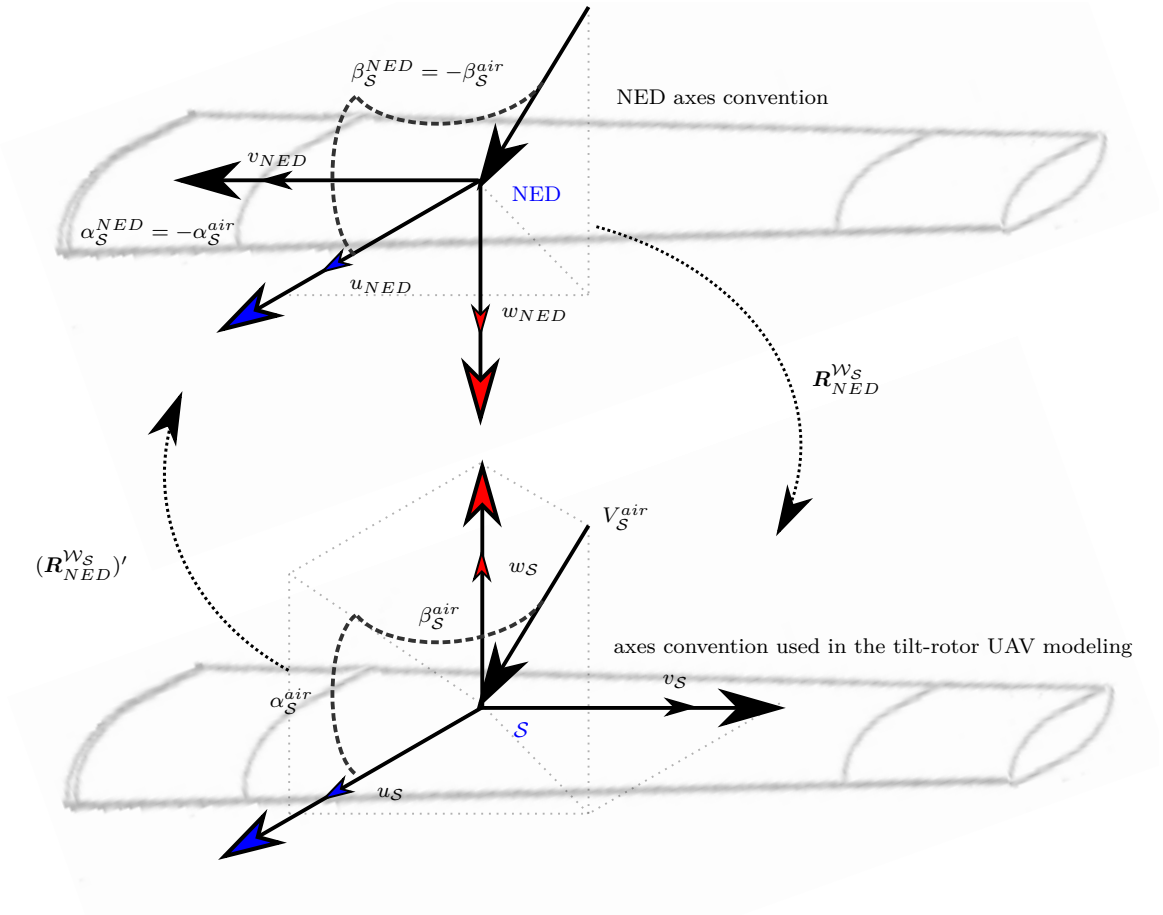

Figure B.7: NED axes and the axes convention used in the tilt-rotor modeling.

$$\begin{bmatrix} f^d_{\mathcal{T}_R} \\ f^y_{\mathcal{T}_R} \\ f^l_{\mathcal{T}_R} \end{bmatrix} = \boldsymbol{R}^{\mathcal{W}_{\mathcal{T}_R}}_{NED} \begin{bmatrix} -\kappa^{air}_{\mathcal{T}_R}\ s_{\mathcal{T}_R}\ \left(c^d_{\mathcal{T}_{R_{xy}}}(\beta^{NED}_{\mathcal{T}_R}) + c^d_{\mathcal{T}_{R_{xz}}}(\alpha^{NED}_{\mathcal{T}_R})\right) \\ -\kappa^{air}_{\mathcal{T}_R}\ s_{\mathcal{T}_R}\ \left(c^y_{\mathcal{T}_R}(\beta^{NED}_{\mathcal{T}_R}) + c^{\delta_r}\delta_r\right) \\ -\kappa^{air}_{\mathcal{T}_R}\ s_{\mathcal{T}_R}\ \left(c^l_{\mathcal{T}_R}(\alpha^{NED}_{\mathcal{T}_R}) + c^{\delta_e}\delta_e\right) \end{bmatrix}, \tag{B.4}$$

$$\begin{bmatrix} f^d_{\mathcal{T}_L} \\ f^y_{\mathcal{T}_L} \\ f^l_{\mathcal{T}_L} \end{bmatrix} = \boldsymbol{R}^{\mathcal{W}_{\mathcal{T}_L}}_{NED} \begin{bmatrix} -\kappa^{air}_{\mathcal{T}_L}\ s_{\mathcal{T}_L}\ \left(c^d_{\mathcal{T}_{L_{xy}}}(\beta^{NED}_{\mathcal{T}_L}) + c^d_{\mathcal{T}_{L_{xz}}}(\alpha^{NED}_{\mathcal{T}_L})\right) \\ -\kappa^{air}_{\mathcal{T}_L}\ s_{\mathcal{T}_L}\ \left(c^y_{\mathcal{T}_L}(\beta^{NED}_{\mathcal{T}_L}) + c^{\delta_r}\delta_r\right) \\ -\kappa^{air}_{\mathcal{T}_L}\ s_{\mathcal{T}_L}\ \left(c^l_{\mathcal{T}_L}(\alpha^{NED}_{\mathcal{T}_L}) + c^{\delta_e}\delta_e\right) \end{bmatrix}, \tag{B.5}$$

$$\begin{bmatrix} f^d_{\mathcal{I}} \\ f^y_{\mathcal{I}} \\ f^l_{\mathcal{I}} \end{bmatrix} = \boldsymbol{R}^{\mathcal{W}_{\mathcal{I}}}_{NED} \begin{bmatrix} -\kappa^{air}_{I}\ s_{I}\ \left(c^d_{I_{xy}}(\beta^{NED}_{I}) + c^d_{I_{xz}}(\alpha^{NED}_{I})\right) \\ -\kappa^{air}_{I}\ s_{I}\ c^y_{I}(\beta^{NED}_{I}) \\ -\kappa^{air}_{I}\ s_{I}\ c^l_{I}(\alpha^{NED}_{I}) \end{bmatrix}, \tag{B.6}$$

$$\begin{bmatrix} L_{\mathcal{F}} \\ M_{\mathcal{F}} \\ N_{\mathcal{F}} \end{bmatrix} = \boldsymbol{R}^{\mathcal{W}_{\mathcal{F}}}_{NED} \begin{bmatrix} 0 \\ \kappa^{air}_{\mathcal{F}}\ s_{\mathcal{F}}\ \bar{c}\ c^M_{\mathcal{F}}(\alpha^{NED}_{\mathcal{F}}) \\ \kappa^{air}_{\mathcal{F}}\ s_{\mathcal{F}}\ b\ c^N_{\mathcal{F}}(\beta^{NED}_{\mathcal{F}}) \end{bmatrix} \tag{B.7}$$

$$\begin{bmatrix} L_{\mathcal{W}_R} \\ M_{\mathcal{W}_R} \\ N_{\mathcal{W}_R} \end{bmatrix} = \boldsymbol{R}^{\mathcal{W}_{\mathcal{W}_R}}_{NED} \begin{bmatrix} 0 \\ \kappa^{air}_{\mathcal{W}_R}\ s_{\mathcal{W}_R}\ \bar{c}\ c^M_{\mathcal{W}_R}(\alpha^{NED}_{\mathcal{W}_R}) \\ \kappa^{air}_{\mathcal{W}_R}\ s_{\mathcal{W}_R}\ b\ c^N_{\mathcal{W}_R}(\beta^{NED}_{\mathcal{W}_R}) \end{bmatrix} \tag{B.8}$$

$$\begin{bmatrix} L_{\mathcal{W}_L} \\ M_{\mathcal{W}_L} \\ N_{\mathcal{W}_L} \end{bmatrix} = \boldsymbol{R}^{\mathcal{W}_{\mathcal{W}_L}}_{NED} \begin{bmatrix} 0 \\ \kappa^{air}_{\mathcal{W}_L}\ s_{\mathcal{W}_L}\ \bar{c}\ c^M_{\mathcal{W}_L}(\alpha^{NED}_{\mathcal{W}_L}) \\ \kappa^{air}_{\mathcal{W}_L}\ s_{\mathcal{W}_L}\ b\ c^N_{\mathcal{W}_L}(\beta^{NED}_{\mathcal{W}_L}) \end{bmatrix} \tag{B.9}$$

$$\begin{bmatrix} L_{\mathcal{T}_R} \\ M_{\mathcal{T}_R} \\ N_{\mathcal{T}_R} \end{bmatrix} = \boldsymbol{R}^{\mathcal{W}_{\mathcal{T}_R}}_{NED} \begin{bmatrix} 0 \\ \kappa^{air}_{\mathcal{T}_R}\ s_{\mathcal{T}_R}\ \bar{c}\ c^M_{\mathcal{T}_R}(\alpha^{NED}_{\mathcal{T}_R}) \\ \kappa^{air}_{\mathcal{T}_R}\ s_{\mathcal{T}_R}\ b\ c^N_{\mathcal{T}_R}(\beta^{NED}_{\mathcal{T}_R}) \end{bmatrix} \tag{B.10}$$

$$\begin{bmatrix} L_{\mathcal{T}_L} \\ M_{\mathcal{T}_L} \\ N_{\mathcal{T}_L} \end{bmatrix} = \boldsymbol{R}^{\mathcal{W}_{\mathcal{T}_L}}_{NED} \begin{bmatrix} 0 \\ \kappa^{air}_{\mathcal{T}_L}\ s_{\mathcal{T}_L}\ \bar{c}\ c^M_{\mathcal{T}_L}(\alpha^{NED}_{\mathcal{T}_L}) \\ \kappa^{air}_{\mathcal{T}_L}\ s_{\mathcal{T}_L}\ b\ c^N_{\mathcal{T}_L}(\beta^{NED}_{\mathcal{T}_L}) \end{bmatrix} \tag{B.11}$$

where $\delta_e \triangleq \frac{1}{2}(\delta_{\mathcal{T}_R} + \delta_{\mathcal{T}_L})$ and $\delta_r \triangleq \frac{1}{2}(\delta_{\mathcal{T}_R} - \delta_{\mathcal{T}_L})$, as illustrated in Figure B.8. Besides, $\bar{c} \in \mathbb{R}_{\geq 0}$ is the mean geometric chord of the wings, $b \in \mathbb{R}_{\geq 0}$ is the wing span, $c^{\delta_a}, c^{\delta_e}, c^{\delta_r} \in \mathbb{R}$ are stability derivatives associated with the deflection of the aerodynamic control surfaces, $\alpha^{NED}_{\mathcal{S}} = -\alpha^{air}_{\mathcal{S}}$, $\beta^{NED}_{\mathcal{S}} = -\beta^{air}_{\mathcal{S}}$, and $\boldsymbol{R}^{\mathcal{W}_{\mathcal{S}}}_{NED} = \boldsymbol{R}_{x,\pi}$, for $\mathcal{S} \in \{\mathcal{F}, \mathcal{W}_R, \mathcal{W}_L, \mathcal{T}_R, \mathcal{T}_L, I\}$. The aerodynamic parameters and control surfaces stability derivatives are presented in Table B.1. The coefficients illustrated in Figures B.5 and B.6 were obtained considering the entire wing and tail-surface, as illustrated in Figure B.3. Therefore, a half of the surface area was considered to compute the contribution of the left and right components.

Concerning the aerodynamic forces and moments (B.1)-(B.11), the terms in (7.18) related to the fuselage, wings, tail surfaces, and aerodynamic interference, are computed

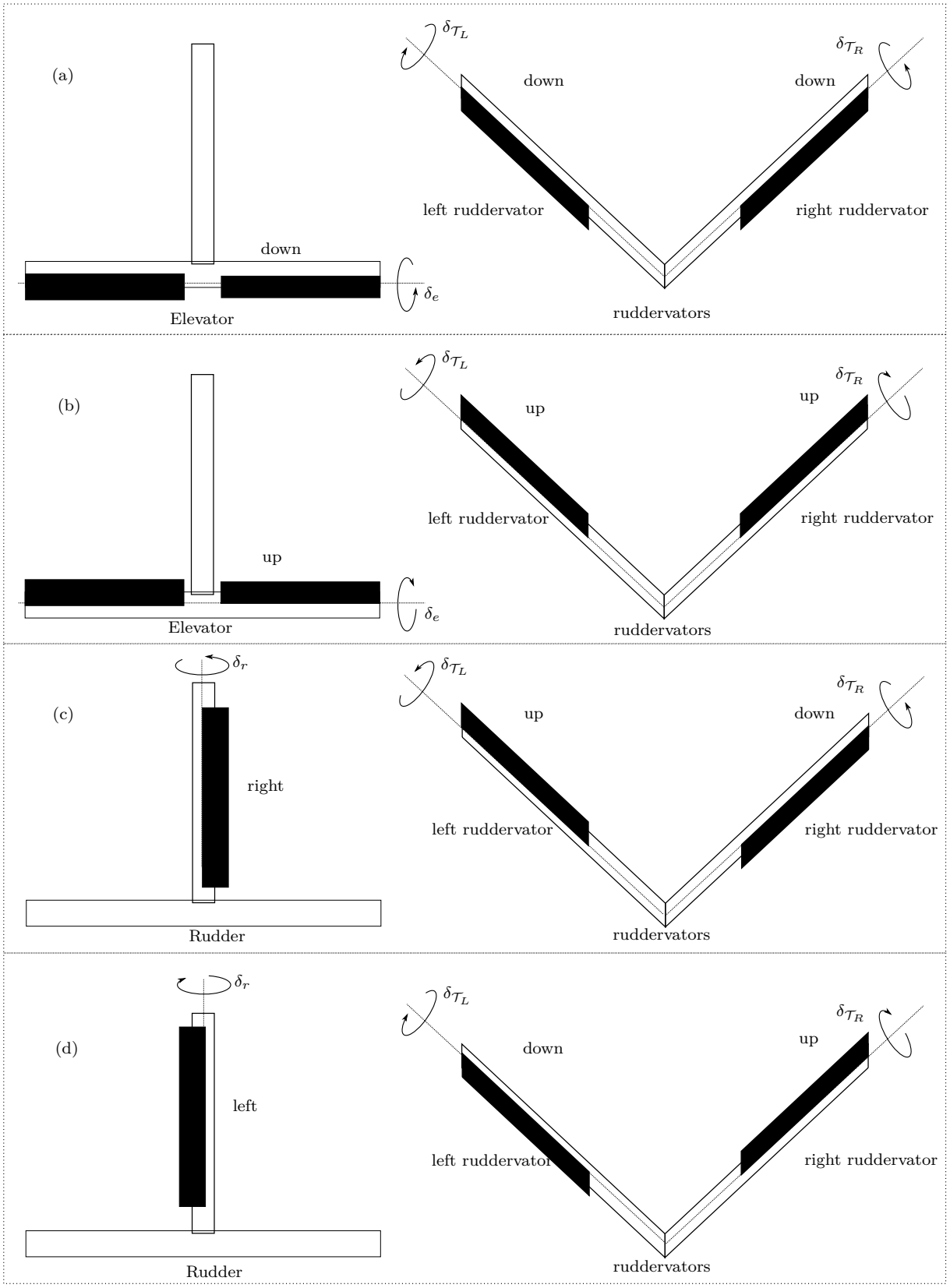

Figure B.8: T-tail and V-tail aerodynamic control surfaces equivalences (back view). In picture (a), both ruddervators are deflected down, which is equivalent to deflect the elevator down. In picture (b), both ruddervators are deflected up, which is equivalent to deflect the elevator up. In picture (c), the right and left ruddervators are deflected down and up, respectively, which is equivalent to deflect the rudder right. In picture (d), the right and left ruddervators are deflected up and down, respectively, which is equivalent to deflect the rudder left.

as follows

$$\boldsymbol{\vartheta}_{\mathcal{F}} = \boldsymbol{J}'_{\mathcal{F}}\boldsymbol{R}^{\mathcal{I}}_{\mathcal{F}}\left(\boldsymbol{R}^{\mathcal{F}}_{\mathcal{W}_{\mathcal{F}}}\begin{bmatrix} f^d_{\mathcal{F}} \\ f^y_{\mathcal{F}} \\ f^l_{\mathcal{F}} \end{bmatrix}\right) + \boldsymbol{W}'_{\mathcal{F}}\boldsymbol{R}^{\mathcal{I}}_{\mathcal{F}}\begin{bmatrix} L_{\mathcal{F}} \\ M_{\mathcal{F}} \\ N_{\mathcal{F}} \end{bmatrix}, \tag{B.12}$$

$$\begin{aligned}\boldsymbol{\vartheta}_{\mathcal{W}} = {} & \boldsymbol{J}'_{\mathcal{W}_R}\boldsymbol{R}^{\mathcal{I}}_{\mathcal{W}_R}\left(\boldsymbol{R}^{\mathcal{W}_R}_{\mathcal{W}_{\mathcal{W}_R}}\begin{bmatrix} f^d_{\mathcal{W}_R} \\ f^y_{\mathcal{W}_R} \\ f^l_{\mathcal{W}_R} \end{bmatrix}\right) + \boldsymbol{W}'_{\mathcal{W}_R}\boldsymbol{R}^{\mathcal{I}}_{\mathcal{W}_R}\begin{bmatrix} L_{\mathcal{W}_R} \\ M_{\mathcal{W}_R} \\ N_{\mathcal{W}_R} \end{bmatrix} \\ & + \boldsymbol{J}'_{\mathcal{W}_L}\boldsymbol{R}^{\mathcal{I}}_{\mathcal{W}_L}\left(\boldsymbol{R}^{\mathcal{W}_L}_{\mathcal{W}_{\mathcal{W}_L}}\begin{bmatrix} f^d_{\mathcal{W}_L} \\ f^y_{\mathcal{W}_L} \\ f^l_{\mathcal{W}_L} \end{bmatrix}\right) + \boldsymbol{W}'_{\mathcal{W}_L}\boldsymbol{R}^{\mathcal{I}}_{\mathcal{W}_L}\begin{bmatrix} L_{\mathcal{W}_L} \\ M_{\mathcal{W}_L} \\ N_{\mathcal{W}_L} \end{bmatrix},\end{aligned} \tag{B.13}$$

$$\begin{aligned}\boldsymbol{\vartheta}_{\mathcal{T}} = {} & \boldsymbol{J}'_{\mathcal{T}_R}\boldsymbol{R}^{\mathcal{I}}_{\mathcal{T}_R}\left(\boldsymbol{R}^{\mathcal{T}_R}_{\mathcal{W}_{\mathcal{T}_R}}\begin{bmatrix} f^d_{\mathcal{T}_R} \\ f^y_{\mathcal{T}_R} \\ f^l_{\mathcal{T}_R} \end{bmatrix}\right) + \boldsymbol{W}'_{\mathcal{T}_R}\boldsymbol{R}^{\mathcal{I}}_{\mathcal{T}_R}\begin{bmatrix} L_{\mathcal{T}_R} \\ M_{\mathcal{T}_R} \\ N_{\mathcal{T}_R} \end{bmatrix} \\ & + \boldsymbol{J}'_{\mathcal{T}_L}\boldsymbol{R}^{\mathcal{I}}_{\mathcal{T}_L}\left(\boldsymbol{R}^{\mathcal{T}_L}_{\mathcal{W}_{\mathcal{T}_L}}\begin{bmatrix} f^d_{\mathcal{T}_L} \\ f^y_{\mathcal{T}_L} \\ f^l_{\mathcal{T}_L} \end{bmatrix}\right) + \boldsymbol{W}'_{\mathcal{T}_L}\boldsymbol{R}^{\mathcal{I}}_{\mathcal{T}_L}\begin{bmatrix} L_{\mathcal{T}_L} \\ M_{\mathcal{T}_L} \\ N_{\mathcal{T}_L} \end{bmatrix},\end{aligned} \tag{B.14}$$

$$\boldsymbol{\vartheta}_{I} = \boldsymbol{J}'_{I}\boldsymbol{R}^{\mathcal{I}}_{I}\left(\boldsymbol{R}^{I}_{\mathcal{W}_{\mathcal{I}}}\begin{bmatrix} f^d_{I} \\ f^y_{I} \\ f^l_{I} \end{bmatrix}\right) \tag{B.15}$$

where the rotation matrix $\boldsymbol{R}^{\mathcal{S}}_{\alpha_{\mathcal{W}_{\mathcal{S}}}} \triangleq \boldsymbol{R}_{y,-\alpha^{air}_{\mathcal{S}}}\boldsymbol{R}_{z,-\beta^{air}_{\mathcal{S}}}$, for $\mathcal{S} \in \{\mathcal{F},\ \mathcal{W}_R,\ \mathcal{W}_L,\ \mathcal{T}_R,\ \mathcal{T}_L\}$, is used to express the lift, drag, and side forces from the wind orientation to the aerodynamic center frame, and the linear and angular velocity Jacobians $\boldsymbol{J}_{\mathcal{S}}$ and $\boldsymbol{W}_{\mathcal{S}}$ are given according to (7.35) and (7.36). In addition, to comply with the orientation of the aerodynamic centers that are considered in the wind tunnel experiments, the following rotation matrix is considered $\boldsymbol{R}^{\mathcal{I}}_{\mathcal{S}} = \boldsymbol{R}^{\mathcal{I}}_{\mathcal{B}}$, for $\mathcal{S} \in \{\mathcal{F}, \mathcal{W}_R, \mathcal{W}_L, \mathcal{T}_R, \mathcal{T}_L, I\}$.

The physical parameters of the ProVANT-Emergentia Tilt-rotor UAV were obtained from the computer-aided-design (CAD) model, which are presented in Table B.1.

Table B.1: ProVANT-Emergentia Tilt-rotor UAV physical parameters.

System Parameters		
$\boldsymbol{g}'_{\boldsymbol{r}}$	$\begin{bmatrix} 0 & 0 & -9.87 \end{bmatrix}$	[m/s^2]
β, ϵ, μ	$\{5, 5, 30\}$	[deg]
ν	0.005	[N · m · s / rad]
$m_{c_1}, m_{c_2}, m_{c_3}$	$\{7,\ 0.3,\ 0.3\}$	[kg]
$\boldsymbol{d}^{\mathcal{B}}_{\mathcal{B},\mathcal{C}_1}$	$\begin{bmatrix} 0.05 & 0 & 0.12 \end{bmatrix}'$	[m]
$\boldsymbol{d}^{\mathcal{B}}_{\mathcal{B},\mathcal{A}_2}$	$\begin{bmatrix} 0.03 & -1.025 & 0.292 \end{bmatrix}'$	[m]
$\boldsymbol{d}^{\mathcal{A}_2}_{\mathcal{A}_2,\mathcal{C}_2}$	$\begin{bmatrix} 0 & 0 & 0.07 \end{bmatrix}'$	[m]
$\boldsymbol{d}^{\mathcal{A}_2}_{\mathcal{A}_2,\mathcal{P}_R}$	$\begin{bmatrix} 0 & 0 & 0.1 \end{bmatrix}'$	[m]
$\boldsymbol{d}^{\mathcal{B}}_{\mathcal{B},\mathcal{A}_3}$	$\begin{bmatrix} 0.03 & 1.025 & 0.292 \end{bmatrix}'$	[m]
$\boldsymbol{d}^{\mathcal{A}_3}_{\mathcal{A}_3,\mathcal{C}_3}$	$\begin{bmatrix} 0 & 0 & 0.07 \end{bmatrix}'$	[m]
$\boldsymbol{d}^{\mathcal{A}_3}_{\mathcal{A}_3,\mathcal{P}_L}$	$\begin{bmatrix} 0 & 0 & 0.1 \end{bmatrix}'$	[m]
$\boldsymbol{d}^{\mathcal{B}}_{\mathcal{B},\mathcal{F}}$	$\begin{bmatrix} 0.1960 & 0 & 0.1200 \end{bmatrix}'$	[m]
$\boldsymbol{d}^{\mathcal{B}}_{\mathcal{B},\mathcal{W}_R}$	$\begin{bmatrix} 0.0060 & -0.4650 & 0.2620 \end{bmatrix}'$	[m]
$\boldsymbol{d}^{\mathcal{B}}_{\mathcal{B},\mathcal{W}_L}$	$\begin{bmatrix} 0.0060 & 0.4650 & 0.2620 \end{bmatrix}'$	[m]
$\boldsymbol{d}^{\mathcal{B}}_{\mathcal{B},\mathcal{T}_R}$	$\begin{bmatrix} -0.4823 & -0.2952 & 0.3532 \end{bmatrix}'$	[m]
$\boldsymbol{d}^{\mathcal{B}}_{\mathcal{B},\mathcal{T}_L}$	$\begin{bmatrix} -0.4823 & 0.2952 & 0.3532 \end{bmatrix}'$	[m]
$\mathbb{I}_{\mathcal{C}_1}$	$\begin{bmatrix} 2.727 & 0 & -0.002 \\ 0 & 7.447 & 0 \\ -0.002 & 0 & 9.95 \end{bmatrix}$	[kg·m^2]
$\mathbb{I}_{\mathcal{C}_2}$, $\mathbb{I}_{\mathcal{C}_3}$	diag(0.005, 0.005, 0.002)	[kg·m^2]
Aerodynamic parameters and stability derivatives		
ρ	1.21	[kg/m^3]
d	0.6096	[m]
b	1.7592	[m]
$\bar{c}$	0.1366	[m]
$s_{\mathcal{F}}, s_{\mathcal{W}_R}, s_{\mathcal{W}_L}, s_{\mathcal{T}_R}, s_{\mathcal{T}_L}, s_I$	0.1250	[m]
c^{δ_a}	0.7104	
c^{δ_e}	0.3759	
c^{δ_r}	−0.0730	

C

Tilt-rotor UAV Input coupling matrix

This Appendix manipulates the vector of generalized forces (7.18) to represent it into the input affine form (7.62), taking into account the aerodynamic coefficients presented in Appendix B.

Initially, one can manipulate (7.32) as follows,

$$\begin{aligned}
\boldsymbol{\vartheta}_{\mathcal{P}} =& \boldsymbol{J}'_{\mathcal{P}_R}\boldsymbol{R}^{\mathcal{I}}_{\mathcal{P}_R}\begin{bmatrix}\mathbf{0}\\ f_{\mathcal{P}_R}\end{bmatrix} + \boldsymbol{W}'_{\mathcal{P}_R}\boldsymbol{R}^{\mathcal{I}}_{\mathcal{P}_R}\begin{bmatrix}\mathbf{0}\\ \lambda_{\mathcal{P}_R} t_{\mathcal{P}_R}\end{bmatrix} + \boldsymbol{J}'_{\mathcal{P}_L}\boldsymbol{R}^{\mathcal{I}}_{\mathcal{P}_L}\begin{bmatrix}\mathbf{0}\\ f_{\mathcal{P}_L}\end{bmatrix} + \boldsymbol{W}'_{\mathcal{P}_L}\boldsymbol{R}^{\mathcal{I}}_{\mathcal{P}_L}\begin{bmatrix}\mathbf{0}\\ \lambda_{\mathcal{P}_L} t_{\mathcal{P}_L}\end{bmatrix},\\
=& \left(\boldsymbol{J}'_{\mathcal{P}_R} + \boldsymbol{W}'_{\mathcal{P}_R}\lambda_{\mathcal{P}_R} d\frac{c_q}{c_t}\right)\boldsymbol{R}^{\mathcal{I}}_{\mathcal{P}_R}\boldsymbol{a}_z f_{\mathcal{P}_R} + \left(\boldsymbol{J}'_{\mathcal{P}_L} + \boldsymbol{W}'_{\mathcal{P}_L}\lambda_{\mathcal{P}_L} d\frac{c_q}{c_t}\right)\boldsymbol{R}^{\mathcal{I}}_{\mathcal{P}_L}\boldsymbol{a}_z f_{\mathcal{P}_L},\\
=& \overbrace{\begin{bmatrix}\left(\boldsymbol{J}'_{\mathcal{P}_R} + \boldsymbol{W}'_{\mathcal{P}_R}\lambda_{\mathcal{P}_R} d\frac{c_q}{c_t}\right)\boldsymbol{R}^{\mathcal{I}}_{\mathcal{P}_R}\boldsymbol{a}_z & \left(\boldsymbol{J}'_{\mathcal{P}_L} + \boldsymbol{W}'_{\mathcal{P}_L}\lambda_{\mathcal{P}_L} d\frac{c_q}{c_t}\right)\boldsymbol{R}^{\mathcal{I}}_{\mathcal{P}_L}\boldsymbol{a}_z\end{bmatrix}}^{\boldsymbol{\Xi}_1}\begin{bmatrix}f_{\mathcal{P}_R}\\ f_{\mathcal{P}_L}\end{bmatrix}, \qquad \text{(C.1)}\\
=& \boldsymbol{\Xi}_1\begin{bmatrix}f_{\mathcal{P}_R}\\ f_{\mathcal{P}_L}\end{bmatrix}, \qquad \text{(C.2)}
\end{aligned}$$

with $t_{\mathcal{P}} = d\dfrac{c_q\left(J_{\mathcal{P}}, \varphi^{air}_{\mathcal{P}}\right)}{c_t\left(J_{\mathcal{P}}, \varphi^{air}_{\mathcal{P}}\right)} f_{\mathcal{P}}$, for $\mathcal{P} \in \{\mathcal{P}_R, \mathcal{P}_L\}$.

In addition, (7.33) can be written as

$$\boldsymbol{\vartheta}_s = \boldsymbol{W}'_{\mathcal{C}_2}\boldsymbol{R}^{\mathcal{I}}_{\mathcal{C}_2}\begin{bmatrix}0\\ \tau_{s_R}\\ 0\end{bmatrix} - \boldsymbol{W}'_{\mathcal{C}_1}\boldsymbol{R}^{\mathcal{I}}_{\mathcal{C}_2}\begin{bmatrix}0\\ \tau_{s_R}\\ 0\end{bmatrix} + \boldsymbol{W}'_{\mathcal{C}_3}\boldsymbol{R}^{\mathcal{I}}_{\mathcal{C}_3}\begin{bmatrix}0\\ \tau_{s_L}\\ 0\end{bmatrix} - \boldsymbol{W}'_{\mathcal{C}_1}\boldsymbol{R}^{\mathcal{I}}_{\mathcal{C}_3}\begin{bmatrix}0\\ \tau_{s_L}\\ 0\end{bmatrix} - \begin{bmatrix}\nu\boldsymbol{I} & \mathbf{0}\\ \mathbf{0} & \mathbf{0}\end{bmatrix}\dot{\boldsymbol{q}},$$

$$= \overbrace{\begin{bmatrix}\left(\boldsymbol{W}'_{\mathcal{C}_2} - \boldsymbol{W}'_{\mathcal{C}_1}\right)\boldsymbol{R}^{\mathcal{I}}_{\mathcal{C}_2}\boldsymbol{a}_y & \left(\boldsymbol{W}'_{\mathcal{C}_3} - \boldsymbol{W}'_{\mathcal{C}_1}\right)\boldsymbol{R}^{\mathcal{I}}_{\mathcal{C}_3}\boldsymbol{a}_y\end{bmatrix}}^{\boldsymbol{\Xi}_2}\begin{bmatrix}\tau_{s_R}\\ \tau_{s_L}\end{bmatrix} - \begin{bmatrix}\nu\boldsymbol{I} & \boldsymbol{0}\\ \boldsymbol{0} & \boldsymbol{0}\end{bmatrix}\dot{\boldsymbol{q}},$$

$$= \boldsymbol{\Xi}_2\begin{bmatrix}\tau_{s_R}\\ \tau_{s_L}\end{bmatrix} - \begin{bmatrix}\nu\boldsymbol{I} & \boldsymbol{0}\\ \boldsymbol{0} & \boldsymbol{0}\end{bmatrix}\dot{\boldsymbol{q}}. \tag{C.3}$$

Moreover, the aerodynamic forces (B.2), (B.3), (B.4), and (B.5) are represented by

$$\begin{bmatrix}f^d_{\mathcal{W}_R}\\ f^y_{\mathcal{W}_R}\\ f^l_{\mathcal{W}_R}\end{bmatrix} = \overbrace{\boldsymbol{R}^{\mathcal{W}_{\mathcal{W}_R}}_{NED}\begin{bmatrix}0\\ 0\\ -\kappa^{air}_{\mathcal{W}_R}\ s_{\mathcal{W}_R}\ c^{\delta_a}\delta_{\mathcal{W}_R}\end{bmatrix}}^{{}^{active}\boldsymbol{f}_{\mathcal{W}_R}} + \overbrace{\boldsymbol{R}^{\mathcal{W}_{\mathcal{W}_R}}_{NED}\begin{bmatrix}-\kappa^{air}_{\mathcal{W}_R}\ s_{\mathcal{W}_R}\ \left(c^d_{\mathcal{W}_{R_{xy}}}(\beta^{NED}_{\mathcal{W}_R}) + c^d_{\mathcal{W}_{R_{xz}}}(\alpha^{NED}_{\mathcal{W}_R})\right)\\ -\kappa^{air}_{\mathcal{W}_R}\ s_{\mathcal{W}_R}\ c^y_{\mathcal{W}_R}(\beta^{NED}_{\mathcal{W}_R})\\ -\kappa^{air}_{\mathcal{W}_R}\ s_{\mathcal{W}_R}\ c^l_{\mathcal{W}_R}(\alpha^{NED}_{\mathcal{W}_R})\end{bmatrix}}^{{}^{passive}\boldsymbol{f}_{\mathcal{W}_R}},$$

$$= {}^{active}\boldsymbol{f}_{\mathcal{W}_R} + {}^{passive}\boldsymbol{f}_{\mathcal{W}_R}, \tag{C.4}$$

$$\begin{bmatrix}f^d_{\mathcal{W}_L}\\ f^y_{\mathcal{W}_L}\\ f^l_{\mathcal{W}_L}\end{bmatrix} = \overbrace{\boldsymbol{R}^{\mathcal{W}_{\mathcal{W}_L}}_{NED}\begin{bmatrix}0\\ 0\\ -\kappa^{air}_{\mathcal{W}_L}\ s_{\mathcal{W}_L}\ c^{\delta_a}\delta_{\mathcal{W}_L}\end{bmatrix}}^{{}^{active}\boldsymbol{f}_{\mathcal{W}_L}} + \overbrace{\boldsymbol{R}^{\mathcal{W}_{\mathcal{W}_L}}_{NED}\begin{bmatrix}-\kappa^{air}_{\mathcal{W}_L}\ s_{\mathcal{W}_L}\ \left(c^d_{\mathcal{W}_{L_{xy}}}(\beta^{NED}_{\mathcal{W}_L}) + c^d_{\mathcal{W}_{L_{xz}}}(\alpha^{NED}_{\mathcal{W}_L})\right)\\ -\kappa^{air}_{\mathcal{W}_L}\ s_{\mathcal{W}_L}\ c^y_{\mathcal{W}_L}(\beta^{NED}_{\mathcal{W}_L})\\ -\kappa^{air}_{\mathcal{W}_L}\ s_{\mathcal{W}_L}\ c^l_{\mathcal{W}_L}(\alpha^{NED}_{\mathcal{W}_L})\end{bmatrix}}^{{}^{passive}\boldsymbol{f}_{\mathcal{W}_L}},$$

$$= {}^{active}\boldsymbol{f}_{\mathcal{W}_L} + {}^{passive}\boldsymbol{f}_{\mathcal{W}_L}, \tag{C.5}$$

$$\begin{bmatrix}f^d_{\mathcal{T}_R}\\ f^y_{\mathcal{T}_R}\\ f^l_{\mathcal{T}_R}\end{bmatrix} = \overbrace{\boldsymbol{R}^{\mathcal{W}_{\mathcal{T}_R}}_{NED}\begin{bmatrix}0\\ -\kappa^{air}_{\mathcal{T}_R}\ s_{\mathcal{T}_R}\ c^{\delta_r}\delta_r\\ -\kappa^{air}_{\mathcal{T}_R}\ s_{\mathcal{T}_R}\ c^{\delta_e}\delta_e\end{bmatrix}}^{{}^{active}\boldsymbol{f}_{\mathcal{T}_R}} + \overbrace{\boldsymbol{R}^{\mathcal{W}_{\mathcal{T}_R}}_{NED}\begin{bmatrix}-\kappa^{air}_{\mathcal{T}_R}\ s_{\mathcal{T}_R}\ \left(c^d_{\mathcal{T}_{R_{xy}}}(\beta^{NED}_{\mathcal{T}_R}) + c^d_{\mathcal{T}_{R_{xz}}}(\alpha^{NED}_{\mathcal{T}_R})\right)\\ -\kappa^{air}_{\mathcal{T}_R}\ s_{\mathcal{T}_R}\ c^y_{\mathcal{T}_R}(\beta^{NED}_{\mathcal{T}_R})\\ -\kappa^{air}_{\mathcal{T}_R}\ s_{\mathcal{T}_R}\ c^l_{\mathcal{T}_R}(\alpha^{NED}_{\mathcal{T}_R})\end{bmatrix}}^{{}^{passive}\boldsymbol{f}_{\mathcal{T}_R}},$$

$$= {}^{active}\boldsymbol{f}_{\mathcal{T}_R} + {}^{passive}\boldsymbol{f}_{\mathcal{T}_R}, \tag{C.6}$$

$$\begin{bmatrix}f^d_{\mathcal{T}_L}\\ f^y_{\mathcal{T}_L}\\ f^l_{\mathcal{T}_L}\end{bmatrix} = \overbrace{\boldsymbol{R}^{\mathcal{W}_{\mathcal{T}_L}}_{NED}\begin{bmatrix}0\\ -\kappa^{air}_{\mathcal{T}_L}\ s_{\mathcal{T}_L}\ c^{\delta_r}\delta_r\\ -\kappa^{air}_{\mathcal{T}_L}\ s_{\mathcal{T}_L}\ c^{\delta_e}\delta_e\end{bmatrix}}^{{}^{active}\boldsymbol{f}_{\mathcal{T}_L}} + \overbrace{\boldsymbol{R}^{\mathcal{W}_{\mathcal{T}_L}}_{NED}\begin{bmatrix}-\kappa^{air}_{\mathcal{T}_L}\ s_{\mathcal{T}_L}\ \left(c^d_{\mathcal{T}_{L_{xy}}}(\beta^{NED}_{\mathcal{T}_L}) + c^d_{\mathcal{T}_{L_{xz}}}(\alpha^{NED}_{\mathcal{T}_L})\right)\\ -\kappa^{air}_{\mathcal{T}_L}\ s_{\mathcal{T}_L}\ c^y_{\mathcal{T}_L}(\beta^{NED}_{\mathcal{T}_L})\\ -\kappa^{air}_{\mathcal{T}_L}\ s_{\mathcal{T}_L}\ c^l_{\mathcal{T}_L}(\alpha^{NED}_{\mathcal{T}_L})\end{bmatrix}}^{{}^{passive}\boldsymbol{f}_{\mathcal{T}_L}},$$

$$= {}^{active}\boldsymbol{f}_{\mathcal{T}_L} + {}^{passive}\boldsymbol{f}_{\mathcal{T}_L}, \tag{C.7}$$

where the superscripts active and passive stand for the terms influenced and uninfluenced, respectively, by the deflection of the aerodynamic control surfaces.

From (C.4), (C.5), (C.6), and (C.7), the vector of generalized forces (B.12), (B.13), (B.14), and (B.15), can be written as

$$\boldsymbol{\vartheta}_{\mathcal{F}} + \boldsymbol{\vartheta}_{\mathcal{W}} + \boldsymbol{\vartheta}_{\mathcal{T}} + \boldsymbol{\vartheta}_{I} = \boldsymbol{J}'_{\mathcal{W}_R}\boldsymbol{R}^{\mathcal{I}}_{\mathcal{W}_R}\boldsymbol{R}^{\mathcal{W}_R}_{\mathcal{W}_{\mathcal{W}_R}}\left({}^{active}\boldsymbol{f}_{\mathcal{W}_R} + {}^{passive}\boldsymbol{f}_{\mathcal{W}_R}\right) + \boldsymbol{W}'_{\mathcal{W}_R}\boldsymbol{R}^{\mathcal{I}}_{\mathcal{W}_R}\begin{bmatrix}L_{\mathcal{W}_R}\\ M_{\mathcal{W}_R}\\ N_{\mathcal{W}_R}\end{bmatrix}$$

$$+ \boldsymbol{J}'_{\mathcal{W}_L}\boldsymbol{R}^{\mathcal{I}}_{\mathcal{W}_L}\boldsymbol{R}^{\mathcal{W}_L}_{\mathcal{W}_{\mathcal{W}_L}}\left({}^{active}\boldsymbol{f}_{\mathcal{W}_L} + {}^{passive}\boldsymbol{f}_{\mathcal{W}_L}\right) + \boldsymbol{W}'_{\mathcal{W}_L}\boldsymbol{R}^{\mathcal{I}}_{\mathcal{W}_L}\begin{bmatrix}L_{\mathcal{W}_L}\\ M_{\mathcal{W}_L}\\ N_{\mathcal{W}_L}\end{bmatrix}$$

$$
\begin{aligned}
&+ \boldsymbol{J}'_{\mathcal{T}_R} \boldsymbol{R}^{\mathcal{I}}_{\mathcal{T}_R} \boldsymbol{R}^{\mathcal{T}_R}_{\mathcal{W}_{\mathcal{T}_R}} \left({}^{active}\boldsymbol{f}_{\mathcal{T}_R} + {}^{passive}\boldsymbol{f}_{\mathcal{T}_R} \right) + \boldsymbol{W}'_{\mathcal{T}_R} \boldsymbol{R}^{\mathcal{I}}_{\mathcal{T}_R} \begin{bmatrix} L_{\mathcal{T}_R} \\ M_{\mathcal{T}_R} \\ N_{\mathcal{T}_R} \end{bmatrix} \\
&+ \boldsymbol{J}'_{\mathcal{T}_L} \boldsymbol{R}^{\mathcal{I}}_{\mathcal{T}_L} \boldsymbol{R}^{\mathcal{T}_L}_{\mathcal{W}_{\mathcal{T}_L}} \left({}^{active}\boldsymbol{f}_{\mathcal{T}_L} + {}^{passive}\boldsymbol{f}_{\mathcal{T}_L} \right) + \boldsymbol{W}'_{\mathcal{T}_L} \boldsymbol{R}^{\mathcal{I}}_{\mathcal{T}_L} \begin{bmatrix} L_{\mathcal{T}_L} \\ M_{\mathcal{T}_L} \\ N_{\mathcal{T}_L} \end{bmatrix} \\
&+ \boldsymbol{\vartheta}_{\mathcal{F}} + \boldsymbol{\vartheta}_I, \\
&= -\boldsymbol{J}'_{\mathcal{W}_R} \boldsymbol{R}^{\mathcal{I}}_{\mathcal{W}_R} \boldsymbol{R}^{\mathcal{W}_R}_{\mathcal{W}_{\mathcal{W}_R}} \boldsymbol{R}^{\mathcal{W}_{\mathcal{W}_R}}_{NED} \boldsymbol{a}_z \kappa^{air}_{\mathcal{W}_R} \; s_{\mathcal{W}_R} \; c^{\delta_a} \delta_{\mathcal{W}_R} \\
&- \boldsymbol{J}'_{\mathcal{W}_L} \boldsymbol{R}^{\mathcal{I}}_{\mathcal{W}_L} \boldsymbol{R}^{\mathcal{W}_L}_{\mathcal{W}_{\mathcal{W}_L}} \boldsymbol{R}^{\mathcal{W}_{\mathcal{W}_L}}_{NED} \boldsymbol{a}_z \kappa^{air}_{\mathcal{W}_L} \; s_{\mathcal{W}_L} \; c^{\delta_a} \delta_{\mathcal{W}_L} \\
&- \boldsymbol{J}'_{\mathcal{T}_R} \boldsymbol{R}^{\mathcal{I}}_{\mathcal{T}_R} \boldsymbol{R}^{\mathcal{T}_R}_{\mathcal{W}_{\mathcal{T}_R}} \boldsymbol{R}^{\mathcal{W}_{\mathcal{T}_R}}_{NED} \boldsymbol{a}_z \kappa^{air}_{\mathcal{T}_R} \; s_{\mathcal{T}_R} \; c^{\delta_e} \delta_e - \boldsymbol{J}'_{\mathcal{T}_R} \boldsymbol{R}^{\mathcal{I}}_{\mathcal{T}_R} \boldsymbol{R}^{\mathcal{T}_R}_{\mathcal{W}_{\mathcal{T}_R}} \boldsymbol{R}^{\mathcal{W}_{\mathcal{T}_R}}_{NED} \boldsymbol{a}_y - \kappa^{air}_{\mathcal{T}_R} \; s_{\mathcal{T}_R} \; c^{\delta_r} \delta_r \\
&- \boldsymbol{J}'_{\mathcal{T}_L} \boldsymbol{R}^{\mathcal{I}}_{\mathcal{T}_L} \boldsymbol{R}^{\mathcal{T}_L}_{\mathcal{W}_{\mathcal{T}_L}} \boldsymbol{R}^{\mathcal{W}_{\mathcal{T}_L}}_{NED} \boldsymbol{a}_y \kappa^{air}_{\mathcal{T}_L} \; s_{\mathcal{T}_L} \; c^{\delta_r} \delta_r - \boldsymbol{J}'_{\mathcal{T}_L} \boldsymbol{R}^{\mathcal{I}}_{\mathcal{T}_L} \boldsymbol{R}^{\mathcal{T}_L}_{\mathcal{W}_{\mathcal{T}_L}} \boldsymbol{R}^{\mathcal{W}_{\mathcal{T}_L}}_{NED} \boldsymbol{a}_z \kappa^{air}_{\mathcal{T}_L} \; s_{\mathcal{T}_L} \; c^{\delta_e} \delta_e \\
&+ \boldsymbol{J}'_{\mathcal{W}_R} \boldsymbol{R}^{\mathcal{I}}_{\mathcal{W}_R} \boldsymbol{R}^{\mathcal{W}_R}_{\mathcal{W}_{\mathcal{W}_R}} {}^{passive}\boldsymbol{f}_{\mathcal{W}_R} + \boldsymbol{W}'_{\mathcal{W}_R} \boldsymbol{R}^{\mathcal{I}}_{\mathcal{W}_R} \begin{bmatrix} L_{\mathcal{W}_R} \\ M_{\mathcal{W}_R} \\ N_{\mathcal{W}_R} \end{bmatrix} \\
&+ \boldsymbol{J}'_{\mathcal{W}_L} \boldsymbol{R}^{\mathcal{I}}_{\mathcal{W}_L} \boldsymbol{R}^{\mathcal{W}_L}_{\mathcal{W}_{\mathcal{W}_L}} {}^{passive}\boldsymbol{f}_{\mathcal{W}_L} + \boldsymbol{W}'_{\mathcal{W}_L} \boldsymbol{R}^{\mathcal{I}}_{\mathcal{W}_L} \begin{bmatrix} L_{\mathcal{W}_L} \\ M_{\mathcal{W}_L} \\ N_{\mathcal{W}_L} \end{bmatrix} \\
&+ \boldsymbol{J}'_{\mathcal{T}_R} \boldsymbol{R}^{\mathcal{I}}_{\mathcal{T}_R} \boldsymbol{R}^{\mathcal{T}_R}_{\mathcal{W}_{\mathcal{T}_R}} {}^{passive}\boldsymbol{f}_{\mathcal{T}_R} + \boldsymbol{W}'_{\mathcal{T}_R} \boldsymbol{R}^{\mathcal{I}}_{\mathcal{T}_R} \begin{bmatrix} L_{\mathcal{T}_R} \\ M_{\mathcal{T}_R} \\ N_{\mathcal{T}_R} \end{bmatrix} \\
&+ \boldsymbol{J}'_{\mathcal{T}_L} \boldsymbol{R}^{\mathcal{I}}_{\mathcal{T}_L} \boldsymbol{R}^{\mathcal{T}_L}_{\mathcal{W}_{\mathcal{T}_L}} {}^{passive}\boldsymbol{f}_{\mathcal{T}_L} + \boldsymbol{W}'_{\mathcal{T}_L} \boldsymbol{R}^{\mathcal{I}}_{\mathcal{T}_L} \begin{bmatrix} L_{\mathcal{T}_L} \\ M_{\mathcal{T}_L} \\ N_{\mathcal{T}_L} \end{bmatrix} \\
&+ \boldsymbol{\vartheta}_{\mathcal{F}} + \boldsymbol{\vartheta}_I, \\
&= \overbrace{\begin{bmatrix} \boldsymbol{J}'_{\mathcal{W}_R} \boldsymbol{R}^{\mathcal{I}}_{\mathcal{W}_R} \boldsymbol{R}^{\mathcal{W}_R}_{\mathcal{W}_{\mathcal{W}_R}} \boldsymbol{a}_z \kappa^{air}_{\mathcal{W}_R} \; s_{\mathcal{W}_R} \; c^{\delta_a} & \boldsymbol{J}'_{\mathcal{W}_L} \boldsymbol{R}^{\mathcal{I}}_{\mathcal{W}_L} \boldsymbol{R}^{\mathcal{W}_L}_{\mathcal{W}_{\mathcal{W}_L}} \boldsymbol{a}_z \kappa^{air}_{\mathcal{W}_L} \; s_{\mathcal{W}_L} \; c^{\delta_a} \end{bmatrix}}^{\boldsymbol{\Xi}_3} \begin{bmatrix} \delta_{\mathcal{W}_R} \\ \delta_{\mathcal{W}_L} \end{bmatrix} \\
&+ \overbrace{\begin{bmatrix} \boldsymbol{J}'_{\mathcal{T}_R} \boldsymbol{R}^{\mathcal{I}}_{\mathcal{T}_R} \boldsymbol{R}^{\mathcal{T}_R}_{\mathcal{W}_{\mathcal{T}_R}} \boldsymbol{a}_z \kappa^{air}_{\mathcal{T}_R} \; s_{\mathcal{T}_R} \; c^{\delta_e} + \boldsymbol{J}'_{\mathcal{T}_L} \boldsymbol{R}^{\mathcal{I}}_{\mathcal{T}_L} \boldsymbol{R}^{\mathcal{T}_L}_{\mathcal{W}_{\mathcal{T}_L}} \boldsymbol{a}_z \kappa^{air}_{\mathcal{T}_L} \; s_{\mathcal{T}_L} \; c^{\delta_e} \end{bmatrix}}^{\boldsymbol{\Xi}_4} \delta_e \\
&+ \overbrace{\begin{bmatrix} \boldsymbol{J}'_{\mathcal{T}_R} \boldsymbol{R}^{\mathcal{I}}_{\mathcal{T}_R} \boldsymbol{R}^{\mathcal{T}_R}_{\mathcal{W}_{\mathcal{T}_R}} \boldsymbol{a}_y \kappa^{air}_{\mathcal{T}_R} \; s_{\mathcal{T}_R} \; c^{\delta_r} + \boldsymbol{J}'_{\mathcal{T}_L} \boldsymbol{R}^{\mathcal{I}}_{\mathcal{T}_L} \boldsymbol{R}^{\mathcal{T}_L}_{\mathcal{W}_{\mathcal{T}_L}} \boldsymbol{a}_y \kappa^{air}_{\mathcal{T}_L} \; s_{\mathcal{T}_L} \; c^{\delta_r} \end{bmatrix}}^{\boldsymbol{\Xi}_5} \delta_r \\
&+ \boldsymbol{J}'_{\mathcal{W}_R} \boldsymbol{R}^{\mathcal{I}}_{\mathcal{W}_R} \boldsymbol{R}^{\mathcal{W}_R}_{\mathcal{W}_{\mathcal{W}_R}} {}^{passive}\boldsymbol{f}_{\mathcal{W}_R} + \boldsymbol{W}'_{\mathcal{W}_R} \boldsymbol{R}^{\mathcal{I}}_{\mathcal{W}_R} \begin{bmatrix} L_{\mathcal{W}_R} \\ M_{\mathcal{W}_R} \\ N_{\mathcal{W}_R} \end{bmatrix} \\
&+ \boldsymbol{J}'_{\mathcal{W}_L} \boldsymbol{R}^{\mathcal{I}}_{\mathcal{W}_L} \boldsymbol{R}^{\mathcal{W}_L}_{\mathcal{W}_{\mathcal{W}_L}} {}^{passive}\boldsymbol{f}_{\mathcal{W}_L} + \boldsymbol{W}'_{\mathcal{W}_L} \boldsymbol{R}^{\mathcal{I}}_{\mathcal{W}_L} \begin{bmatrix} L_{\mathcal{W}_L} \\ M_{\mathcal{W}_L} \\ N_{\mathcal{W}_L} \end{bmatrix}
\end{aligned}
$$

$$
\begin{aligned}
&+ \boldsymbol{J}'_{\mathcal{T}_R} \boldsymbol{R}^{\mathcal{I}}_{\mathcal{T}_R} \boldsymbol{R}^{\mathcal{T}_R}_{\mathcal{W}_{\mathcal{T}_R}}{}^{passive}\boldsymbol{f}_{\mathcal{T}_R} + \boldsymbol{W}'_{\mathcal{T}_R} \boldsymbol{R}^{\mathcal{I}}_{\mathcal{T}_R} \begin{bmatrix} L_{\mathcal{T}_R} \\ M_{\mathcal{T}_R} \\ N_{\mathcal{T}_R} \end{bmatrix} \\
&+ \boldsymbol{J}'_{\mathcal{T}_L} \boldsymbol{R}^{\mathcal{I}}_{\mathcal{T}_L} \boldsymbol{R}^{\mathcal{T}_L}_{\mathcal{W}_{\mathcal{T}_L}}{}^{passive}\boldsymbol{f}_{\mathcal{T}_L} + \boldsymbol{W}'_{\mathcal{T}_L} \boldsymbol{R}^{\mathcal{I}}_{\mathcal{T}_L} \begin{bmatrix} L_{\mathcal{T}_L} \\ M_{\mathcal{T}_L} \\ N_{\mathcal{T}_L} \end{bmatrix} \\
&+ \boldsymbol{\vartheta}_{\mathcal{F}} + \boldsymbol{\vartheta}_I, \\
&= [\boldsymbol{\Xi}_3 \;\; \boldsymbol{\Xi}_4 \;\; \boldsymbol{\Xi}_5] \begin{bmatrix} 1 & 0 & 0 & 0 \\ 0 & 1 & 0 & 0 \\ 0 & 0 & \frac{1}{2} & \frac{1}{2} \\ 0 & 0 & \frac{1}{2} & -\frac{1}{2} \end{bmatrix} \begin{bmatrix} \delta_{\mathcal{W}_R} \\ \delta_{\mathcal{W}_L} \\ \delta_{\mathcal{T}_R} \\ \delta_{\mathcal{T}_L} \end{bmatrix} \\
&+ \boldsymbol{J}'_{\mathcal{W}_R} \boldsymbol{R}^{\mathcal{I}}_{\mathcal{W}_R} \boldsymbol{R}^{\mathcal{W}_R}_{\mathcal{W}_{\mathcal{W}_R}}{}^{passive}\boldsymbol{f}_{\mathcal{W}_R} + \boldsymbol{W}'_{\mathcal{W}_R} \boldsymbol{R}^{\mathcal{I}}_{\mathcal{W}_R} \begin{bmatrix} L_{\mathcal{W}_R} \\ M_{\mathcal{W}_R} \\ N_{\mathcal{W}_R} \end{bmatrix} \\
&+ \boldsymbol{J}'_{\mathcal{W}_L} \boldsymbol{R}^{\mathcal{I}}_{\mathcal{W}_L} \boldsymbol{R}^{\mathcal{W}_L}_{\mathcal{W}_{\mathcal{W}_L}}{}^{passive}\boldsymbol{f}_{\mathcal{W}_L} + \boldsymbol{W}'_{\mathcal{W}_L} \boldsymbol{R}^{\mathcal{I}}_{\mathcal{W}_L} \begin{bmatrix} L_{\mathcal{W}_L} \\ M_{\mathcal{W}_L} \\ N_{\mathcal{W}_L} \end{bmatrix} \\
&+ \boldsymbol{J}'_{\mathcal{T}_R} \boldsymbol{R}^{\mathcal{I}}_{\mathcal{T}_R} \boldsymbol{R}^{\mathcal{T}_R}_{\mathcal{W}_{\mathcal{T}_R}}{}^{passive}\boldsymbol{f}_{\mathcal{T}_R} + \boldsymbol{W}'_{\mathcal{T}_R} \boldsymbol{R}^{\mathcal{I}}_{\mathcal{T}_R} \begin{bmatrix} L_{\mathcal{T}_R} \\ M_{\mathcal{T}_R} \\ N_{\mathcal{T}_R} \end{bmatrix} \\
&+ \boldsymbol{J}'_{\mathcal{T}_L} \boldsymbol{R}^{\mathcal{I}}_{\mathcal{T}_L} \boldsymbol{R}^{\mathcal{T}_L}_{\mathcal{W}_{\mathcal{T}_L}}{}^{passive}\boldsymbol{f}_{\mathcal{T}_L} + \boldsymbol{W}'_{\mathcal{T}_L} \boldsymbol{R}^{\mathcal{I}}_{\mathcal{T}_L} \begin{bmatrix} L_{\mathcal{T}_L} \\ M_{\mathcal{T}_L} \\ N_{\mathcal{T}_L} \end{bmatrix} \\
&+ \boldsymbol{\vartheta}_{\mathcal{F}} + \boldsymbol{\vartheta}_I,
\end{aligned} \tag{C.8}
$$

Therefore, taking into account (C.2), (C.3), and (C.8), the vector of generalized forces (7.18) can be written as

$$
\boldsymbol{\vartheta}(\dot{\boldsymbol{q}}, \boldsymbol{q}, \boldsymbol{u}, \boldsymbol{\zeta}) = \overbrace{[\boldsymbol{\Xi}_1 \;\; \boldsymbol{\Xi}_2 \;\; \boldsymbol{\Xi}_3 \;\; \boldsymbol{\Xi}_4 \;\; \boldsymbol{\Xi}_5]}^{\boldsymbol{B}(\boldsymbol{q},\dot{\boldsymbol{q}})} \begin{bmatrix} 1 & 0 & 0 & 0 & 0 & 0 & 0 & 0 \\ 0 & 1 & 0 & 0 & 0 & 0 & 0 & 0 \\ 1 & 0 & 1 & 0 & 0 & 0 & 0 & 0 \\ 0 & 0 & 0 & 1 & 0 & 0 & 0 & 0 \\ 0 & 0 & 0 & 0 & 1 & 0 & 0 & 0 \\ 0 & 0 & 0 & 0 & 0 & 1 & 0 & 0 \\ 0 & 0 & 0 & 0 & 0 & 0 & \frac{1}{2} & \frac{1}{2} \\ 0 & 0 & 0 & 0 & 0 & 0 & \frac{1}{2} & -\frac{1}{2} \end{bmatrix} \begin{bmatrix} f_{\mathcal{P}_R} \\ f_{\mathcal{P}_L} \\ \tau_{s_R} \\ \tau_{s_L} \\ \delta_{\mathcal{W}_R} \\ \delta_{\mathcal{W}_L} \\ \delta_{\mathcal{T}_R} \\ \delta_{\mathcal{T}_L} \end{bmatrix} \tag{C.9}
$$

$$
\begin{aligned}
&+ \boldsymbol{J}'_{\mathcal{W}_R} \boldsymbol{R}^{\mathcal{I}}_{\mathcal{W}_R} \boldsymbol{R}^{\mathcal{W}_R}_{\mathcal{W}\mathcal{W}_R}{}^{passive} \boldsymbol{f}_{\mathcal{W}_R} + \boldsymbol{W}'_{\mathcal{W}_R} \boldsymbol{R}^{\mathcal{I}}_{\mathcal{W}_R} \begin{bmatrix} L_{\mathcal{W}_R} \\ M_{\mathcal{W}_R} \\ N_{\mathcal{W}_R} \end{bmatrix} \\
&+ \boldsymbol{J}'_{\mathcal{W}_L} \boldsymbol{R}^{\mathcal{I}}_{\mathcal{W}_L} \boldsymbol{R}^{\mathcal{W}_L}_{\mathcal{W}\mathcal{W}_L}{}^{passive} \boldsymbol{f}_{\mathcal{W}_L} + \boldsymbol{W}'_{\mathcal{W}_L} \boldsymbol{R}^{\mathcal{I}}_{\mathcal{W}_L} \begin{bmatrix} L_{\mathcal{W}_L} \\ M_{\mathcal{W}_L} \\ N_{\mathcal{W}_L} \end{bmatrix} \\
&+ \boldsymbol{J}'_{\mathcal{T}_R} \boldsymbol{R}^{\mathcal{I}}_{\mathcal{T}_R} \boldsymbol{R}^{\mathcal{T}_R}_{\mathcal{W}_{\mathcal{T}_R}}{}^{passive} \boldsymbol{f}_{\mathcal{T}_R} + \boldsymbol{W}'_{\mathcal{T}_R} \boldsymbol{R}^{\mathcal{I}}_{\mathcal{T}_R} \begin{bmatrix} L_{\mathcal{T}_R} \\ M_{\mathcal{T}_R} \\ N_{\mathcal{T}_R} \end{bmatrix} \\
&+ \boldsymbol{J}'_{\mathcal{T}_L} \boldsymbol{R}^{\mathcal{I}}_{\mathcal{T}_L} \boldsymbol{R}^{\mathcal{T}_L}_{\mathcal{W}_{\mathcal{T}_L}}{}^{passive} \boldsymbol{f}_{\mathcal{T}_L} + \boldsymbol{W}'_{\mathcal{T}_L} \boldsymbol{R}^{\mathcal{I}}_{\mathcal{T}_L} \begin{bmatrix} L_{\mathcal{T}_L} \\ M_{\mathcal{T}_L} \\ N_{\mathcal{T}_L} \end{bmatrix} \\
&+ \boldsymbol{\vartheta}_{\mathcal{F}} + \boldsymbol{\vartheta}_I - \begin{bmatrix} \nu \boldsymbol{I} & \boldsymbol{0} \\ \boldsymbol{0} & \boldsymbol{0} \end{bmatrix} \dot{\boldsymbol{q}} \\
&= \boldsymbol{B}(\boldsymbol{q}, \dot{\boldsymbol{q}}) \bar{\boldsymbol{\tau}} + \boldsymbol{\vartheta}_{passive}, \qquad \text{(C.10)}
\end{aligned}
$$

with $\bar{\boldsymbol{\tau}} \triangleq \begin{bmatrix} f_{\mathcal{P}_R} & f_{\mathcal{P}_L} & \tau_{s_R} & \tau_{s_L} & \delta_{\mathcal{W}_R} & \delta_{\mathcal{W}_L} & \delta_{\mathcal{T}_R} & \delta_{\mathcal{T}_L} \end{bmatrix}'$, and

$$
\begin{aligned}
\boldsymbol{\vartheta}_{passive} \triangleq\ & \boldsymbol{J}'_{\mathcal{W}_R} \boldsymbol{R}^{\mathcal{I}}_{\mathcal{W}_R} \boldsymbol{R}^{\mathcal{W}_R}_{\mathcal{W}\mathcal{W}_R}{}^{passive} \boldsymbol{f}_{\mathcal{W}_R} + \boldsymbol{W}'_{\mathcal{W}_R} \boldsymbol{R}^{\mathcal{I}}_{\mathcal{W}_R} \begin{bmatrix} L_{\mathcal{W}_R} \\ M_{\mathcal{W}_R} \\ N_{\mathcal{W}_R} \end{bmatrix} \\
&+ \boldsymbol{J}'_{\mathcal{W}_L} \boldsymbol{R}^{\mathcal{I}}_{\mathcal{W}_L} \boldsymbol{R}^{\mathcal{W}_L}_{\mathcal{W}\mathcal{W}_L}{}^{passive} \boldsymbol{f}_{\mathcal{W}_L} + \boldsymbol{W}'_{\mathcal{W}_L} \boldsymbol{R}^{\mathcal{I}}_{\mathcal{W}_L} \begin{bmatrix} L_{\mathcal{W}_L} \\ M_{\mathcal{W}_L} \\ N_{\mathcal{W}_L} \end{bmatrix} \\
&+ \boldsymbol{J}'_{\mathcal{T}_R} \boldsymbol{R}^{\mathcal{I}}_{\mathcal{T}_R} \boldsymbol{R}^{\mathcal{T}_R}_{\mathcal{W}_{\mathcal{T}_R}}{}^{passive} \boldsymbol{f}_{\mathcal{T}_R} + \boldsymbol{W}'_{\mathcal{T}_R} \boldsymbol{R}^{\mathcal{I}}_{\mathcal{T}_R} \begin{bmatrix} L_{\mathcal{T}_R} \\ M_{\mathcal{T}_R} \\ N_{\mathcal{T}_R} \end{bmatrix} \\
&+ \boldsymbol{J}'_{\mathcal{T}_L} \boldsymbol{R}^{\mathcal{I}}_{\mathcal{T}_L} \boldsymbol{R}^{\mathcal{T}_L}_{\mathcal{W}_{\mathcal{T}_L}}{}^{passive} \boldsymbol{f}_{\mathcal{T}_L} + \boldsymbol{W}'_{\mathcal{T}_L} \boldsymbol{R}^{\mathcal{I}}_{\mathcal{T}_L} \begin{bmatrix} L_{\mathcal{T}_L} \\ M_{\mathcal{T}_L} \\ N_{\mathcal{T}_L} \end{bmatrix} \\
&+ \boldsymbol{\vartheta}_{\mathcal{F}} + \boldsymbol{\vartheta}_I - \begin{bmatrix} \nu \boldsymbol{I} & \boldsymbol{0} \\ \boldsymbol{0} & \boldsymbol{0} \end{bmatrix} \dot{\boldsymbol{q}}. \qquad \text{(C.11)}
\end{aligned}
$$